



UNIVERSITAT POLITÈCNICA
DE CATALUNYA
BARCELONATECH

Contributions to the development and validation of fMRI-based biomarkers for drug discovery in social anxiety disorder

by

Héctor Ortiz València

ADVERTIMENT La consulta d'aquesta tesi queda condicionada a l'acceptació de les següents condicions d'ús: La difusió d'aquesta tesi per mitjà del repositori institucional UPCommons (<http://upcommons.upc.edu/tesis>) i el repositori cooperatiu TDX (<http://www.tdx.cat/>) ha estat autoritzada pels titulars dels drets de propietat intel·lectual **únicament per a usos privats** emmarcats en activitats d'investigació i docència. No s'autoritza la seva reproducció amb finalitats de lucre ni la seva difusió i posada a disposició des d'un lloc aliè al servei UPCommons o TDX. No s'autoritza la presentació del seu contingut en una finestra o marc aliè a UPCommons (*framing*). Aquesta reserva de drets afecta tant al resum de presentació de la tesi com als seus continguts. En la utilització o cita de parts de la tesi és obligat indicar el nom de la persona autora.

ADVERTENCIA La consulta de esta tesis queda condicionada a la aceptación de las siguientes condiciones de uso: La difusión de esta tesis por medio del repositorio institucional UPCommons (<http://upcommons.upc.edu/tesis>) y el repositorio cooperativo TDR (<http://www.tdx.cat/?locale-attribute=es>) ha sido autorizada por los titulares de los derechos de propiedad intelectual **únicamente para usos privados enmarcados** en actividades de investigación y docencia. No se autoriza su reproducción con finalidades de lucro ni su difusión y puesta a disposición desde un sitio ajeno al servicio UPCommons. No se autoriza la presentación de su contenido en una ventana o marco ajeno a UPCommons (*framing*). Esta reserva de derechos afecta tanto al resumen de presentación de la tesis como a sus contenidos. En la utilización o cita de partes de la tesis es obligado indicar el nombre de la persona autora.

WARNING On having consulted this thesis you're accepting the following use conditions: Spreading this thesis by the institutional repository UPCommons (<http://upcommons.upc.edu/tesis>) and the cooperative repository TDX (<http://www.tdx.cat/?locale-attribute=en>) has been authorized by the titular of the intellectual property rights **only for private uses** placed in investigation and teaching activities. Reproduction with lucrative aims is not authorized neither its spreading nor availability from a site foreign to the UPCommons service. Introducing its content in a window or frame foreign to the UPCommons service is not authorized (*framing*). These rights affect to the presentation summary of the thesis as well as to its contents. In the using or citation of parts of the thesis it's obliged to indicate the name of the author.

PhD dissertation

Contributions to the development and validation of fMRI-based biomarkers for drug discovery in Social Anxiety Disorder

Submitted by

Héctor Ortiz València

under the supervision of

Dr. Jesús Pujol Nuez and Prof. Dr. Javier Rosell Ferrer

in partial fulfillment of the requirements for a Doctor of Philosophy degree from
the Universitat Politècnica de Catalunya

Barcelona, November of 2015



**UNIVERSITAT POLITÈCNICA
DE CATALUNYA
BARCELONATECH**

To my son, Oriol. Use this as a proof that you can get further than what you can see.

Contributions to the development and validation of fMRI-based biomarkers for drug discovery in Social Anxiety Disorder

Author: Héctor Ortiz València

Thesis supervised by:

Jesús Pujol Nuez, MD, PhD

MRI Research Unit, CRC Mar, Hospital del Mar, Barcelona, Spain

Centro Investigación Biomédica en Red de Salud Mental, CIBERSAM
G21, Barcelona, Spain

Prof. Javier Rosell Ferrer, PhD

Department of Electronic Engineering, Universitat Politècnica de
Catalunya, Barcelona, Spain

Doctoral degree in Biomedical Engineering. Universitat Politècnica de Catalunya

This work has been supported by the FPU grant AP2006-2869 from the Ministry of Education of Spain

Copyright © 2015 by Héctor Ortiz València, Barcelona, Spain. All rights reserved.
Reproduction by any means or translation of any part of this work is forbidden without permission of the copyright holder.

Abstract

This document presents the theoretical background and experimental work made to develop and validate a set of experiments based on functional magnetic resonance imaging (fMRI). These experiments are aimed to demonstrate that fMRI can be a valuable tool to objectivize drug treatment response in Social Anxiety Disorder (SAD) patients.

Functional MRI is a non-invasive imaging technique which provides localized indicators of brain activity. The analysis of fMRI data has recently facilitated neuroscience to make a leap forward in the understanding of the human brain.

Psychiatric clinical research, however, hasn't fully embraced yet the potential of fMRI. In parallel, the societal costs of new psychiatric drug discovery are reaching unbearable limits. It has been hypothesized that the addition of fMRI in clinical trials of pharmacologic treatments of SAD can provide new biomarkers of treatment response which, in the future, shall reduce the temporal and economic burden of drug discovery. Five studies are presented in this dissertation in an evolving path towards the validation of the hypothesis.

In study 1, a widely validated state-of-the-art emotional face processing paradigm was piloted in a non-clinical sample. Task-related activations were in line with the findings previously reported in the literature. However, the results of experiment did not show a correlation with symptom severity. An additional exploratory psychophysiological interaction analysis revealed that the relationship between two emotion-processing areas had a significant correlation with SAD symptom severity. This emphasized the potential value of studies based on functional connectivity for our objectives.

Study 2 explored the reproducibility of connectivity analysis of fMRI data. To do so, a brain network was selected and explored with Independent Component Analysis (ICA) on data collected from three categorically differentiated paradigms: A resting task, a moral dilemma task and in a cognitive-challenging Stroop task. The selected network was systematically identified in the three cases, exemplifying the robustness of the technique in three extreme cases.

Study 3 explores the sensitivity of ICA by analyzing resting-state data acquired before and after an experimental induction of sad mood. Multiple regions reflected changes in their intranetwork connectivity after sad mood induction. Results were validated using a split-half re-analysis and confirmatory seed-based functional connectivity measurements. These results support the idea that spatial ICA of fMRI is not only reliable, but also a sensitive paradigm.

Study 4 presents a novel SAD symptom-provoking paradigm that was validated on SAD patients and controls. The analysis of this pilot revealed a striking non-linear relationship between task activation and social anxiety scores. This non-linear relationship is compatible with some of the divergences found in literature regarding the alteration of emotional regulation brain areas in SAD.

Study 5 presents the results of a small placebo-controlled clinical trial using a common treatment for SAD (paroxetine) in SAD patients. Subjects underwent the emotional face processing, the symptom-provoking and resting state tasks that were administered and analyzed following the experience obtained in studies 1 to 4. The selected fMRI paradigms and analysis methods showed significant sensitivity to the effects of paroxetine treatment on SAD. Treatment effects were identified in areas related to the processing of fear stress and anxiety, which are known to be altered in SAD. Remarkably, ICA revealed sensitivity to pharmacologically-induced clinical improvement in the same areas and direction than the symptom-provocation task.

Along with the evidences reported in the literature review, the methods and results obtained throughout this dissertation provide a proof of concept on the usage of fMRI as a biomarker for SAD pharmacologic research.

Acknowledgements

I would like to express my most sincere gratitude to Jesús Pujol for his guidance through this exciting journey. With Jesús, I've acquired knowledge that goes far beyond these pages and that I will treasure for life. However, it is not only the knowledge that I want to thank him for, but also for the personal experiences and the memories collected on the way.

Jesús' passion for what we do creates very vivid days. Most of these days are very demanding, but often colorfully spotted with intense situations of joy, laughter, success or failure, intrigue or even fear. Any harsh sensation was rapidly outweighed by one those "whoa" moments in which we realized that we had brought the understanding of the brain one step further.

This experience wouldn't have been possible without my travel colleagues, who know that deserve my thanks. I could have never imagined how hilarious and delusional could it be doing research surrounded of psychologists, psychiatrists and creatures alike. Carles was for long time the balancing element of the lab, until he had one of those moments which made us break into tears of laughter. We were lucky of getting Monica's organization skills in-house. Ben's postdoc stay brought from overseas a toolset and an academic perspective that made a difference, in addition to a huge human quality. I impatiently look forward to his yearly visits since he left. Alicia is the living proof that top-notch neuroradiology and romanticism can coexist. The periodic visits of Joan, Narcís and Rosa brought us an invaluable reference from the "real" world of mental health, and often fresh air into the lab. Marina's emotion bombs could revolution up any gray day behind Matlab scripts, something I ended being truly thankful for. Oren's permanent smile managed to cheer up any situation. While all these amazing individuals can be considered singular, our performances as an orchestra left memorable moments, especially those during our Wednesday's brainstorming paellas in front of the Mediterranean Sea. For all of those moments, many, many thanks.

I can't continue the acknowledgements without mentioning how glad I am to see that the latest to arrive to the lab: Laura, Marina, Gerard ... have contributed to keep alive the singular atmosphere that is the soul of the group. I'm particularly grateful to Dídac for joining the family. Finally, after ten years, one colleague with what I call an engineer's mind – although he is actually a physicist, a historian, an artist and an entrepreneur-. His fast ramp up has brought to me the peace of mind feeling that the lab now has the best potential than ever to develop revolutionary methods of neuroimaging.

A special thanks go to Javier Rosell. Despite not being part of our day to day momentum, he has been a thorough supporter of this endeavor since the first day. Thanks for patiently waiting to hear news from the "basement" and for providing wise academic and vital advice in our warm encounters throughout all these years.

I also want to thank my family. Thanks to my parents Toni and Hemi, for giving me the values and self-confidence that brought me here. Thanks as well to my extended family for the understanding shown on what I chose to spend my "free" time in.

Last but not least, my deepest appreciation is for my beloved wife Anna. Thanks for your relentless support, motivation and patience during this journey. You're the best travel companion I could imagine.

Contents

Abstract i

Acknowledgements iii

List of abbreviations ix

| | | |
|----------|--|-----------|
| 1 | Introduction..... | 1 |
| 1.1 | <i>Context and motivation</i> | <i>1</i> |
| 1.2 | <i>Thesis outline</i> | <i>3</i> |
| 2 | Introduction to the technological state of the art | 5 |
| 2.1 | <i>Physics to technology: From magnetism to brain function maps</i> | <i>5</i> |
| 2.2 | <i>Overview of analysis methods of fMRI studies</i> | <i>19</i> |
| 3 | Introduction to the application’s state of the art: Psychiatry research from a neuroimaging perspective | 31 |
| 3.1 | <i>Contributions of neuroimaging to the clinical practice of psychiatry</i> | <i>31</i> |
| 3.2 | <i>Potential contributions of neuroimaging in psychiatric drug discovery: biomarkers and surrogate markers.....</i> | <i>32</i> |
| 3.3 | <i>The Social Anxiety Disorder.....</i> | <i>39</i> |
| 4 | Hypothesis and specific objectives of this dissertation | 43 |
| 4.1 | <i>Hypothesis.....</i> | <i>43</i> |
| 4.2 | <i>Objectives.....</i> | <i>43</i> |
| 5 | Study 1 - Exploratory analysis of altered emotional face processing as a SAD symptom biomarker in healthy volunteers: Proof of concept on the value of functional connectivity and validation of the imaging setup..... | 47 |
| 5.1 | <i>Introduction</i> | <i>47</i> |
| 5.2 | <i>Methods.....</i> | <i>50</i> |
| 5.3 | <i>Results.....</i> | <i>70</i> |
| 5.4 | <i>Discussion and Conclusions.....</i> | <i>79</i> |
| 6 | Study 2: Specificity and reproducibility of independent component analysis of fMRI datasets in cognitive, emotional and resting state experiments | 83 |
| 6.1 | <i>Introduction</i> | <i>83</i> |
| 6.2 | <i>The concept of the default mode brain network.....</i> | <i>84</i> |
| 6.3 | <i>Methods.....</i> | <i>85</i> |

| | | |
|-----------|--|------------|
| 6.4 | <i>Results</i> | 93 |
| 6.5 | <i>Discussion and conclusions</i> | 96 |
| 7 | Study 3: Validation of sensitivity of resting-state experiments to emotional state differences | 101 |
| 7.1 | <i>Introduction</i> | 101 |
| 7.2 | <i>Methods</i> | 103 |
| 7.3 | <i>Results</i> | 111 |
| 7.4 | <i>Discussion and conclusions</i> | 120 |
| 8 | Study 4: Characterization of SAD’s expression using a novel symptom provoking fMRI experiment in patients and controls. | 125 |
| 8.1 | <i>Introduction</i> | 125 |
| 8.2 | <i>Methods</i> | 127 |
| 8.3 | <i>Results</i> | 133 |
| 8.4 | <i>Discussion and conclusions</i> | 139 |
| 9 | Study 5: Validation of an imaging protocol aimed to characterize pharmacological response in Social Anxiety Disorder patients | 143 |
| 9.1 | <i>Introduction</i> | 143 |
| 9.2 | <i>SSRI action principles in SAD.</i> | 145 |
| 9.3 | <i>Experimental setup</i> | 147 |
| 9.4 | <i>Methods</i> | 147 |
| 9.5 | <i>Results</i> | 154 |
| 9.6 | <i>Discussion and Conclusions</i> | 161 |
| 10 | Ethical considerations | 165 |
| 10.1 | <i>Limitations of the inference through this thesis’ results</i> | 165 |
| 10.2 | <i>Neuroethics</i> | 166 |
| 10.3 | <i>A new window to the brain: Privacy of the subjects</i> | 168 |
| 11 | Conclusions | 171 |
| 12 | Publications derived from this thesis | 173 |
| 13 | Bibliography | 175 |

List of figures

| | |
|---|-----|
| Figure 1 Rate of publication of fMRI papers..... | 10 |
| Figure 2 Hemodynamic response function | 14 |
| Figure 3 Point spread function | 16 |
| Figure 4 Thesis outline..... | 44 |
| Figure 5 EFPT task as implemented in study 1 | 52 |
| Figure 6 LSAS score histogram..... | 53 |
| Figure 7 MRI-compatible goggles | 57 |
| Figure 8 MRI-compatible response devices | 58 |
| Figure 9 Model for Psychophysiological interaction analysis..... | 68 |
| Figure 10 Main faces-matching task effects..... | 71 |
| Figure 11 Psychophysiological interaction induced by the faces processing task | 73 |
| Figure 12 Amygdala regions that correlate with LSAS after regressing out the activation of the fusiform gyrus. | 77 |
| Figure 13 Plots between amygdala activation and LSAS scores after regressing out the activation of fusiform gyrus | 79 |
| Figure 14 Examples of moral dilemma task | 89 |
| Figure 15 Components of the default mode network..... | 95 |
| Figure 16 ICA-extracted Default Mode Network overlap across tasks | 96 |
| Figure 17 Resting state networks common across states | 113 |
| Figure 18 Results of the split-half reproducibility analysis..... | 114 |
| Figure 19 Modulation of Resting-State Networks by Mood Induction | 117 |
| Figure 20 Spectral analysis of ICA results | 118 |
| Figure 21 Cross-Correlation analysis of representative resting-state Networks | 120 |
| Figure 22 The PERPT Task..... | 129 |
| Figure 23 Task-induced activation..... | 134 |
| Figure 24 Differences in task-induced activation | 135 |
| Figure 25 Correlation of brain activation with task-related anxiety ratings | 136 |
| Figure 26 Correlation of brain activation with Liebowitz Social Anxiety Scale (LSAS) scores | 137 |
| Figure 27 Physiological assessment of task response for patients and controls | 138 |
| Figure 28 Eye tracking assessment..... | 139 |

| | |
|---|-----|
| Figure 29 EFPT task..... | 149 |
| Figure 30 Visuo motor control task | 151 |
| Figure 31 ICA components selected for second level analysis..... | 153 |
| Figure 32 EFPT and PERPT activation maps..... | 155 |
| Figure 33 ANOVA 2x2 results of interaction between treatment and time..... | 157 |
| Figure 34 Correlation of paroxetine effect on PERPT or resting and CGI scores | 159 |
| Figure 35 Resting state effect of treatment | 160 |

List of tables

| | |
|---|-----|
| Table 1 Publications with model free analysis methods | 25 |
| Table 2 Key economic statistics of top drug companies | 37 |
| Table 3 Study sample descriptors..... | 54 |
| Table 4 Main faces-matching task effects | 71 |
| Table 5 Segmented faces-matching task effects..... | 72 |
| Table 6 Differential task effects: Fear > Happy | 73 |
| Table 7 Correlations of LSAS with brain response to emotional faces in the task's activation peak coordinates. | 75 |
| Table 8 Correlation of amygdala response to emotional faces with LSAS after controlling for fusiform gyrus activation | 78 |
| Table 9 Treatment effects of paroxetine on PERPT activation in ROIs | 158 |

List of abbreviations

| | |
|--------------|--|
| 5-HT | 5-Hydroxytryptamine, serotonin |
| AC | Anterior commissure |
| ACC | Anterior cingulate cortex |
| AF | Angry faces |
| ANOVA | Analysis of variance |
| AR | Autoregressive |
| ATP | Adenosine triphosphate |
| BOLD | Blood oxygenation level dependent |
| CBF | Cerebral blood flow |
| CBT | Cognitive behavioral therapy |
| CBV | Cerebral blood volume |
| CGI | Clinical global impression scale |
| CRF | Clinical research facilities |
| CRO | Contract research organization |
| CS | Cluster size |
| CSF | Cerebrospinal fluid |
| DMN | Default mode network |
| DNA | Deoxyribonucleic acid |
| DSM | Diagnostic and statistical manual of mental disorders |
| EBIT | Earnings before interests and taxes |
| EFPT | Emotional face processing task |
| EMA | European medicines agency |
| EPI | Echo planar imaging |
| FC | Functional connectivity |
| FDA | Food and drug administration of the United States of America |
| FDR | False discovery rate |
| FF | Fearful faces |
| fMRI | Functional magnetic resonance imaging |
| FWHM | Full width at half maximum |
| GE | Gradient echo |
| GLM | General linear model |
| HF | Happy faces |
| IC | Independent component |
| ICA | Independent component analysis |
| IND | Investigational new drug |
| LSAS | Liebowitz social anxiety scale |
| MAOI | Monoamine oxidase inhibitor |
| MDL | Minimum description length |
| MEG | Magnetoencephalography |
| MNI | Montreal neurological institute |
| MR | Magnetic resonance |
| MRI | Magnetic resonance imaging |

| | |
|--------------|--|
| NMR | Nuclear magnetic resonance |
| PC | Posterior commissure |
| PCA | Principal components analysis |
| PD | Pharmacodynamics |
| PERPT | Public exposition of recorded performance task |
| PET | Positron emission tomography |
| PFC | Prefrontal cortex |
| PK | Pharmacokinetics |
| PPI | Psychophysiological Interaction |
| PSD | Power spectral density |
| PSF | Point spread function |
| RESEL | Resolution element |
| RF | Radio frequency |
| RIMA | Reversible inhibitors of monoamine oxidase |
| ROI | Region of Interest |
| RSN | Resting state network |
| SAD | Social anxiety disorder |
| SD | Standard deviation |
| SE | Spin echo |
| sICA | Spatial independent component analysis |
| SNR | Signal to noise ratio |
| SNRI | Serotonin noradrenaline reuptake inhibitor |
| SPM | Statistical parametric map (or mapping) |
| SSRI | Selective serotonin reuptake inhibitor |
| STAI | Spielberger state-trait anxiety inventories |
| TE | Time of echo |
| TR | Time of repetition |
| USD | United States dollars |

1 Introduction

1.1 Context and motivation

Anxiety disorders form the group of most common psychiatric disorders. The most relevant medical authorities, including the World Health Organization and the American Psychiatric Association, recognize a subtype in it named Social Anxiety Disorder (SAD) or social phobia (WHO 1992; APA 2000). SAD patients are characterized by fearing and avoiding the scrutiny of others that leads them to the avoidance of social situations, significantly impairing their life. SAD has been reported to have a lifetime prevalence up to 12.1% over the US general population (Ruscio et al. 2008). This bears huge costs to our society (François et al. 2010), who calls for new and more effective treatments (Stein & Stein 2008).

Neuropsychopharmacologic research eagerly requires the development of research protocols able to objectivize drug effectivity assessment. In some cases, biomarkers simplify and accelerate the characterization of patient populations and the quantification of the effect of new treatments on their therapeutic targets (Frank & Hargreaves 2003). Unfortunately, these are still scarce or with limited effectivity to model psychiatric conditions (Macaluso & Preskorn 2012). Due to this lack of biomarkers, psychiatry research often has to infer treatment response through self-reports of large samples of patients.

This situation makes translational research difficult in anxiety-related disorders. Often, the treatment effect needs to be inferred from behavioral observations of the animals under study. These provide standardized and reproducible results, but with limited capacity to predict human response to new pharmacological treatments (Cryan & Sweeney 2011).

From the perspective of the pharmacological industry, the lack of biological markers adds risks and costs to the assessment of effectivity of new molecules. As a result, the pharmacologic industry's costs are increasing dramatically while the amount of new treatments launched has been barely maintained (Trist & Bye 2014).

Recent advancements in human functional magnetic resonance imaging and its analysis indicate the possibility of its usage in the development of new paradigms for psychiatric drug discovery (Nathan et al. 2014). In particular, fMRI has proven able to identify activity in emotional processing and anxiety related brain circuits, which are known to be altered in SAD (Goldin, Manber, et al. 2009).

The complex nature of SAD makes difficult the development of biomarkers that require to trigger the symptoms consistently across subjects or trials. Techniques based on symptom provocation have an interpretation closer to the context of clinical practice, and are the most used in SAD. However, biomarkers that directly explore the underlying neuropsychological mechanisms may better support drug development in its early phases, as they are more compatible with translational research (Cryan & Sweeney 2011) and early microdosing studies (Bergström et al. 2003). Extensive neuroscience studies and techniques are still to be developed in order to reach the stage in which biomarkers become validated and widely accepted for drug discovery in the Social Anxiety Disorder.

Concurrently to the issues presented, in the research context, there has been a growing interest and advancements in the interpretation of fMRI brain signals collected while the subject is performing no task (being in resting state). The further development of methods able to analyze resting-state fMRI datasets suggests the possibility to study treatment response without the need of relying on a full cooperation of the individuals under study nor symptom-provoking paradigms.

Resting state assessments of disease severity biomarkers in SAD patients would avoid the variability across subjects or time of the effectivity of symptom-provoking tasks. Importantly, it could also be highly compatible with translational research, as resting state studies have proven highly translational on animal models (Barks et al. 2015). This enables the creation of cross-species biomarkers (Becerra et al. 2013; Grimm et al. 2015)

A protocol for assessing drug effectivity in SAD using resting state had not been published when this thesis was started. Recent publications show similar working lines in other labs. As part of this dissertation, and prior to its design and development, it has been necessary to explore some pre-requisites such as the expression of SAD in brain

connectivity, the reproducibility, specificity and sensitivity of resting state studies in this particular context. After designing the protocol and analysis methods, a pilot study with actual patients is presented for its validation.

1.2 Thesis outline

This thesis presents the theoretical background and experimental work made to explore fMRI-based biomarkers aimed to objectivize drug treatment response in Social Anxiety Disorder (SAD) patients. The assessed biomarkers are based on tasks previously validated by the scientific community, a task developed during the development of this work and an analysis that can be performed while the subject performs no task (resting state analysis). Results of the different task types are analyzed as biomarker candidates in pilot studies including controls and patients.

Section 2 introduces the reader into the technical background of fMRI. Section 3 describes the context of psychiatry, neuroimaging and drug discovery research. Section 4 sets the hypotheses and objectives of this work along with their conceptual arrangement throughout this dissertation. Section 5 shows the initial exploratory experiment aimed to validate the imaging technique and to explore the value of connectivity analysis in SAD research. Section 6 validates reproducibility and specificity of ICA of fMRI collected in resting state, cognitive and emotional tasks. Section 7 shows the results of an exploratory experiment aimed to test the sensitivity of resting-state ICA to emotional state changes. Section 8 shows the results of an experiment aimed to compare SAD patients and controls. Section 9 shows the first results obtained with the described protocol, and analyzes them to validate its effectivity. Section 10 contains an ethical review of the results obtained during the development of this thesis. Section 11 summarizes the conclusions made through this piece of work.

2 Introduction to the technological state of the art

2.1 Physics to technology: From magnetism to brain function maps

2.1.1 The journey towards Nuclear Magnetic Resonance

Magnetism is a phenomenon that has been known by mankind for millennia. We can find references to magnetism even in Thales of Miletus' works (VI century BC). However, for long time, magnetism remained as a non-understood phenomenon. It was not until 1820 when Christian Oersted published a clear relationship between electric current and magnetism. Even then, the phenomenon was not mathematically modeled until André-Marie Ampère published his seminal works in 1826 (Ampère 1826).

The accelerated growth of knowledge on the atom and quantum physics of the early XX century originated a singular situation in which the *Nuclear Magnetic Resonance* (NMR) phenomenon was described simultaneously by two researchers of distant centers. (Bloch 1946; Purcell et al. 1946). A surprised editor of the Physical Review Journal received their two groundbreaking papers, describing NMR, within 4 weeks of difference.

Immediately after, and for almost 4 decades, NMR was considered as a technique used to characterize chemical samples. Its adoption was mainly in physics and chemistry research. Nonetheless, there are early reports of its application to study histological samples (Odeblad & Lindström 1955).

The physical principle behind NMR is understood through quantum physics: Isotopes that contain an unpaired number of protons or neutrons – such as hydrogen ^1H – present a quantum mechanical property named *spin*. To make a macroscopic mechanical analogue, *spin* behaves as if a small magnet was inside the atom, spinning on its north-south axis. This magnet can be imagined with some inertial momentum, like a spinning top has. In normal conditions, these atomic spins would be randomly oriented, creating a null macroscopic magnetization vector.

However, when an external magnetic field B_0 is applied, the spins orient themselves either parallel or antiparallel to the magnetic field. Because parallel alignment

to B_0 is a lower energy state, thus more stable, than antiparallel alignment, an excess of nuclei will be aligned towards the parallel state. In conditions compatible with a biologic exploration, this excess is very small, on the order of 1 out of 10 million spins. This excess is, however, enough to create a measurable macroscopic magnetization vector.

Spins naturally precess according to the Larmor frequency ω , which is proportional to the magnetic field B_0 and to the gyromagnetic ratio γ of the nucleus ($\omega = \gamma \cdot B_0$). The gyromagnetic ratio of hydrogen is 42.6 MHz/Tesla. Again, in stable conditions, precession phases will be incoherent and therefore no macroscopic effect will be detectable due to this precession. However, if an electromagnetic signal (at Larmor frequency) is applied to the sample, spins will start precessing coherently, creating a macroscopic magnetic component perpendicular to B_0 that will rotate along direction B_0 and that will briefly remain after we stop applying the electromagnetic signal. As the spin returns to its relaxed state, it will release an electromagnetic signal. This is the origin of the term magnetic *resonance*. The macroscopic transversal component of the spin –and its decay- can be measured using suitable antennas for the application's Larmor frequency.

After cessation of the stimulating signal, the transverse magnetization will decay exponentially in the process we know as relaxation. This decay will depend on the physicochemical surrounding of the nuclei, and therefore vary depending on it. The principles of NMR are based on measuring the relaxation times in the longitudinal axis (T_1) or in the transversal plane (T_2 and T_2^*) to detect the concentration and state of substances or tissues.

The difference between T_2 and T_2^* parameters only relies on how they are measured: T_2 is measured as the difference between the echo after the (90°) excitation pulse and the echo after and 180° refocusing pulse. T_2^* is measured as the rate of decay of the pulse right after the excitation pulse. T_2^* measurements are more sensitive to local magnetic field inhomogeneity, which dephases faster the spins. In an ideally homogeneous magnetic field and sample, T_2 would be exactly as T_2^* . In general practice $T_2^* \ll T_2$, this is also a reason why T_2^* is widely used in fast imaging sequences.

2.1.2 Images based on NMR: Magnetic Resonance Imaging

Note that, as described before, NMR would not be able to discriminate the signal from different positions within the sample. This made the technique barely usable in *in vivo* tests until magnetic resonance *imaging* was developed, using a simple addition: Small spatial variations of the field strength were used to spatially encode the Larmor frequency, and therefore the collected signal. Receivers also faced the challenge of changing from measuring a decaying tone, to processing a broadband signal that needed to be explored band by band to record the signal from different spatial locations at once.

Raymond Vahan Damadian is considered one of the key fathers of NMR *imaging* (MRI) systems. Initially, the system he invented and patented was based on a simple execution of NMR spectroscopies run *in vivo* on patients aiming to detect cancerous tissue (Damadian 1971). The usefulness of his invention and its commercial application were deeply controversial for years.

It is not until 1973 when Paul Lauterbur published in *Nature* the first image generated by MRI as the technique is conceived today. For the first time, spatially encoded magnetic gradients were being applied on a sample to give its atoms a location-specific resonant frequency (Lauterbur 1973). In the following years, Lauterbur's lab developed many technical solutions that are still in use in today's MRI systems. In parallel, Peter Mansfield developed excitation and reconstruction algorithms that would allow retrieving images within a timespan that enabled their usage in clinical practice (Mansfield 1977). Among them, the Echo Planar Imaging sequence (EPI), which still is widely used today. The simultaneous developments of Lauterbur and Mansfield made them eligible to share them the 2003 Nobel's prize of medicine.

The first commercial MRI systems were placed on the market in the early eighties. Most of the early manufacturers (Bruker, EMI) chose to develop systems operating at magnetic fields below 0.5 Tesla. A remarkable step forward was made with the introduction of the *Signa* systems that General Electric, together with Advanced NMR systems, presented in 1983. These systems operated at a magnetic field of 1.5 Tesla. This represented the onset of the era of high field MRI. As it will be presented later, this step

was key for the evolution towards functional MRI. Functional MRI of the human brain, as we understand it today, is practically considered to be technically feasible only at 1.5 T or higher fields.

2.1.3 Imaging the biophysics of brain function: functional Magnetic Resonance Imaging

Later in the eighties, MRI had become a modern imaging technique, relatively accessible in clinical and research environments and opening new windows to neuroscience (Pujol et al. 1988). However, at that time, the technique of reference for brain activity imaging was still Positron Emission Tomography (PET).

The work of Fox and Raichle had showed that, upon activation, the cortical brain tissue changed its local Cerebral Blood Flow (CBF) in a proportion much larger than the change in its Cerebral Metabolic Rate of Oxygen (CMRO₂) (Fox & Raichle 1986). This effect induces the paradox in which a local increase of brain activity is accompanied by a local increase of the fraction of oxygenated blood in the local capillary bed.

In 1990, Ogawa et al demonstrated the idea that local blood oxygenation could be mapped using MRI (Ogawa & Lee 1990). Ogawa et al modulated cerebral blood flow in a rat model using a high-CO₂ gas mixture that the animal breathed. The vasodilation property of CO₂ dramatically increases brain blood flow, while the oxygen metabolic rate of the brain could be assumed to remain constant. Therefore, upon breathing the CO₂, the brain blood was more oxygenated, with less presence of deoxyhemoglobin. Ogawa observed a significant change in the signal of an MRI technique, based on the measurement of T₂, which is sensitive to magnetic field heterogeneity. They termed it the Blood Oxygenation Level Dependent (BOLD) signal.

With the findings of an MRI technique sensitive to local blood oxygenation and knowing that PET studies pointed that brain activity would be accompanied by a local change of oxygenation, the quest for an MRI technique sensitive to brain activity had started.

In 1992, two groups published, almost simultaneously, results showing the feasibility of techniques able to map BOLD signal in human brains without the need to administer any external agent (Kwong et al. 1992; Ogawa et al. 1992). These are considered the first successful experiments of *functional Magnetic Resonance Imaging* (fMRI) as we understand it today. The momentum of that period can be exemplified by the fact that multiple groups also published successful fMRI results in the following months (Frahm et al. 1993; Menon et al. 1993; Blamire et al. 1992; Turner et al. 1993). Soon after, the global neuroscientific community was aware that the technique was aware of the potential of this technique for clinical and scientific interests (Pujol et al. 1995).

The BOLD signal detected by fMRI sequences is based in the magnetic properties of hemoglobin. Hemoglobin is present in the blood of all vertebrates, with the exception of the ice fish family Channichthyidae (di Prisco et al. 2002). When hemoglobin flows through the capillary bed and loses its oxygen, it turns into deoxyhemoglobin. Magnetic properties of hemoglobin and deoxyhemoglobin differ categorically (Pauling & Coryell 1936). The binding of oxygen to the protein's ferrous nucleus makes hemoglobin to behave as diamagnetic and to turn into paramagnetic when it loses this oxygen, becoming deoxyhemoglobin.

At MRI's high magnetic fields, the paramagnetic property of deoxyhemoglobin introduces an inhomogeneity into its environment's magnetic field. This inhomogeneity induces a drop in the transverse relaxation time $T2^*$ of the hydrogen nuclei of the water present in blood. In particular, the blood's rate of relaxation $T2^{-1}$ has a quadratic dependency of the external magnetic field's strength and the blood's concentration of deoxyhemoglobin (Thulborn et al. 1982).

In contrast to PET studies, fMRI allowed for the first time recording an activity indicator of the whole brain tissue every few seconds. Therefore, it allowed creating 3D maps of brain activity with an unprecedented combination of spatial and temporal precision. Also, in favor against PET, fMRI did not require exposing the subject to any contrast agent nor to ionizing radiation. Consequently, the technique was considered as non-invasive since its beginning. This extremely facilitated the recruitment of volunteers

and approval of experiments avoided many burdensome approvals. Some of the subjects of the first experiments were, in fact, young researchers that years later became successful Neuroimaging authors (Blamire 2012; Uğurbil 2012) .

With an effective sampling frequency, at that time, around 0.5 Hz, fMRI had positioned inbetween the two most accepted neuroimaging techniques of the moment: PET (with a temporal resolution in the order of minutes) and EEG (with a temporal resolution in the area of milliseconds). In terms of space resolution, it presented a resolution and precision one order of magnitude above PET and EEG. The cost of the instruments and its maintenance was similar to a PET setup. However, the fact that explorations were noninvasive and that spent no consumables quickly raised the interest from the neuroscientific community (Illes et al. 2003). Currently, the rate of usage of fMRI continues growing, while PET is in decline (Cumming 2014) despite it has some unmatched strengths. See Figure 1 for a graph on the rate of appearance of the keyword “fMRI” in title/abstract headers of peer-reviewed articles published per year (2015 volume was projected from the run rate at August 2015).

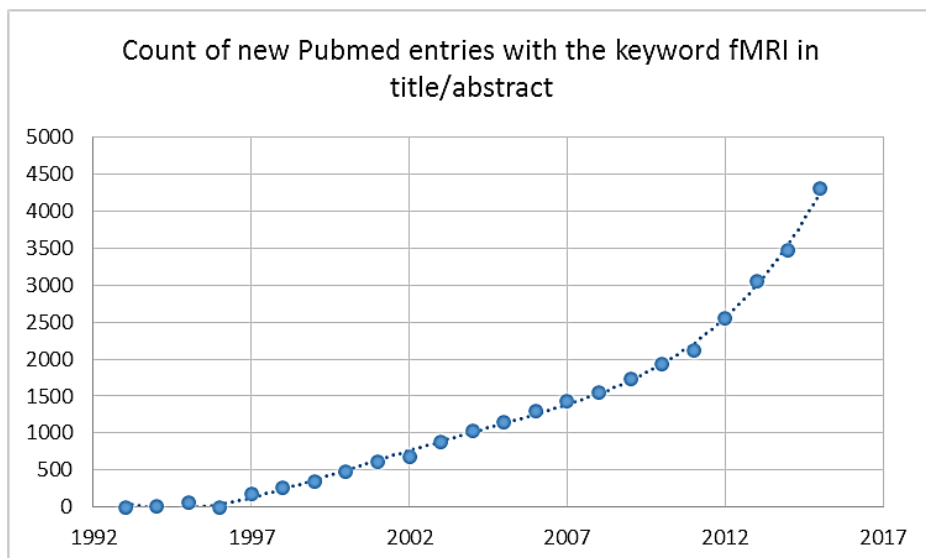


Figure 1 Rate of publication of fMRI papers

Rate of apparition of the keyword fMRI in peer-reviewed articles indexed by the US national library of medicine. Quantity indicates yearly amount of articles. 2015 data is a projection from rate in august 2015.

Currently, fMRI has clearly become the technique of first choice in cognitive neuroscience to study brain activity (Rosen & Savoy 2012) in a time-space window constrained down to 1 second temporal resolution and 1 mm³ of spatial precision.

2.1.4 Physiological principles behind fMRI

As introduced in section 2.1.3, the BOLD contrast was named after the observation that focal brain activity generates a local increase of the blood flow that exceeds the increase of oxygen tissue the same area. This induces an increased oxygenation in the capillary bed of the activated cortex. Some MRI sequences are sensitive to these local changes. Therefore, the brain activity *detection* made with fMRI is a deeply indirect approach. The observed BOLD signal is generated by a chain of physiologic effects that needs to be fully understood before it is interpreted. Each of the mediators can also act as a potential source of confounds for the measurement. This section covers the minimum concepts needed to be able to interpret the inferences made in this thesis.

The source of the BOLD effect was originally described as the “uncoupling” of the activation-induced changes in local cerebral blood flow (CBF) and in the cerebral metabolic rate of oxygen (CMRO₂) (Fox & Raichle 1986). However, it soon became clear that the relationship between brain activity and these physiologic phenomena needed to be clearer understood in order to correctly interpret fMRI results.

The increase in CMRO₂ that accompanies brain activity is related to the increased oxidative metabolism of glucose that is triggered by synaptic activity (Erecińska & Dagan 1990). Neural activity is also known to induce anaerobic glycolysis (Fox et al. 1988), but this has a small contribution to the neuron’s ATP supply due to its much smaller yield. The relationship between synaptic activity and neuronal energetic metabolism is still partially quantified (Ivannikov & Macleod 2013).

Activity-related changes in local Cerebral Blood Flow (CBF) are still to be precisely described, but it is widely accepted that hemodynamic regulatory mechanisms are independent of substrate depletion nor metabolite buildup (Davis & Hill 1999). The brain’s

capillary bed is highly responsive to the changes that neuronal activity introduce in the chemical composition of the extracellular fluid. Level of K^+ change due to membrane potential shifts and are considered the main driver of CBF regulation. Some neurogenic regulation of CBF can also occur: The fastigial nucleus of the cerebellum (Iadecola & Reis 1990) and the basal forebrain (Sato et al. 2001) have been demonstrated to drive changes in CBF, which are unrelated to local metabolic rates.

Generally, CBF regulation is mainly achieved by increasing capillary blood velocity rather than by additional capillary recruitment (Keyeux et al. 1995). However, some studies using vasoactive challenges did manage to induce changes in vessel recruitment (Hutchinson et al. 2006). These results are key to compare fMRI results obtained with different MRI sequences, as they show different sensitivity to the vascular state of the tissue (Duong et al. 2003).

While the CMRO₂ changes are immediately tied to neuronal metabolism, CBF is related to slower physical changes that need to take place in the vascular bed. These changes have lags in the order of magnitude of seconds. Because of their longer sampling times, the early PET studies on CBF were not sensitive to these hemodynamics, but this lag became evident since the earliest fMRI results because of the technique's highest temporal resolution (Kwong et al. 1992). The initial approaches for modeling the relationship between CMRO₂ and the BOLD signal involved modeling it as a linear filter (K. J. Friston et al. 1994). Its impulse response would be convolved with the expected neuronal activity related to stimulus to predict BOLD signal. Posterior works developed more complete –and complex- non-linear models of BOLD hemodynamics (Buxton & Frank 1997; Mandeville et al. 1999; Friston et al. 2000). Models like these are used in practically every fMRI analysis, although some details of them are still under discussion (van Zijl et al. 2012).

Buxton's nonlinear "balloon" model (Buxton et al. 1998) along with its posterior expansions (Griffeth & Buxton 2011), has been one of the most influencing physiologic models to map neuronal activity to its expression in fMRI's BOLD signal. Buxton's model introduces cerebral blood volume into the equation: Some of the effects identified are

not directly related to blood oxygenation changes, but to the temporal evolution of the intravascular/extravascular ratio of volume within each acquisition voxel. Capillaries' response to activity displaces extravascular tissue, as they inflate like elastic balloons (hence the origin of the model's name), changing the local cerebral blood volume (CBV). In typical BOLD sequences, most of the signal change will be related to the venous fraction of the capillary bed, because there is where most of deoxyhemoglobin is (the arteriole fraction is normally saturated of oxygen). The effects of a CBV change become larger in higher magnetic fields, and have an important dependence with sequence settings such as Echo Time (TE) (Uludağ et al. 2009).

The impulse response defined by the model (BOLD signal triggered by a brief neuronal activity) incorporates three characteristic phases:

- a) An initial undershoot, when CMRO₂ has increased, but the vascular bed has not yet responded effectively. The timing of this phase is related to the arteriole's smooth musculature response to neural signaling and to their biomechanical elastic properties (Behzadi & Liu 2005).
- b) The increased BOLD signal period, related to the excessive compensation of CBF in response to increased CMRO₂, which leads to an effective decrease in the Oxygen Extraction Fraction (OEF), and therefore an increase in transverse MRI relaxation time.
- c) A trailing undershoot, which was originally attributed to slow biomechanical recovery of CBV. This effect has been proven to have significant spatial dependence (Yacoub et al. 2006). Contrarily, the undershoot has been also attributed to increased post-activation levels of CMRO₂ (Dechent et al. 2011), or to a CBF undershoot (Griffeth et al. 2011). The huge discrepancies found across serious studies suggest that this effect may be generated by multiple factors.

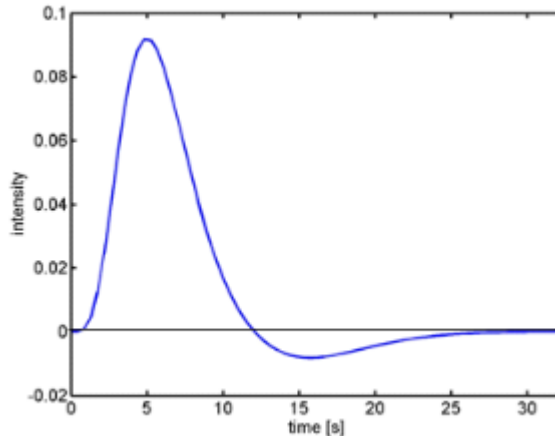


Figure 2 Hemodynamic response function

Impulse response of the hemodynamic response function, as implemented in SPM5 by default. This response function models the BOLD signal response to a “spike” (delta function) of neural activity. The convolution of the model of neural activation (typically matching the task or stimulus) with this impulse response will allow the generation of BOLD activation model to which the observed fMRI signal is tested against.

2.1.5 Functional magnetic resonance imaging sequences

Going back to the technical description of MRI initiated in section 2.1.1, we can summarize saying that magnetic resonance imaging is based in creating *in vivo* maps – images- of tissue’s NMR properties. A careful selection of the scanner’s pulse sequence settings will define the different weights given to T1, T2 and T2* properties in the MRI signal readings. This weighting defines the image contrast, which will allow the sought discrimination between different tissues or tissue states in the resulting MRI image.

Practical implementations of MRI imaging do not simply measure the signal decay immediately after the excitation pulse. This would lead to unfeasibly long acquisition times. Instead, it uses refocusing pulses generated with the radio frequency (RF) generator or with the magnetic gradient coils. The time between the excitation pulse and the recovered signal is called *echo time* (TE). The time between excitation pulses is called *repetition time* (TR). The specific combination of RF pulses and magnetic gradients is what we call the fMRI sequence, which highly defines the characteristics of the images collected.

Gradient-Recalled Echo Planar Imaging (GE-EPI) is by far the most used sequence to explore brain activity. GE-EPI quickly took over other early fast imaging sequences such as FLASH (Haase et al. 1986), GRASE (Oshio & Feinberg 1991) or PRESTO (Liu et al. 1993). However, these sequences are not completely abandoned and remain being found advantageous in singular experimental setups (van Gelderen et al. 2012; Zuo et al. 2013; Kemper et al. 2015).

Spin Echo EPI is likely to be the second most widely-used BOLD imaging technique. SE-EPI is known to give similar, but lower BOLD signals than GE-EPI at 1.5 Tesla (Bandettini et al. 1994). At 3 T scanning, these results are less obvious: They are replicated or indicating the opposite direction depending on the brain area (Naganawa et al. 2002). At 3 T, however, SE-EPI has been reported to suffer less susceptibility artifacts, which are a common concern at high fields. SE-EPI is also known to generate a signal more specifically driven by the oxygenation of the microvascular bed (weighting down large vessels), especially at high fields (Zhao et al. 2006). This makes SE-EPI still a preferable technique in certain experimental setups.

As it is described in the methods section of each individual study, all studies that compose this dissertation have been acquired using a single-shot gradient-recalled echoplanar imaging sequence (GE-EPI).

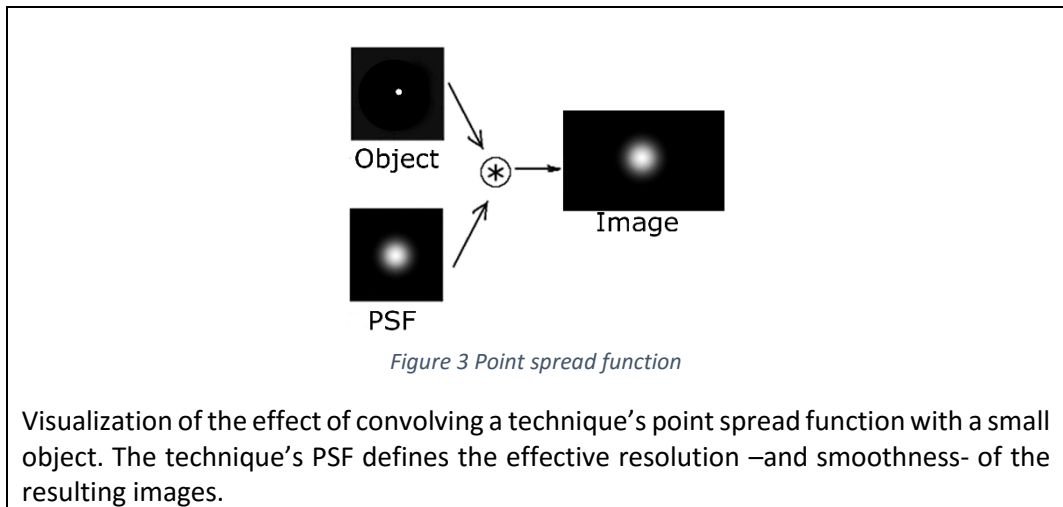
2.1.6 Technical characterization of common fMRI datasets.

A typical fMRI experiment on a subject generates a four-dimensional set of BOLD signal measurements, which can also be interpreted as a (true) 3-D video of BOLD activity within the field of view under exploration (typically covering the complete head).

Spatial resolution

In all imaging techniques, the spatial resolution obtained from the phenomenon under observation depends on two main elements: The sampling matrix (the spatial density of sampling points –voxels-) and the sharpness of the sensing technique, which is typically characterized by its *point spread function* (PSF).

The PSF is derived from the model of the filter that imaging technique applies onto the signal. Typically modelled by a Gaussian convolving kernel and measured by the full width at half maximum (FWHM) of its impulse response. For visualization purposes of this principle, see Figure 3: In it, we see the effect of a technique that has captured the image of a perfect dot. The PSF's FWHM would be the diameter of the resulting's blurb core, defining the core as the signal that exceeds 50% of the peak signal.



The effective spatial resolution of an imaging technique will be mainly driven by the worse of either the sampling spacing or the technique's PSF function. While the technique's PSF function is largely intrinsic to the imaging system and the sample under study, the sampling spacing (the acquisition matrix) is a decision made during the pulse sequence programming. In a methodological study, a 1.5 T scanner with a Gradient Echo sequence showed a PSF function of 3.5 mm FWHM when exploring small (column-like) areas in the visual cortex (Engel et al. 1997). This system can be considered highly equivalent to the techniques used in the works of this dissertation. Similar PSF characteristics have been reported in posterior works with 3 T scanners (Parkes et al. 2005), although a higher spatial resolution is known to be possible at high field fMRI (Logothetis 2008), compromising signal-to-noise ratio. Knowing the signal's smoothness allows selecting a sampling matrix that optimizes signal to noise ratio and radiofrequency energy absorption. Posteriorly, it supports the statistical-wise calculation of cluster-wise significance of the activations detected.

Temporal resolution

Thanks to multi-echo scanning techniques, an Echo Planar Imaging slice can be collected in less than 100 ms. Technically, a slice can be collected much faster, but losing SNR. The practical threshold of around 100 ms allows collecting a 20-24 slices volume in 2 seconds, which becomes the effective TR, or sampling rate of the volume. That is, the signal of each volume element is recorded once per TR. While the electric neural discharges behind neural processes occur in a time window a 100 times shorter than the mentioned TR, the neurovascular response associated to the BOLD signal has much slower dynamics (See section 2.1.4) and a TR between 2 and 3 seconds has become a standard practice in terms of tradeoff between SNR and temporal resolution. However, some experimental setups have successfully used TR rates as low as 100 ms (Feinberg & Yacoub 2012).

Noise content

Functional MRI datasets are affected by multiple known sources of noise. Knowing them allows developing more robust analysis methods. One of the most characteristic noises of fMRI datasets is the low-frequency drift. This noise has been observed since the early days of fMRI and it has been described to have a $1/f$ shape in its spectral power density (Aguirre et al. 1997). This noise source is frequently isolated using autoregressive models (Woolrich et al. 2001; Gautama & Van Hulle 2005) or other implementations of high-pass filters (Bullmore et al. 2001). Aguirre et al reported that this type of noise is observed in human acquisitions and in water phantoms. Therefore it is not attributed to physiologic sources. The relatively large energy of this noise source prevents the direct comparison of task activations across very distant time points as it prevents absolute readings of BOLD signal intensity. Note that most of fMRI techniques focus in signal *change* rather than in signal *level* due to this noise source.

Another source of noise is that of physiologic origin, but not related to the biologic process under observation. This is a form of self-interference of the subject on his/her own BOLD signal. Respiration motion and heart beat pulsations are known to introduce noise to the fMRI datasets that degrades the statistical significance of activation signals.

This type of noise has been isolated by measuring and incorporating the cardiac and respiratory phase as regressors in the statistical analysis (Glover et al. 2000). Cardiac rate, in addition to phase, has also been described as a source of noise, and therefore as a candidate regressor to reduce noise (Shmueli et al. 2007). However, physiologic fluctuations have also found to share variance with brain processes of interest, including resting state functional connectivity signals (Chang & Glover 2009). The fact that physiologic fluctuations are also being associated with cognitive (Bucks & Seljos 1994) or self-regulatory sympathetic and parasympathetic activity (Chang et al. 2013) calls for extreme caution before taking actions to remove them from an fMRI dataset (Bright & Murphy 2015).

Other, sources of noise include artifacts generated by movements of the head, eyeball (Zhang et al. 2011) or mouth (Kemeny et al. 2005). These artifacts have a spontaneous nature and should be minimized by experimental setup design and training of the subject. When in certain experiments or populations it is not possible to avoid these sources of noise, some specific artifact-removal algorithms may have to be used to prevent the unwanted effects of these noise sources (Diedrichsen & Shadmehr 2005).

Dataset size

The datasets used in this thesis are highly representative of the datasets used in a typical whole-brain neuroscience study. For example, the dataset used in study 1 consists of 270 volumes of 22 slices composed of a scan matrix of 64 x 64 pixels. Each pixel has a grayscale depth of 2 bytes.

Therefore, the effective information of one subject's exploration is:

$$size [Mb] = 270 \text{ volumes} \cdot \frac{22 \text{ slices}}{1 \text{ volume}} \cdot \frac{64 \times 64 \text{ pixel}}{1 \text{ slice}} \cdot \frac{2 \text{ byte}}{1 \text{ pixel}} \cdot \frac{1 \text{ kb}}{1024 \text{ byte}} \cdot \frac{1 \text{ Mb}}{1024 \text{ kb}} = 46.4 \text{ Mbyte}$$

Which provide the following amount of independent BOLD signal measurements per subject:

$$size [samples] = 270 \text{ volumes} \cdot \frac{22 \text{ slices}}{1 \text{ volume}} \cdot \frac{64 \times 64 \text{ pixel}}{1 \text{ slice}} = 24.33 \text{ million samples}$$

The size of this dataset makes some analysis challenging in terms of computational power, although it is common to conduct fMRI analysis on standard desktop computers. Note that the practical amount of information is increased by application-based add-ons like headers and redundancy information.

2.2 Overview of analysis methods of fMRI studies

The purpose of this section is to introduce the basics in terms of fMRI analysis. Details of the specific methods used in the presented studies are included in the corresponding sessions.

As presented in section 2.1, the BOLD signal is driven by a set of complex phenomena driven by the processes of the brain, which is in turn a complex system as well. As a result, the interpretation of BOLD-sensitive MRI sequences requires some awareness of statistic procedures and of neuroscience. The basics are presented below to make this document self-contained.

The first concept that needs to be taken into account when planning fMRI-based research is the fact that the fMRI BOLD signal is affected by noise sources related to unwanted thermal, physiologic or scanner-related effects. These unwanted effects can even exceed the effect size of the signal of interest ($SNR < 0$ dB) (Krüger & Glover 2001). This presence of noise often requires the usage of high order filtering –or statistical tests- to reach appropriate confidence levels (Murphy et al. 2007). The amount of signal time points needed for a particular study depends on the technique used and the expected effect size of the task, but few fMRI experiments use less than 50 time points due to the mentioned SNR limitations. This need to obtain a large number of representative samples will significantly condition experimental design: In some contexts such as phobic symptom induction or positive reward, repeatedly inducing the same effect on the subjects under study can be a challenge.

A second important concept to be taken into account is the complexity of the human mind: A myriad of processes are in concurrent execution in the human brain. All these processes are based on neuronal activity – and thus BOLD signal- which could be

considered as an interference. The experiment and analysis will be designed taking into account that the signal of interest will be mixed with a number of uncontrolled signal sources.

A large number of experimental design and analysis methods have been developed for neuroimaging studies. However, a basic split is proposed in this section. The intention of the proposed division is to provide the reader with the basic understanding of the techniques presented in this dissertation.

2.2.1 Analysis based on a model of the expected BOLD signal

Model-based analyses were the first models used in neuroimaging studies and are those that provide a more direct interpretation. In these studies, a hypothesis is made on the expected neuronal response to a given experimental condition. Then, statistical analyses are typically made with methods to compare the significance of the given model versus a null hypothesis. This analysis is analogous to the matched filter approach in signal processing.

It is important to note that these analyses basically answer to which point the signal behaves according to the model. Therefore, the sensitivity of these methods heavily relies on the ability to make valid predictions on the expected BOLD signal. This involves not only having a neuroscientific hypothesis on the neural activity triggered by a stimulus, but also dealing with a model of the hemodynamic response function that “translates” from neuronal activity to BOLD signal.

In this type of analysis, confound signals need to be modelled or to be cancelled by experimental design. As it has already been introduced, during our experiment, self-regulatory, sensorial, attention-related or cognitive processes are running in parallel. This generates brain activity and therefore confound BOLD signals.

A common way to cancel confound signals by experimental design consists on designing an experiment containing at least two conditions, and making these conditions to differ only in the process of interest. The assumption that confound signals are

stationary processes, and that therefore will have the same effect size in both conditions, allows comparing conditions to explore only the expression of the process of interest.

To illustrate the cancellation of confound signals, observe the following example: If we want to map the brain activity related to seeing an angry face, the first line of thought could be just presenting the angry face pictures and comparing it against epochs of a dark screen. In an experiment like this, a huge primary visual activation would be expected (seeing something versus not seeing it), along with the deactivation of an extensive cortical and limbic network related to cognitive load (placing the attention into something versus not doing so) these activations would be large, overlapping our activation of interest and not specifically tied to it (any complex visual stimulus would generate similar results). To obtain specific results, the control condition may be changed from a blank screen to neutral faces. That is, we would compare BOLD signal of looking angry faces versus looking at neutral faces. In this second case, as task and control conditions are highly matched in neurocognitive terms, the results obtained would show the specific effect of looking at angry faces. However, if this experiment is carried on SAD patients and with the intention of mapping the activity in the areas related to angry face processing, a neuroscience literature research may warn us that SAD patients are prone to interpret neutral faces as salient (like angry faces) (Cooney et al. 2006) or that SAD may encompass an impaired ability to discriminate between relevant and irrelevant social stimuli (Ahrens et al. 2015). Therefore our analysis would have suboptimal sensitivity. In this context, using happy faces as the control condition could be more appropriate (Phan et al. 2006).

The purpose of the example above is to show the important need of having robust *a priori* knowledge of the phenomenon under study when building the experimental design or model.

In some cases, the confound signals cannot be expected to behave as stationary processes across task and control conditions. This can be the case of heart rate or blood CO₂ levels. In these cases, these variables may be added to the analysis as nuisance regressors, provided that the transfer function (variable to BOLD) is known.

2.2.1.1 *The General Linear Model*

The most widespread approach for model-based analysis of fMRI data is through the general linear model (GLM). The GLM is an equation $Y=X\beta+\epsilon$ that expresses the observed variable Y in terms of a linear combination of beta-weighted explanatory variables X plus an error term (Friston et al. 1995). The term GLM is widely used across the neuroimaging world. However, in other scientific disciplines, the concept of GLM is also known as 'analysis of covariance' or 'multiple regression analysis'.

In GLM, the matrix X that contains the explanatory variables is called the *design matrix*. Each column of the design matrix corresponds to some effect the researcher has modelled, measured or included into the experiment. These columns are commonly referred to as regressors, explanatory variables or covariates. The relative contribution (β) of each of these columns (X) to the observed variable (Y) is assessed using standard least squares. Inferences about these contributions are typically made using T or F statistics, depending upon whether one is looking at a particular linear combination (*e.g.* a subtraction), or all of them together. Note that the Y variable can contain either direct measurements (such as an individual's BOLD signal readings) or the results already obtained in a GLM. In the context of this dissertation, these cases are referred to as *first level* and *second level* analysis, respectively.

From a conceptual point of view, a conventional analysis of an fMRI time series is conducted in a voxel by voxel basis. That is, the signal in each voxel is modelled as the Y of an independent GLM. However, this involves that a whole-brain study has an order of magnitude of 10^5 independent observations. Attempting to make a direct multiple comparisons censoring (Bonferroni's correction) to the inference in this context could make the analysis extremely insensitive. On the other hand, a formal indicator of significance is still needed.

The challenge described above stimulated the application of Gaussian Random Fields (GRF) theory to the interpretation of neuroimaging data (Chumbley & Friston 2009), leading to the concept of Statistical Parametric Mapping. Statistical Parametric Mapping (SPM) involves the construction of *spatially* extended null-hypothesis models to test

hypotheses about regionally specific effects (Friston et al. 1991). The interest of SPM largely relies on the simplicity of the idea. Voxels can be initially analyzed using any standard (univariate) statistical test. The resulting statistical parameters are then assembled into an image, which is also typically named a statistical parameter map (SPM). To calculate significance of the results contained in SPMs, these are interpreted as spatially extended statistical processes by referring to the probabilistic behavior of Gaussian fields (Worsley et al. 1992; K. Friston et al. 1994). Gaussian random fields model both the univariate probabilistic characteristics of a SPM and any non-stationary *spatial* covariance structure. 'Unlikely' excursions of the SPM are interpreted as regionally specific effects, attributable to the variables contained in the design matrix.

GRF is not the only approach to set appropriate significance thresholds to fMRI data. Monte Carlo permutations or cluster extent thresholding are also used. However GRF is the most widely adopted solution to support inference on SPM (Nichols 2012). In these cases, the GLM is used to estimate parameters that could explain the spatially continuous data in exactly the same way as in conventional analysis of discrete data. GRF theory is used afterwards to resolve the multiple comparison problem that arises when making inferences over a relatively large volume of the brain. Therefore, GRF theory provides a method for correcting p values for the search volume of a SPM and plays the same role for *continuous* data (*i.e.* images) as the Bonferroni correction for the number of discontinuous or *discrete* statistical tests.

It is important to note that most of the statistical tests conducted in neuroimaging can be explained taking as a basis the general linear model. This can include the comparison of 2 groups, an analysis of variance (ANOVA) or the calculation of the correlation coefficient between a signal and its model. Even the idiosyncratic psychophysiological interaction analysis presented in section 5.2.4.2 is based in a two-steps GLM. Mathematically, these analyses are fitted with identical equations and algorithms. The two parameters that distinguish analyses amongst them is the design matrix that defines the experimental design and the contrasts extracted to compare the fitting of different columns of X .

2.2.2 Model-free analysis.

As the title of the section announces, this section covers the description of analysis methods that do not rely on comparing the observed BOLD signal against a pre-defined model for it. Instead, these techniques characterize the signal properties with voxel-by-voxel descriptors or by the relationship of the signal across voxels.

These techniques may seem to have an exploratory nature. However, the measurements of these techniques can still be compared across subjects or states of the same subject. Therefore, model-free analysis are also valid to test n-sample or parametric hypothesis.

While model-free analysis of fMRI data can be done on sequences in which the subject is executing a task, a particular interest has been raised by experiments that observe the spontaneous neural-driven fluctuations of the BOLD signal while the subject is at rest (Snyder & Raichle 2012). The term resting-state fMRI (rs-fMRI) is now widely used in the world of neuroscience.

One of the strong points of rs-fMRI experiments is that they do not require the subject to understand and execute a task nor a control condition. This can be a great benefit in the context of psychiatry or animal research, where compliance to complex tasks cannot always be assumed. Resting state fMRI results have been shown sensitive to certain psychiatric conditions, although inconsistent results have also been reported (Fornito & Bullmore 2010). In their comprehensive review, Fornito and Bullmore provided a thorough classification of the techniques used in the psychiatric context. This classification has been used as the basis for the literature search presented in Table 1. This breakdown of the usage of model-free techniques in fMRI research has been done with PubMed searches in the title or abstract of peer-reviewed journals using the keywords indicated. The results indicate that ICA and seed-based correlation analysis are the most used model-free analysis techniques, followed by graph theory analyses.

| Method | PubMed search terms: (fMRI OR "functional MRI" OR "functional magnetic resonance imaging") and | Quantity of articles [2005-2015] |
|--|---|-------------------------------------|
| Independent Component Analysis | ICA OR "independent component analysis" | 1076 |
| Seed-based correlation | Seed | 710 |
| Graph analysis | Graph | 496 |
| Spectral power | "spectral analysis" or "spectrum analysis" or fALFF or ALFF | 253 |
| Regional homogeneity (ReHo) | "Regional homogeneity" OR ReHo | 223 |
| Granger causality, multivariate autoregressive methods | Granger OR multivariate autoregressive | 89 |
| Hurst and Holder exponents | Hurst OR Holder OR fractal | 51 |
| Network homogeneity | "Network homogeneity" | 5 |
| Resting-state Activity Index | "Activity Index" RSAI | 2 |

Table 1 Publications with model free analysis methods

Quantitative results of a literature search made in August 2015 using model-free fMRI analysis methods as key words in Pubmed.

The basic concepts behind seed connectivity and independent component analysis are described below, as they are the two model-free techniques used in the works that compose this dissertation.

2.2.2.1 Seed-based functional connectivity mapping

The concept of functional connectivity was observed and described soon after the development of BOLD fMRI sequences (Biswal et al. 1995). This term refers to the measurement of synchronization between oscillations of brain activity measurements (BOLD signal in this case) in different brain areas. Although many studies use pairwise correlation coefficients as a measurement of functional connectivity, the broader statistical term *dependence* may be more appropriate to describe what it is explored in such analyses. Functional connectivity differs from anatomical connectivity by the fact that it doesn't identify regions that necessarily have more dense axonal connections, but regions in which activity is statistically dependent, suggesting they form a functional brain network which may be related by direct or complex physical connection paths (Deco et al. 2013).

Seed-based functional connectivity maps refer to a map of the cross-correlation coefficient of the time course in each of the volume's voxels against the signal of one of them (the seed). In some cases, instead of a seed voxel, the average signal of a small

volume of interest is used. This provides higher robustness to noise. Therefore, seed-based functional connectivity maps highlight the brain areas functionally connected to the seed region.

Despite seed-based functional connectivity analysis are frequently obtained from resting state data, functional connectivity studies in the context of a task are becoming common and provide new optics to classic experiments (Lee et al. 2013).

Seed-based connectivity analyses require the selection of a seed amongst thousands of voxels. Consequently these studies are frequently used with narrow hypothesis or in post-hoc analysis, rather than in exploratory approaches.

2.2.2.2 Independent component analysis

Independent component analysis (ICA) is a data-driven statistical method that is able to decompose high-dimensionality data into discrete signal and noise covariance components (Comon 1994; Bell & Sejnowski 1995). In a more general context, it belongs to the group called Blind Source Separation techniques. ICA has successfully been applied in fMRI data to identify temporal signals (McKeown 1998) and anatomical networks that define functional connectivity (Calhoun & Adali 2006).

Typically, ICA assumes a generative model in which observations are linear mixtures of independent non-Gaussian sources. That is, in the context of fMRI, that the signal in each location is influenced by an overlapping set of spatial networks that oscillate with an independent intrinsic signal –or components, in ICA jargon-. The central limit theorem tells us that the mixture of independent random variables tends towards a Gaussian distribution, under certain assumptions. Thus, the sum of two independent random variables is expected to have a distribution that resembles more a Gaussian distribution than any of the two original random variables, provided none of them originally has a Gaussian distribution. This explains why the algorithm will provide consistent results only if at most one of the true sources is Gaussian. The Gaussianity measurement method is one of the parameters that shape the performance of an ICA implementation. Kurtosis

and negentropy Gaussianity estimators are common choices. See (Hyvärinen & Oja 2000) for details in the different implementations of ICA algorithms.

ICA will therefore use high order statistics to split the dataset into a number of independent sources with the same dimensionality as an observation of the original dataset. It is important to highlight that, while PCA splits the data by minimizing correlation, ICA uses higher order statistics, aiming to achieve maximal statistical *independence* among components. ICA is, therefore, an appealing method to solve the classical cocktail party problem (Haykin & Chen 2005), which sets an scenario with multiple people talking at the same time, with independent speeches that need to be unmixed.

In our context it is relevant to note that in the typical cocktail party problem the situation is having long recordings in a few locations. In the typical fMRI dataset we will have a much larger amount of locations than the limited number of time points where we collected data. The transposition of the fMRI data matrix (with dimensions defined as “number of time samples” x “number of voxels”) will make the dataset highly equivalent to the cocktail party dataset mentioned before. However, the interpretation of the results requires taking into account that this has happened: We are obtaining spatial locations maximally independent amongst them, rather than time courses maximally independent themselves. The emphasis on this matter has caused that, in the fMRI context, this common practice makes the analysis being often called *spatial ICA* (sICA) (Calhoun et al. 2001b). From the signal processing perspective, this has little effect and all the ICA literature and algorithms are equally applicable to spatial or temporal ICA of fMRI data.

In the formal description of an ICA, the signal of an individual’s fMRI time series is modelled by $X=AS$. Where X is a matrix containing the BOLD signal readings of the complete exploration, arranged in M rows and N columns. In the sICA arrangement, M is the number of time points and N the number of voxels in the field of view. $A_{M \times n}$ and $S_{n \times N}$ are initially unknown and named as the mixing matrix (A) of n spatial components contained by S . In sICA, the matrix A is often referred to as the set of characteristic time courses of the M spatial maps contained by the matrix S .

The outcome of an ICA algorithm is the estimation of an unmixing matrix $W_{n \times M}$ such that y is a good approximation to the true sources s . Therefore, $y = Wx = W \cdot A \cdot s$. In some contexts, W will be simply referred to as the pseudoinverse of A (\hat{A}^{-1}). The algorithm will iterate attempting to obtain a maximally independent set of components in y .

Infomax (Bell & Sejnowski 1995), -a contraction of *information maximization*- is the algorithm most commonly used to optimize the independence of the components of the unmixing matrix W . Infomax is based on the principle of numerically maximizing the absolute value of the entropy of the above auxiliary signal y . Entropy of a discrete signal, as defined by Shannon is:

$$H(y) = - \sum_k p_k(y) \log(p_k(y))$$

Where $p_k(y)$ refers to the probability of y taking the discrete value k . This can be done iteratively by minimizing the mutual information across pairs of components, which is defined as:

$$I(x; y) = H(x) - H(x|y)$$

Where $H(x|y)$ is the conditional entropy. That is, the entropy of x conditional to y taking a particular value y_i .

Similar algorithms such as fastICA and JADE have also been applied to fMRI data. Comparisons amongst them have showed that consistent and reliable results can be obtained with the three mentioned algorithms (Correa et al. 2007) despite minor performance differences have been described between them (Calhoun & Adali 2006). In these comparisons, Infomax has been shown to perform better in super Gaussian datasets, which is a common situation when estimating independent fMRI sources from the spatial perspective, but not the temporal ones (Correa et al. 2007). This limitation has been known since the early days of Infomax (Lee et al. 1999) so some sophisticated proposals analyze the component's Gaussianity to select the algorithm depending on the dataset's properties (Choi et al. 2000).

The application of ICA to groups of subjects is not straightforward because of potentially having a different mixing matrix for each subject (Calhoun et al. 2001a). This is typically addressed by a concatenation of the spatially-normalized BOLD images, prior to the source separation, followed by a segmentation after the split. The dataset generated by the concatenation may be very large (see section 2.1.6 for an order of magnitude analysis). Therefore, due to computational power constraints, the group dataset often needs to be reduced. This is done with lossy signal compression techniques such as Pareto-decimated Principal Component Analysis (PCA). The amount of sources to be extracted is also numerically determined during the analysis employing minimum description length (Rissanen 1983) or Akaike's information criterion (Akaike 1974).

Group ICA methods have received increasing attention in the analysis of fMRI studies for their robust and flexible modeling nature (Calhoun & Adali 2012). In addition to providing a data-driven characterization of fMRI studies, ICA results can also provide an estimate of functional connectivity in such studies. In the case of Group ICA, "functionally connected" networks of voxels or regions are defined spatially by their signal as a system, which is estimated in the higher-order statistical sense. Calhoun et al. showed that, after reconstruction, ICA results using this group approach are similar to those performed for each individual subject. This indicates that group ICA technique is robust to cross-subject variability (Calhoun et al. 2001a).

3 Introduction to the application's state of the art: Psychiatry research from a neuroimaging perspective

The etymology of the term *psychiatry* refers to healing the mind (or in some strict interpretations, the *soul*). Some historic views of the mind-body duality used somehow ethereal concepts to describe the mind's nature. However, today's neuroscientific community shares a clear vision of the mind being a functional manifestation of a complex nervous system. Consequently, in this dissertation a strict physicalism-driven perspective will be kept, without forgetting the extraordinary complexity of the system we are exploring.

Therefore, in our perspective, pathologies of the mind are potentially related to alterations in its biophysical substrate, which may actuate as pathology drivers or just as risk factors. Unfortunately, the anatomical, biochemical and electrical complexity of the brain, along with the limitations of the imaging techniques, makes many of the possible alterations virtually impossible to measure with today's equipment. Instead, today's neuroimaging can still only offer just macroscopic or indirect measurements.

For two centuries, psychiatry has evolved without the support of neuroimaging tools. Disease definitions, patient classifications and treatments have been developed based on behavioral observations of patients and healthy controls. During the last four decades, neuroscientists have worked to explain the biophysical principles behind psychiatric diseases and treatments. This has brought an explosion of knowledge on the brain, which entails many exciting opportunities for psychiatry (Linden 2012). However, it is also openly recognized that still there is a long way to go.

3.1 Contributions of neuroimaging to the clinical practice of psychiatry

While the understanding of the mind-body duet has made a leap forward thanks to fMRI, functional magnetic resonance imaging is still seldom used in the clinical practice of psychiatry (Rosen & Savoy 2012). This can be illustrated by the lack of apparition of fMRI as a diagnostic technique in the latest edition of the Diagnostic and Statistical

Manual of Mental Disorders DSM-5 (APA 2013). In the clinical day to day, neuroimaging is mainly devoted to simply exploring the encephalic tissue integrity.

After decades of formal neuroscience research, which included the “decade of the brain”, there seems to be a general consensus that not a single psychiatric disorder can be explained by a simple biological mechanism (Paulus & Stein 2007). Multiple biological alterations have been solidly associated to psychiatric disorders. However, the human mind manifests the dynamic (Gazzaniga 2011) complexity of its host: A self-adapting network of roughly 100 billion neurons (Azevedo et al. 2009), 160 trillion synapses (Tang et al. 2001) and over 500 million years of evolution (Shu et al. 1999). This amazing organ is, still today, just partially understood. As a consequence, the mind and its malfunctions are just partially understood as well.

Another limitation of the contribution of neuroimaging to psychiatry is that the current definition of psychiatric disorders is mainly based on symptom observation on a phenomenological level. Neuroimaging provides data much more related to biological measurements. Different biological expressions (or a combination of them) can converge to the same set of symptoms. This involves that a single psychiatric definition can be mapped with different imaging alterations. Being the psychiatric practices the gold standard, these differences can be initially interpreted as inconsistent results from the neuroimaging community.

3.2 Potential contributions of neuroimaging in psychiatric drug discovery: biomarkers and surrogate markers

As introduced in section 3.1, the usage of fMRI in the clinical practice of psychiatry is modest. Consequently, its usage in clinical trials to assess the state of patients is still uncommon. However, since its earliest days, fMRI has been regarded as a tool with high potential to develop biomarkers to support drug discovery (Borsook et al. 2006).

It is important to highlight that, in the context of drug discovery, a biomarker is defined as a laboratory measurement that reflects the activity of a disease process (Katz 2004). When a biomarker is fully validated as a direct measure on how the patient feels, functions or survives and is expected to predict the effect of the therapy, it may start

being used in clinical trials as a surrogate markers (Temple 1999). That is, only some biomarkers can become surrogate markers in clinical trials.

In order to be validated as a surrogate marker, a biomarker is expected to meet all the following requirements (Paulus & Stein 2007):

- A consistent response across studies and drugs
- A clear response of the biomarker to therapeutic doses
- A dose-response relationship
- A plausible relationship between the biomarker and pharmacology or pathogenesis.

An increasing amount of studies are showing the capacity of fMRI to feed biomarkers for early clinical research in psychiatry. Promising fMRI-based studies have showed the effects of pharmacological treatments on disease-relevant brain circuitry of depression (Fu et al. 2013), anxiety disorders (Nitschke et al. 2009), schizophrenia (Snitz et al. 2005) and addictions (Myrick et al. 2008; Goudriaan et al. 2013). These results keep the expectations high on the opportunities that fMRI has to support drug discovery through the development of surrogate markers (Nathan et al. 2014). However, further studies are still clearly needed to fully demonstrate the validity and reliability of fMRI to predict the outcome of pharmacologic treatments.

From a regulatory perspective, the influential Food and Drug (FDA) administration of the USA makes an explicit acceptance of clinical trials based on surrogate markers that are “reasonably likely” to predict clinical benefit (FDA 2015). The usage of this path is frequent: In the period of 2005-2012, 91 of out the 206 newly approved indications were based on surrogate endpoints (Downing et al. 2014).

The convenience of using biomarkers or surrogate markers is widely recognized in the early phases of drug development (Frank & Hargreaves 2003). However, the usage of surrogate endpoints in pivotal phase III studies has been overtly questioned (Fleming 1996) and clinical trials based on them not always remain trouble-free (Sacks et al. 2014).

3.2.1 The phases of clinical trials

In our context, clinical trials are experiments done on human participants to determine safety and efficacy of new treatments. These experiments are tightly regulated by laws and cannot be conducted without approval of medical and ethical committees representing the authorities. These committees will assess risk/benefit of conducting the experiment along with legal and ethical compliance. Ethical compliance will require, amongst others, that the experiment generates scientific validity and reproducibility of the results. The need for clinical trials has developed a large industry especially visible in the shape of Contract Research Organizations (CRO) and Clinical Research Facilities (CRF), which operate guaranteeing strict observance of the ethical principles set by the declaration of Helsinki.

The context of clinical research has, to some extent, developed its own language (NIH 2015). Clinical trials are divided in phases that have barely changed in the last 50 years. Only seen a recent addition of a “phase 0” has been seen in a limited amount of studies. See below the common naming and description of the main phases of the drug development process.

3.2.1.1 *Phase I*

The main purpose of Phase I is to assess drug safety, pharmacokinetics and pharmacodynamics. The molecules under study may have been synthesized or isolated from nature. Extensive studies in animal models are often required prior gaining approval to initiate Phase I of a clinical trial.

Typically, this phase involves testing the drug on small groups of healthy volunteers for dose ranging. At this stage, dose may still be subtherapeutic. In these trials, a single or multiple doses are administered to the volunteers in a controlled environment. Subjects participating in the trial are exhaustively monitored during multiple drug half-lives to describe the drug effects and to detect any possible side effects. In most of cases, Phase I encompasses the “first time in humans” step of clinical trials (see section 3.2.1.5 for exceptions).

3.2.1.2 Phase II

The purpose of this phase is to test drug safety and efficacy or effectiveness in a small group of patients. When testing for efficacy, the question to answer is whether the drug is able to improve the patient's condition. When testing for effectiveness, the question to answer is whether the patients will improve when following the standard clinical practice (patient compliance comes into the equation). Still, in this case, the experiment is driven in the clinical research context (not by personal physicians)

3.2.1.3 Phase III

The purpose of phase III is to test the effectiveness of a treatment in the context of clinical practice. This involves administering the drug in a large sample of patients through the conventional clinical practice. In some cases, multiple phase III studies are conducted before the drug launch. Local agencies may require a phase III study to be conducted in their region prior granting approval for drug launch. A large amount of workforce is needed to monitor the trials. This workforce is typically provided by a Contract Research Organization (CRO).

3.2.1.4 Phase IV

Typical phase IV studies are based in post-launch surveillance. This phase is intended to detect rare effects or effects related to the patient context (for example due to comorbidity or interaction with other drugs). In this phase, a large amount of data needs to be collected and analyzed. Depending on the results, the drug may be withdrawn from the market or restricted to certain uses.

3.2.1.5 Exploratory "Investigational New Drug" studies or "Phase 0" studies

The decay of the last two decades in R&D productivity of the global pharmacological industry raised concerns on the sustainability of the tight regulatory scheme of clinical trials (Merlo Pich 2011). The tight waterfall model of phase I to Phase IV has proven very effective to maintain patient's safety. However, its early phases have proven a low effectivity in discarding molecules that will fail in posterior phases (Kola & Landis 2004).

In a modernization attempt, the US food and drug administration (FDA) and the European Medicines Agency (EMA) have generated procedures to allow an earlier human exposition to novel drugs with the purpose of better predicting drug efficacy. While there still is a strict surveillance for the safety of the subjects that participate in clinical trials, the new schemes may grant authorization for early (pre-phase I) exposure of the subjects to small doses of the drug. These procedures were named “exploratory Investigational New Drug (IND)” by the FDA and “Phase 0” by the EMA. These experiment may be done in healthy volunteers or, rarely, even in patients. The purpose of these new phases is not identifying therapeutic effect, but to obtain early indicators such as pharmacokinetics, pharmacodynamics or the effect on selected biomarkers. The formal definition of phase 0 clinical trials raised controversy (The Lancet editors 2009). But soon provided proof of effectiveness to accelerate drug development in certain cases (Kummar et al. 2009)

Microdosing in humans before a formal phase 1 study is not completely new and had been proposed earlier to accelerate clinical trials and to validate animal models (Lappin & Garner 2003). However, when the US FDA published guidelines for exploratory IND studies, this boosted the interest for these practices and for the development and validation of biomarkers and surrogate markers that could assist in these studies (Collins 2005).

3.2.2 Potential contribution of fMRI biomarkers to drug discovery success rate enhancement

The need to increase productivity of clinical trials is not just a simple business interest: Due to the increasing regulatory pressure and the complexity of new drugs, the costs related to drug validation (through clinical trials) have surged over the last decades. If we take into account the means needed to conduct clinical trials and the success rate of these trials, the current average R&D costs for bringing a neurological drug from phase I to the market (a successful phase III) are in the region of 1000 million USD (Adams & Van Vu 2010). This is still excluding basic science, *in vitro* or animal drug discovery costs.

One billion USD per new drug launch is a huge cost even for the top pharmaceutical companies. In order to contextualize, see in Table 2 the key company size

indicators of the world’s top 6 pharmaceutical industries at July 2015. As a rule of thumb, we can see that launching a new drug can require between the 5% and 10% of the yearly’s EBIT of the world’s largest pharmaceutical companies.

| Company | Market capitalization ·10⁹\$ | Revenue ·10⁹\$ | EBITDA ·10⁹\$ |
|-----------------------|--|--------------------------------------|-------------------------------------|
| Pfizer (PFE) | 212 | 49,1 | 20,3 |
| Novartis (NVS) | 250 | 52,8 | 16,4 |
| Sanofi (SNY) | 135 | 38,8 | 11,8 |
| Roche (RHHBY) | 248 | 52,6 | 13,02 |
| Merck (MRK) | 164 | 41,4 | 14,7 |
| GlaxoSmithKline (GSK) | 103 | 35,4 | 9,79 |

Table 2 Key economic statistics of top drug companies

Market capitalization annual revenue and EBITDA was based on avg values of the 2014 exercise. Data extracted 12/7/2015 from CapitalIQ (www.capitaliq.com).

A large fraction of the drug development cost is driven by the high failure rate of new drugs in late phases, which can be over a 90% in central nervous system drug trials (Kola & Landis 2004). Duration of clinical trials also worsens the financial concern: It takes over 8 years in average to move from phase I to Phase IV (Kaitin 2010). Despite unprecedented investment in drug discovery over the last years, the amount of new drugs approved by the US Food and Drug administration hasn’t changed drastically in decades (Munos 2009). Patients also pay a toll, as every failure in phase III involves that a cohort of patients have been exposed to a non-suitable treatment.

As introduced in section 3.2.1.5, the huge drug development costs, together with its worsening trend, has opened debates questioning the tight “waterfall model” of clinical trials. In phase 0 studies (or investigational IND studies) biomarkers make possible an early assessment of drug effectiveness before the trial progresses to posterior phases (Trist & Bye 2014).

Functional magnetic resonance imaging has been proposed as a screening stage for early assessment of effectivity of new psychoactive drugs (Wise & Preston 2010). Some fMRI-based biomarkers have proven helpful to pre-assess treatments for psychiatric diseases such as schizophrenia (Minzenberg & Carter 2007), although further technical

improvements are still obviously needed (Iannetti & Wise 2007). Once these biomarkers are validated enough, they may be considered suitable to be used in early stages of clinical trials to prune molecules with less likelihood of success. This would be done before phase II or even before phase I, in micro dosing studies. Early pruning of non-successful drugs can avoid substantial clinical trial costs and unnecessary exposure of volunteers to suboptimal treatments.

Another practice that is becoming more common in clinical research is the usage of adaptive and *Bayesian* experimental designs (Orloff et al. 2009). This line of action involves continuous processing of the clinical trial data, and distributing the decision making throughout the duration of the clinical trial. This is opposed to phase-end decision points of the classical model. These decisions can be used to adjust cohort size or dosing. Decision making can even include the continuity of the study. The decision making can be based on parameters such as PK/PD, symptom severity or in novel biomarkers.

Besides clinical trials, another area of pharmacology that can benefit from the advancement of biomarkers are the treatments called “personalized medicines”. This is a growing approach based on delivering customized treatments, highly adapted to the patient (Costa e Silva 2013). This approach eagerly requires novel techniques to predict and to measure treatment response (ESR 2015). Technically speaking, personalized medicine has something in common with clinical trials: The need to assess or predict drug effectivity as early as possible.

3.3 The Social Anxiety Disorder

The understanding of the social anxiety disorder has evolved from the concept of it being a heightened shyness to a more complex set of symptoms tied to behavioral and neurobiological alterations (Stein & Stein 2008). It is important to highlight that shyness is a normal personality trait and therefore is not regarded as pathological. However, today, social anxiety disorder is widely recognized as a high-prevalence mental disorder, with high impairment of the patient's quality of life and significant costs to our society (François et al. 2010).

From an evolutionary perspective, social anxiety is hypothesized to act as a mechanism to detect and react in front of potential attacks of dominant group members (Trower & Gilbert 1989). Therefore, it may have played a vital role in the evolution of social groups as it avoids unnecessary challenge to the dominant group members and keep submissive individuals in the safety of the group. Today this function is still highly valuable and generally supports the acquisition and execution of social skills (Gilbert 2001). However, when a heightened social anxiety impairs significantly the individual's ability to carry on with a normal life, the individual may be diagnosed of a social anxiety disorder.

3.3.1 SAD in the domestic context

Individuals with SAD fear the scrutiny of others and are highly concerned by the possibility of saying or doing something that could result in embarrassment or humiliation. These concerns can be so intense that the individual avoids interpersonal encounters, or just go through them with high discomfort (Stein & Stein 2008).

SAD is a chronic disease (Reich et al. 1994) and one of the most prevalent mental disorders, with estimates of lifetime as high as 12.1% in general population of the US (Ruscio et al. 2008), although other surveys reported lifetime prevalence estimations down to 5.0% (Grant et al. 2005). Similar results have been reported in other western countries, while studies in eastern cultures report much lower prevalence, presumably due to culture-driven differences in the interpretation of the disease (Iancu et al. 2006).

Certain collectives, such as musicians, show a higher awareness on social phobia, as it is highly correlated with performance anxiety (Cox & Kenardy 1993). Musicians have also been reported to develop particular coping strategies (Fehm & Schmidt 2006).

SAD significantly impairs quality of life (Mendlowicz & Stein 2000). In a European survey, it was identified as one of the top ten diseases in terms of lost work days (Alonso et al. 2004). Associated costs are also substantial (Stuhldreher et al. 2014). SAD is associated with high comorbidity (Schneier et al. 1992), specially with depression (Stein & Kean 2000) and presents a high risk of substance abuse (Sareen et al. 2006).

3.3.2 SAD in the clinical context

Three decades ago, social phobia was reported as “a neglected anxiety disorder” (Liebowitz et al. 1985). However, over the last years it has become widely studied and recognized with the more modern “social anxiety disorder”. Today, Social phobia (or social anxiety disorder) is a well-described condition with a single diagnostic category in general (WHO 1992) and psychiatry-specific diagnostic manuals (APA 2000). In order to support diagnose, today’s clinicians can benefit from using tools like the Brief Social Phobia Scale (Davidson et al. 1991; Davidson et al. 1997) or the Liebowitz Social Anxiety Scale (LSAS) (Liebowitz 1987), being this later a widespread well-validated symptom-based questionnaire (Heimberg et al. 1999).

Despite of SAD being highly impairing, it is often difficult to detect and diagnose. It has been observed that SAD patients often do not seek treatment unless they need medical help for any of the comorbidities (Lipsitz & Schneier 2000; Fehm et al. 2005). Even during treatment, due to their condition, patients may avoid sharing information about their symptoms for fear of being negatively evaluated.

According to a public health treatment guide of UK (NICE 2013), Patients diagnosed with Social Anxiety Disorder may be first offered cognitive behavioral therapy (CBT). CBT based on the Clark and Wells (Clark et al. 2003) or the Heimberg models (Heimberg 2002) are specifically developed to treat SAD and therefore became the primary choices. For individuals that do not accept CBT or do not respond adequately to

it, a pharmacological treatment may be offered. Selective Serotonin Reuptake Inhibitors (SSRI) such as escitalopram or sertraline are typical first choices for treatment. Patients not responding to the first SSRI treatment may be offered an alternative SSRI (fluvoxamine or paroxetine) or an alternative class of anxiolytic drugs, including serotonin noradrenaline reuptake inhibitors (SNRI) such as venlafaxine (Stein et al. 2004; Liebowitz et al. 2005), reversible inhibitors of monoamine oxidase (RIMA) such as moclobemide (D. J. Stein et al. 2002) or, still, a non-selective irreversible monoamine oxidase inhibitor (MAOI) such as phenelzine (Blanco et al. 2003; Canton et al. 2012). It is important to note that, like in most psychiatric treatments, there are relevant regional differences on the approved or preferred treatments for SAD. For example, in USA, the FDA-approved prescription drugs for SAD are limited to paroxetine, sertraline, extended-release venlafaxine and extended-release fluvoxamine (Schneier 2011). However, off-label drug usage (Wittich et al. 2012) and comorbidity (Ruscio et al. 2008) open the practical span of medication that SAD patients receive. Benzodiazepines such as clonazepam or alprazolam have been historically widely used to treat anxiety symptoms. However, its usage is today is diminished due to its fast-building dose tolerance and side effects (Brown et al. 2015). Its fast effectivity still keep them as a valid option for acute episodes (Benítez et al. 2008; Schneier 2011).

3.3.3 SAD in the clinical research context

Conducting research with SAD patients requires understanding the condition's nature and adapting the clinical setting to the requirements of the cohort. The recommendations on the interactions with the individuals do not differ much from these given to clinical practitioners. An example of these can be found in the guide published by the British Psychological Society and The Royal College of Psychiatrists (NICE 2013) and include:

Improving access to services: Provide clear information on where to go on arrival and where to wait. Provide a private space for waiting and inform upfront on the location of toilets or clinical personnel in the facilities. Provide the opportunity to fill forms or eat

in private. Minimize the distress of interacting with different professionals. Develop and maintain an accompanying liaison throughout the trial.

Adapting communication style: When working with a person with social anxiety disorder, researchers must bear in mind that the individual may be vulnerable to stigma and embarrassment. It is common that SAD patients avoid interaction with researchers to disclose information about them, to ask questions or to complain. Therefore, it is important that researchers actively encourage patients to communicate in the way they feel most comfortable (including writing) and to raise any questions or concerns they have. Attention to this aspect should be maintained throughout the complete clinical trial.

Recruitment of SAD patients for a clinical trial arises a very unique situation. Conventional advertising in media asking for volunteers involves that the patients would have to take the initiative to contact the clinical research team. This step can be very difficult for the SAD population. Cooperation with healthcare providers, which can introduce the clinical trial to the patients and offer to initiate contact would be a preferred recruitment procedure.

4 Hypothesis and specific objectives of this dissertation

4.1 Hypothesis

This dissertation aims to demonstrate that fMRI is a tool applicable to the development of valuable biomarkers for the characterization of treatment response in clinical research of Social Anxiety Disorder. The building blocks needed to validate this hypothesis were broken down as objectives for the five studies embedded in this dissertation, which are presented in the section below.

The applicability of the technique will be determined by its capacity to provide sensitive and reproducible measurements with a scientifically proven relationship to pharmacology or pathogenesis.

4.2 Objectives

The initial literature review revealed that emotional face processing paradigms had already been proposed as candidate biomarkers for pharmacologic treatment in anxiety disorders (Paulus et al. 2005). Therefore, the first set of objectives was set in the replication and pilot of such methods in our specific imaging setup (Study 1). An exploratory connectivity-based analysis was added to the study as recent findings pointed that connectivity could be a valuable contribution in our context. Given these positive results, we proceeded to further explore connectivity-based analysis, this case using Independent Component Analysis. This involved setting as objectives the validation that results obtained through this technique were reproducible across paradigms (Study 2) and that the results were sensitive enough to detect subtle changes in the subject's emotional state (Study 3). It was perceived necessary to compare any connectivity findings with a symptom-provoking task. This set the objectives to define and validate the experimental setup of study 4. A pilot clinical trial is presented in study 5 using the literature-reviewed task of study 1, the ICA technique validated in studies 2 and 3 and the novel symptom provoking task of study 4. These 3 paradigms were executed on the same trial, exploring coincidences, power and specificities of their results. Figure 4 shows a graphic representation of the flow of these objectives.

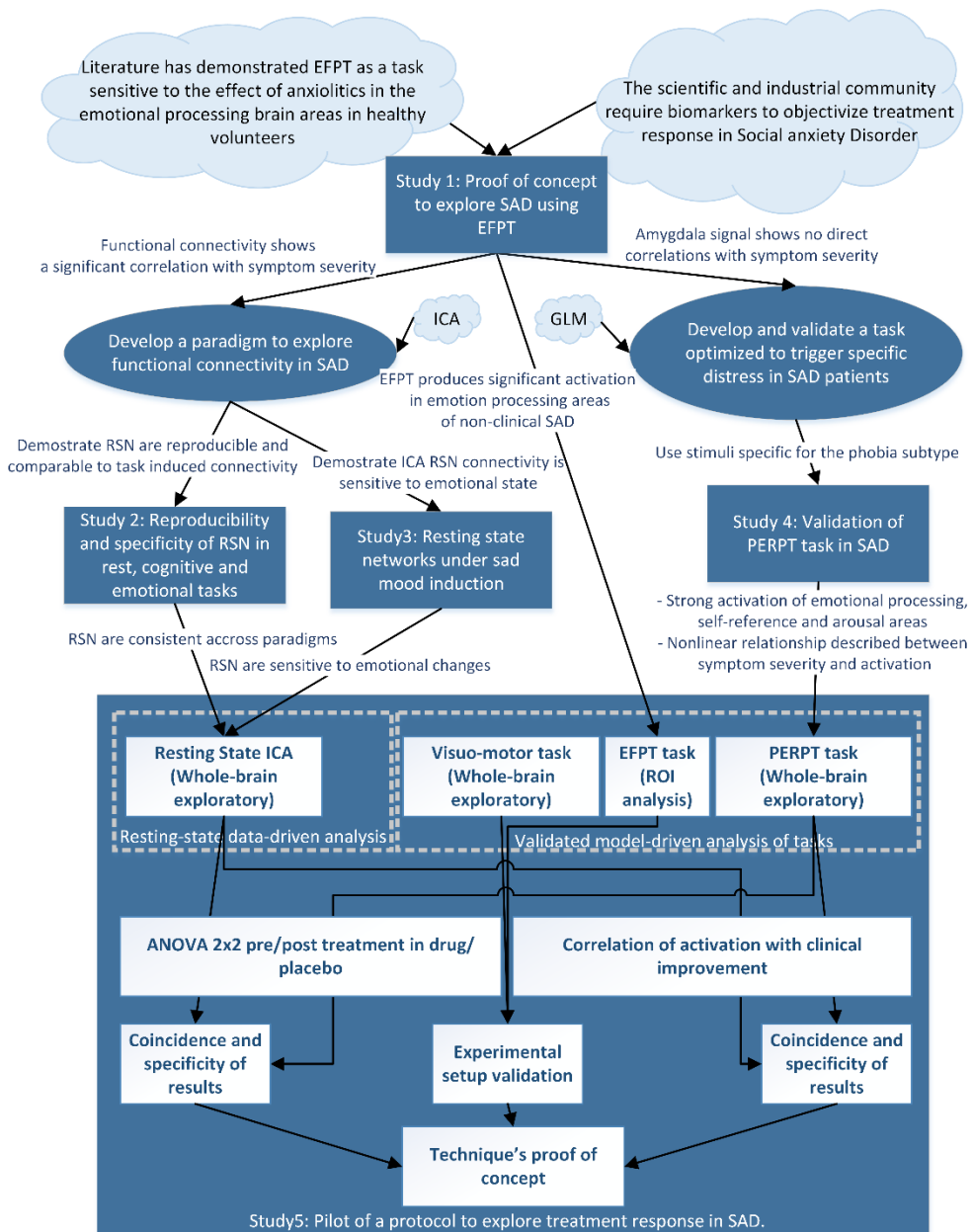


Figure 4 Thesis outline

The following sub-objectives were specifically defined for each of the mentioned studies:

4.2.1 Study 1: Replication of the state of the art and pilot of novel connectivity-based biomarkers.

- 1) To develop and validate an imaging setup and analysis methods able to replicate the findings of previous studies in terms of brain activations induced by the emotional face processing task.
- 2) To determine if there is a significant relationship between task-induced activation and the social phobia scores.
- 3) To describe the interaction between the fusiform gyrus and amygdala, including its relationship with social phobia scores.

4.2.2 Study 2: Reproducibility of ICA results

- 1) To implement and validate an Independent component analysis pipeline able to obtain indicators of functional connectivity within resting state networks, from the BOLD images obtained in our system.
- 2) To validate that, with our methods, the extraction of a particular network is reproducible despite the images being acquired while the subjects are executing a cognitive-demanding task, a self-referential exercise or no particular task (rest).

4.2.3 Study 3: Sensitivity of ICA results

- 1) To validate that Independent Component Analysis of fMRI data is able to detect brain connectivity changes related to emotional states.
- 2) To validate that the changes detected are not related to coupling of the network with physiological noise sources, which have a spectral power density different than the spontaneous brain activity oscillations that drive network connectivity.
- 3) To validate that the networks obtained are directionally reproducible with the “golden standard” seed-based functional connectivity estimator.

4.2.4 Study 4: Pilot of a novel symptom-provoking task as a new potential biomarker.

- 1) To develop and pilot a customized SAD symptom-provoking experimental condition able to drive robust activations in the emotional and arousal brain networks.
- 2) To characterize the differential response between SAD patients and controls when exposed to the experimental condition.
- 3) To characterize the relationship between task-related activation and SAD symptom severity.
- 4) To validate that the new experiment is well tolerated by SAD patients and controls by not creating overwhelming physiologic responses.
- 5) Using an eye tracking system, to validate that SAD patients do not react to the experiment with gaze avoidance strategies which could minimize the exposure to the stimuli.

4.2.5 Study 5: Pilot of the explored techniques in a clinical trial.

- 1) To characterize the effects of treatment in the activations of the emotional face processing task presented in Study 1.
- 2) To characterize the effects of treatment on the resting-state network connectivity measurements presented in Studies 2 and 3.
- 3) To characterize the effects of treatment in the activations of the symptom-provoking task presented in Study 4.
- 4) To characterize the correlation of drug-driven clinical improvement scores with the results three experiments.

5 Study 1 - Exploratory analysis of altered emotional face processing as a SAD symptom biomarker in healthy volunteers: Proof of concept on the value of functional connectivity and validation of the imaging setup

5.1 Introduction

The assessment of disease severity in most of medical disciplines is backed up by objective measurements such as biochemical concentrations or mechanical properties. However, the assessment of psychiatric diseases' severity in clinical practice and research is still mainly relying on structured interviews and questionnaires. This involves that the patient and researcher or physician rely on the accuracy in which patients self-reports their symptoms and experience.

For the severity assessment of Social Anxiety Disorders, the usage of self-reported scales such as the Clinical Global impression (CGI) and the Liebowitz social anxiety scale (LSAS) is the most widespread approach. CGI and LSAS ratings are reasonably well accepted as condition severity indicators by the healthcare and research community. These scales have been demonstrated to have moderate but similar effect sizes (Hedges et al. 2009).

Despite this generalized usage, there has always been some concerns in the accuracy and repeatability of such instruments (Beneke & Rasmus 1992; Busner et al. 2009). In fact, a conceptual issue arises when relying on data extracted from an interview with social phobia patients: The nature of their condition is prone to limit the individual's ability to describe or acknowledge their symptoms (Rapee & Heimberg 1997). On the other side, individuals with social anxiety are likely to experience disruptions in the workplace, family, friendship or romantic relationships (Stein & Kean 2000). These disruptions are often captured by the questionnaires and structured interviews as symptomatic queues. It is possible that, after treatment, the individual remains anxious by these social situations, but being no longer disabled by the disease. This could be

captured by the instruments as a remaining symptom, reducing its sensitivity to improvement.

The recent developments of neuroimaging techniques has raised the interest towards the development of biomarkers able to derive disorder severity from physical measurements made on the subject under study (Valenzuela et al. 2011). It is important to stress that, in this context, neuroimaging-based biomarkers are typically targeted to explore the physical or functional integrity of the neural circuitry that supports the impaired function.

Anxiety is regulated by a complex brain circuit involving cortical and subcortical structures. Alterations of this circuitry are associated to anxiety-related mental disorders, including social phobia. The amygdala is a key part of this circuit and it is frequently viewed as the central target for anxiolytic treatments (Mathew et al. 2008), because of its pivotal role in fear acquisition (Phelps & LeDoux 2005) and emotion processing (Phelps 2006). In a pioneer $H_2^{15}O$ PET study, Furmark et al. showed correlation between treatment response and amygdala's CBF attenuation in SAD patients during a symptom-provoking task (Furmark et al. 2002).

Emotional face processing tasks have proven effective to induce amygdala activation that can be detected with fMRI and explored under different states of patients and controls (Gentili et al. 2015). These tasks have captured attention as candidates for the development of symptom-measuring biomarkers: In multiple studies, SAD patients have shown increased amygdala activation (with respect to controls) while doing emotional face processing tasks (M. B. Stein et al. 2002; Veit et al. 2002; Straube et al. 2005; Phan et al. 2006; Etkin & Wager 2007; Brühl et al. 2014). However, results also indicate that the amygdala activation related to emotional processing may not be stable across time (Campbell et al. 2007), especially in SAD patients (Sladky et al. 2012).

Despite the limitations of the emotional face processing paradigm, the appeal of these results is that amygdala is clearly associated to the brain system processing social, emotional and threatening information (Haxby et al. 2002). A circuit formed by the amygdala and its cortical extensions is frequently reported to be altered in social phobia

patients (Clark & Mcmanus 2002; Duval et al. 2015). Therefore, standardized tasks able to functionally challenge this brain circuit are good candidates to identify differences between patients and controls, patient phenotypes or differences related to treatment response.

Previous studies suggest that the brain activations induced by the emotional face processing tasks (EFPT) can be sensitive to the effect of psychoactive drugs –mainly benzodiazepines and selective serotonin reuptake inhibitors- in healthy subjects (Paulus et al. 2005; Arce et al. 2008) and patients (Kilts et al. 2006; Faria et al. 2012; Phan et al. 2013; Brown et al. 2015). Some studies also indicate that this type of experiments can be useful to predict treatment response (McClure et al. 2007; Whalen et al. 2008; Nitschke et al. 2009)

Development of an experimental setup able to explore such relationships requires extensive design and validation activities. At the time this study started, no emotional face processing studies had been performed at our R&D center. Therefore, it was necessary to conduct a first study including the replication of the results of the literature to proof the setup's sensitivity and specificity. This was, therefore, the first step prior to exploring the relationship between brain activation during the EFPT and the expression of Social Phobia symptoms.

It would have been very difficult to justify running an exploratory paradigm in a clinical population. A non-clinical population was used instead: Healthy volunteers were recruited in the University environment. Individuals were selected based on social anxiety ratings to evenly cover the spectrum of social anxiety degrees in non-patient population. This range overlaps with the range of LSAS scores for patients. Having a uniform coverage of degrees of expression of social phobia symptoms will facilitate performing correlation analyses of brain activation versus symptom severity.

The amygdala is a well-known emotional processing area with observed alteration in social phobia patients. However, amygdala is also part of a complex brain circuit processing emotional face stimulus, which includes the fusiform gyrus (Kanwisher et al. 1997). Alterations in the fusiform gyrus have been inconsistently reported in social phobia

patients (Straube et al. 2004). In a parallel context, alteration in the fusiform-amygdala system has been deemed instrumental in the social deficits of autism (Schultz 2005; Dziobek et al. 2010).

A neuromodulatory effect of the amygdala in face processing areas has been described in PET studies using PsychoPhysiologic Interaction (PPI) (Morris et al. 1998), but not in fMRI at the time of the study. A posterior study used a similar PPI method in fMRI, obtaining results consistent with ours (Frick et al. 2013).

Provided this context and as described in section 4.2.1, three specific objectives were defined for this study:

- 1) To validate that our imaging setup and analysis methods can replicate the findings of previous studies in terms of brain activations induced by the emotional face processing task.
- 2) To determine if there is a significant relationship between task-induced activation and the social phobia scores.
- 3) To describe the interaction between the fusiform gyrus and amygdala, including its relationship with social phobia scores.

5.2 Methods

A model-based approach was selected for this study. As introduced in section 2.2.1, this involves that neural response to a given stimulus is hypothesized and statistical comparison is made between the observed BOLD signals and the model.

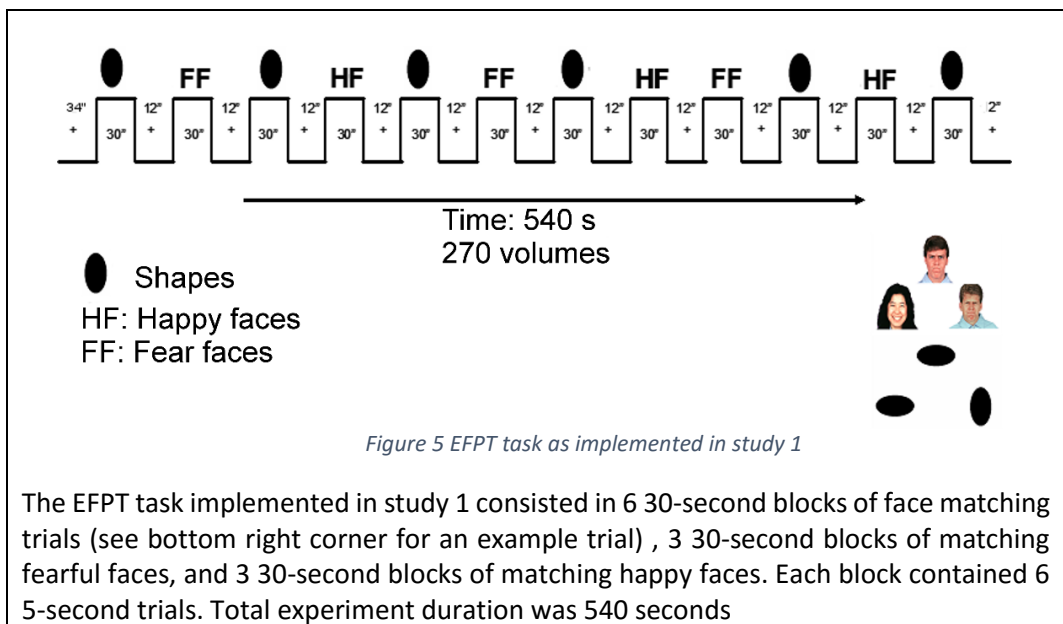
Due to the unpredictability of neural processes at an uncontrolled rest, subjects need to be explored in two very similar conditions (task and control), and signal is to be compared to obtain a differential contrast. Task and control conditions are designed to differ only in the neural process under study (in this case, emotional face processing). Simplifying, the activation of the system of interest will be determined by the difference in BOLD signal between the task and control conditions. The low signal-to-noise ratio of fMRI studies require us to take repeated measures in order to increase statistical power. Additionally, the low frequency psychophysiological changes that subjects can

experiment during the task requires us to interleave control and experimental conditions to avoid results being biased by this background drift. All these requirements condition the behavioral paradigm that subjects execute during the fMRI exploration.

5.2.1 Behavioral paradigm

Subjects were explored with fMRI while executing a modified version of the emotional face-processing task developed by Hariri et al. (Hariri et al. 2002). The task was configured using the same stimulus as used by Paulus et al (Paulus et al. 2005), but the variety of faces used was reduced to fearful and happy only. The reason for selecting this version is that Paulus et al reported that the level of amygdala activation created by this task in healthy volunteers was specifically attenuated by the administration of lorazepam, a benzodiazepine widely used for its anxiolytic effects. These results make the task a good candidate biomarker for SAD.

In this task, subjects execute a sequence of 5 second trials in which they are presented with three images, one in the center and two below, separated towards the sides. Subjects are asked to indicate which of the bottom images matches the center image. In the task condition, images are standardized faces of individuals making emotional expressions (Ekman et al. 1983). All faces were different and the target was always either happy or fearful to match complexity with the control condition. In the control condition, geometric shapes (ovals) were presented. A total of 24 5-second trials were run for each of the task and control conditions, this provides 60 full-brain images per condition (TR= 2 seconds per image). Trials were presented in blocks of 6 (30 s) of the same condition (task/control), spaced by a 15-second fixation cross to enhance independence across the measurement blocks. This totals 9.00 minutes, thus providing a time series of 270 full-brain BOLD images per subject.



5.2.2 Population selection

Twenty-four volunteers were recruited for this study. Individuals were selected from a larger pool on the basis of their score on the Liebowitz Social Anxiety Scale (LSAS) (*Liebowitz 1987*), which has been validated to quantify the level of social anxiety in young Spanish non-clinical populations (*Zubeidat et al. 2008*). A pre-screening self-report was conducted in the students of Barcelona University and Barcelona Autonomous University, obtaining 146 valid answers. Volunteers were selected based on their social anxiety score to uniformly cover the range of social phobia in normal subjects. A confirmatory and differential assessment was conducted on the selected sample by a senior psychiatrist using a Structured Clinical Interview for DSM-IV (SCID) non patient version (*First et al. 2002*). This interview confirmed that selected volunteers did not meet criteria for social phobia, nor were seeking medical treatment. Subjects with a relevant history of medical disorders (including psychiatric) or substance abuse were excluded. The resulting sample ranged from 11 to 61 points of the LSAS scale, with a fairly uniform distribution (see histogram in Figure 6). As a reference, patients with social phobia usually score more than 60 points above this scale, while the range of 30 to 60 is considered a subclinical score (*Mennin et al. 2002*).

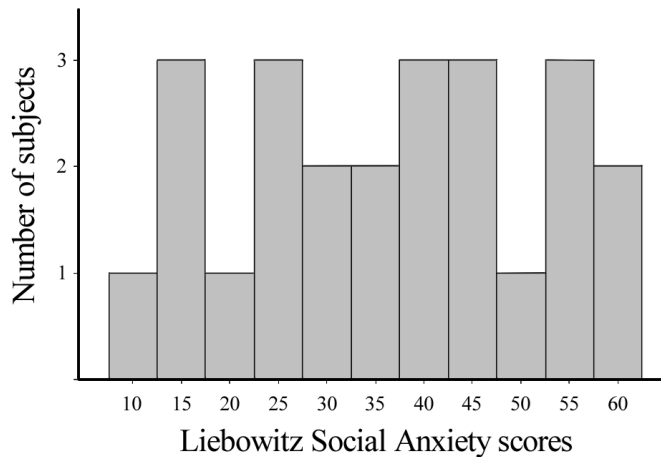


Figure 6 LSAS score histogram

Distribution of LSAS scores of the recruited sample. LSAS provides a dimensional assessment of the degree of social anxiety of the individual, being larger to higher social anxiety. Participants were selected to provide a roughly homogeneous distribution of LSAS scores. Note that scores from 30 to 60 points are considered a subclinical expression of social anxiety.

A comprehensive set of demographic and psychometric questionnaires was used to characterize the population sample, but was not used to further censor nor select the subjects. This included the following items, with its scores summarized in the table below. The table includes the values for 22 subjects, as 2 were excluded from the final analysis due to unsuccessful fMRI exploration.

- A handedness questionnaire: The Edinburgh Handedness Inventory (Oldfield 1971). This provides a laterality scale (degree of dominance of right/left hand). However, for the descriptive statistics, only right/left dominance was considered.
- A simplified intelligence test. In particular, the vocabulary subscale of the Wechsler Adult Intelligence Scale – Revised (WAIS-R) (Wechsler 1981). A reduced version was chosen as this variable is secondary and it would take more than two hours of a mental health professional per subject to administer and score a full WAIS-R test (Camara et al. 2000).
- The Beck Anxiety and Depression Inventories (Beck et al. 1988) to support the absence of comorbidity

- The Spielberger State-Trait Anxiety Inventories (STAI) (Spielberger 1983), which provides indicators of state anxiety (at the precise moment of the assessment) and trait anxiety (experienced in a continuous way). A generalized anxiety score allows the comparison against the specific social anxiety scores. A high social anxiety score with a moderate generalized score support the specificity of the social anxiety expression.
- The Cloninger Temperament and Character Inventory – Revised (TCI-R Spanish version) (Gutiérrez-Zotes et al. 2004), which provided personality descriptors related to novelty seeking and harm avoidance trends.
- The Sensitivity to Punishment and Sensitivity to Reward Questionnaire (SPSRQ) (Torrubia et al. 2001) which provided two additional personality describing metrics. These two metrics, along with those provided by the TCI, facilitate the psychologic assessment of the sample. This is relevant in this study due to the atypical recruitment procedure.

Table 3 Study sample descriptors

| | |
|--------------------------------------|-------------|
| Sex: female/male | 12 / 10 |
| Age, years | 26.0 (3.5) |
| Handedness: Right/left handed | 20 / 2 |
| Education level, years | 17 (3) |
| WAIS-R vocabulary | 11.8 (2.8) |
| Liebowitz Social Anxiety Scale | 37.5 (15.2) |
| Beck Anxiety Inventory | 8.7 (7.8) |
| Beck Depression Inventory | 5.6 (6.3) |
| Sielberger's State Anxiety Inventory | 32.9 (22.9) |
| Sielberger's Trait Anxiety Inventory | 30.5 (27.2) |
| Cloninger's TCI-Novelty seeking | 52.1 (6.3) |
| Cloninger's TCI-Harm avoidance | 52.8 (10.2) |
| Sensitivity to punishment | 6.3 (4.8) |
| Sensitivity to reward | 7.0 (4.6) |

Sample descriptors as revealed by the battery of tests. Mean (SD) where applicable

5.2.3 Imaging setup

5.2.3.1 MRI system

The MRI equipment used was a Signa Excite 1.5 Tesla system (General Electric, Milwaukee, WI, USA) equipped with an eight-channel phased-array coil.

While 1.5 T systems were the most common choice for fMRI studies in the past, we can recognize a clear trend now to use 3 T systems instead. Doubling the magnetic field strength provides an increased sensitivity to BOLD signal contrast that depends on settings, but that has been reported to be in the order of magnitude of a 25% higher in cortical structures (van der Zwaag et al. 2009). However, when the areas of interest are near the frontal or sphenoid sinuses (such as the orbitofrontal cortex or the amygdala) the advantages of using a 3 T system over a 1.5 T may not be seen (Krasnow et al. 2003). The air-bone-brain interface creates spatial discontinuity of the magnetic properties which induces, in that area, a larger signal dropout at 3 Tesla. The loss of sensitivity in 3 T systems can be partially corrected using custom hardware and fMRI pulse sequences optimized for a given brain structure (Weiskopf et al. 2006), but the applicability of these methods to whole-brain studies remains highly experimental.

At the time the study was planned, a 3 T system was not easily available to explore the advantages and disadvantages of higher fields in the context of this particular study.

5.2.3.2 MRI Sequences

Single-shot echo planar Imaging (EPI), gradient-recalled images were collected in the steady state. Time of Repetition (TR) was 2000 ms. Common settings were selected for Time of Echo (50 ms) and Pulse angle (90°). Experimental data has proven that, in 1.5 T systems, selection of a TE around 50 ms ($TE \approx T2^*$) provides an optimal contrast between the activated and baseline state (Gati et al. 1997).

Images covered a field of view of 24 cm with an original pixel matrix of 64x64 and with slice thickness of 4 mm plus an interslice gap of 1 mm. Twenty-two interleaved slices were collected parallel to the anterior-posterior commissure line. The functional time series consisted in 270 consecutive volumes (which covered 9 minutes of acquisition).

Four additional dummy volumes were collected and discarded at the beginning of the acquisition to reach the equilibrium state.

An extra anatomical image was collected for posterior reference. This provided high-resolution landmarks of the subject. The anatomical sequence selected in this case was a 3-D fast spoiled gradient (SPGR) inversion-recuperation prepared sequence with 130 contiguous slices (TR 11.8ms; TE 4.2 ms; flip angle 15° and a field of view 30 cm divided in 256x256 pixels with slice thickness of 1.2 mm.

5.2.3.3 Stimulus presentation and response collection

The presentation of visual stimuli in the fMRI context is particularly challenging due to the bulky MRI instrumentation. The Signa's MRI magnet's leaves a confined space (0.6 m diameter cylinder, 1 m long approximately) where the subject has to stay quiet while the images are collected. In a typical brain imaging sequence, the subject lays in supine position with the head fixed with straps to the center of this cylindrical space. The whole-brain surface antenna array takes extra space as it is placed like an American football helmet surrounding the subject's head.

Most models of MRI head antennas include a small mirror positioned at 45° with respect to the horizontal. This mirror provides the subject a vector of vision parallel to the body's axis towards the subject's feet. Many fMRI paradigms have used this mirror to successfully provide visual stimulus to the subject by retro projecting them on a screen placed at the subject's feet.

In this case, however, we determined we needed a deeper immersion of the subject on the stimulus, a high quality of images to make emotional face processing feasible and the biggest isolation possible of the subjects from the MRI environment.

For this reason, the chosen mechanism for stimulus delivery was a set of MRI-compatible high-resolution goggles (Visuastim digital System, Resonance technology inc, Northridge, CA, USA) which were acquired for the study. These goggles are placed directly on the subject's eyes, between the face and the head antenna. The goggles are built with diamagnetic materials and highly counterbalanced current-induced magnetic fields. This

makes them effectively “transparent” to the fMRI technique. The system consists in 2 small LCD displays of 600x800 pixels which cover 30 degrees of horizontal field of view. The viewing experience is therefore equivalent to watching a 50” 4:3 TV from a distance of approximately 1.9 meters, in a dark room. A set of embeddable lenses allow the usage of the system by persons with myopia or hyperopia.

The usage of this system helps in minimizing the head movement during the task by avoiding instinctive head movements to explore the surroundings or the edges of the field of view.



Figure 7 MRI-compatible goggles

The usage of goggles fitted with LCD displays facilitated an immersive experience into the paradigm and isolation of the subject from the surroundings during the experiment. Model shown: Visuastim digital System, Resonance technology inc, Northridge, CA, USA

Subject’s responses (left or right matching) were collected using two trigger-equipped handles (ResponseGrip, NordicNeuroLab AS, Bergen, Norway) which were held by the patient throughout of the scan. Patients could answer left or right using the corresponding hand’s index finger. As this system is entirely passive (a button press acts as a diaphragm on a fiber optic link) and contains no paramagnetic materials, there is no doubt on its compatibility with the fMRI environment. The “pistol-type” trigger avoids distractions by the subject to (blindly) look for the button, as they are always under the left and right index fingers.



Figure 8 MRI-compatible response devices

MRI-compatible response buttons embedded in a handle allow a simple positioning of the response fingers, even when the response buttons are out of the visual field of the subject. Model shown: ResponseGrip, NordicNeuroLab AS, Bergen, Norway.

Subject's heart rate and respiration rhythm were monitored using a pulse oximeter (4500MRI, Invivo research, Winter park, FL, USA) and a home-built pneumatic plethysmograph.

5.2.4 Image analysis

The flow from raw fMRI images to statistical results can be segmented in two differentiated stages: The data preprocessing and the statistical testing itself. As some of these steps are very similar across the 5 studies presented in this dissertation, they are described in detail in this section and posteriorly referenced along this document.

5.2.4.1 Image preprocessing

Preprocessing includes all the image modifications that take place since the volumes are collected from the scanner until they are fed into statistical analysis tools. The purpose of image preprocessing is increasing the robustness of the analysis methods by correcting nuisance factors such as spatial motion, anatomical variability of the individuals or noise from the imaging technique.

In our studies, image preprocessing was conducted entirely on Statistical Parametric Mapping software (SPM5; The Wellcome Department of Imaging

Neuroscience, London, UK) running on Matlab v6.5 (The MathWorks Inc., Natick, MA, USA). SPM5 is a freely available academic software toolkit developed and maintained mainly by members & collaborators of the Wellcome Trust Centre for Neuroimaging of University College London (UCL). This software package was originally developed by Karl Friston at the Medical Research Council (MRC) and first made available to the neuroimaging community in 1991 (Friston et al. 2007). In few years SPM became the most used neuroimaging software. Many researchers have contributed to develop posterior versions, fully backed up with peer-reviewed methodological articles (Ashburner 2012). The software package is currently distributed under the terms of the GNU General Public License as published by the Free Software Foundation.

A common preprocessing process was selected, which involves three steps: Realignment, normalization and smoothing, which are described below.

Realignment:

As the statistics applied to the images are based in a voxel-by-voxel comparison, it is essential that every piece of tissue is always compared to itself during the complete time-series. Small movements during the task could misalign these voxels and compromise the following analysis phases (note that in this case the original “pixel” measures 3,75 X 3,75 x 4 mm), so a displacement in this order of magnitude is considered extremely large.

In our fMRI sequences, the subject was explained the importance of staying steady and had the head restrained by pillows and elastic straps. However, small movements are still possible. These movements are especially concerning during statistical image processing and inference as they act in two ways: Adding variance to the test residuals, thus reducing sensitivity of the analysis or, when they are correlated to the task, biasing the results of the statistical tests against the models.

In order to minimize the effects of small movements, an iterative rigid-movement algorithm is applied to each of the images to realign them to the first image in the series. This algorithm uses rotation and displacement transformations while attempting to

minimize a least squares cost function of the difference between the realigned image and the first one in the series. The optimal spatial transformation for each image is saved in a separate file, but images do not get re-written as posterior transformations can include these motion correction parameters in the transformation function.

In most of the cases, only sub-millimetric corrections need to be made to realign the series. Large movements can induce additional non-geometric effects on the image quality: Note that it takes 2 seconds to collect a whole brain, so intra-image movement can create a “blurring” effect, where signal of the same point of tissue influences more than one image element. Also, the MRI technique uses sequential spatial encoding to excite-recover signal from the tissue. Therefore, a sudden movement can create a wrong area to be excited, encoded or recalled, inducing a loss of signal in a part of the image, typically a slice. For this reason, the magnitude of the realignment needed is often taken as a data quality criteria.

In this study, we defined an acceptance criterion of a maximum of 2 mm of displacement or one degree of rotation, in order to deem the images suitable for further analysis. Note that one degree of rotation involves a displacement of approximately 2 mm at the edge of the field of view (120 mm radius → displacement [mm] = $120 \tan(1^\circ) = 2,09$ mm).

In order to avoid resampling errors to build up, images are not rewritten at this stage. Only an affine transformation matrix (containing the displacement and rotation parameters for each of the 3 axis) is saved for each image, and will be added to the transformation made in the next step.

In this study, one subject was excluded from the statistical analysis due to exceeding 2 mm movement in the z-axis, as detected during the realignment preprocessing step.

Normalization:

After realignment we can assume that all images within a subject’s time series are co-registered. That is, that every coordinate (pixel position) points to the same portion of

tissue in each of the images that compose the time series. However, this correspondence cannot be assumed between subjects due to the variability in the individual's anatomy.

Most of neuroimaging studies, like this one, require multiple subjects to be analyzed as a group. However, inter-subject voxel-based statistics, like averaging, is possible only after ensuring that each voxel in the volume corresponds to the same anatomic location of the individual.

Normalization involves deforming the individual's volumes to a common "standard brain" space, so each voxel coordinate corresponds to the same anatomical region in all the subjects of the study. When the selected common space is a widely known template, results from different studies can be easily compared and extrapolated to the general population's anatomy. One of the earliest formal reference spaces, which is still in wide use today, is the Tailarach-Tornoux coordinate system (Talairach & Tournoux 1988). This coordinate system is based on an orthogonal division of a single subject's brain using anatomical landmarks.

In this study, the common space selected for normalization is the ICBM-152 template developed in the Montreal Neurological Institute (MNI). This template was developed as part of the ICBM project (Mazziotta et al. 1995) by averaging the high-resolution anatomical MR images of 152 healthy subjects, which had been previously coregistered to a series of earlier MNI templates that in turn had been coregistered to the Tailarach-Tournoux space. In few years, the usage of the MNI system of coordinates to report results of neuroimaging studies become as used as the previously omnipresent Tailarach-Tournoux coordinate system (Laird et al. 2010). However, the wide usage of the Talairach-Tournoux coordinate system in medicine and in research make it to remain as a reference for reporting landmark's coordinates.

The existence of small differences across the two previously mentioned reference spaces raised methodological concerns and controversies in the neuroimaging community, and even multiple inter-space transformation functions (Brett, Johnsrude, et al. 2002; Lancaster et al. 2007). These differences are particularly problematic in the case of coordinate-based meta-analysis studies. In studies where the individual's anatomy is

available, a neuroanatomic assessment may still prevail to pinpoint the anatomical location of certain resulting coordinates, especially if they are in the regions where the different spaces differ mostly.

In our study, the algorithm used to calculate the optimal warping from the individual's image to the common template was developed by the SPM creators (Ashburner & Friston 2005). The algorithm was made available for first time in SPM5 and shows performance improvements compared to the algorithm previously implemented in SPM (Klein et al. 2009). This algorithm is highly optimized for human brain images and combines *a priori* probabilistic tissue classification (segmentation) with the spatial deformation log-likelihood cost function. This generates a "mixture of Gaussians model" that is used to calculate the optimal parameters of the cost function. The combination of tissue segmentation with normalization is known to reduce the dependence of the normalization results from the fMRI physic acquisition parameters (Fischl et al. 2004).

For this specific case, normalization was carried over in 4 steps:

- 1) Rigid-body coregistration of the low resolution average BOLD image with the same subject's high-resolution anatomic image.
- 2) Calculation of the normalization of the high resolution image to match the space of the MNI template.
- 3) Application of the normalization (deformation) parameters to each of the functional BOLD images, on top of the realignment parameters calculated in the previous step. Resulting functional and anatomical images are re-written (resampled) after applying the transformation.
- 4) Visual inspection of the resulting images:
 - a. Anatomical comparison of the original and normalized images to detect deformation artifacts (excessive warping, aberrant misalignment...).
 - b. Matching comparison of the normalized images and the template space to detect a possible failure to match.

Although failures of the normalization algorithm are not frequent, step 4 is extremely important to ensure data integrity and, therefore, validity of the downstream results. The normalization and coregistration algorithms are based in heuristic cost function minimizations. Therefore, it is possible that the algorithm converges into an aberrant local minimum. When this happens, it is often sufficient to slightly adjust the initial alignment so the algorithm converges to the absolute minimum of the cost function.

Smoothing:

A last step of spatial smoothing is very commonly done before moving into statistical analysis. This procedure consists in a 3-D convolution of the imaging data with a filtering kernel. The most commonly used kernel shape is Gaussian, which is described by the “Full Width at Half Maximum” (FWHM) parameter.

Smoothing with an appropriate FWHM can mitigate high (spatial) frequency MRI noise, including residual effects of motion, inter-subject variability and resampling-related artifacts (Maas & Renshaw 1999). This can involve a potential increase the Signal to Noise Ratio (SNR) and therefore an increase of sensitivity and specificity of the statistical results. As per the matched filter theory, a single filter size won't be optimal for all the activation foci. Sensitivity and specificity will be optimized for activation foci of a size matching the smoothing kernel (White et al. 2001). A large smoothing filter can also cause a loss in spatial resolution of the results. For example, two separate activation foci can merge into a single activation cluster if the distance between them is smaller or comparable to the smoothing filter's FWHM. It is therefore prime to take into consideration the data smoothness when interpreting fMRI data.

A minimum data smoothness is also required to use the common parametric statistics implemented in the SPM software package. The statistical inference using this software is based in the Gaussian Random Field theory. Therefore, it is assuming that the dataset is a set of discrete samples collected from a smooth Gaussian field (Friston et al. 1996; Worsley et al. 1996). A rule of thumb that can be used as an entry criteria in these analysis is that the data smoothness (or “RESEL” – RESolution ELEMENT) should be at least the double of the voxel size (Worsley & Friston 1995; Strother et al. 2004). Data smoothness (FWHM) is linearly additive: Convoluting two times a spatial impulse function -a dot- with a 4 mm FWHM leads to an 8 mm FWHM dataset. Therefore, to meet this rule of thumb, the minimum FWHM convolution filter would be the voxel size, provided that the voxel signals are independent from one to the other.

In this study, an isotropic Gaussian filter of 8 mm FWHM was used to smooth the data, as it meets the rule for minimum size (larger than the 3,75x3,75x4 mm voxel size),

it is comparable to the smallest structure of interest (amygdala) and it has shown as optimal for group statistical analysis in similar datasets (Mikl et al. 2008).

5.2.4.2 *Statistical analysis*

In order to explore the activations induced by the task, a classical two-step General Linear Model (GLM) statistical analysis is conducted:

- 1) A first-level analysis is made for each individual to determine the amount of activation related to the task (contrast estimation).
- 2) A second-level analysis is made using all the individual's contrasts to obtain, for each voxel in the brain, a group-wise statistical test against the null hypothesis (In this case, that the voxel does not activate according to the task model).

The details of these analysis steps can be seen below:

First level analysis: This analysis is executed voxel by voxel on the signal's time course (BOLD signal as collected during each moment of the task) modeling the signal with a parametric statistical model containing experimental, confound and residual variables. Best fit of the model and the data is calculated numerically, deriving parameter estimates (beta values) for each voxel and variable of the model, leaving a residual noise, which is the non-explained fraction of the signal. Classical statistical inference can be used to test hypotheses that are expressed in terms of the variables of the General Linear Model and referenced to the residual noise.

In this study, the General linear model contained three experimental variables: Shapes, Happy faces and Fearful faces. Each of these 3 variables was constructed by a box-car function (value of 1 when the subject is executing this task and 0 otherwise) convolved with the "canonical" SPM-default model of the hemodynamic task-to-BOLD transfer function, which is based in two gamma functions (Friston et al. 1999). This is not the most versatile model, but it is widely used as it is fairly simple to use and interpret (Lindquist et al. 2009). A 128 s high pass filter was applied to the resulting time course model to remove its drift component. After the beta values were estimated, 4 sets of beta comparisons

(contrasts) were extracted for its significance testing in the second level analysis: $\beta_{\text{faces}} - \beta_{\text{shapes}}$; $\beta_{\text{fearful}} - \beta_{\text{shapes}}$; $\beta_{\text{happy}} - \beta_{\text{shapes}}$; $\beta_{\text{fearful}} - \beta_{\text{happy}}$. Note that “faces” experimental condition is the union of “happy” and “fearful” experimental conditions. The rationale behind task and control experimental condition in this experiment is introduced in section 5.2.1 “Behavioral paradigm”.

Second level analysis: In this step we conduct group-wise statistical tests on the task effect under the contrasts extracted in the first level analysis. In this case, the null hypothesis is “average first-level beta values equal zero”. One-sample T-test where used to test each contrast condition. A whole-brain significance threshold was set at voxel level to $p < 0.05$, being p corrected by the false discovery rate method (Genovese et al. 2002; Chumbley & Friston 2009). Anatomical interpretation was mainly conducted in the MNI space, but supported case by case by the individual’s 3D image and the landmarks of the Talairach and Tournoux atlas, particularly for the fusiform gyrus, as it is one of the areas with highest discrepancy between the Talairach and MNI reference spaces (Lancaster et al. 2007). All results are reported in the Talairach and Tournoux coordinate space.

Psychophysiological interaction analysis:

Psychophysiological interaction (PPI) analyses test the model in which the response of a cortical area is explained in terms of an interaction between another area's activity (the physiological factor) and an experimental parameter (the psychological factor). That is, PPI analyses are used in fMRI studies to quantify the extent to which an experimental task changes the influence that one brain region has over another (Friston et al. 1997).

With Friston's PPI approach, the BOLD signal of all voxels throughout the brain (target regions) are attempted to be explained (via a general linear model) by the activity of a single "seed" region of interest (ROI), the psychological (task-related) factor and their interaction.

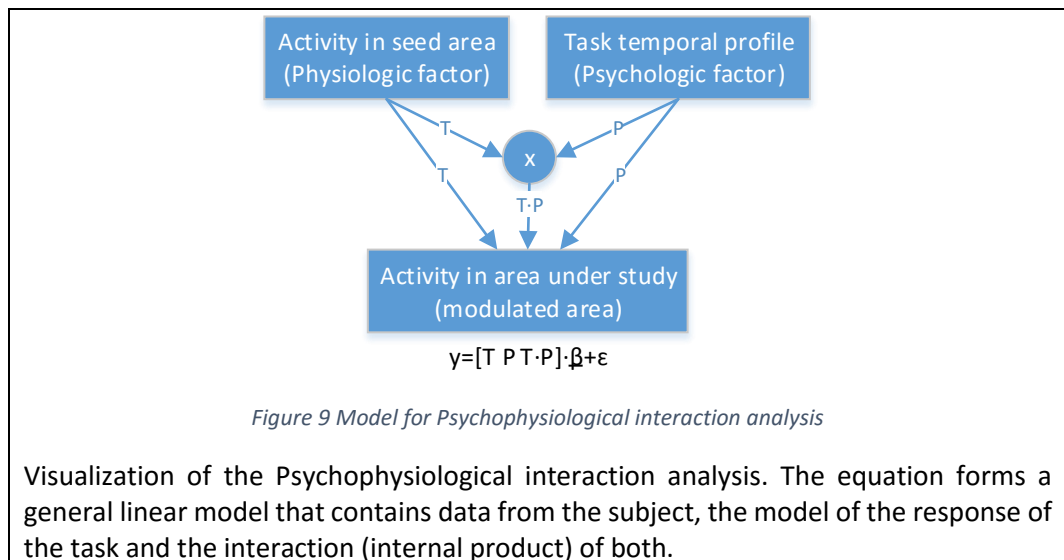
When building a GLM for a PPI analysis, we will use one regressor representing the deconvolved (Gitelman et al. 2003) activation time course of the ROI (the physiological variable), one regressor representing the psychological variable of interest (the weighted task contrast) and a third regressor representing the cross-product of the previous two (the psychophysiological interaction - PPI- term). Solving the GLM will provide us, for each voxel in the brain, beta values for each regressor plus an error term. These will be used to map areas where activation is significantly predicted by the PPI term. That is, the physiological and psychological regressors are treated as confound variables.

More specifically, a GLM design matrix X is generated containing four columns of variables as follows:

- X_1 or P , The psychological variable representing the experimental paradigm (here, the task's emotional face stimuli versus shapes).
- X_2 or T , The time-series variable containing the amygdala-representative signal, extracted as the average time course from a 5 mm radial sphere ROI centered on the cluster maxima identified inside the amygdala in the group analysis.
- X_3 or I , The interaction variable containing the product between P and T .

- X_4 , A constant term included by default into the model to capture the grand mean signal.

This model is then numerically fitted at each voxel in the brain as: $y=X\beta+e$ using a pseudoinverse algorithm. Where y is the “observed” voxel’s signal, β are the parameter estimates and e is the error term. Note that, despite the results are obtained via a general linear model, the addition of the interaction variable involves the inclusion of non-linear relationships into the tested model.



For each individual, the regression coefficient for the interaction term I (β_i) gives a measure of PPI. Significance of PPI will be determined by a random effects analysis of β_i and the error term ϵ (One-sample T-test). A strong significance of PPI indicates that the correlation between the source and the target region(s) during the presentation of emotional faces is significantly different from that during presentation of shapes. Note that, in neuroimaging, the correlation between the BOLD signals of two regions is commonly described as functional connectivity.

Group results were obtained by feeding individual’s whole-brain β_i estimates into a second level one-sample T-test.

Amygdala correlation with LSAS scores Amygdala activation (1st level contrast for happy and fearful faces) was correlated against individual's LSAS score. To assess the influence of the fusiform gyrus on amygdala, a representative signal of the fusiform gyrus was introduced into the model as a regressor. In order to obtain this representative signal, the average contrast value of a 5 mm spherical region of interest (ROI) was extracted. The center of the ROI was defined by the peak activation within the fusiform area functionally related to face processing (Kanwisher et al. 1997). ROI's signal was extracted using the MarsBar toolbox for SPM (Brett, Anton, et al. 2002). Separate extractions and analysis of right and left fusiform gyrus were done given the supporting evidence of lateralized functional specialization in this structure (Koutstaal et al. 2001; Sorger et al. 2007; Meng et al. 2012). The correlation analysis was restricted to the region of the hypothesis (amygdala nucleus and its cortical extensions) to avoid the loss of sensitivity induced by the multiple comparisons correction that would need to be made in a whole-brain analysis. Analysis significance threshold was adjusted following the Montecarlo simulations performed by Stein, Paulus et al (Paulus et al. 2005; Stein et al. 2007) using the AlphaSim software distributed with the AFNI software package (Cox 1996). These simulations reveal the relationship between an *a priori* voxel wise probabilistic threshold and the resulting corrected threshold, when activations are only considered if they reach a minimum number of suprathreshold contiguous voxels. In this case, only clusters of 2 or more contiguous voxels (equivalent to 128 μ l of tissue) are considered within the amygdala ROI, with an *a priori* voxel wise probabilistic threshold of $p=0.05$. This corresponds to a corrected cluster wise $p=0.05$ or to a corrected voxel wise $p=0.01$.

5.3 Results

5.3.1 Behavioral performance indicators during the task

Subjects showed a high accuracy in the task execution. This indicates that the selected task is not excessively demanding for this context. Average failure rate was 1.5%, or an average of 1.1 errors out of the 72 trials that compose the paradigm (total amount of errors ranged from 0 to 5). Having a lenient task is an advantage of this paradigm for future replications of this experiment: Patients or healthy volunteers under the effect of drugs may show a diminished functional performance.

Reaction times to match faces differed between happy (1.079 ± 0.207 s) and fearful (1.505 ± 0.307 s). Difference (0.426 s) was statistically significant (paired Student's $T=10.6$, $p<0.00001$). This suggests that the task induces a different level or type of cognitive demand to process the fearful faces than the happy ones.

5.3.2 Brain response to emotional faces

5.3.2.1 *Main task effect*

Group level voxel-wise comparison (One sample T-test on individual's contrasts) between matching shapes versus matching emotional faces (being happy and fearful part of the same group) showed significant bilateral activation in the visual cortex, fusiform gyrus, amygdala and prefrontal cortex. Note that activation, as described here, refers to strong statistical correlation between BOLD signal and the task model, with statistic strength above the pre-defined significance level. See Figure 10 and Table 4 for details in the activations identified in this analysis. These activations are in line with those identified in previous works using this same task (Paulus et al. 2005; Stein et al. 2007). Therefore, these results can be used to validate that the experimental setup and analysis methods are sensitive enough to detect face-processing brain activations.

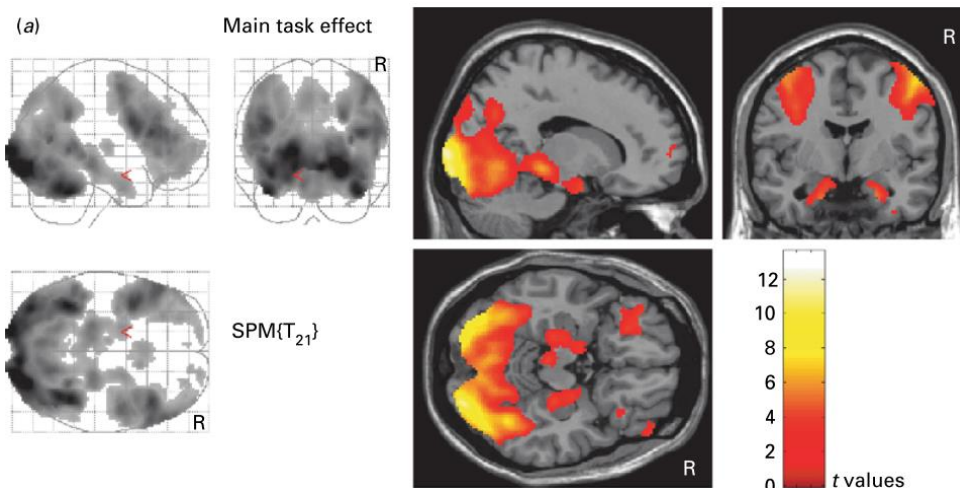


Figure 10 Main faces-matching task effects

Group (second-level) statistical test of the activations related to matching emotional faces (happy and fearful) versus the control shape-matching condition. Group results are thresholded at $p < 0.05$, False Discovery Rate (FDR) corrected. The color bar represents Student's T scores. R indicates the right hemisphere.

Table 4 Main faces-matching task effects

| Main task effect (fearful+happy > Shapes) | | | |
|---|---|---------|---------------------------------------|
| | | Z score | Talairach coordinates (x, y, z mm) |
| Visual cortex | | | |
| | R | 6.9 | 26, -86, -5 |
| | L | 6.5 | -18, -97, 8 |
| Fusiform gyrus | | | |
| | R | 6.3 | 40, -50, -13 |
| | L | 6.4 | -38, -50, -13 |
| Amygdala | | | |
| | R | 4.1 | 20, -5, -22 |
| | L | 3.9 | -20, -5, -23 |
| Frontal cortex | | | |
| | R | 5.7 | 44, 22, 17 |
| | L | 5.8 | -40, 7, 25 |

Coordinates and z score of the cluster's peak value. All contrasts show $p < 0.05$ False Discovery Rate corrected significance.

The effects of both face conditions (fearful and happy) showed a similar activation pattern to the task's main effect (same functional areas were activated), see Table 5 for details.

Table 5 Segmented faces-matching task effects

| Fearful>Shapes | | | | Happy>Shapes | | | |
|--------------------------|---------|------------------------------------|---|------------------------|------------------------------------|--|---------|
| | Z score | Talairach coordinates (x, y, z mm) | | Z score | Talairach coordinates (x, y, z mm) | | Z score |
| Visual cortex | | | | Visual cortex | | | |
| R | 6.9 | 26, -86, -6 | R | 7.0 | 20, -97, -1 | | |
| L | 6.8 | -18, -99, 8 | L | 6.4 | -14, -95, 4 | | |
| Fusiform gyrus | | | | Fusiform gyrus | | | |
| R | 6.0 | 40, -50, -11 | R | 6.2 | 40, -57, -9 | | |
| L | 6.3 | -38, -52, -13 | L | 6.1 | -38, -50, -13 | | |
| Amygdala | | | | Amygdala | | | |
| R | 3.6 | 20, -9, -16 | R | 2.9 | 20, -3, -22 | | |
| L | 4.2 | -16, -5, -13 | L | 3.0 | -22, -11, -18 | | |
| Frontal cortex | | | | Frontal cortex | | | |
| R | 5.8 | 51, -1, 52 | R | 3.9 | 46, 2, 48 | | |
| L | 5.9 | -44, 11, 20 | L | 4.4 | -55, 26, 19 | | |

Coordinates and z score of the cluster's peak value. All contrasts show $p < 0.05$ False Discovery Rate corrected significance, except for amygdala in the happy condition which showed uncorrected $p < 0.002$ (L) and $p < 0.001$ (R)

The comparison between happy and fearful, revealed a significantly stronger activation for the fearful condition in bilateral fusiform gyrus and middle frontal gyrus (See Table 6 for details). This suggest that the extended reaction time observed for fearful face matching may be related to heightened activity in the face processing areas.

Table 6 Differential task effects: Fear > Happy

| Differential task effect (fearful > happy) | | | |
|--|---|---------|---------------------------------------|
| | | Z score | Talairach coordinates (x, y, z mm) |
| Fusiform gyrus | | | |
| | R | 3.6 | 42, -51, -1 |
| | L | 3.4 | -40, -51, -6 |
| Frontal cortex | | | |
| | R | 4.3 | 48, 5, 26 |
| | L | 4.7 | -44, 11, 27 |

Coordinates and z score of the cluster's peak value. All contrasts show $p < 0.05$ False Discovery Rate corrected significance.

5.3.2.2 Psychophysiological interaction

The Psychophysiological interaction analysis (PPI) showed that the emotional face processing blocks significantly and specifically increased connectivity between the amygdala and the fusiform gyrus. Note that the seed region was extracted from the peak amygdala coordinate of the task's main effect (right amygdala). The peak connectivity within the target region of interest (fusiform gyrus) was identified in coordinates -40 -50 -13, with a T-value of 4.27 ($p = 0.003$), p false discovery rate (FDR) corrected for the target area's volume. See Figure 11 for anatomy.

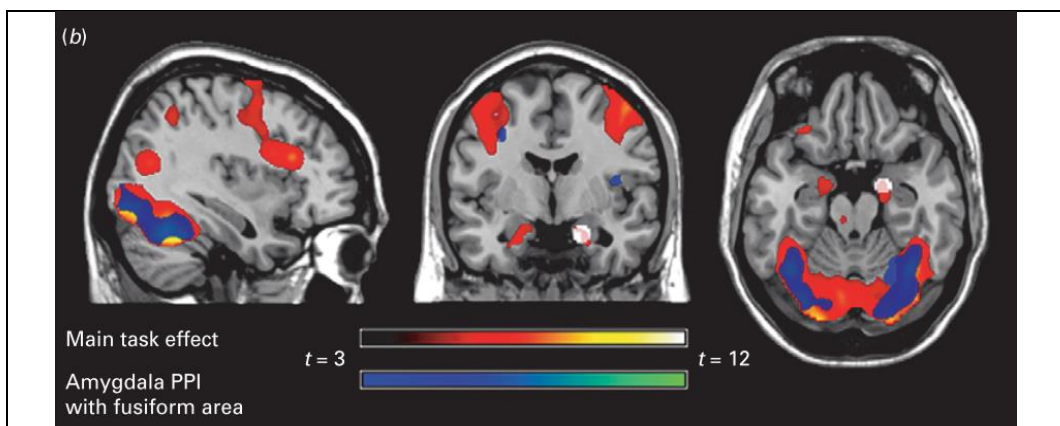


Figure 11 Psychophysiological interaction induced by the faces processing task

Results from the psychophysiological interaction (PPI) analysis revealing functional connectivity modulation by the face processing task between the 5 mm amygdala source region (white circles) and fusiform gyrus [target region of interest (ROI): right fusiform gyrus (40,-50,-13), z score=3.52, T value=4.27, small volume correction $p_{FDR} = 0.003$].

5.3.3 Correlation of brain activation with social anxiety scores and behavioral variables

The Liebowitz Social Anxiety Scale (LSAS) score of each subject was used as a symptom severity indicator to explore if the task activations in the face processing areas showed a Pearson's correlation with SAD expression. The average activation of a 5mm radius sphere was extracted from the activation's peak to feed it to the statistical test.

In this analysis, we found that none of the region's peak activation, including amygdala's, showed a significant positive correlation with LSAS scores. The fusiform gyrus activation did, however, show a moderate ($r=0.47$) negative correlation in the fearful condition. Note the fearful condition is also the condition that showed the strongest activation for the fusiform gyrus, and the condition with highest response times.

Table 7 Correlations of LSAS with brain response to emotional faces in the task's activation peak coordinates.

| | Happy | | Fearful | |
|-----------------------|-------------|-------|-------------|-------|
| | Pearson's r | p | Pearson's r | p |
| Visual cortex | | | | |
| R | -0.13 | 0.576 | -0.22 | 0.338 |
| L | -0.08 | 0.701 | -0.22 | 0.323 |
| Fusiform gyrus | | | | |
| R | -0.18 | 0.431 | -0.47 | 0.029 |
| L | -0.31 | 0.168 | -0.42 | 0.051 |
| Amygdala | | | | |
| R | -0.14 | 0.551 | 0.12 | 0.602 |
| L | -0.01 | 0.971 | -0.05 | 0.827 |
| Frontal cortex | | | | |
| R | 0.29 | 0.191 | 0.24 | 0.286 |
| L | 0.04 | 0.877 | -0.18 | 0.413 |

Pearson's correlation between individual brain activation at group's peak coordinate and individual's Liebowitz Social Anxiety Scale Scores. R, Right; L, left.

The relationship of peak amygdala and fusiform gyrus activation was further explored by calculating its correlation with the clinical and behavioral scores presented in Table 3. Again, in this analysis we didn't find significant findings for the amygdala. Right fusiform gyrus's peak activation did show a moderate correlation with two personality dimension scores: Harm avoidance ($r=-0.53$, $p=0.012$) and Sensitivity to punishment ($r=-0.74$, $p<0.001$), but not with the rest of behavioral scales.

5.3.4 Region of interest correlation with social anxiety scores

Provided that the activation in the amygdala's peak coordinate hadn't shown a significant correlation with social anxiety scores, an additional exploratory analysis was conducted. In particular, the whole amygdala region of interest was mapped using voxel-wise correlation between individual's activation and LSAS scores. The mapping was

conducted for separately for both happy and fearful faces and for left and right amygdala ROIs. In none of these cases we found correlations surviving our significance threshold.

The analysis was repeated but this time including the signal of the fusiform gyrus as a nuisance regressor in the correlation analysis. This analysis showed that amygdala activation had a significant correlation with LSAS scores only after regressing out the effect of fusiform gyrus. Using this model, a suprathreshold cluster was identified for the happy condition in the left amygdala region (see Figure 12a). In the fearful condition, activation was identified in both left and right amygdala ROIs (see Figure 12b). See Table 8 for size, position and significance of the clusters detected.

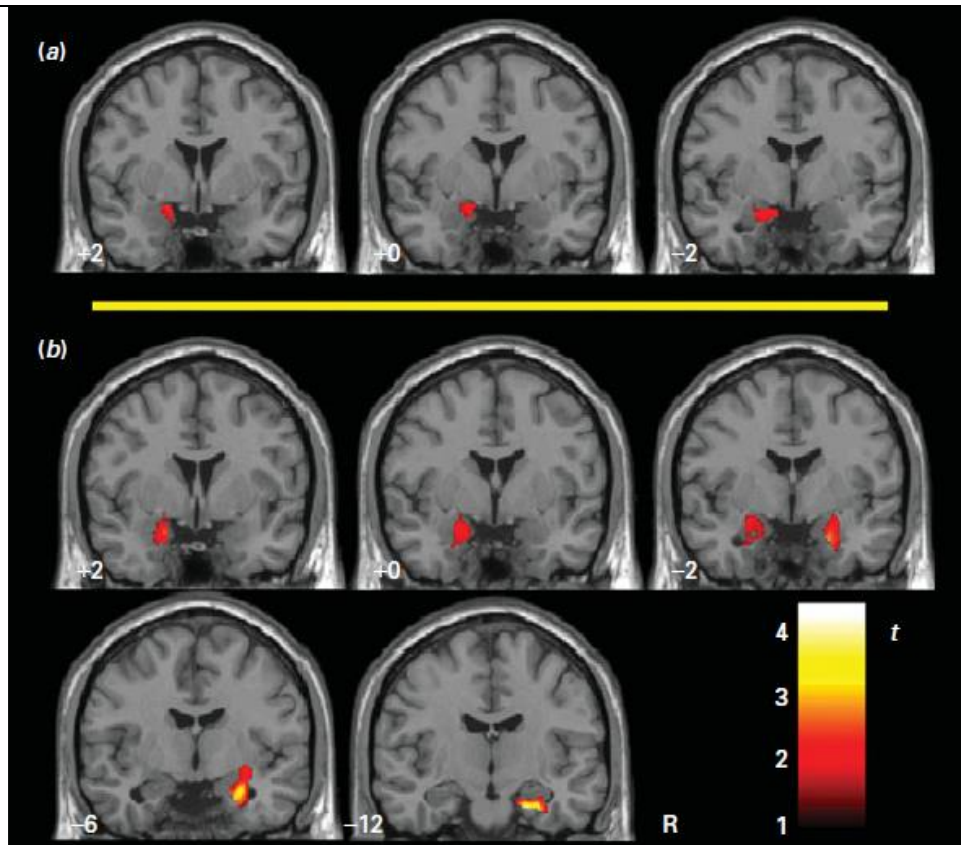


Figure 12 Amygdala regions that correlate with LSAS after regressing out the activation of the fusiform gyrus.

Mapping of the voxel-wise correlation in the amygdala region between the Liebowitz Social Anxiety Scale (LSAS) scores and task activation after controlling for (regressing out) activation in the right fusiform gyrus: (a) Correlations obtained for the happy condition; (b) Correlations obtained for the fearful condition. Only clusters above the reference threshold (volume > 128 μ l with $p < 0.05$) are displayed. The color bar represents t scores. R indicates the right hemisphere.

Table 8 Correlation of amygdala response to emotional faces with LSAS after controlling for fusiform gyrus activation

| | Talairach coordinates (x,y,z) | Partial correlation <i>r</i> | T score | p | Cluster volume (μ l) |
|----------------------------|-------------------------------------|---------------------------------|---------|-------|---------------------------------|
| Happy vs shapes L | -16, -3, -15 | 0.43 | 2.14 | 0.023 | 184 |
| Fearful vs shapes R | -20, 1, -17 | 0.51 | 2.63 | 0.008 | 824 |
| Fearful vs shapes L | 20, -13, -21 | 0.63 | 3.72 | 0.001 | 696 |

Partial correlation coefficients of Liebowitz Social Anxiety Scale with amygdala activation after regressing out activation in the fusiform gyrus (20 degrees of freedom). Coordinates, correlation coefficient, T value and p refer to the cluster's peak.

For data visualization, the relationship between amygdala activation (residuals after regressing out the fusiform gyrus activation) was plotted against the corresponding individual's LSAS score. Figure 13 shows these plots for the peak left and right amygdala in the fearful condition. Results are clearly not driven by outliers.

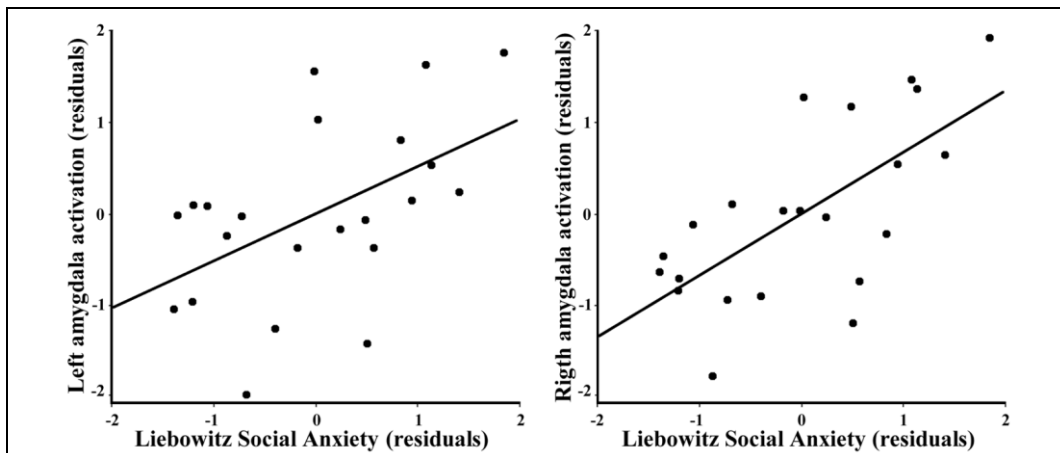


Figure 13 Plots between amygdala activation and LSAS scores after regressing out the activation of fusiform gyrus

Plots showing the correlation between LSAS scores and amygdala activation in the fearful faces condition after controlling for right fusiform gyrus activation. The activations were extracted from a 5 mm-diameter ROIs centered at the peak correlation in the left amygdala (partial correlation, $r = 0.51$, $df = 20$, $p = 0.017$ two-tailed) and right amygdala (partial correlation, $r = 0.63$, $df = 20$, $p = 0.002$ two-tailed).

To explore specificity of the observed correlations after regressing out the activation of the right fusiform gyrus, the analysis was repeated but regressing out the activation at the peak coordinates of the other regions involved in the emotional face processing task (left fusiform gyrus, bilateral visual and prefrontal areas). In the fearful condition, controlling for none of these regions replicated the effect seen in the amygdala's activation. In the happy condition, only controlling for left fusiform gyrus replicated the left amygdala correlation with LSAS. In particular, by identifying a cluster of 640 μl with $p < 0.05$ with peak correlation at Talairach coordinates (-22, 1, -20) and peak significance of $p = 0.007$.

5.4 Discussion and Conclusions

The presented experimental setup and analysis method was proven able to generate and detect significant activation in a network related to facial emotion processing, including visual cortices and bilateral amygdala in a non-clinical population. These activations are in line with the dominant works modeling emotional face processing (Haxby et al. 2000; Gobbini & Haxby 2007; Stein et al. 2007).

The observed amygdala activation did not show a direct correlation with social anxiety disorder symptom severity until a modulatory effect of the fusiform gyrus was considered in the model. The univariate statistical model detected involvement of emotional processing areas in healthy subjects, but was unable to provide dimensional results. Some studies have shown a heightened amygdala response to emotional (mainly harsh) faces in SAD patients (M. B. Stein et al. 2002; Phan et al. 2006; Evans et al. 2008; Goldin, Manber, et al. 2009), but we are not aware of similar findings in a non-clinical population such as ours. The psychophysiological interaction observed guided the exploratory analysis towards considering a bivariate model of the relationship between symptom severity and activation of not one, but two emotional processing areas (fusiform gyrus and amygdala). Recent studies suggest that this functional connectivity interaction may also be altered in Social anxiety and correlated to symptom severity (Frick et al. 2013). Also, a recent magnetoencephalography (MEG) study (which provides a temporal resolution 100 times higher than fMRI) has described a complex pattern of activation of fusiform gyrus, with an early (150-200 ms) under activation (in SAD patients) followed by a late (250-300 ms) over activation (Riwkes et al. 2015). The early undershooting pattern would be within the temporal timeframe of the amygdala response, but amygdala signal was not collected in Riwke's study due to the technical limitations of MEG. These results suggest that the processes related emotional face processing may have complexity within a temporal timeframe smaller than the typical time resolution of fMRI. This scenario emphasizes the methodological value of connectivity-related analysis, which provide an intrinsic synchronization of the dataset used for the analyses.

The bivariate model (including fusiform gyrus' interaction with amygdala) revealed a linear relationship between task-induced activations in areas related to the disease and symptom severity. These findings suggest this relationship should be further explored as a biological marker candidate for symptom severity exploration using fMRI. Previous studies identified related alterations in the fusiform gyrus with SAD (Straube et al. 2004; Gentili et al. 2008). But these findings have not always been consistent across studies (M. B. Stein et al. 2002; Phan et al. 2006). Functional connectivity studies will reveal further details of these modulatory relationships. The indicator of fusiform gyrus

activation may be related to the activity of a brain network extended further than the amygdala: In a similar experiment, Gaebler et al identified that high-frequency heart rate variability was modulated by the faces matching task and that this modulation correlated with fusiform gyrus activation (Gaebler et al. 2013).

In the context of emotional face processing tasks, fusiform gyrus could be a good indicator of task immersion, being activated proportionally to the cognitive load placed on face processing or to the fixation time on the face stimulus. Its involvement in emotional processing may therefore act as an indicator of the amount of attention placed to the faces stimuli. The inclusion of an eye tracking system in the experimental setup may be able to show correlation between fusiform activation and the time spent analyzing the faces stimulus. Unfortunately, this system was not available in our experimental environment. See study 4 (section 8 of this document) for a follow-up on this issue, including the results of an eye tracking analysis in the context of a similar experiment.

When executing this paradigm in our non-clinical population, we have observed a modulation of the brain activity in the circuitry previously shown to be recruited and altered in patient populations. The fact that both populations activate similar structures reinforces the interest of using a dimensional, not categorical (active/not active) approaches as a biomarker. The nature of symptom severity is also non binary, despite medical criteria does end up categorizing patients as patients or non-patients. Measuring the strength of the interaction between emotion processing areas, which is a dimensional approach, can therefore be particularly helpful, as this study suggests this can act as a specific biological marker correlating with SAD symptom severity.

Our results did not reveal significant differences between happy and fearful faces, although fearful faces triggered a stronger effect, with stronger activations and correlations. A methodological study reported higher test-retest reliability in the amygdala's response to fear faces than in response to neutral faces (Johnstone et al. 2005). Also, a comprehensive meta-analysis associated fusiform hyper-activity to specifically negative emotional stimuli in SAD (Etkin & Wager 2007). It is important to note that our experiment was not aimed to discriminate the effect between accepting and

harsh faces, as random expressions appear in the non-target option of every trial. We neither controlled for neutral faces, which have been reported to also trigger an abnormal amygdala response in SAD patients (Birbaumer et al. 1998; Cooney et al. 2006).

In conclusion, the results of this work suggest that our setup and implementation of the emotional face processing task induces brain activations in line with those found in the literature. The task also was seen to modulate amygdala-fusiform connectivity. The exploratory analysis considering fusiform and amygdala activation has revealed brain activation patterns linearly related to symptom severity in the non-clinical population. Increasing knowledge on these inter-related brain activation patterns (functional connectivity) in SAD patients may be extremely helpful to develop biomarkers able to identify and objectivize treatment response or patient's symptom severity.

6 Study 2: Specificity and reproducibility of independent component analysis of fMRI datasets in cognitive, emotional and resting state experiments

6.1 Introduction

The results of study 1 (section 5 of this document) pointed that a connectivity-based measurement could provide a biomarker reflecting symptom severity in SAD. This triggers the interest of further exploring functional connectivity techniques to develop fMRI-based biomarkers for SAD.

The interpretation of functional connectivity (that is, of the dependence between the brain activity registered in different areas of the brain) as the expression of brain networks which support certain functions is not new. The first fMRI connectivity study was limited to the calculation of cross-correlation of the signal of a (seed) point of the brain's motor cortices versus the rest of voxels (Biswal et al. 1995). These results remained relatively non-interpreted for several years. However, the understanding of functional connectivity measurements has evolved very fast in the XXI century (Sporns 2012). In this period, a new and exciting perspective has been provided to neuroimaging through the study of the human connectome (Behrens & Sporns 2012) and its dynamics (Calhoun et al. 2014). This later is becoming relevant in neuroscience and it has brought up the concept of the study of the chronnectome. This later illustrates the understanding that functional connectivity maps can reflect dynamic states rather than a mere footprint of an underlying neuronal system.

As introduced in section 2.2.2.2, Independent Component Analysis is a convenient and attractive method to explore whole-brain networks defined by functional connectivity. The fact that this technique can explore the brain's functional connectivity even in resting state, makes it a very good candidate for translational research or for clinical research with human patients with which full cooperation cannot be taken for granted. It is not surprising then that the clinical applications for which resting-state studies have shown earlier development include Alzheimer's disease, schizophrenia and

disorders of consciousness (which cover coma and vegetative states) (Rosazza & Minati 2011).

In light of this interest, it is considered necessary to demonstrate that our experimental system and analysis methods can obtain valid connectivity maps from healthy volunteers, and that these connectivity maps are indeed representing an underlying brain network that remains regardless of the activity the subject is carrying.

In this study, a characteristic brain network has been selected and it will be examined using a model-free analysis of three extremely different tasks that the subject will be performing. The selected network for study is the “default mode brain network”, due to the interest that its unconventional dynamics have arisen. A recent literature review pointed that the main findings on resting state connectivity alterations in anxiety-related patients are related to this network (Peterson et al. 2014). Reproducibility of the results will be explored as part of the validation of the experimental setup and the analysis methods.

6.2 The concept of the default mode brain network

The name of the “default mode” network (DMN) was coined after a few years of PET studies identifying a set of brain structures that, paradoxically, would decrease their activity when the subject was performing non-referential attention-demanding tasks (Shulman et al. 1997; Raichle et al. 2001).

An intense debate and expectation has been generated around the interpretation of the brain functions related to this network, and even on its existence (Morcom & Fletcher 2007). This controversial situation has reverted in a fast growth on the awareness on this network, as evidenced by the large amount of recent publications on the topic (Raichle 2013).

Despite there are still multiple open unknowns, today the DMN observations are widely accepted as the proof of existence of an ongoing and anatomically organized mode of neuronal activity that is preferentially engaged in the brain and that is suspended only during specific goal-directed behaviors. In humans, this default mode system has been

linked, in part, to: The spontaneous thought processes or self-referential mental activity (Andrews-Hanna et al. 2010), to the support of emotional processing (Gusnard et al. 2001) and to the recollection of prior experiences (Vincent et al. 2006).

There are methodological concerns related to the unknown contribution of physiological noise to the connectivity metrics obtained in these analysis (Birn, Murphy, et al. 2008). However, the functional connectivity shown by this group of brain structures has been widely reproduced across the globe and are now backed up by studies showing highly matching anatomical connectivity across the nodes of this network (Hagmann et al. 2008; Deco et al. 2013). The DMN is, therefore, a widely recognized brain network, still under study. This gives it a great scientific interest that pulls attention for neuroscientific and methodological works like the one presented below.

6.3 Methods

6.3.1 Subjects

Twenty-two healthy subjects were included in this study (12 female; 10 male; mean age \pm SD = 26.0 \pm 3.5 years) from an original sample of 24. Two male subjects were excluded from the final analysis, one because of failure to complete the fMRI session and the second because of excessive head movement. None of the individuals had a personal history of neurological or psychiatric illness and all subjects had normal or corrected-to-normal vision. Each subject underwent the Structured Clinical Interview for DSM-IV (SCID) non-patient version (APA 2000). The mean education level of the group was 17 \pm 3 years. All subjects gave written informed consent to participate in the study, which was approved by local research and ethics committees.

6.3.2 Task selection for comparison with spontaneous activity

Previous literature has identified that brain activity in the so-called default-mode brain network can be consistently modulated depending on the activity of the subject. While this brain network has been identified to oscillate while the subject performs no task, the activity of this network is now well known to significantly decrease while the subject performs an attention-demanding task (Greicius & Menon 2004). At the same

time, activity in this network has been seen to increase when the individual is performing involving self-judgments, autobiographical memory recall, moral dilemma, and prospective thinking, among others (Gusnard et al. 2001; Pujol et al. 2008).

This study sought to investigate the reproducibility ICA-extracted default mode network maps obtained by three distinct fMRI contexts: Passive rest, task-related deactivation and task- related activation.

6.3.2.1 *Resting state condition*

A 4-minute continuous resting-state scan was acquired for each subject. Subjects were instructed to relax, to stay awake and to lie still without moving, while keeping their eyes closed at all times. This scan generated 120 whole-brain EPI volumes and was acquired as the first functional imaging sequence for each subject.

6.3.2.2 *Deactivating task*

To study functional deactivations of default mode regions, we developed a self-paced computerized version of the Stroop color-word interference task. This task is known to be highly cognitive demanding as it defines both speed and accuracy as performance criteria. The choice of the task being self-paced is to promote robust deactivation of the default network by keeping subjects continually engaged regardless of their ability to perform the task.

This Stroop paradigm involved three conditions: resting visual-fixation (R), congruent color-word stimulus blocks (C), and incongruent color-word stimulus blocks (I). The paradigm began with an initial resting block of 32 seconds, followed by four 30-second congruent and incongruent stimulus blocks, interleaved sequentially by eight 12-second blocks of resting visual-fixation, defining the sequence [RCRIRCIRRCRIRCIR]. During congruent trials, the stimulus “XXXXX” was centered on a black screen in either one of three colors: red, green, or blue. Correct responses were mapped to the following target stimuli; “RED,” “GREEN,” or “BLUE,” located in the screen below the cue stimulus and displayed in congruent caption color. The location of the targets (left, middle, right) corresponded to the hand-held button device responses presented in section 5.2.3.3.

During incongruent trials, the same stimulus configuration was presented. However, the cue stimulus was instead one of the same three words presented in incongruent caption color.

Subjects were instructed to match the color of the cue stimulus with the corresponding target word stimulus as quickly and accurately as possible, while mentally vocalizing their response (color naming). There was no inter-stimulus interval between consecutive stimulus presentations. Instead, new stimuli appeared immediately, at a pace determined by each subjects' rate of responding. The paradigm ran for a total duration of 6 minutes, generating 180 whole-brain EPI volumes.

6.3.2.3 Activating task

For the activation task, a version of the moral dilemma challenge previously used by the same group (Pujol et al. 2008) was selected. In this task, subjects are familiarized with stories with and without moral challenges and, for the morally challenging situations, are asked to provide their answer on what would they do.

As the logistics of the fMRI setup do not allow developing the story during the acquisition, subjects were familiarized in detail with the 24 moral dilemma and 24 control task situations, illustrated with vignettes, within one week of the exploration. This training session lasted approximately 1h and was performed to ensure that subjects had a clear understanding of the task and to assist the recall of each control and dilemma vignette on the study day.

On the day of the experiment and before commencing scanning, subjects verified that they could remember each task vignette and were then instructed how to respond during the actual scan. For the control condition, subjects were told to simply indicate the outcome of each event when voice-prompted for a "yes/no" answer, by raising either their index finger (yes) or index and middle fingers (no). For the moral dilemma condition, subjects were informed that during scanning they would be prompted for their own moral judgment to each of the dilemma vignettes, again by raising their index finger to indicate "yes" or index and middle fingers to indicate "no." All of the voice prompts that

accompanied the presentation of the control and moral dilemma vignettes were prerecorded and programmed to occur one second after the presentation of the visual stimuli. The total stimulus interval for each visual presentation was 5 s. Subjects' responses were made within a four second window using the response commands described above, which were recorded by an examiner. The control (C) and dilemma (D) scenarios were presented as four 30-second long, alternating blocks of six stimulus presentations each (CDCDCDCD). The exploration lasted 4 minutes in total, generating 120 whole-brain EPI volumes. See below a sample of a moral dilemma situation and an episodic recall (control) condition.



Mr. Jones is walking down the street when he finds across a wallet lying on the ground. He opens the wallet to see that it contains \$900 in cash as well as the owner's driver's license and credit cards. From the contents, Mr. Jones can see that the owner has been hit by hard times. He considers mailing the wallet back to the owner with all its contents from the address on the driver's license, or keeping the \$900 and sending back just the credit card and license.

Voice prompt: Would you keep the \$900?



Mr. Jones is out in the main shopping street downtown. He enters a clothes store where he tries on several garments. After thinking for a long while he makes up his mind and selects the red t-shirt.

Voice Prompt: Will he buy the blue t-shirt?

Figure 14 Examples of moral dilemma task

Figures presented to immerse the subject in each of the stories (left) and story accompanying the image (right) subjects were trained with these stories prior to the fMRI exploration. Note that the top story corresponds to a dilemma condition, while the bottom story corresponds to a control condition.

6.3.3 Image acquisition

The MRI system and MRI sequence was the same as used in Study 1 and described in section 5.2.3.2. In summary, a 1.5 T Signa Excite system (General Electric) equipped with an eight-channel phased-array head coil and single-shot echoplanar imaging (EPI) software was used. Functional sequences consisted of gradient recalled acquisition in the steady state [time of repetition (TR), 2,000 ms; time of echo (TE), 50 ms; pulse angle, 90°] within a field of view of 24 cm, with a 64 x 64 pixel matrix and a slice thickness of 4 mm (plus an interslice gap of 1 mm). Twenty-two interleaved slices, parallel to the anterior–

posterior commissure (AC–PC) line, were acquired to cover the whole-brain for all functional sequences. The first four (additional) images in each run were discarded to allow the magnetization to reach equilibrium.

As introduced in section 6.3.2, the number of acquired volumes was 120 for the resting state sequence and the dilemma (activating) task and 180 for the Stroop (deactivating) task.

6.3.4 Image analysis

6.3.4.1 *Preprocessing*

Image preprocessing followed a similar pipeline as in study 1 (See section 5.2.4.1 for a detailed description). In summary, it was preprocessed using SPM5 (www.fil.ion.ucl.ac.uk/spm) by doing motion correction, spatial normalization to the MNI template and smoothing using a Gaussian filter of 8 mm of full-width to half-maximum. Data was resliced to 3 mm isotropic voxels to contain computational power demand in the ICA analysis. One subject was excluded due to presenting excessive head movement (z axis translation > 2 mm).

6.3.4.2 *Independent Component Analysis*

Independent Component Analysis was performed using the Group spatial ICA for fMRI Toolbox (GIFT, Version 1.3b; <http://icatb.sourceforge.net/>) run on MATLAB 7, using settings and algorithms similar to those reported in the studies of the toolbox developers i.e. (Calhoun et al. 2004). This involved that, for each of the three fMRI experiments, a single Group ICA was performed at the group level after concatenation of all subjects along the spatial dimension. Single-subject time courses and spatial maps were back reconstructed after the analysis from the raw data matrix. As detailed in Calhoun's works, GIFT performs this procedure as three stages: (1) data reduction, (2) application of the ICA algorithm, and (3) back reconstruction.

During stage 1, principal component analysis (PCA) (with three reduction steps) was used to reduce individual subjects' data in dimensionality (for computational feasibility). The dimensionality of these data, or number of components, was estimated

using the minimum description length (MDL) criterion as implemented in GIFT, which attempts to minimize mutual information between components (Li et al. 2007). For the resting-state study, data from each subject ($n = 22$) were initially reduced from 120 to 17 dimensions, followed by a second concatenation into five groups ($n = 4, 4, 4, 4, 6$), each of which was reduced from 68 or 102 dimensions to 17. This was followed by an ultimate concatenation and reduction into one group with 17 components. An identical data reduction was estimated for the activation (moral dilemma) study. For the deactivation (Stroop) study, as it had a longer acquisition time, data from each subject ($n = 22$) were first reduced from 184 to 19 dimensions followed by a second concatenation into five groups ($n = 4, 4, 4, 4, 6$), each of which was reduced from 76 dimensions to 19. This was followed by an ultimate concatenation and reduction to one group with 19 components.

In stage 2, the estimation of independent sources was performed using the Infomax algorithm (Bell & Sejnowski 1995). See section 2.2.2.2 for an overview of the rationale behind this algorithm.

During stage 3 of back-reconstruction, individual subject image maps and time courses were estimated using the group solution and the individual data to accurately represent the subject-to-subject variability existing in the data (Calhoun et al. 2001a). The resulting single-subject time course amplitudes were then calibrated (scaled) by using the raw data to reflect a proportional percentage of fMRI-BOLD signal strength. In this process, the estimated time course is treated as the model and is linearly fitted to the raw data using an intercept term. This fit is then used to scale (or normalize) the component images into effect size “z score” units. Z-score effect size estimators also reflect the deviation of the data from the mean, enabling second-level (subtractive or conjunctive) random effects analyses to be performed.

6.3.4.3 Identification of the extracted components

This work focused mainly in one pre-defined network, which was expected to be represented by one of the ICA-extracted components. In order to maintain impartiality in the component selection, we performed an automatic (blind) spatial sorting analysis of the GIFT output. For each respective set of Group ICA results, independent components

were spatially correlated with an anatomically predefined default mode template and were ranked according to a “highest correlation” criterion (Pearson’s r) with this anatomy. For a similar approach see (Greicius & Menon 2004). This template was created using the Wake Forest University “WFU Pick atlas” (www.fmri.wfubmc.edu), which is based on the Talairach labeling system. The basic anatomy of the template included the posterior cingulate cortex, and medial frontal and inferior parietal lobes. Although objective, this process essentially confirmed what was evident upon a visual inspection of the data.

6.3.4.4 Statistical Significance Testing of Networks

One-sample T-tests in SPM5 were used to assess the statistical significance of each identified default mode network pattern. For a particular pattern, each subject’s respective independent component image (z score spatial correlation map) was entered into a second-level random-effects analysis and assessed statistically against a threshold of $P_{FDR} < 0.05$ (whole-brain corrected) with a minimum cluster size of >8 contiguous voxels.

6.3.4.5 Anatomical comparison of Identified networks

Consistency in the spatial distribution of the default mode pattern across the three study conditions was assessed by calculating the percentage of overlap of voxels in each activity map in a series of pairwise comparisons. Initially, each map was scaled and binarized as a global mask that represented all suprathreshold brain voxels. The total number of voxels in each map was then calculated. For each comparison, the number of voxels contained within a union of the two given masks was also estimated. With these data, it was then possible to determine the percentage of overlap of voxels, and the percentage of unique voxel space, of one network relative to the other.

The consistency of regional activity in the three default mode network patterns was examined using a conjunction analysis as implemented in SPM5 adopting the global null approach (Friston et al. 2005). That is, the condition tested is whether the activation takes place in all conditions (AND condition). Evidence for a conjunction between the three task states was assessed statistically using a threshold of $P_{FDR} < 0.05$ (whole-brain

corrected). The results of these analyses indicate those voxels that showed significantly consistent connectivity to the DMN across the three experiments.

6.4 Results

6.4.1 Identification of the default mode brain network

For each experiment, we identified a statistically significant pattern of spatially correlated BOLD signal activity [an independent component (IC)] that reproduced the major anatomical features of the default mode network with statistical significance ($P_{\text{FDR}} < 0.05$). This was tested further and directly, using the described spatial sorting analysis that estimated the spatial correlation of all IC patterns from a given set of Group ICA results using an anatomical template of the default mode network created by using a Talairach and Tournoux atlas labeling system.

In each case, the default mode network pattern that we identified from each Group ICA demonstrated the highest correlation to this anatomical template with respect to other estimated ICs (Pearson's r range = 0.40 to 0.60).

Figure 15 shows the default mode network patterns and their associated time courses that were identified in each of the fMRI experiments. For each of these observations, primary clusters of activity were located in the dorsal and polar medial frontal cortex, ventral posterior cingulate cortex, the inferior parietal and frontal cortices and lateral cerebellum.

After the initial spatial identification of networks, a temporal sorting analysis was performed to determine the degree of "task-relatedness" of the moral dilemma and Stroop task default mode network patterns. For each set of ICA results, the associated time course for all ICs was correlated with an idealized reference function (task waveform) of the moral dilemma and Stroop experiments, respectively. In both cases, the identified default mode networks (Figure 15 B and C) demonstrated the highest correlation to each corresponding task waveform of the relevant task periods. As seen in Figure 15B, the degree of task-relatedness of the default mode network activity pattern to the moral dilemma task was strong. This pattern was positively and most robustly correlated with

the specific moral dilemma condition blocks (Pearson's $r = 0.53$) relative to other estimated ICs.

Similarly, the degree of task-relatedness of the default mode network pattern to the Stroop task was also high (Figure 15C). This pattern was positively and most robustly correlated with the interleaved rest-fixation periods during Stroop task performance (Pearson's $r = 0.53$) relative to other estimated ICs.

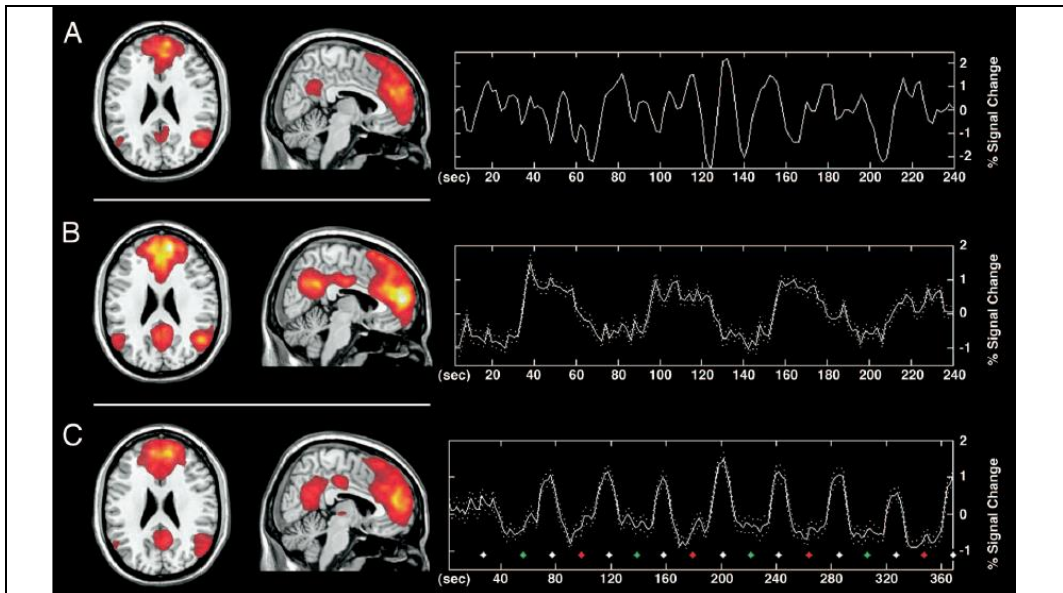


Figure 15 Components of the default mode network

Map of the group-defined default mode network during (A) Rest (z score range = 3.5 to 7) and the time course of a representative subject. (B) The moral dilemma experiment (z score range=3.5 to >8) and the average task-related activity (solid line) \pm standard error (dashed line). (C) The Stroop task experiment (z score range = 3.5 to 7) and the average task-related activity (solid line) \pm standard error (dashed line) Diamonds located below this time course correspond to the middle point of each Stroop task block. White diamonds, rest-fixation periods; green diamonds, congruent trials; red diamonds, incongruent trials. Image display: Radiologic convention (left = right).

6.4.2 Anatomical comparison of the identified networks

After the initial identification of default mode network activity patterns, our first aim was to assess the consistency of the spatial anatomy of the network across the three imaging contexts: Activation, deactivation and rest. The primary intention of this analysis was to determine the extent to which the task-related activity patterns may reproduce the spontaneous anatomy of the network as characterized at rest. This was performed by calculating the percentage of common and unique voxel space in each activity map in a series of pairwise statistical comparisons.

A spatial overlap of 97.3% was observed from the resting-state to dilemma task activity map, such that the dilemma map reproduced almost the entire voxel space of the

default mode network represented at rest. The dilemma activity map was also 41.6% larger in additional voxel space compared with rest—an effect that was expressed predominantly in the anterior, mid, and posterior cingulate regions; right inferior parietal cortex; and dorsolateral frontal cortex (see Figure 16A).

A spatial overlap of 94.7% was observed from the resting-state to Stroop task activity map, such that the Stroop map also reproduced the original voxel space of the default mode network at rest. The Stroop task activity map was also found to be 48.5% larger in additional voxel space compared with rest. This effect was expressed predominantly in the anterior, mid, and posterior cingulate cortex regions (see Figure 16B).

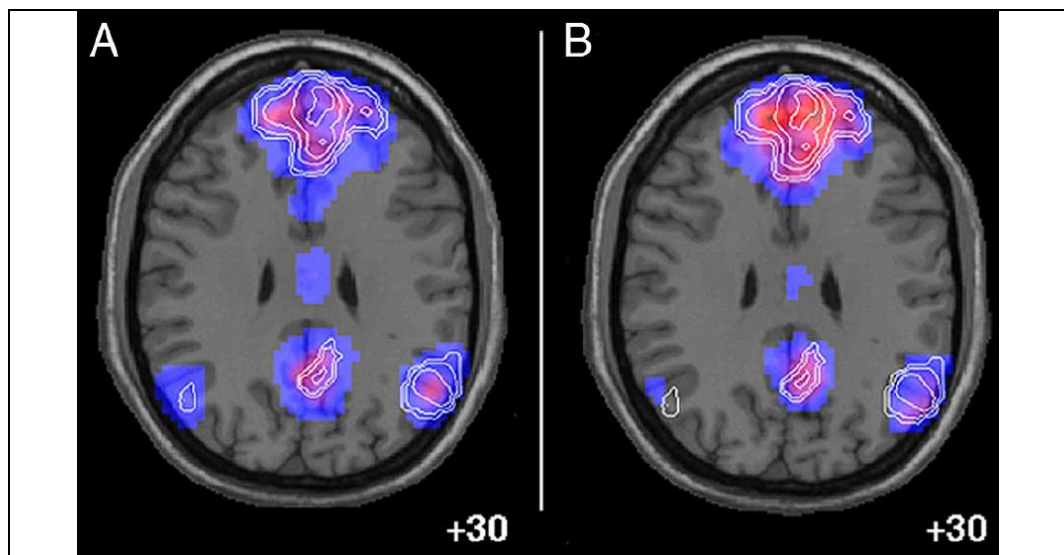


Figure 16 ICA-extracted Default Mode Network overlap across tasks

Figure 16 shows the anatomical overlap of default mode network activities. (A) Representative axial slices showing the moral dilemma activation map (color) overlaid with the corresponding anatomy of the default mode network at rest (white contour lines). (B) Representative axial slices showing the Stroop task deactivation map (color) overlaid with the corresponding functional anatomy of the default mode network at rest (white contour lines). Image display: Radiological convention (left = right).

6.5 Discussion and conclusions

The selected Independent component analysis technique consistently identified the functional connectivity of the chosen brain network (the *default mode network*) in

three paradigms very different among them (highly emotional, highly cognitive and task-free). The model-free independent component analysis results showed a high spatial coherence across functional network footprint identified in each of the three paradigms. This network was selected because the interest and open questions the neuroscientific community recently raised on it (Raichle 2013). Piling scientific work is contributing to the vanishing of the concerns expressed on the value of resting state functional connectivity studies (Morcom & Fletcher 2007). Nowadays, the DMN has now been robustly identified across imaging techniques, including positron emission tomography (Raichle et al. 2001), electroencephalography (Laufs et al. 2003), near infra-red spectroscopy (White et al. 2009) and magnetoencephalography (Brookes et al. 2011). Using fMRI, the DMN has also been identified in resting monkeys (Vincent et al. 2007), cats (Popa et al. 2009), rats (Lu et al. 2012) and mice (Stafford et al. 2014). The availability of methods to image connectivity of resting state networks in animal models boost the interest of characterizing SAD improvement biomarkers based on resting state functional connectivity, as these could be explored across species in translational research.

The analysis of the time course identified to be driving the network's connectivity revealed that the emotional (moral dilemma) task increased the activity in the DMN. The opposite effect was observed in the cognitive (Stroop) task. From the neuroscientific perspective, these results support the idea that this brain network is also functionally related to self-referential process in humans (Harrison et al. 2008).

The fact that the network identified was anatomically highly coincident across experiments supports the reproducibility of the results obtained by the implemented group ICA approach. That is, the implemented approach is able to isolate underlying brain networks despite of them having large differences in their activity during the imaging session. In an experiment that was executed around the same timeframe as ours, Calhoun et al also explored the reproducibility of the brain networks extracted with group ICA. In Calhoun's work, they reported a robust replication of the spatial map of the default mode network obtained by analyzing data obtained during resting state and during a cognitive-demanding auditory oddball task (Calhoun et al. 2008). In this work, they found a large spatial correlation in a large fraction of the networks explored, but not in all of them.

The extension differences observed in the results of our experiment (see Figure 16) are likely to be related to the applied thresholding. In our context, thresholding can only be based on an arbitrary value and must not be assumed to provide the same results across experiments. It is important to note that in fMRI's ICA, the signal of each voxel is generally expected to be influenced by more than one source (Calhoun et al. 2013). Changes in the coupling with regions of other networks will affect the effect size measured by the analysis procedure. This is very likely to expand or contract the network borders when these are defined by a fixed effect size threshold. Therefore, neuroscience-literate qualitative assessments are often used to set the boundary threshold and to determine whether a voxel in the network's border has a relevant participation in the detected network or not. Expansion of the spatial ICA analysis with temporal independence analysis on the component's time course has proven to provide high robustness to the issue of having highly overlapping networks (Smith et al. 2012). However, the initial works using this approach required over 100 times more data points and the associated computational power, making it to be considered not yet usable in our context.

One of the limitations of this study to support reproducibility of the group ICA method implemented is that it is focused on a single set of tasks and in a single brain network. The results found in this study, even when reproduced, cannot be used to infer a robust reproducibility in all tasks and networks. Similar validating assessments will have to be carried before alternative networks and tasks can be validated as fMRI biomarkers.

Another limitation of this study is the limited sample size ($n=22$). A study on 1093 resting-state datasets acquired in 2 different centers also concluded that resting state fMRI provides a remarkable stability of the functional connectome (Biswal et al. 2010). In Biswal's *et al.* study, however, subtle differences related to gender and age were identified. The fact that our identified default mode network is anatomically highly overlapping with the findings of large-sample studies further supports the conclusion that the technique's implementation is robust and reliable.

Concluding, the selected group spatial independent component analysis technique has been able to robustly reproduce the anatomy of the default mode network in data acquired during two very distinct tasks and while the subject was in rest condition.

7 Study 3: Validation of sensitivity of resting-state experiments to emotional state differences.

7.1 Introduction

The robustness of spatial independent component analysis of fMRI data in systematically isolating functionally connected brain networks is now becoming widely accepted. This can be rapidly inferred from a basic literature review in the general case, or from study 2 in the particular context of our setup and analysis methods.

It has been highlighted that spatial independent component analysis may not just be able to robustly identify brain networks, but may also be sensitive to certain characteristics or states of the subject (Beckmann 2012). In this study we will study the feasibility of using spatial ICA results as psychiatric biomarkers by attempting to detect subtle short-term changes in the subject's emotional state. Significant progresses have been made in characterizing ICA-based biomarkers in other psychiatry areas of knowledge, such as schizophrenia (Du et al. 2014), but models of ICA expression of most psychiatric alterations are still deeply underdeveloped.

When comparing the results of spatial independent component analysis across two states or populations, it is essential to describe in detail the metric being compared. Subtle details can deeply condition the inference that can be made from the results.

The concept most broadly used to explore functional changes of brain networks is Functional Connectivity (FC). FC is defined as the correlation (or other kinds of statistical dependency) among two spatially remote brain regions (Friston 2002). Due to its simple interpretation, the FC estimator most broadly used is the Pearson's correlation coefficient between two given voxels or ROIs. Note that, when this correlation coefficient is mapped from a particular location to a broad set of regions of the brain, we are using the technique described in section 2.2.2.1 as seed-based functional connectivity.

In the context of spatial independent component analysis (sICA, described in section 2.2.2.2), the unmixing matrix obtained as part of the analysis defines a temporal

signal that drives the connectivity within each identified network. In sICA, the obtained spatial component (images) are maximally independent. This does not apply to the obtained time courses, for which independence has not been maximized during the process. Therefore, the network's time courses can exhibit temporal dependencies between them. These temporal dependencies among components are typically not as large as those between regions within a component (otherwise they would likely have been included within a single component) (Calhoun et al. 2001b; Calhoun et al. 2003). The study of the dependence between network's time course is now commonly known as the study of functional *network* connectivity (Jafri et al. 2008).

A method conceptually in between the two analysis previously described consists in the assessment of the dependence of each voxel's raw time course with the time course of a given (ICA-extracted) functional network. This method allows assessing to which extent a network's characteristic signal explains the variance of a given voxel. This gives an indicator of functional connectivity of the pixel to the network's estimated characteristic signal. In this context, the most commonly used effect size estimator is the standardized score (z-score). This method is also commonly used to determine which voxels are significantly modulated by a network's time course (Beckmann et al. 2005). To do so, a map is typically created containing the z-scores of voxels that survive a pre-defined significance threshold. These are the characteristic "Independent network map" images used to present a network's anatomy in most ICA-based works, including this one. Provided that the differences versus basic functional connectivity have been presented in this section, in the context of this work, these "z-score" maps will be simply referred to as "component connectivity maps".

In this study, changes in functional connectivity through experimental manipulation of the subjects are explored through comparison of component connectivity maps. As it has been exemplified in section 6, ICA allows modeling the independent component networks behind an fMRI dataset with fair spatial robustness across subjects and conditions. Z-score component connectivity maps have been successfully used to determine to which extent component connectivity maps differ in certain populations such as Alzheimer's disease patients (Greicius & Menon 2004) or schizophrenic patients

(Çetin et al. 2014). It has also been described that functional alterations related to task execution can be observed in component connectivity maps (Calhoun et al. 2008). Some studies revealed that the resting state networks could be sensitive even to the task that the subject had performed just before (not during) the scan session (Waites et al. 2005; Tailby et al. 2015). This supports the idea that the subject's state could, to some extent, influence component connectivity maps.

One of the main objectives of this study is exploring whether ICA component connectivity maps can be sensitive to experimentally induced emotional states. We are not aware of any previous study that has tested this hypothesis and we believe that these results can contribute in the understanding that ICA of fMRI data is a technique highly sensitive to the status of the subject under study. A positive result reinforces that this technique could be a valuable contributor to the characterization of psychiatric patient's symptom severity or response to psychopharmacologic treatments.

7.2 Methods

7.2.1 Subjects

Twenty-four, right-handed, healthy volunteers were recruited for this study (12 female; mean age and SD=31.0 ± 8.3 years). All subjects spoke English as a first language (they were recruited and explored in the area of Melbourne, Australia) and had no history of neurological disorder or psychiatric illness. Subjects' mean education level was 15.3 ± 2.4 years and general intelligence scores (Wechsler 1999) 114 ± 10.8. All subjects gave written, informed consent to participate in the study, which was approved by the Mental Health Research Institute of Victoria and Melbourne Health Research and Ethics Committees

7.2.2 Experimental protocol

For mood induction, we used a modified version of the paradigm reported by Damasio *et al* (Damasio et al. 2000). During an initial interview session, one week prior to scanning, participants were told that they would be required to think about two events in their past - one especially non-emotional experience and one especially sad experience- .

Subjects were told that they would be asked to provide broad (not detailed) accounts of the contents of their imagery after scanning. As described in Damasio *et al*, there was no attempt to constrain the themes artificially by limiting the recall to episodes involving the same persons or places or a certain time span, because we were interested in gaining access to the autobiographical episodes that the subjects considered to be emotionally most powerful. For the neutral recall condition, subjects were asked to recall in detail a specific but unemotional day in their lives (e.g., a typical day at work in which everything is routine) assisted by the musical piece 'Chopin Waltzes numbers 11 and 12' (played at half-speed). Subjects were asked to recall this day chronologically, i.e., from waking up in the morning, preparing breakfast, getting dressed, hearing the news, leaving for work, arriving at work etc. For the sad recall condition, subjects were asked to recall in detail a specific, personal episode or event of particular sadness in their lives and to attempt to re-experience the emotions, aided by the musical piece 'Russia under the Mongolian Yoke' by Prokofiev. To encourage that true autobiographical recalls were generated for both conditions, subjects were instructed not to imagine or interject untrue events (i.e. worst/best case scenarios) but rather to think about events that actually happened.

During scanning, subjects were instructed to close their eyes and attempt to recall and re-experience the specific neutral or sad emotional episodes (i.e., scan 1 = neutral recall, scan 2 = sad recall). Subjects were told to actively visualize, think and ruminate about the specific episodes rather than to concentrate on their feelings of relaxedness or sadness. They were also instructed to maintain as long as they could these specific feeling states until the end of the scanning period, i.e., after they had indicated each scan to commence (see further). Each condition commenced with the selected music pieces being played. The choice of music to accompany the sad recall condition was based on previous studies indicating that this piece, together with the sad memory recall, consistently and specifically induced dysphoric mood without co-producing other related emotional states (e.g. anxiety) (Clark & Teasdale 1985; Martin 1990; Segal et al. 2006). This approach to mood induction, including the specific sad music piece, have been used successfully in previous PET and fMRI studies e.g., (Baker et al. 1997; Lewis et al. 2005), albeit to assess the influence of induced mood states on latter cognitive task performance. In our study,

the presentation of music pieces during the pre-scanning (induction) period was also employed to reduce distraction to surrounding noise in the MRI environment.

Each musical piece (presented via headphones) was played for between one and five minutes on average before each of the four-minute scans commenced, depending on the time it took for the participant to achieve the mood state. Scanning commenced only after the subject indicated (via button press) that they felt a certain intensity of neutral or sad mood had been reached. While we allowed up to five minutes for subjects to achieve the desired mood states, in practice, all subjects indicated to commence the scans within a three-minute period. For the neutral recall condition, this period lasted on average between one to two minutes while for the sad recall condition this lasted typically two to three minutes. Throughout the scanning sequences, subjects laid in a relaxed position and were instructed to keep their eyes closed at all times without falling asleep. Mood state ratings and alertness was assessed by self-report and communication with the subjects between the neutral and sad recall conditions. All subjects spent approximately 30 minutes in a mock scanner prior to the actual study period in order to familiarize themselves with the MRI environment.

Subjects' mood state was assessed by verbal response to an 11-point rating scale of the seven dimensions, 'alertness', 'anxiety', 'happiness', 'sadness', 'fear', 'anger' and 'disgust'. Scale range was from 0–10, with 0 reflecting 'not at all' and 10 reflecting 'extremely'. In a debriefing session following scanning, subjects were also asked to indicate the extent to which they were actively engaged in the sad autobiographical recall, rating on an 11-point scale (0–10) their relative 'ease of inducing sadness' (mean \pm SD = 7.1 ± 2.1); 'similarity of feelings when compared to actual life event/episode' (mean \pm SD = 6.7 ± 2.1); and the 'approximate proportion of time sadness was maintained throughout the four-minutes' (mean \pm SD = 5.5 ± 2.1). Behavioral data were analyzed using the Statistical Package for the Social Sciences v. 11 (SPSS, Chicago, Illinois).

7.2.3 Imaging acquisition

Individual MRI sequences were acquired in a single scanning session using a 3 Tesla GE Signa Horizon LX whole body scanner (General Electric, Milwaukee, WI, USA).

Subjects' heads were fixed using a Velcro® strap over the forehead. Functional MRI data were acquired as a series of single shot gradient-recalled echo planar imaging volumes providing T2*-weighted BOLD contrast (repetition time, 3000 ms; echo time, 40 ms; flip-angle 60°; field of view, 24 cm; voxel size, 1.875×1.875×4.0 mm; 25 slices). For each condition, the functional time-series consisted of 80 consecutive whole-brain images (duration of 4 minutes) after automatically discarding the first (additional) four images in each run to allow the magnetization to reach equilibrium.

7.2.4 Image analysis

7.2.4.1 Preprocessing

Image preprocessing followed a similar pipeline as in study 2 (See section 5.2.4.1 for a detailed description). In summary, images were preprocessed using SPM5 (www.fil.ion.ucl.ac.uk/spm) by doing motion correction, spatial normalization to the MNI template and smoothing using a Gaussian filter of 5 mm of full-width to half-maximum. Data was resliced to 3 mm isotropic voxel to contain computational power demand in the ICA analysis.

Provided this was a paired-sample experimental design, we further compared the translation and rotation estimates (x, y, z) from both scans (neutral and sad recall conditions) using repeated measures analysis of variance (ANOVAs) to ensure equivalent data quality. Translation and rotation estimates (x, y, z) were all less than 1 mm or 1°, respectively. For translation estimates, we observed no main effect of condition ($F(1, 23) = 1.43, p = 0.23$) or translation estimate by condition interaction ($F(1, 23) = 0.30, p = 0.74$). For rotation estimates, we observed no main effect of condition ($F(1, 23) = 3.59, p = 0.07$) or rotation estimate by session interaction ($F(1, 23) = 0.35, p = 0.71$).

7.2.4.2 Independent Component Analysis

The ICA analysis performed in this study was the same as in Study 2. See section 6.3.4.2 for details. Briefly, the Group ICA for fMRI Toolbox (GIFT v1.3b; <http://icatb.sourceforge.net>) was used to perform ICA at the group level for the neutral and sad recall conditions per separate. This involves that the Infomax ICA algorithm was

executed after the previously described subject-wise data concatenations, and followed by a back reconstruction of single-subject time courses and spatial maps from the raw data matrix.

The algorithm's initial self-adjusting parameters did converge to a singular configuration in terms of data reduction and number of detected components that is described next.

During Stage 1, three steps of PCA were used to reduce individual subjects' data to a dimensionality estimated following a minimum description length algorithm. For the neutral recall condition, data from each subject ($n = 24$) were firstly reduced from 80 to 21 dimensions, followed by a second concatenation into six groups of $n = 4$ subjects each. The dimensionality of each subgroup (i.e., $n = 4$ sets of 21 dimensions) was reduced from 84 to 21 dimensions using PCA. This was followed by a final concatenation and reduction into one group with 21 components. For the sad recall condition, data from each subject ($n = 24$) were first reduced from 80 to 24 dimensions followed by a second concatenation into six groups (of $n = 4$ subjects), each of which was reduced from 96 dimensions to 24. This was followed by a final concatenation and reduction to one group with 24 components.

In Stage 2, the estimation of independent sources was performed using the Infomax algorithm (Bell & Sejnowski 1995). During this stage the spatially independent component maps were created, while during Stage 3 of back reconstruction, individual subject image maps and time courses were estimated using the group solution to accurately represent the subject-to-subject variability existing in the data (Calhoun et al. 2001a).

The resulting single-subject time course amplitudes were then calibrated (scaled) using the raw data to reflect percent fMRI signal strength, followed by normalization to z score values. In this process, the estimated time course is treated as the model and is fitted to the raw data using an intercept term. This fit is then used to scale (or normalize) the component images into z score units also reflecting the data's deviation from the mean, thus, enabling second-level random effects analyses to be performed.

7.2.4.3 *Identification and assessment of Resting-State Networks*

For the neutral and sad recall conditions, ICA produced respectively 21 and 24 maximally independent patterns (ICs). Both the spatial pattern and frequency spectra (see below) of each component were visually inspected to determine their appearance as potential RSNs or possible image artifacts.

Examples of noise ICs published in previous ICA works (Cordes et al. 2001; Beckmann et al. 2005; De Luca et al. 2006; Fukunaga et al. 2006) were used to detect components that corresponded to distinct and clear image artifacts. The noise components identified were related to subject's head motion and related susceptibility artifact at the frontal sinus; eyeball movement, cardiac-induced pulsatile fluctuation at the base of the brain and/or surrounding major vessels, and cerebrospinal fluid (CSF) signal fluctuation due the respiratory and cardiac cycles.

For the neutral and sad recall conditions, respectively 7 and 5 task-related relevant RSNs were identified with neurophysiological relevance criteria for further analysis. The components were matched across conditions following neuroanatomical criteria.

Before testing for possible mood state-related changes in the functional connectivity pattern of the five common RSNs, we examined the reproducibility of these results by performing a simple split-half analysis of both of the datasets, repeating the procedure of the original group ICAs. This analysis was considered necessary because although measurements of functional connectivity of RSNs have demonstrated spatial consistency across fMRI studies, it is less clear how reliable these measurements are in detecting changes of functional connectivity strength in the context of repeated measurements and task performance. To assess the reproducibility of our main effects using group ICA (Shown in Figure 17), we compared the findings of each split-half analysis qualitatively (by visual inspection) as shown in Figure 18. It is important to note that some of the discrepancies shown could be attributed to the loss of statistical power when reducing to the half the amount of subjects in the analysis.

7.2.4.4 Significance testing of changes in Resting-State Networks

SPM5 was used to estimate second-level group RSN maps to compare the common RSNs for differences in their relative functional connectivity strength between the neutral and sad recall conditions. Group statistical maps were estimated for each RSN separately, by first entering each subject's respective independent component images (z-score maps) into voxel-wise one-sample t tests ($p_{FDR} < 0.05$, corrected). To assess for differences in the functional connectivity pattern of common RSNs, a global mask was created by combining all regions from RSN patterns that survived the previous correction of $p_{FDR} < 0.05$ in both conditions. Paired samples t tests were then used to test for differences in functional connectivity strength of the common RSNs restricted only to voxels contained in the global mask. Regional differences were considered significant if surviving $p < 0.005$ (uncorrected), with a minimum cluster extent of at least 5 contiguous voxels.

7.2.4.5 Signal analysis of the resting state networks

Analyzing the signal of the identified networks served two basic purposes in the current study:

- 1) To confirm that all selected RSNs showed dominant a Power Spectrum Density (PSD) in the expected 'very low frequency' domain (Cordes et al. 2001; Kiviniemi et al. 2003; Kiviniemi et al. 2005).
- 2) To assess for any significant differences in the PSD parameters for the common RSN patterns identified in association with the neutral and sad recall conditions, which may reflect different sources of signal variation.

Transformation of group ICA associated time courses into the frequency domain is necessary because phase synchrony of these slow signal fluctuations cannot be assumed across subjects under resting-state conditions. By characterizing ICA-associated time courses on the basis of PSDs, inter-subject averaging becomes possible and, in turn, facilitates the assessment of frequency characteristics and differences between components.

To perform this analysis, we derived the PSD estimate using a modified periodogram method (with a Hamming window of 240 s) for each subject's respective RSN time-series (i.e., 5×2 common RSN patterns + 2 specific RSNs per subject = 12 in total). Components were normalized in energy ($\sigma^2 = 1$) prior to the analysis. We also computed each RSN's average PSD across subjects.

Our specific interest was to compare the proportion of power in this frequency domain among the common RSNs. To perform this comparison without an operator-driven bias, we divided our frequency range into three domains based on the literature's descriptions; 'very low frequency' ranging between 0.01–0.04 Hz; 'low frequency' ranging between 0.04–0.10 Hz; and 'higher frequencies' ranging between 0.1–0.17 Hz (Cordes et al. 2001; Kiviniemi et al. 2003; Kiviniemi et al. 2005). Note that, provided TR=3 s, 0.17 Hz is our Nyquist frequency.

For each extracted RSN, the proportion of the total power in each of these bands was estimated (see one example in Figure 20). Focusing on the 'very low frequency' range of interest, paired-samples Wilcoxon Signed Ranks Tests were used to assess for differences in the proportion of power across this frequency range between common RSNs.

7.2.4.6 Confirmatory Cross-Correlation Analysis

Seed-based cross-correlation analyses (CCAs) were performed to assess for specific changes in functional connectivity strength among key ROIs (seed and target) in the 'paralimbic' and 'default mode' RSNs. The ROI placements and size (i.e., volume) were derived from a conjunction analysis in SPM5 of the ICA functional connectivity maps for each RSN, as described above. This analysis identified clusters whose activity was highly and jointly significant in both the neutral and sad recall conditions (p FDR<0.05). These SPM activity clusters were converted to ROIs using the MarsBaR region of interest (ROI) toolbox (<http://marsbar.sourceforge.net>).

All ROI placements and dimensions were determined via a conjunction analysis of the exploratory ICA connectivity maps, which identified those regions whose activity was highly and jointly significant to both conditions ($p_{\text{FDR}} < 0.05$).

Initially, reference time courses were extracted from the neutral and sad recall condition scans for each subject, for each seed ROI. These time courses were calculated as the average time courses across all voxels inside each ROIs, which were then entered into first-level (single-subject) whole-brain, linear regression analyses in SPM5. To minimize the effect of global drift, voxel intensities were proportionally scaled by dividing each time point's value by the mean value of the whole-brain image at that time point. A high-pass filter set at 120 s cutoff period was used to remove low frequency drifts below ~ 0.008 Hz. Data were corrected for first-order serial autocorrelations using the AR(1) model in SPM5. Contrast images were generated for each subject by estimating the regression coefficient between each voxel and the reference time-series. These contrast images were then included in second-level (group) random-effects analyses using one-sample t tests. Resulting z transformed (Gaussianized) SPMs were thresholded at $p_{\text{FDR}} < 0.05$ (corrected) and represent the strength of functional connectivity from each seed to target ROI respectively (see Figure 21). Differences between conditions were considered significant at $p < 0.05$ FDR corrected after small volume correction (search volume used during significance testing was the target ROI's volume).

7.3 Results

7.3.1 Behavioural

The effect of task conditions on subjects' mood state was assessed in a two-way repeated-measures analysis of variance with mood dimensions and condition type (neutral and sad recall) as within-subject variables, which indicated a significant interaction ($F(1, 6) = 41.21, p = 0.0001$). Post-hoc t tests showed no significant change in subjective ratings of 'alertness' between the neutral and sad recall conditions (indicating score of neutral recall minus sad recall) [$t(1, 23) = 0.67, p = 0.51$], but significant changes in self-reported levels of anxiety [$t(1, 23) = -3.78, p = 0.001$]; happiness [$t(1, 23) = 7.47, p = 0.0001$], sadness [$t(1, 23) = -11.44, p = 0.0001$]; and fear [$t(1, 23) = -3.55, p = 0.002$].

In a pairwise comparison of the change scores for each mood state dimension, the magnitude of change for self-reported sadness between the neutral and sad recall conditions was found to be greater than for each of the other dimensions (p value range <0.023 to 0.0001).

7.3.2 Identification and assessment of resting-state networks

From the group ICAs, we identified 5 significant independent component patterns of interest (i.e., RSNs) that were common to both of the task conditions (See Figure 17). The two unmatched components were related to visual and sensorimotor cortices, but they did not appear robustly during the sad recall condition.

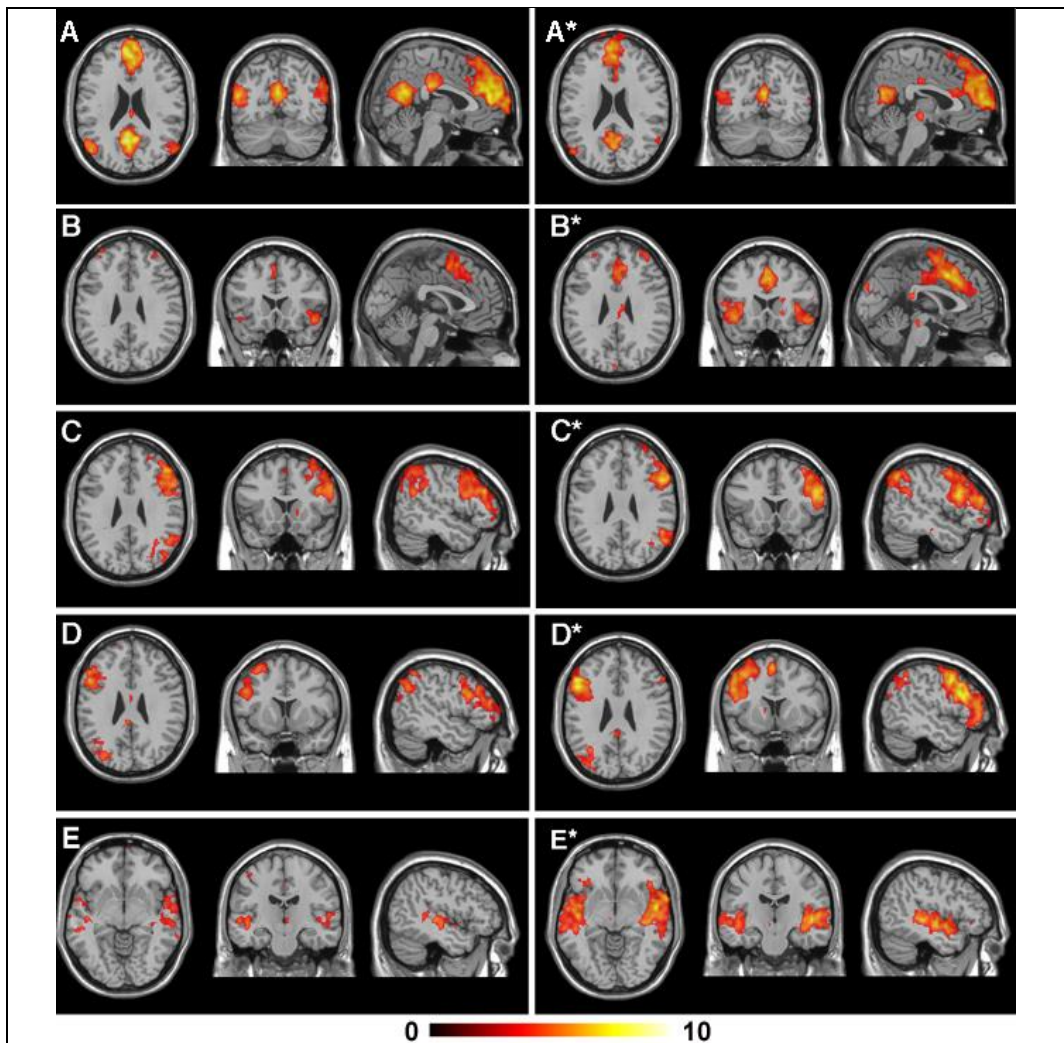


Figure 17 Resting state networks common across states

Global functional connectivity maps of the common RSN patterns that were identified in the mood induction experiments ($p_{FDR} < 0.05$). The left-most panel displays axial, coronal and sagittal views of the pattern under the neutral recall condition, while the right-most panel displays each corresponding pattern under the sad recall condition. All images are presented on a high-resolution single-subject MRI in standard neuroanatomical space (Montreal Neurological Institute, Colin-27). Corresponding color bars indicate the t score ranges of the displayed maps. Images are displayed in neurological convention (left = left).

In the reproducibility-confirmatory analysis of both datasets, we observed an 80% reproducibility of the five common RSN patterns. For the RSN patterns that reproduced in both split halves, there appeared to be good agreement (similarity) in the strength of functional connectivity estimated within-condition (neutral or sad recall), as well as

apparent changes in the extent and magnitude of functional connectivity between these conditions as suggested from the original full-sample analysis.

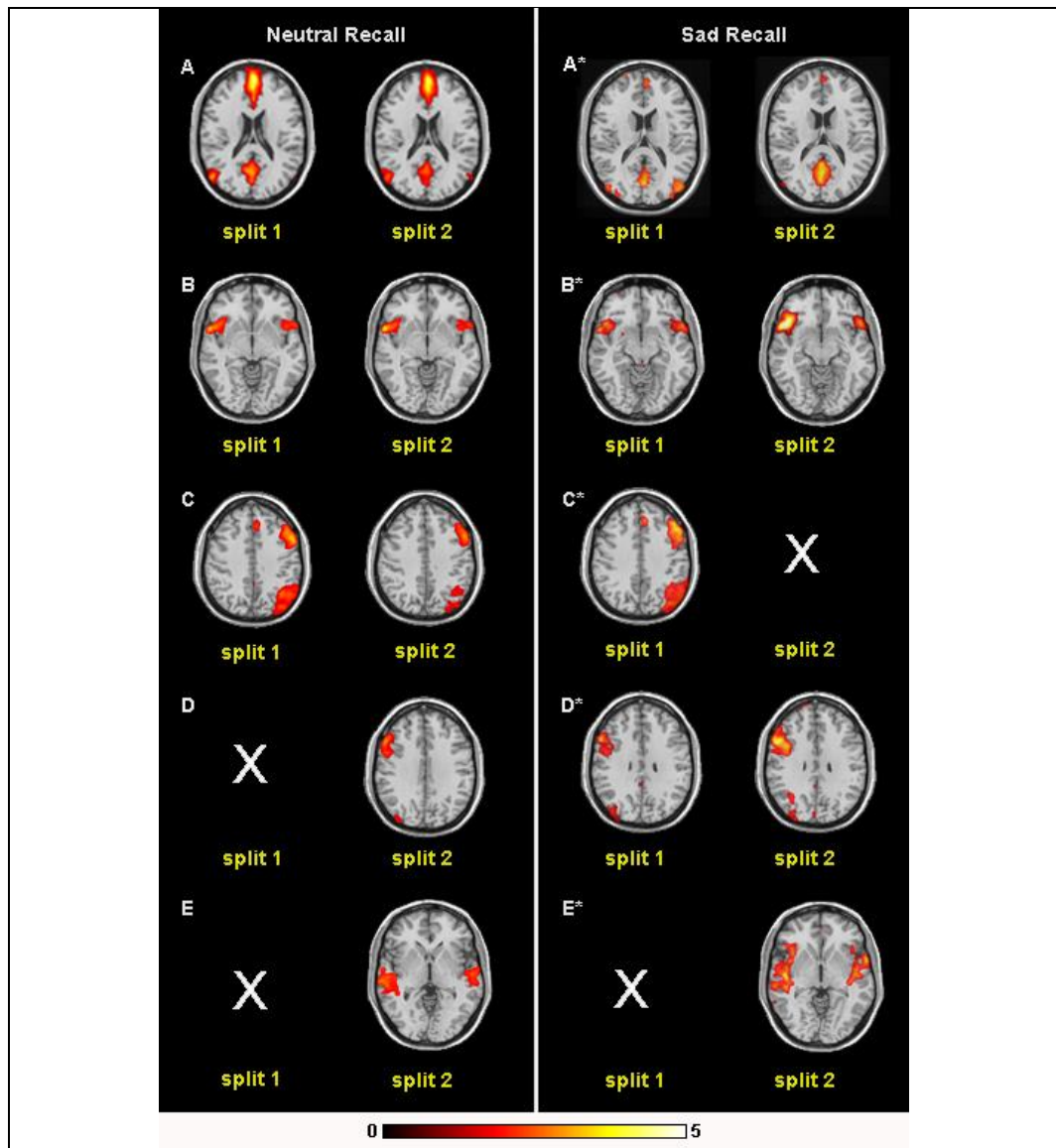


Figure 18 Results of the split-half reproducibility analysis

Split-half analysis of resting-state networks. Assessment of the reproducibility of group ICA findings with the use of simple half-sample analysis repetition of the neutral and sad recall conditions. For both analyses, the split groups were assigned using a pseudo-random order. All images are presented on a high-resolution single-subject MRI in standard neuroanatomical space (Montreal Neurological Institute, Colin-27). Corresponding color bars indicate the z score ranges of the displayed maps. Images are displayed in neurological convention (left = left).

7.3.3 Significance testing of changes in resting state networks

Figure 19 shows the relative changes of functional connectivity that were observed in each RSN between the two task conditions (visualization threshold at $p < 0.005$). These changes occurred as either increases or decreases in the statistical magnitude and/or extent of regional clusters showing correlated activities in the very low frequency domain (< 0.04 Hz) as shown by the signal analysis below. These five common networks and their changes can be summarized as follows. All statistics are reported as peak z-score in coordinates (mm) according to the MNI standard space, CS=cluster size.

Default Mode Network: included primary clusters in the posterior cingulate and medial prefrontal cortices as well as the angular gyri. Specific regions that showed decreased functional connectivity during the sad recall condition (A-A*) included the dorsal and ventral posterior cingulate cortex (-9,-63,27 mm; $Z=4.1$; CS=226 voxels), bilateral angular gyri (45,-78,36 mm; $Z=3.53$; CS=61 voxels) (-54,-63,21 mm; $Z=2.93$; CS=62 voxels), ventral medial frontal cortex (-3,48,21 mm; $Z=3.34$; CS=251 voxels) and caudate nucleus (9,12,3 mm; $Z=3.61$; CS=26 voxels).

Paralimbic network: included clusters located primarily in the dorsal anterior cingulate and insula cortices, supplementary motor area and dorsal medial frontal cortex. Specific regions that showed increased functional connectivity during the sad recall condition (B* -B) included the dorsal anterior cingulate (3,-6,42 mm; $Z=3.44$; CS=168 voxels) and supplementary motor area (3,-9,60 mm; $Z=2.97$; CS=21 voxels), left anterior insula (-42,15,-9 mm; $Z=3.64$; CS=50 voxels) and opercular region (-57,12,-3 mm; $Z=3.47$; CS=22 voxels).

Right frontoparietal network: included clusters lateralized to the right hemisphere, including the lateral prefrontal (medial and inferior frontal gyri), the inferior parietal cortices, caudate nucleus and supplementary motor area. Specific regions that showed increased functional connectivity during the sad recall condition (C* - C) included the right inferior frontal gyrus (3,36,51 mm; $Z=3.04$; CS=53 voxels), anterior insula (39,24,-9 mm; $Z=2.54$; CS=11 voxels), superior frontal gyrus (3,36,51 mm; $Z=3.04$; CS=53 voxels) and inferior parietal cortex (51,-66,45 mm; $Z=2.8$; CS=36 voxels).

Left Frontoparietal Network: included clusters lateralized to the left hemisphere, including the lateral prefrontal cortex (superior, medial and inferior frontal gyri), inferior and superior parietal cortices, thalamus and caudate nucleus. Specific regions that showed increased functional connectivity during the sad recall condition ($D^* - D$) included the left medial (-39,3,45 mm; $Z=3.92$; $CS=849$ voxels) and superior frontal gyrus (-3,6,57 mm; $Z=3.26$; $CS=98$ voxels) and inferior parietal cortex (-42,-54,39 mm; $Z=2.69$; $CS=8$ voxels).

Auditory Cortex Network: included clusters located primarily in the lateral superior temporal cortex and posterior insular cortex. Specific regions that showed increased functional connectivity during the sad recall condition ($E^* - E$) included the right posterior insula (39,-12,6 mm; $Z=3.79$; $CS=287$ voxels) and left mid-temporal cortex (-54,-9,0 mm; $Z=3.63$; $CS=79$ voxels).

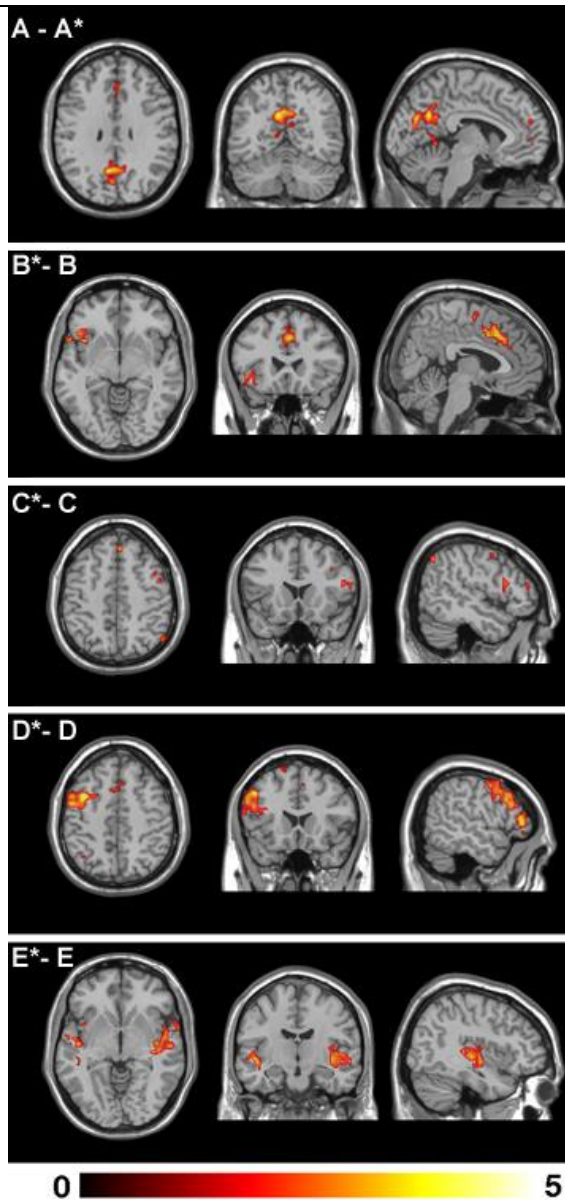


Figure 19 Modulation of Resting-State Networks by Mood Induction

Global functional connectivity differences observed between the neutral and sad recall conditions for the common RSNs. The top panel A - A* indicates an apparent *decrease* in intranetwork functional connectivity of the default mode network between the neutral and sad recall conditions. All other panels indicate apparent *increases* of intranetwork functional connectivity during the sad compared to neutral recall condition. All images are presented in standard neuroanatomical space. Corresponding color bars indicate the t score ranges of the displayed maps. Images are displayed in neurological convention (left = left)

7.3.4 Signal analysis of the resting state networks

Each RSN's PSD averaged across subjects showed good fitting to the $a+bf^{-1}$ model previously described for raw BOLD signal analysis, with a Pearson's r^2 range of 0.97 to 0.55. Dominant oscillating frequencies were observed as one or more clear peaks above this baseline, typically around 0.03 Hz.

All networks had predominant power density distributions in the very low frequency domain (0.01–0.04 Hz), similar to previously published fMRI studies of spontaneous resting-state conditions (Biswal et al. 1995; De Luca et al. 2006; Kim et al. 2013). An example of this assessment is provided in Figure 20. For the five common RSN pairs, there were no significant differences in their relative proportions of power distributed within this range (p value range = 0.19–0.58), indicating that these signal variations were similar between the neutral and sad recall conditions.

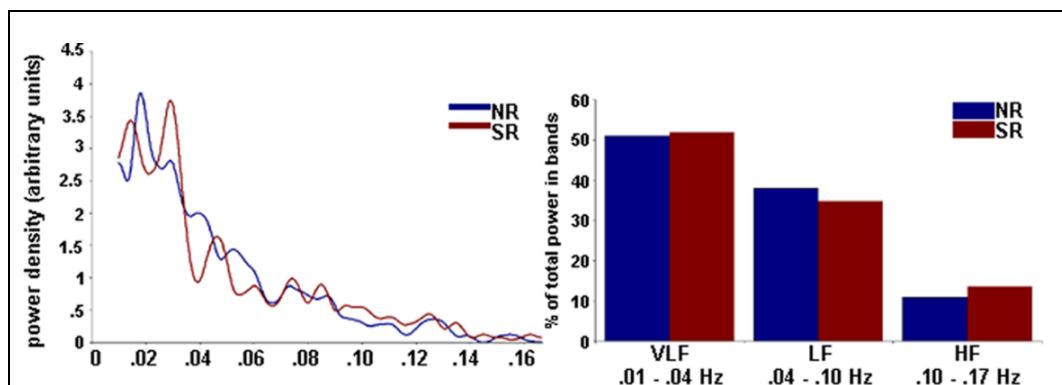


Figure 20 Spectral analysis of ICA results

Left: A representative mean power spectral density plot for one component of interest (default mode network; represented as A and A* in Figure 17). For all networks, the highest power density was observed below 0.04 Hz. *Right:* Proportion of power in the three non-overlapping frequency bands for the default mode RSN associated with the neutral and sad recall conditions. All identified components showed the highest percentage of power in the very low frequency band. LF = low frequency; VLF = very low frequency; HF = higher frequency. NR = neutral recall; SR = sad recall.

7.3.5 Confirmatory seed-based cross-correlation analysis

To confirm the changes in functional connectivity identified with ICA in the major regions of interest, our primary seed ROIs were located in the dorsal anterior cingulate cortex ('paralimbic' RSN; MNI $x, y, z = 3, -3, 51$ mm; 260 voxels) and the posterior cingulate cortex ('default mode' RSN; MNI $x, y, z = -3, -69, 21$ mm; 367 voxels), respectively. Our primary target ROIs were located in the right anterior insula cortex ('paralimbic' RSN; MNI $x, y, z = 48, 18$ mm, -12 ; 145 voxels) and the medial frontal cortex ('default mode' RSN; MNI $x, y, z = -9, 51, 36$ mm; 1062 voxels), respectively.

Consistent with the group ICA findings, both RSN patterns were reproduced by the seed-based cross-correlation approach (Figure 21). For the paralimbic network, we observed a significant increase of functional connectivity between the dorsal anterior cingulate and right anterior insula cortex in the sad recall relative to neutral recall condition (MNI $x, y, z = 48, 21$ mm, -15 ; $z = 2.86$; 24 voxels). By comparison, for the default mode network, there was also decreased of functional connectivity between the posterior cingulate and medial frontal cortex in the sad relative to neutral recall condition (MNI $x, y, z = 6, 54, 12$ mm; $z = 2.93$; 23 voxels).

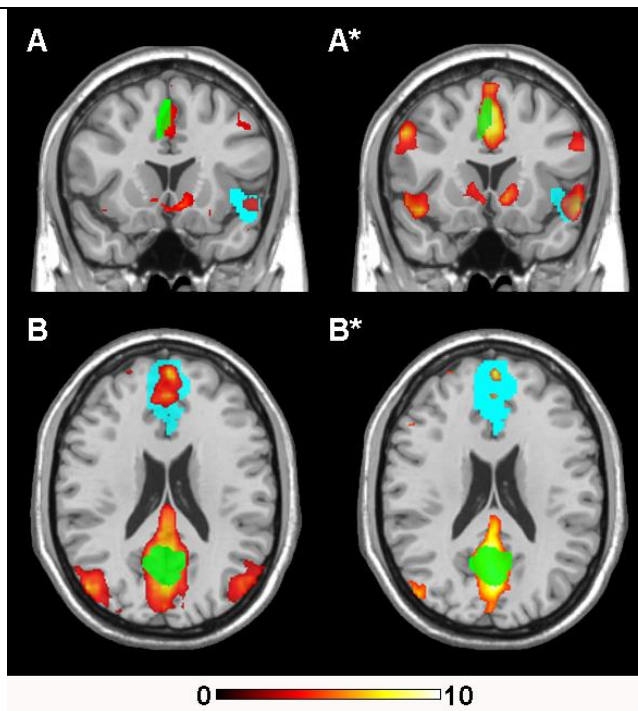


Figure 21 Cross-Correlation analysis of representative resting-state Networks

Regional functional connectivity maps of the ‘paralimbic’ (A) and ‘default mode’ (B) resting state networks. Green clusters represent the two seed ROIs while the blue clusters represent their respective target ROIs. Both ROI types are overlaid on the regional functional connectivity maps derived from the cross-correlation analyses. All images are presented in standard neuroanatomical space. Corresponding color bars indicate the t score ranges of the displayed maps. Images are displayed in neurological convention (left = left).

7.4 Discussion and conclusions

The results obtained in this study support the idea that measurable changes in component connectivity maps can be obtained from very subtle changes in the individual’s state. In this study, the five networks explored showed significant changes in the connectivity scores after sad mood induction. The selected behavioral task was proven effective to induce a significant emotional change to the individuals explored and the selected analysis methods generated results that are in line with the results of previous studies on mood induction (Phan et al. 2002).

While we consider that the subjects under study were in a “resting-equivalent” status, it is important to recognize that the mood induction task involved an active

memory recall exercise of a sad event. This was counterbalanced by experimental design in the neutral condition by the recall of a routine day. Despite being very mild cognitive-demanding tasks, the conditions we used may have subtle differences compared to a pure “resting state” experiment, in which mind wandering may drive a singular profile of brain activity (Braboszcz & Delorme 2011). Therefore, caution shall be taking before directly inferring our results to pure resting state paradigms. Further experiments shall be conducted to demonstrate if the observed network alterations are also evident in pure resting state paradigms.

The results obtained may be limited by the relatively short scan length used in this study. However, as in study 2, ICA was able to isolate a set of resting state networks that was majorly reproducible across subject states and that in most of the cases survived to the split-half confirmatory analysis. This is relevant, provided that the stability of ICA connectivity studies has been reported to have a steep decrease in scan durations below 4 minutes (Birn et al. 2013). On the other hand, sustaining an induced sad mood for longer periods of time would have been more difficult for the volunteers, setting the compliance of the experimental condition at risk. Further studies may benefit from recent methodological works developing chronnectomic techniques, which try to disentangle the short term existence of connectivity patterns (Allen et al. 2014). Short-term existence of networks conflicts with the spatial stationarity assumption that our ICA approach used.

The usage of ICA component connectivity maps to compare two experimental conditions poses an unsolved methodological question: The spatial independent component analysis can be performed by concatenation of the complete dataset (that is the two conditions merged into a single analysis) or by estimating component connectivity effect size per separate in each condition and later comparing across them. Both options have been used in the literature (Calhoun et al. 2008; Arbabshirani et al. 2013) by the team who developed GIFT, the software package that implements the algorithms used in our study. When concatenating all image sets in a single ICA, the analysis is vulnerable to lose sensitivity in cases where networks are spatially different across conditions, as ICA’s performance is optimum when the network is spatially stationary. On the other hand, executing the analysis in two runs requires an additional step of matching the identified

networks across the results of two analyses, which requires expert neuroscientific judgement and is subject to human error. In the event of having a network that significantly changes its anatomy across the two analyses, inference on its comparison may be doubtful and should not be performed without extreme awareness of its limitations.

It is important to stress the limitations in the ability to infer connectivity strength from the comparison of ICA spatial maps. The comparison of seed-based cross-correlation is much more widespread as this analysis is simpler and relates to the complete fraction of signal. Despite a moderate correlation has been reported in the comparison of resting-state seed-based maps and ICA maps (Rosazza et al. 2011), when comparing ICA maps across populations or states it is important to bear in mind the “variance segmentation” nature of the signal processing made. Having 2 regions of interest with strongly correlated time courses will lead to a clear result if the signal of one of the ROIs is used as a seed in a seed-based cross-correlation analysis: The connectivity of both ROIs will be solidly identified. This will also be the case in ICA analysis as long as the signal of these two ROIs majorly corresponds to that of one of the identified spatially independent components identified. In an opposite situation, if the variance of the signal of these ROIs is explained by a mixture of a mid to large amount of components, these two ROIs may not be identified as part of any network, despite being strongly correlated. When comparing spatial connectivity effect size of two different states with ICA, it is important to question whether there could have been a significant reorganization of the functional connectivity of the brain networks involved, before assuming that these changes reflect real changes in functional connectivity. Confirmatory post-hoc seed-based cross-correlation analysis (with or without regressing out the signal of other ROIs) are a wise recommendation for studies attempting to infer macroscopic functional connectivity changes using ICA.

We cannot hypothesize why two components were not reproduced in the sad recall condition. A number of reasons could explain it, ranging from technical limitations or because of true experimental effect on connectivity of these areas. The fact that a large number of components were considered noise or non-relevant evidences that a fraction

of the fMRI signal was excluded from the analysis because of being considered noise or not being coherent enough to generate a component in the ICA.

The signal spectrum of the networks identified was highly reproducible across networks and states, emphasizing the idea that the networks identified effectively show a stable large-scale set of networks. These networks are also backed up by basic neuroscience knowledge and in line with the regions recruited or affected by an experiment such as ours. Similar signal spectrum results have been obtained in the intraoperative context using direct optical readings of oxyhemoglobin concentration in the capillary bed (Rayshubskiy et al. 2014). Our spectral analysis procedure was similar to that used by Calhoun et al in a study aimed to reveal differences between schizophrenic patients and controls in the connectivity changes related to a cognitive task versus rest (Calhoun et al. 2008). Calhoun et al also reported that the power spectrum distribution of the temporal signal representing the extracted components did not significantly change across experimental conditions.

The seed-based connectivity analysis provided a valuable confirmation that the changes identified by analyzing the ICA results were indeed representative of the macroscopic connectivity changes in the brain. Note that the seed-based connectivity analysis is not affected by the exclusion of “unstable” or “noise” components, the complete signal is used in this case.

These results support recent findings that the resting state functional connectivity may be affected by the subject’s state immediately before the scanning (Tailby et al. 2015). Therefore, executing resting state paradigms in rigid protocols that replicate the conditions before the scan may reduce the variance observed across subjects.

Taking everything into account, our findings suggest that ICA-extracted component connectivity maps reflect very subtle changes in the emotional state of the subject. This reinforces our hypothesis that resting state ICA analyses could become valuable contributors in the spectrum of biomarkers for clinical improvement on psychiatric patients.

8 Study 4: Characterization of SAD's expression using a novel symptom provoking fMRI experiment in patients and controls.

8.1 Introduction

In the study of the neural expression of phobias, study of the brain activations encompassing specific symptom provocation is a common choice (Etkin & Wager 2007). While some potential biomarkers exploit differences in indirect brain mechanisms – like the emotional face processing paradigm in study 1-, it is still interesting to evaluate SAD patients in a direct approach involving symptom provocation. Given the nature of the fMRI setup, it is impossible to fully replicate a natural social interaction scenario. Therefore, fMRI experiments aiming to explore brain responses to symptom-provocation stimuli always require some degree of abstraction of the stimuli and, therefore, a thorough validation of the model.

Social anxiety symptom-provocation PET-based studies have been frequently reported using overt speaking situations in front of a reduced public (Tillfors et al. 2001; Åhs et al. 2006; Furmark et al. 2008). However, overt speaking in fMRI is considered as a highly unfavorable situation due to the induced artifacts (Birn et al. 1998; Barch et al. 1999; Birn et al. 2004) and its usage is restricted to experiments in which it is indispensable, such as surgical planning (Croft et al. 2013).

Functional MRI studies of SAD have been performed using a wide range of symptom-provoking stimuli. This includes angry face visualization (M. B. Stein et al. 2002), although similar results have been reported with neutral faces (Cooney et al. 2006). Actually, simple gaze is now considered as a salient symptom-provoking stimulus, which has been shown to trigger powerful responses in SAD patients (Cavallo et al. 2015). Other fMRI experiments involved the processing of anger prosody (Quadflieg et al. 2008), script-driven imaginary of anxiety-provoking social situations (Kilts et al. 2006), responding to cognitive challenging tests (Sareen et al. 2007), anticipation of a public speaking task (Lorberbaum et al. 2004) or exposure to criticism and negative self-beliefs (Ziv et al. 2013).

Like in all fMRI-based phobic symptom-provoking paradigms, it is important to take into account that social phobia responses can encompass intense physical symptoms including blushing, heart rate acceleration, sweating, trembling or nausea (Stein & Stein 2008). The associated physiologic alterations can create irreversible artefactual degradation of the fMRI BOLD signal or even lead the individual to avoid the anxiety-provoking situation. Therefore, in such experiments, it is key to carefully contain the degree of distress induced to the subject by the experimental condition to mild and bearable levels.

Despite the brain networks related to harsh social stimulus processing are fairly described, the differential neural circuitry activations detected when comparing patients with controls in these experiments has led to heterogeneous results, which may be related to the methodological differences (Freitas-Ferrari et al. 2010). Until the neural expression of SAD becomes fully understood, it is highly valuable that the neuroimaging community continues developing paradigm variants and continues reporting the differential findings so a more holistic model can be developed.

In this study, we assessed the neural response of patients to self-recognition when exposed to scrutiny and evaluation by others. Specifically, the experiment involved presenting patients and controls with prerecorded video sequences of themselves performing a verbal memory task, in a session during which the examiners acted as a scrutinizing audience and rated the performance of the subject under study through the examination of his/her video recording.

We anticipated that the neural response in this situation would involve robust activation of distributed brain regions in patient and control groups. Indeed, simple visual recognition of one's own face is associated with the activation of a complex cortical network involving the inferior occipito-temporal cortex, inferior frontal and parietal cortices, the medial frontal gyrus and the anterior cingulate cortex (Devue & Brédart 2011). We also expected that a potentially tense scrutiny perception situation would lead to relevant engagement of emotion and arousal systems including the activation of the

amygdala and the thalamus in addition to the insular, cingulate and prefrontal cortices (Barrett et al. 2007).

The first line of thought could lead us to expect that the anxiety generated by a symptom provocation task in SAD would be associated with a heightened activation in response to the stimulus. However, the literature review reveals that, in SAD symptom provocation tasks, it is common finding a reduced activation in brain areas devoted to evaluative processes of emotion (Tillfors et al. 2001; Lorberbaum et al. 2004). Similarly, imagining socially threatening situations was associated with cortical activity reductions in SAD patients (Kilts et al. 2006; Nakao et al. 2011). Of note, confronting patients with negative self-beliefs (Goldin, Manber-Ball, et al. 2009) and first-person negative appraisals (Blair et al. 2011) has also been associated with reduced early activation in cortical areas related to cognitive emotion control.

In the context of our task, we predicted that SAD patients overall would not show a generally higher response than control subjects. Instead, we anticipated that patients would demonstrate a combination of activation increases in systems mediating emotional reactions (Tillfors et al. 2001), together with reduced activation of cortical areas driving the cognitive control of anxiety (Bishop et al. 2004).

8.2 Methods

8.2.1 Subjects

A total of 20 patients with generalized SAD were recruited through public media advertisement (local newspapers and poster advertisements). Participants contacted the study center (Pharmacology Research Unit) by email and then a clinical researcher performed a preliminary interview by telephone. A screening visit was performed thereafter to confirm inclusion/exclusion criteria and good physical health by a complete physical examination. Inclusion criteria were: (a) out-patients with a primary psychiatric diagnosis of generalized SAD according to DSM-IV-TR criteria (APA 2000) (b) A Liebowitz Social Anxiety Scale (LSAS; Liebowitz, 1987) score ≥ 50 , and (c) participants aged between 18 and 60 years. Patients with relevant medical or neurological disorders, or other DSM-

IV Axis I disorders, were not considered for inclusion. All subjects were free of any history of substance dependence or current substance abuse, and all provided a negative urine toxicity and breath alcohol screen. In addition, subjects receiving any current psychotherapy or pharmacological treatment were not included. The finally selected sample represents a notably homogeneous SAD group of generalized type (no cases showing only performance-related SAD were included) with childhood onset of symptoms and significant distress and interference in the patient's life, but with no current treatment that could confound the study results. The LSAS score of this patient cohort was (mean \pm SD) 80.7 ± 16.2 .

A group of 20 healthy volunteers matched by age, educational status and gender distribution were recruited. These control participants satisfied the same health conditions and also showed negative results in the toxicity screen. All participants were right-handed. The LSAS score of the control cohort was (mean \pm SD) 24.4 ± 5.6 .

Written informed consent was obtained from all participants. The study was approved by the local ethics committee (CEIC-IMAS, Barcelona) and in compliance with the declaration of Helsinki.

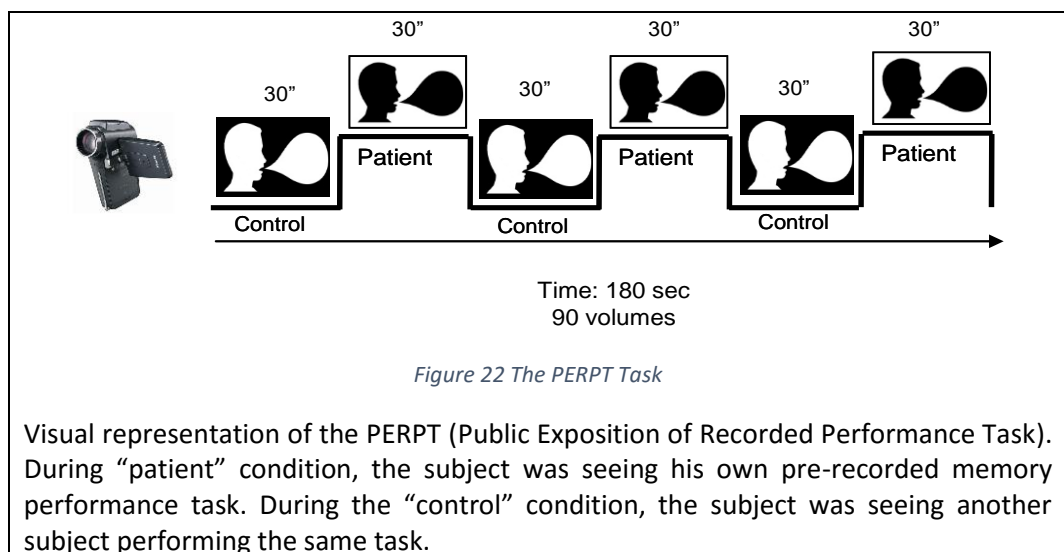
8.2.2 The novel experimental task

Before scanning, participants' verbal task performances were video-recorded privately in a laboratory setting. They underwent a memory task adapted from the Wechsler Memory Scale – Revised (Wechsler 1981), which involves a single presentation of verbal narratives to be recalled and repeated immediately. Subjects were asked to listen to and repeat aloud three stories. During each repetition, video sequences of 30 seconds duration were recorded at a short distance. Public exposure to the video segments occurred only during the fMRI session when both the subject and the research team viewed the scenes.

Participants were informed that a clinical psychologist would evaluate their memory performance during the imaging session according to formal guidelines. As a control condition, equivalent video segments featuring unknown 'other' subjects

responding to the same stories were used. These ‘others’ were matched in terms of age and gender to each individual study participant. We maintained a stable background (neutral white color) and framing (fixed general short plane) in all videos, and avoided possible distracters such as loud colors for clothes, hairstyle or accessories (large pendants or earrings).

In total, the fMRI experiment consisted of six alternating 30-second blocks of the control (other) and experimental (self) conditions. It is important to note that the experiment required no actual performance during scanning. In this way, the neural response shows no influence from actions and mental operations related to performance nor speech. This may facilitate the interpretation of results and provide data less affected by head motion artifacts. Total recall execution scores during the videos were not collected, as the task finished once a 30-second video was successfully recorded. To assess the quality of execution, we considered relevant that participants were talking during most (80%) of the recording periods. That is, periods of silence during recording never exceeded 20% of the time. Experimental and baseline conditions were also equated in this performance parameter.



8.2.3 Out of scanner behavioral experiment

Because of the complexity of the fMRI session, the assessment of task behavioral effects was completed in a separate experiment that included eye-tracking records to rule out possible visual avoidance strategies in SAD patients during symptom provocation (Horley et al. 2004).

The separate experiment was conducted in a subgroup of 30 participants (15 SAD patients and 15 control subjects, also matched by age, educational status and gender distribution), who consented to undergo the behavioral study protocol a second time. This assessment was carried out several months after the primary study, minimizing possible retest effects. The evaluation procedures adopted during the fMRI session were reproduced in this experiment and the subjects' gaze was monitored using an eye-tracking system. At the end of the session, the subjects were asked to fully describe their subjective experience and to rate the emotion perceived using 101-numerical rating scales (0 being not at all, 100 the maximum possible). Rates for "anxiety" were used as the main outcome measurement and 18 additional descriptors served to characterize the nature of the generated emotion (i.e., alert, anger, apathy, calm, discouragement, displeasure, distress, embarrassment, lack of interest, negative excitement, negative thoughts, nervousness, pleasure, positive excitement, problems to maintain the attention, restlessness, stress and tension).

Real-time "free binocular viewing" behavior was recorded continuously during the task using a high resolution eye tracking system (T60 Tobii Technology AB, Stockholm) and the data were analyzed using Tobii Studio™ analysis v2.1.1.3 software. The stimuli videos were presented full-screen on a 17" monitor with a resolution of 1280x1024 pixels. The Eye Tracker device collected eye movement data with a 60-Hz sampling rate. For the analysis, we computed for each block (i) the total number of visual fixations on the presented scenes, (ii) fixations specifically on the eyes of the person appearing in the video, and (iii) time spent for visual fixation on this eye area (expressed as a percentage of block duration).

Between-groups differences in behavioral and physiological variables were tested using parametric (Student-t) tests when normally distributed and non-parametric (Mann-Whitney) tests when distribution did not follow a normal pattern.

8.2.4 Physiological data acquisition

Heart rate was monitored continuously during fMRI scans using a photoplethysmograph placed on the left index finger (Model 4500MRI, Invivo Corp., USA). The device provided an output signal for each arterial pulsation that was registered using software developed in-house on the Labview 8.0 platform (National Instruments Corp., USA). Scanner trigger pulses were also registered to allow accurate synchronization of physiological signals with the fMRI data. Data were analyzed and plotted using procedures similar to those we reported in a previous study (Caseras et al. 2010). The beat-to-beat interval was calculated and the inverse of each interval was designated as the beat-to-beat heart rate. The evoked response to the experimental (self) condition was calculated as the heart rate increase in relation to the preceding control (other) block. Group mean heart rate was also calculated for each block.

8.2.5 Image acquisition

The MRI system was the same as used in Studies 1 and 2. That is, a 1.5 Tesla Signa Excite system (General Electric) equipped with an eight-channel phased-array head coil and single-shot echoplanar imaging (EPI) software was used. The MRI sequence was highly equivalent to that described in section 5.2.3.2. Functional sequences consisted of gradient recalled acquisition in the steady state [time of repetition (TR), 2000 ms; time of echo (TE), 50 ms; pulse angle, 90°] within a field of view of 24 cm, with a 64 x 64 pixel matrix and a slice thickness of 4 mm (plus an interslice gap of 1.5 mm). Twenty-two interleaved slices, parallel to the anterior–posterior commissure (AC–PC) line, were acquired to cover the whole brain for all functional sequences. The first four (additional) images in each run were discarded to allow the magnetization to reach equilibrium.

8.2.6 Image analysis

8.2.6.1 Preprocessing

Image preprocessing followed a similar pipeline as in studies 1 and 2 (See section 5.2.4.1 for a detailed description). In summary, it was preprocessed using SPM5 (www.fil.ion.ucl.ac.uk/spm) by doing motion correction, spatial normalization to the MNI template and smoothing using a Gaussian filter of 8 mm of full-width to half-maximum.

8.2.6.2 Task effect statistical analysis

Single-subject (first-level) SPM contrast images were estimated comparing the 'self' condition with the 'other' condition. For these analyses, the fMRI signal response at each voxel was modeled using the SPM canonical hemodynamic response function (Friston et al. 1999). The resulting first-level contrast images were then carried forward to subsequent second-level random-effects (group) analyses.

One-sample t-statistic maps were calculated to obtain task-related activations and deactivations, and two-sample t tests were performed to map between-group differences.

Voxel-wise analysis in SPM5 was also performed to map the correlation between brain activation and both task-related anxiety ratings and LSAS scores. The task-related anxiety ratings were (i) 'anxiety before minus anxiety after scanning', as a representative measurement of anticipatory anxiety obtained in the fMRI session day, and (ii) 'anxiety during 'self' condition minus anxiety during 'other' condition', as a task-evoked anxiety measurement obtained in the out-of-scanner experiment.

A threshold $p_{\text{FDR}} < 0.05$ whole-brain corrected was used throughout this study. In one-sample t-test maps, only activations surviving this conservative threshold are reported. For between-group comparisons and correlation maps, changes involving a minimum cluster extension of 15 voxels at $p < 0.001$ uncorrected were also reported, which may provide an optimal balance between type I and type II errors (Lieberman & Cunningham 2009). In figures, an activation threshold of $p < 0.01$ is used for display purposes.

8.3 Results

8.3.1 Task-induced brain activation

The neural response to the 'self' versus 'other' condition produced robust activation in regions involved in self-face recognition (extrastriate visual cortex, right inferior frontal gyrus and medial frontal gyrus) and emotional response/general arousal (bilateral anterior insula, anterior cingulate cortex, bilateral amygdala, upper brainstem, thalamus, basal ganglia and cerebellum) in both SAD patients and control subjects. SAD patients showed additional activation in the primary visual cortex but the activation in midline regions was less extensive (see top row of Figure 23). Significant deactivation during the 'self' condition was observed only in the patient group in the dorsal prefrontal and parietal neocortex (see bottom row of Figure 23). The direct between-group comparison showed no differences surviving the false-discovery rate (FDR)-corrected threshold. Nevertheless, as shown in Figure 24, increased activation in the primary visual cortex, reduced activation in the medial frontal gyrus and the anterior cingulate cortex, and more pronounced deactivation in the dorsolateral prefrontal cortex were identified in SAD patients compared to control subjects when observed with a significance threshold of $p < 0.001$ uncorrected (minimum cluster extension >15 voxels).

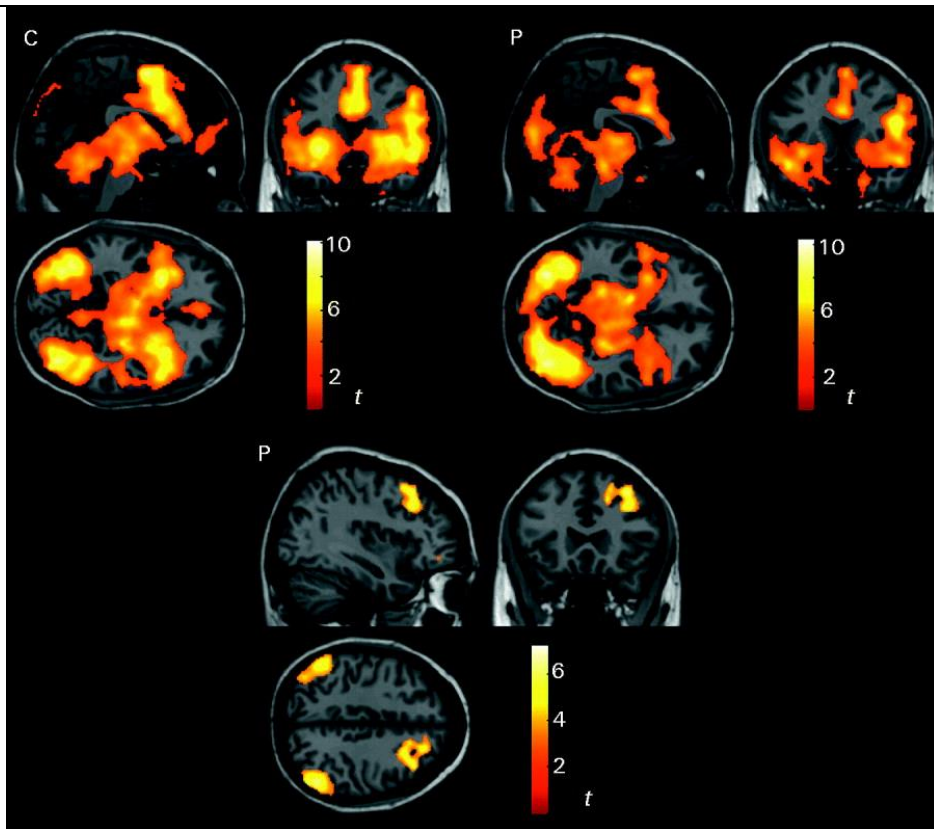
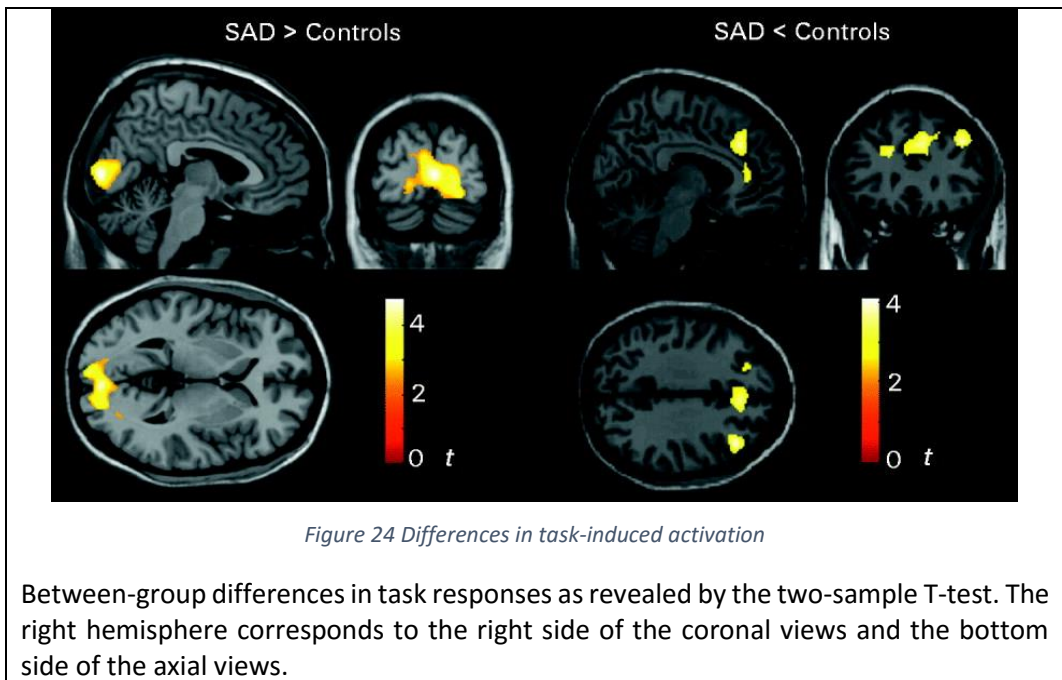


Figure 23 Task-induced activation

Top: neural response to the task –activations- as revealed by separate one-sample T-tests for control subjects (C) and social anxiety disorder (SAD) patients (P).

Bottom: Deactivation maps for SAD patients. Deactivation in control subjects did not reach the significance level. The right hemisphere corresponds to the right side of the coronal views and the bottom side of the axial views.



8.3.2 Correlation of brain activation with task-related anxiety ratings

SAD patients showed a notable amount of anxiety before the fMRI assessment (mean \pm SD = 54.5 \pm 19.8 %). Using ‘anxiety before minus anxiety after scanning’ as a measurement of anticipatory anxiety, we observed a negative correlation with cortical activation within the patient group ($p < 0.001$ uncorrected, cluster >15 voxels) (Figure 25a). Anxiety ratings obtained in the separate behavioral experiment similarly showed negative correlations with brain activation, in this case combining patients and controls in the measurement of anxiety during ‘self’ condition minus anxiety during ‘other’ condition (Figure 25b). Notably, in both analyses the areas with negative correlations implicated the frontoparietal-cingulate network that showed significant deactivation or reduced activation during the task in patients.

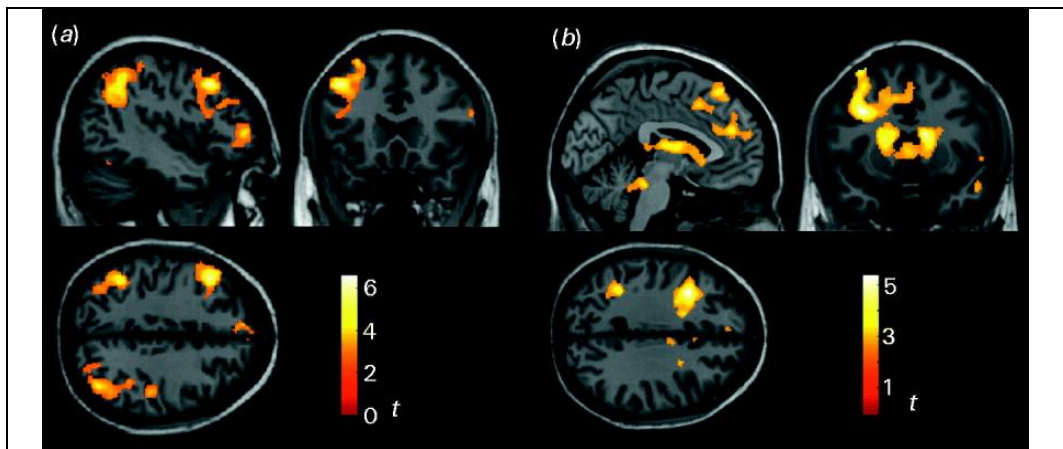


Figure 25 Correlation of brain activation with task-related anxiety ratings

a) Correlation maps of brain activation with anticipatory anxiety before functional magnetic resonance imaging (fMRI) in 20 patients.

(b) Correlation maps of brain activation with anxiety provoked by the task in the separate experiment combining patients and control subjects (total $n = 30$). The right hemisphere corresponds to the right side of the coronal views and the bottom side of the axial views.

8.3.3 Correlation of brain activation with social anxiety scores

The correlation between LSAS scores and the observed brain response showed a clear tendency to differ between groups. LSAS correlated positively with brain activation in control subjects in regions where SAD patients showed negative correlations. The map of the interaction between groups for the correlation of LSAS with brain response summarizes this effect (Figure 26). Regions showing an interaction effect included the mesencephalic tegmentum, the thalamus, hypothalamus, ventral striatum, medial and posterior orbitofrontal cortex, occipitotemporal areas and the right dorsal (medial and lateral) frontal cortex. The interaction effect is illustrated with a plot including both controls and patients in Figure 26. For this plot, the relationship between LSAS and brain activation was best explained by a quadratic or inverted U-shaped function ($r = 0.75$, $r^2 = 0.56$, $p < 0.00001$).

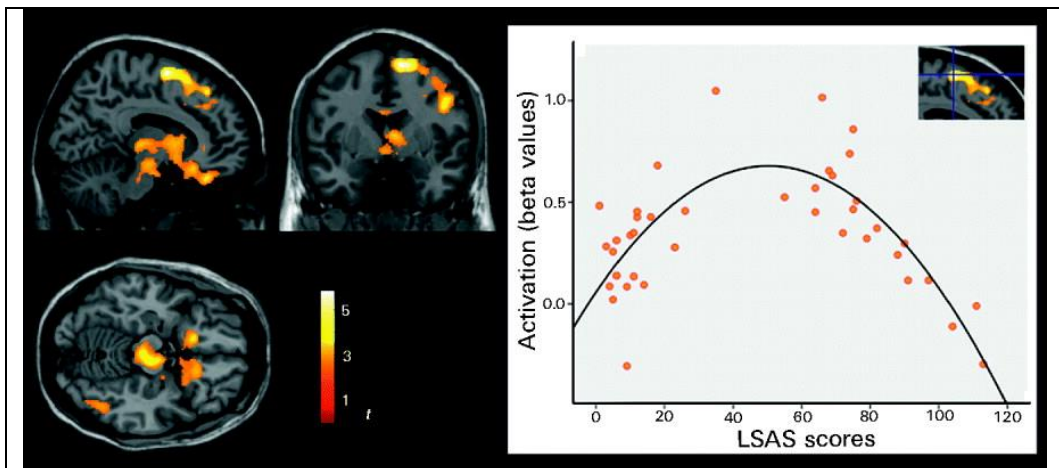


Figure 26 Correlation of brain activation with Liebowitz Social Anxiety Scale (LSAS) scores

The map corresponds to the interaction between groups and displays voxels showing a positive correlation significantly greater in control subjects than in patients (or a negative correlation significantly greater in patients than in controls). The right hemisphere corresponds to the right side of the coronal view and the bottom side of the axial view. The plot illustrates the interaction effect. A quadratic function or an inverted-U function provided the best explanation for the relationship.

8.3.4 Analysis of physiologic monitoring data

Recorded heart beat data were optimal (>95% of beats registered) for all but three participants who were subsequently excluded from this analysis (one control subject and two patients). SAD patients showed a tendency to lower heart rate during each paradigm phase; in terms of the whole experiment, control subjects showed an average heart rate of 78.8 ± 10.3 beats/min and SAD patients 72.2 ± 9.5 beats/min ($t = 2.0$ and $p = 0.051$). The response to the 'self' condition was characterized by an initial increase in heart rate in control subjects (Figure 27). This physiological reaction, however, was mostly absent in SAD patients. The mean initial (5 seconds window) heart rate increase across the three 'self' condition blocks was 1.9 ± 2.6 beats/min in control subjects and 0.4 ± 1.1 beats/min in SAD patients ($t = 2.4$ and $p = 0.025$).

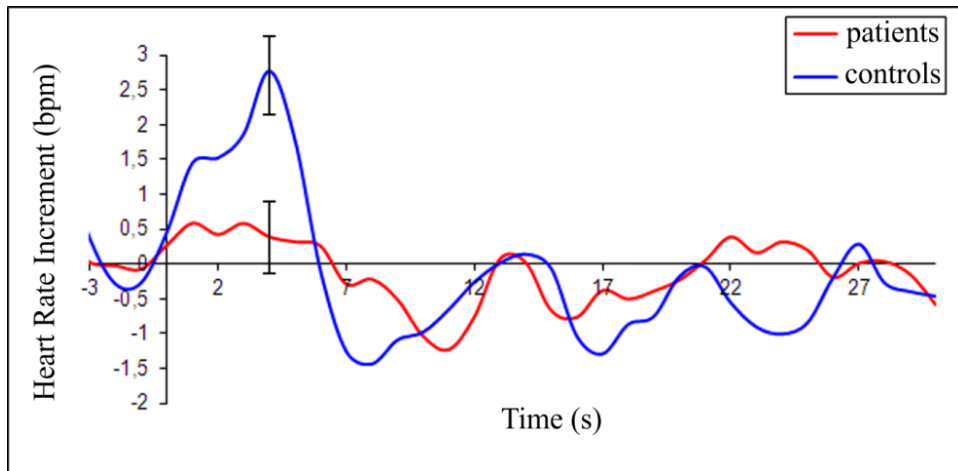


Figure 27 Physiological assessment of task response for patients and controls

Plot of heart rate evolution during the “self” condition averaged across blocks and subjects. Note that the initial heart rate increment observed in the control subject group was almost absent in patients. Vertical bar denotes standard error of the mean.

8.3.5 Out of scanner behavioral experiment

Anxiety ratings: The exposure to one’s own pre-recorded performance generated a significant amount of anxiety in SAD patients (mean+SD points in the 101-numerical rating scale in controls, 15.3+18.5; in SAD, 58.3+29.0; $Z=-3.8$; $p=0.00006$). Group differences were also significant for the variable “anxiety during *self*” condition minus “anxiety during *other*” condition (10.7+20.9 in controls and 37.7+26.8 in SAD; $Z=-3.0$; $p=0.002$). SAD patients gave higher scores to all descriptors closely related to anxiety.

Eye tracking: During the “self” condition, SAD patients made more visual fixations on the screen than control subjects (controls: 111.7+41.5; SAD patients: 144.6+31.6; $Z=-2.4$ and $P=0.016$). The number of visual fixations specifically on the eye area, however, did not significantly differ between groups (controls: 36.6+23.2; SAD patients: 34.20+17.4; not significant). Additionally, there were no significant group differences in the percentage of time involving visual fixations on the eyes during this condition (controls: 37.4%+25.9%; SAD patients: 25.8%+12.8%; not significant). No between-group differences were observed for any measurement related to the “other” condition. The overall results indicate that patients showed a different visual scanning approach (Figure

28), although the data do suggest that patients' strategy did not overtly involve eye area avoidance.

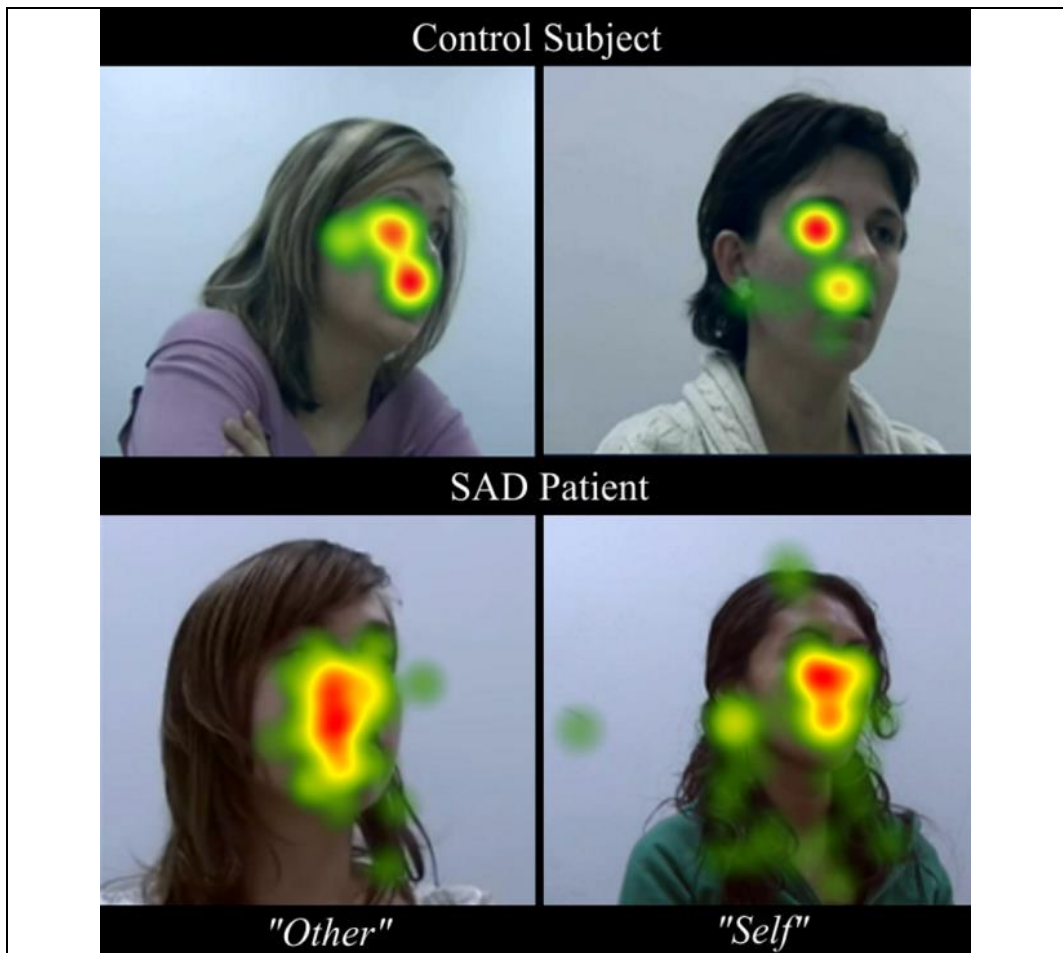


Figure 28 Eye tracking assessment

The pictures show the data from an illustrative single control subject (top) and a patient (bottom). The color “heat maps” typically represent visual fixations on each screen point averaged across blocks for the “other” condition (left) and “self” condition (right). (Red color indicates the most observed areas).

8.4 Discussion and conclusions

We have developed and piloted an fMRI-compatible experimental situation in which participants are explored while they see themselves as if viewed from an observer's perspective during exposure to scrutiny and evaluation by others.

SAD patients were highly sensitive to the situation, as reflected by their behavioral ratings. However, both patients and controls showed robust activation in brain regions related to self-face recognition, emotion and general arousal. The patients showed greater activation than the controls only in primary visual areas. By contrast, the patients showed deactivation or smaller activation in dorsal frontoparietal and anterior cingulate cortices. Task-related anxiety ratings revealed a pattern of negative correlation with activation in this frontoparietal/cingulate network. Social anxiety scores were positively correlated with brain activation in control subjects and negatively in patients, a pattern that was best explained by an inverted-U function.

The lack of a strong contrast between patients and controls may be associated with the disease complexity pointed by this inverted-U function. In fact, in a literature review of symptom provocation tasks it is frequent to find both activity increases and decreases when comparing patients with controls.

In our assessment, symptom provocation was not associated with increased psychophysiological arousal, but instead SAD patients showed reduced heart rate responses. This is in line with the altered cardiac regulation observed in previous studies on SAD patients (Gaebler et al. 2013). Heart rate deceleration in response to gaze has been observed in healthy subjects with high trait of social anxiety (Tsuji & Shimada 2015). Several independent research groups have reported an absence of a significant increase in heart rate and other physiological measures between SAD patients and controls in response to threatening faces (Staugaard 2010) or during stressful speaking tasks (Heiser et al. 2009; Schmitz et al. 2011). The importance of this finding relies in the fact that an altered heart rate responsivity in the context of emotional regulation can be associated to alterations in autonomic, sympathetic or parasympathetic regulatory mechanisms (Appelhans & Luecken 2006). These alterations, have not been associated with enhanced fear conditioning in SAD (Tinoco-González et al. 2015). Cardiac regulation has, however, been seen modulated by SSRI intake in patients with panic disorder (Mueller et al. 2014).

From a technical experimental design point of view, the lack of an exacerbated physiologic reaction of the subjects should be regarded as a success of the task design. An

aberrant increase in arousal could be a concern due to the sensitivity of fMRI to large changes in the physiologic state of the subject. This is known to create significant artifacts in the analysis results through alterations in respiratory (Birn et al. 2006; Birn, Smith, et al. 2008) or heart rates (Shmueli et al. 2007). However, physiologic oscillations may also be related to the experimental effect, for example through a top-down regulation related to attention or emotion. Consequently, in this case we took a cautionary approach by not including them into the analysis as regressors. An excessive regression out of “confound” variables would have a potentially detrimental effect on the signal of interest.

A literature review may bring us to suspect that arousal response may be different in particular patient subgroups or experimental conditions. Significant heart rate acceleration during speech presentation was observed in social phobia patients who complained of blushing (Gerlach et al. 2001), elderly socially anxious women (Grossman et al. 2001), social phobia patients without associated avoidance personality disorder (Hofmann et al. 1995), and selective public speaking phobics (as opposed to generalized social phobia) (Heimberg et al. 1990; Levin et al. 1993).

Nevertheless, it is important to emphasize that differences between patients and control subjects have been more consistent for the subjective perception of physiological reactions than for the reactions themselves, which supports cognitive theories of social anxiety emphasizing negative interpretation of bodily sensations as part of the anxiety response (Klumbies et al. 2014).

In conclusion, the task we developed, which involved self-recognition when exposed to scrutiny and evaluation by others, was well tolerated by patients and controls and generated a robust neural response in regions relevant to emotional reactivity. However, group differences for the activations were not evident in these domains. Social anxiety was more specifically associated with changes in the dorsal frontal and cingulate systems mediating top-down emotion regulation. These results may emphasize the relevance of the cognitive component of anxiety in SAD. Disorder severity showed a nonlinear relationship with the neural activation pattern, which was characterized by a

significant cortical reduction in the most severe cases. This observation may help to explain some of the divergent results that can be found in research studies of SAD

9 Study 5: Validation of an imaging protocol aimed to characterize pharmacological response in Social Anxiety Disorder patients

9.1 Introduction

Along this dissertation we have presented the socio-economical need of developing and validating biomarkers able to characterize treatment response in Social Anxiety Disorder. The availability of validated biomarkers could reduce the long time to market and the failure rate of new SAD treatments (Merlo Pich 2011). Potentially, it would also enhance the currently limited contribution of animal models (Cryan & Sweeney 2011). This could revert in significant savings for our society (Adams & Van Vu 2010) and the reduction of patients unnecessarily exposed to unsuccessful experimental treatments (Trist & Bye 2014).

Also along this document, we have reviewed the latest findings in fMRI research on social anxiety disorders. These findings suggest an engaging possibility to explore SAD treatment response using fMRI biomarkers in novel paradigms for drug discovery (Valenzuela et al. 2011; Nathan et al. 2014). The first attempts to characterize treatment response in SAD works focused on measuring the response to emotional or stressful stimuli as BOLD activation level in the amygdala and insula (Paulus & Stein 2007; Arce et al. 2008). These brain regions are considered representative of an extended network that processes fear, stress and anxiety (Etkin & Wager 2007; Shin & Liberzon 2010). In some of these studies, amygdala was described as over-responsive when SAD patients were exposed to socially stressful or harsh emotional stimuli (Etkin & Wager 2007). This over-responsiveness of the fear and stress network was suggested to reflect a disease-related susceptibility. This view led to the proposal that a pharmacologic agent attenuating amygdala hyper-responsiveness would be also an effective treatment for clinical anxiety. Promising findings were obtained using standard therapeutics (Nathan et al. 2014). However, amygdala over-responsiveness was not always observed in Anxiety Disorders (Marsh et al., 2008, Whalen et al., 2008) which may be attributed to dependency of this biomarker on subtle methodological differences (Freitas-Ferrari et al. 2010). This

highlights the complex dynamics of this brain network (Riwkes et al. 2015). The inconsistency of the findings on brain activations in the fear circuitry challenges the usability of these as SAD symptom severity biomarkers in clinical research, as first we would need to be understand them further.

In our exploratory experiment presented as study 1, we identified that a state-of-the-art emotional face processing task created a solid activation in the emotional face processing structures in a non-clinical sample. These results were in line with the literature review. However, we did not identify a direct correlation of this activation with SAD symptom severity. Notably, an exploratory interaction measurement did show significant correlations with symptom severity. This finding is in line with growing evidence in literature that SAD disorder expresses in functional connectivity alterations (Liao et al. 2010; Giménez et al. 2012; Demenescu et al. 2013; Dodhia et al. 2014; Liu et al. 2015).

Functional connectivity studies provide the advantage of reducing dependence on activation models, which is highly advantageous when exploring complex brain networks (Calhoun & Adali 2012). Unfortunately, results of model-free connectivity-based analysis methods are not always simple to interpret (Barkhof et al. 2014) and this raised some controversies in the neuroimaging community (Morcom & Fletcher 2007).

In Studies 2 and 3 of this dissertation we presented results supporting a high reproducibility and sensitivity of functional connectivity studies based on spatial Independent Component Analysis of fMRI BOLD data (Calhoun & Adali 2006). Similar methods have been recently proposed as biomarkers for nicotine addiction (Fedota & Stein 2015).

On the other hand, in study 4 we presented the results of a novel model-based symptom-provocation task. In our pilot study including SAD patients and matched controls, this task neither revealed alterations in the activations of the fear and anxiety brain network. Instead, social anxiety scores showed a significant non-linear relationship with the dorsal frontal and cingulate systems, which mediate top-down emotion regulation (Bishop et al. 2004). These results were in line with growing literature reports

that support that SAD alterations do not limit to amygdala and its emotional processing network, but to a much more complex network, including emotion regulation areas (Gentili et al. 2015)

The aim of this study is to characterize, for first time, treatment response in SAD patients using fMRI and a resting state functional connectivity paradigm. In particular, response to a commonly used anxiolytic drug (Paroxetine) is assessed. Along with the resting state ICA analysis, two additional model-based tasks are included in the paradigm. One of the tasks has been widely used in literature as a lenient challenge to the emotion-processing brain circuitry (and piloted in our setup in study 1). The second task is the novel one presented in study 4 to explore the subject's reactions in a context of SAD symptom provocation. An additional visuo-motor control task is also included to validate that no significant physiologic disruption takes place due to the administration of the drug.

9.2 SSRI action principles in SAD.

As introduced in section 3.3.2, Selective Serotonin Reuptake inhibitors (SSRIs) such as paroxetine currently are the widest choice for pharmacologic treatment of SAD, with vast evidence of their effectivity (Blanco et al. 2013). SSRIs are known to modulate the physiology related to the monoamine neurotransmitter 5-Hydroxytryptamine (5-HT, serotonin), which has been associated with a wide variety of emotional, cognitive and behavioral control processes (Cools et al. 2008).

The action principle of SSRIs is by avoiding the reabsorption of serotonin into the presynaptic cell. This is believed to increase the extracellular level of serotonin, modulating signaling across synapses in which serotonin serves as the primary neurotransmitter. Effects have been observed to differ on chronic vs acute treatments and to show a nonlinear response to dose (Fischer et al. 2014).

In some contexts, acute doses of an SSRI have been observed to produce the opposite effects than chronic treatments (Burghardt et al. 2004). As an example, acute administration of the SSRI citalopram has been observed to enhance the recognition of fear emotion in healthy volunteers (Browning et al. 2007; Harmer et al. 2003) whereas

administration for seven days has been observed impairs its recognition (Harmer et al. 2004).

Biological models explain this phenomenon by predicting that SSRI administration will quickly increase extracellular serotonin availability, which also excites autoregulation receptors, thus inhibiting the release of serotonin. These autoregulation receptors may become desensitized after few weeks of treatment (Gray et al. 2013), leading to the sought increased serotonin availability in the synapse. The predictions of these models are backed up by the experimental results of dietary restriction of the 5-HT precursor (the essential amino acid tryptophan). As an essential amino acid, tryptophan cannot be synthesized and must be obtained through the diet. Tryptophan depletion is known to reduce serotonin levels and has been shown to reverse the effect of chronic SSRI in SAD patients (Argyropoulos et al. 2004).

Serotonergic neuronal cell bodies are restricted to discrete groups of cells or nuclei located along the midline of the brainstem, found largely within the boundaries of the raphe nuclei (Molliver 1987). These nuclei have a wide fan out of axonal projections. The limbic and paralimbic systems are heavily innervated by axonal projections from the median raphe nucleus (to dorsal hippocampus, medial septum and hypothalamus) and dorsal raphe nucleus (to prefrontal cortex, lateral septum, amygdala, striatum and ventral hippocampus), conforming the so-called serotonin pathways. See the review of Hensler *et al.* for a detailed description of the serotonin pathways to the limbic system (Hensler 2006).

Unfortunately, there is not yet a clear understanding on how SSRIs work to normalize abnormal cognitive and emotional processes (Andrews et al. 2015) nor to increase social behavior in healthy volunteers executing a problem-solving task and (Knutson et al. 1998). However, a well-established assumption is that the therapeutic effects of SSRI are related to modulation of activity in brain structures densely connected to the serotonin pathways, particularly those in the limbic and paralimbic systems. Consequently, these regions have been, and still are, frequent subject of study to

understand the relationship between brain activity and SSRI's therapeutic effects (Stahl 1998; Phan et al. 2013).

9.3 Experimental setup

The experimental setup used for this study was exactly as the setup described and validated in studies 1, 2 and 4 (see section 5.2.3 for a detailed description). This involved exploring subjects in a GE 1.5 Tesla Signa Excite MRI system, using single-shot echo planar Imaging (EPI) gradient recalled acquisition in the steady state. MRI settings were also reproduced: Whole-brain images were acquired with a Time of Repetition (TR) of 2000 ms, Time of Echo 50 ms and 90° of pulse angle. The number of images acquired for each task is presented along with the experimental paradigm description.

The MRI setup was equipped with the stimulus presentation system described in section 5.2.3.3, which allowed an immersive presentation of audiovisual stimulus.

Replicating the setup used in studies 1, 2 and 4 allowed being able to use the previous results as a validation of the setup effectiveness and as reference in the interpretation of the results.

9.4 Methods

9.4.1 Subjects

A total of 33 subjects (28 female and 5 male), with a DSM-IV-TR guided primary diagnosis of SAD (APA 2000) obtained using the structured clinical diagnostic interview SCID-I (First et al. 2002) were included into the study via public media advertisement. Inclusion criteria also involved LSAS score > 50, the acceptance to restrict alcohol intake to 2 units/day, the absence of any other psychiatric disorders and co-morbidity with diabetes, hypertension, cardiovascular, renal, hepatic or endocrine disorders, no psychotropic medications use in the month before trial initiation with exception of low-dose hypnotics, no participation in any other trial in the last 6 months and no reported suicidal ideation. Demography, subject disposition, State-Trait anxiety inventory (STAI) questionnaire (Spielberger 1983) and Patient Health Questionnaire (PHQ) (Spitzer 1999) were collected during screening.

Each subject was randomized (1:1 ratio) to daily receive either 20 mg of paroxetine or placebo as oral capsules for 8 weeks, with controlled visits and tablet refilling every 2 weeks. At the end of the study, subjects of the active treatment group received 10 mg/day of paroxetine as a tapering dose for one additional week before discontinuation. One subject was withdrawn from the study on day 17 due to a protocol violation

9.4.2 Experimental paradigms

The main objective of this experiment is to explore the capacity of fMRI to detect SAD treatment response. For this reason, the three categorically different paradigms presented in the previous studies of this dissertation were executed by the SAD and control populations under treatment and placebo condition.

The selected experimental paradigms were those presented in study 1 (emotional faces matching), study 2 (resting state) and study 4 (delayed public exposition) of this dissertation, plus a control visuomotor task. Note this selection of tasks allowed testing the individuals under:

- 1) A well-validated task in the SAD context (emotional faces matching)
- 2) Our novel symptom-provocation task (delayed public exposition).
- 3) A resting state condition with the technical parameters validated in studies 2 and 3 plus
- 4) A universal control task (visuomotor paradigm) that will allow to test for unwanted physiologic effects of the drug under study.

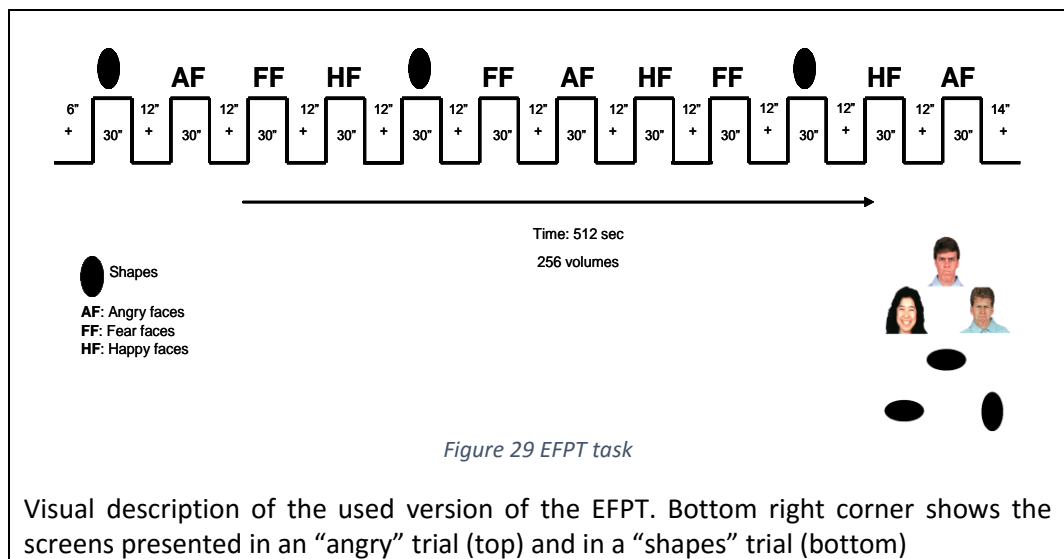
For readability of this document, a brief description is provided below for all paradigms, including the reused ones. Cross-references are also provided to guide the reader to the detailed descriptions of the tasks in earlier sections of this document.

9.4.2.1 EFPT – Emotional Face processing task

This task was executed exactly as presented by Paulus et al. (Paulus et al. 2005) and highly similar to that used in study 1 (see section 5.2.1 for details). The emotional faces pictures, display layout and trial duration were exactly the same as in study 1. This

study incorporated the “angry” faces block, originally present in Paulus’ study but that had been excluded in study 1.

Summarizing the rationale of this task, subjects performed a simple matching exercise where the items to match are either emotional faces or shapes. The overall task consisted of an 8.32 minutes sequence, comprising 12 blocks (9 for faces –fear, anger or happiness-, 3 for shapes) and a fixation cross presented between blocks. An “angry block”, for example, is defined by the emotion expressed by target image, which would be “angry” in this case. See Figure 29, bottom right corner for an example of an angry faces (AF) trial and a shapes trial. Each run comprised the acquisition of 256 volumes (15 brain volumes in each trial block, spaced by 12 seconds of fixation cross with 2000 ms per volume).



This task is generally considered a lenient set of stimulus that allow the selective recruitment of the emotional face processing brain circuits without a specific SAD symptom provocation. Tasks related to emotional face processing are widely used in multiple variants to study SAD. See (Gentili et al. 2015) for a recent review.

9.4.2.2 PERPT – Public Exposition of Recorded Performance Task

This task, developed and presented in study 4, was executed exactly as presented in study 4 and in (Pujol et al. 2013) (see section 8.2.2 for details).

To summarize the task, subjects were presented with stimuli consisting of a pre-recorded “private” video with three 30-s sequences of the same subject while executing a memory test that consisted in memorizing and narrating a story. The control condition were clips of the same length of another subject performing the same memory test. The whole task consisted of 6 alternated blocks (“other” and “self”), each block resulting in 15 brain volumes, 2000 ms per volume.

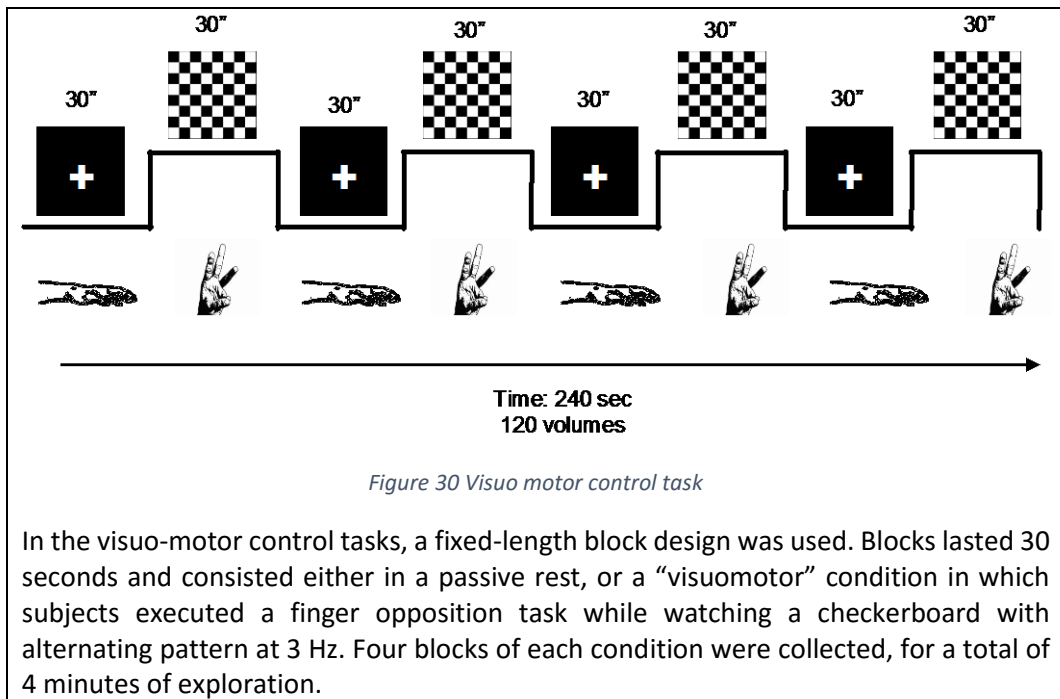
9.4.2.3 Resting state scanning

Subjects were asked to lie quietly in the scanner with eyes open and fixed to a neutral dimmed green spot during the acquisition for 6 minutes, thus generating 180 volumes acquired every of 2000 ms . Subjects had been indicated that the green color of the spot indicated they were not being scrutinized during that period.

9.4.2.4 Visuomotor control task

The visual-motor task was selected as a control test to rule out “unspecific” effects of drug treatment on the BOLD signal. Subjects were scanned while performing a visual-motor paradigm consisting of a repeated finger opposition task while watching checkerboard square flashing (alternating black and white) at 3 Hz.

The fMRI sequence, based on a block design, included the visual-motor condition and a baseline condition in which the subject was asked to fix the eyes onto the screen while remained immobile. The 4 minute sequence was organized in 8 blocks (4 task, 4 rest), with each block lasting 30 s. Each run comprised the acquisition of 120 volumes (15 brain volumes in each block, 2 s per volume).



9.4.3 Image analysis

The analysis methods used were highly similar to those presented in Studies 1 to 4. After preprocessing of all fMRI images, first level analysis was based in the general linear model for the EFPT, PERPT and visuomotor tasks. ICA was used to analyze the resting state task. A GLM-based ANOVA was performed as a second level analysis of the four studies. An overview of these analysis methods is presented below for readability of this document.

9.4.3.1 Preprocessing

Image preprocessing followed a similar pipeline as in studies 1 to 4 (See section 5.2.4.1 for a detailed description). In summary, it was preprocessed using SPM5 (www.fil.ion.ucl.ac.uk/spm) by doing motion correction, spatial normalization to the MNI template and smoothing using a Gaussian filter of 8 mm of full-width to half-maximum. During normalization, images were resampled to a 2x2x2 mm³ voxel size, except for the resting-state sequence which was resampled to a voxel size of 3x3x3 mm³ like in studies 2 and 3, due to computational power limitations.

9.4.3.2 First level - General linear model

The emotional face processing task, public exposition of recorded performance task and visuomotor control tasks were analyzed using a general linear modeling analogous to that those in study 1 (described in section 5.2.4.2) and study 4 (described in section 8.2.6.2).

Summarizing, first level analysis were performed in SPM5 using as the model box-car designs following the experimental conditions, convolved with the canonical hemodynamic response function. The contrasts extracted were those leading robust results in study 1 (harsh faces > shapes) and in study 4 (“viewing self” > “viewing other”). For the visuomotor task, the extracted contrast was sensorimotor activity>rest.

9.4.3.3 First level – Independent Component Analysis

The ICA analysis performed in this study was the same as in Studies 2 and 3. See section 6.3.4.2 for details. Briefly, time-series were concatenated and processed using GIFT v1.3d; (<http://icatb.sourceforge.net>) running on Matlab 7. This included a component back-reconstruction following the individual’s source data, as previously described. Attending the purposes of the current study, four components related to anxiety, self-referential emotion and arousal processes were selected (see the selected networks in Figure 31).

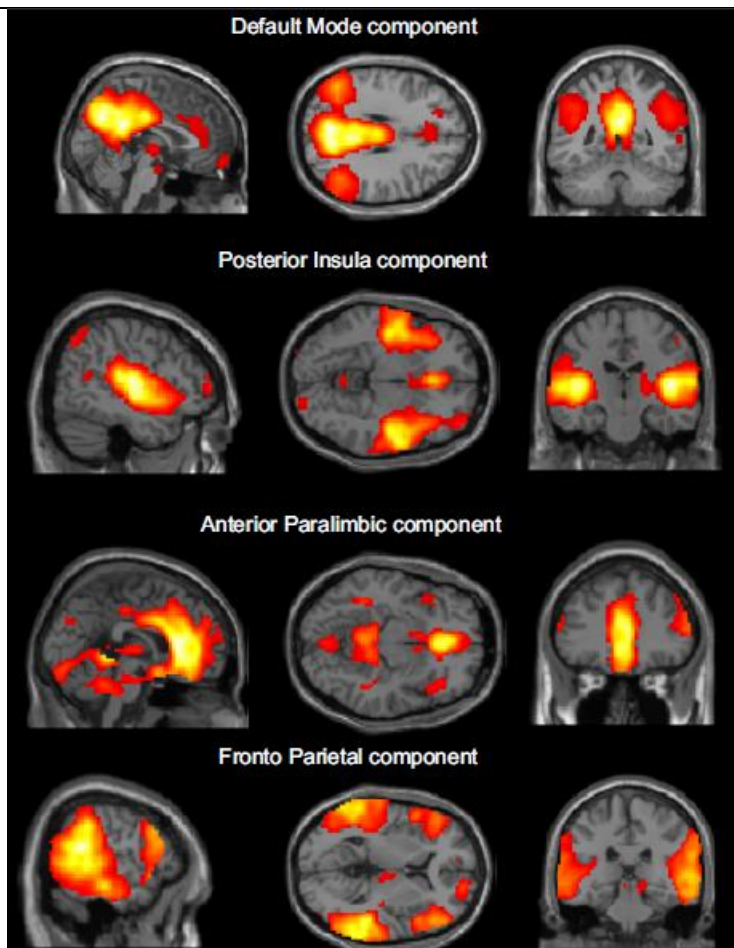


Figure 31 ICA components selected for second level analysis

Components extracted by ICA from the resting state sequence and selected as relevant for the second level analysis. Each ICA component shows brain voxels with a particular activation dynamics (temporal time course). These are presented in a single- subject MRI standard MNI anatomical space.

9.4.3.4 Second level Analysis

Inferential analysis of each of the 4 experiments were conducted on SPM using a 2x2 repeated measures ANalysis Of VAriance (ANOVA), where 2 factors were defined as treatment (paroxetine or placebo) and time (baseline or week 8). Significance was tested for the “drug vs placebo” interaction and for individual treatment effects.

For the three tasks analyzed with GLM at the first level, the described contrasts of interests were fed to SPM to calculate the ANOVA statistics. For the resting state task,

component connectivity effect size (z-score maps) were fed, separately for each component, to the same repeated-measures ANOVA statistical calculation.

Baseline task effect (one-sample T-test) second level analysis were also performed to validate the brain areas recruited by the experiment. For the emotional face processing task, GLM inference was constrained using the WFU pick atlas v 3.1 to *a priori* regions of interest, previously reported as potential treatment response biomarkers: Bilateral amygdala and insula (Paulus et al. 2005; Arce et al. 2008). For the novel PERPT, data was analyzed with both a ROI and a whole-brain approach.

Additionally, a correlation coefficient analysis was performed between clinical improvement (as revealed by CGI-I) and the ANOVA's time contrast (week 8 versus baseline) for placebo and paroxetine.

9.5 Results

9.5.1 Baseline of behavioral tasks

The baseline analysis of behavioral tasks revealed, for each task, the brain areas for which activity is significantly modulated by the paradigm. These results were used to confirm that the experimental design effectively engages the brain regions targeted by the experiment.

9.5.1.1 EFPT

At baseline, the EFPT produced a significant bilateral activation of amygdala and insula, as well as other areas included in the fear, stress and anxiety circuit, e.g., hippocampus, orbitofrontal cortex, and fusiform gyrus. See the anatomy in Figure 32, left panel.

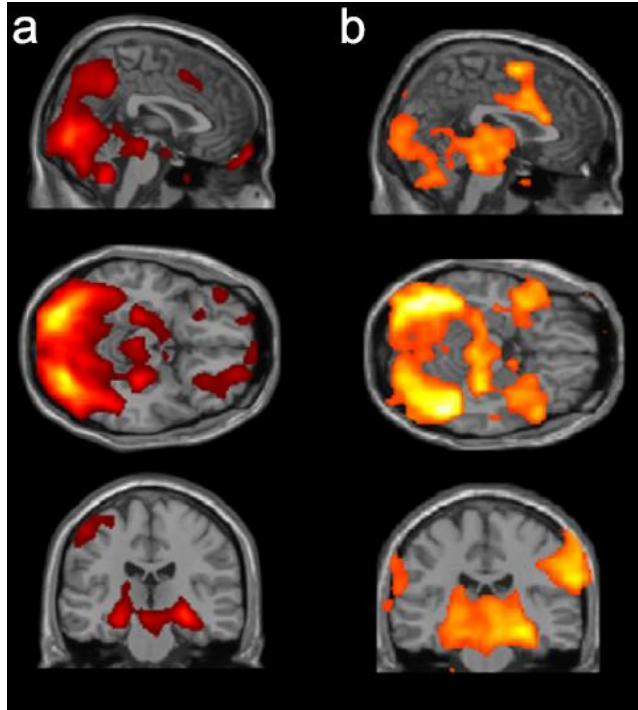


Figure 32 EFPT and PERPT activation maps

Activation maps observed in SAD subjects during EFPT (a) and PERPT (b). Color maps represent group-wise activation T-values (black, $t = 0$; red, $t = 4$; yellow, $t = 8$; white, $t = 10$).

9.5.1.2 PERPT

At baseline, the PERPT produced a more intense and extended bilateral activation of the same areas as the EFPT, with an additional distinctive activation in the regions related to self-recognition, i.e., extrastriate visual cortex, the right inferior frontal gyrus and medial frontal gyrus. See the anatomy in Figure 32, right panel.

9.5.2 Effects of treatment

Treatment effect analysis revealed the differential brain activity induced by the pharmacologic treatment. It is important to read these results in conjunction with the baseline results presented in the previous section. Provided the experimental design, factorial (ANOVA) and dimensional (correlation coefficient) results are presented.

9.5.2.1 ANOVA on EFPT activations

The effect of paroxetine on the activation produced by the EFPT was analyzed by a ROI approach, focusing on amygdala and insula bilaterally, and as an exploratory analysis in the prefrontal cortex (PFC) and anterior cingulate cortex (ACC). Two-way ANOVA treatment x time interaction was found significant in right amygdala (cluster size=122, $t=2.11$ in MNI 24 -4 -20, $p=0.019$), left insula (cluster size=205, $t=2.96$ in MNI -40 -80, $p=0.002$) and right insula (cluster size=532, $t=3.78$ in MNI 30 -14 20, $p<0.0005$). These results were mostly explained by paroxetine producing more activation at study-end when compared to placebo (Figure 33, upper panel). Placebo alone did not directly affect amygdala and insula, but reduced the signal in the hippocampus and in the right thalamus (Figure 33, yellow arrows). No significant effect of paroxetine or placebo treatment was observed in PFC or ACC (data not shown).

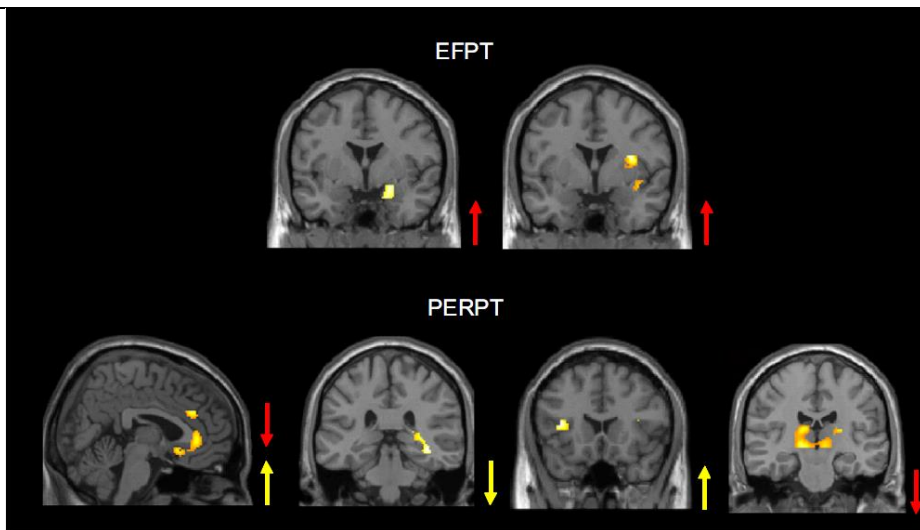


Figure 33 ANOVA 2x2 results of interaction between treatment and time

Statistical maps of the ANOVA 2x2 interactions between treatment and time (paroxetine vs. placebo, study-end vs. baseline). Threshold was $p < 0.05$ at voxel level, color maps representing t-values (red, $t = 1.5$; yellow, $t = 2.5$; white, $t = 3.5$). Top panel: Results from the EFPT in the amygdala and the insula ROI. Lower panel: Results from the PERPT assessed as fear, stress and anxiety circuit, showing BOLD signal changes in orbitofrontal and ACC, posterior hippocampus, insula and thalamus respectively. In PERPT, amygdala activation was attenuated by both placebo and paroxetine and did not show significant interaction. Arrows represent the increase (upwards) or the decrease (downwards) of activation found at study-end versus baseline for paroxetine (red arrow) and placebo (yellow arrow).

9.5.2.2 ANOVA on PERPT activations

In the PERPT, the two-way ANOVA treatment x time interaction showed effects in various components of the fear, stress and anxiety circuit (Figure 33, lower panel). In addition to subcortical structures, engagement of a medial prefrontal cluster was observed, including anterior cingulate cortex and the subgenual cortex (Brodmann areas 34 and 25). Significant interaction was found in the left insula (cluster size=87, $t = 3.10$ in MNI -38 20 10, $p = 0.002$), right insula (cluster size=31, $t = 2.65$ in MNI 30 32 -2, $p = 0.005$), left hippocampus (cluster size=72, $t = 2.30$ in MNI -18 -40 0, $p = 0.013$), right hippocampus (cluster size=146, $t = 3.10$ in MNI 40 -36 -10, $p = 0.001$), left extended prefrontal and ACC (cluster size=705, $t = 2.60$ in MNI -6 38 8, $p = 0.006$), right extended prefrontal and ACC (cluster size=248, $t = 3.67$ in MNI 10 32 28, $p < 0.0005$), right thalamus (cluster size=54,

t=2.81 in MNI 20 -30 14, p=0.003) and left thalamus (cluster size=18, t=1.88 in MNI -8 -16 14, p=0.032). The study of the main effects (Table 9) showed that the amygdala response was significantly attenuated at study-end versus baseline in both treatment groups.

Table 9 Treatment effects of paroxetine on PERPT activation in ROIs

| ROI | Cluster size (voxels) | MNI coordinates (x y z mm) | T value | p value (uncorrected) |
|--|-----------------------|----------------------------|---------|-----------------------|
| Paroxetine effect (study end < baseline) | | | | |
| Bilateral thalamus | 895 | 10 -30 -2 | 3.69 | <0.0005 |
| | 33 | 22 -20 14 | 2.42 | 0.009 |
| Left PFC and ACC | 48 | -6 46 28 | 2.29 | 0.013 |
| Right amygdala | 36 | 18 -10 -26 | 2.72 | 0.004 |
| Placebo effect (study end < baseline) | | | | |
| Left hippocampus | 385 | -18 -40 -2 | 3.11 | 0.001 |
| Right hippocampus | 243 | 28 -10 -26 | 3.35 | 0.001 |
| | 142 | 38 -34 -12 | 2.61 | 0.006 |
| | 26 | 24 -42 -2 | 2.13 | 0.018 |
| Right amygdala | 25 | 28 -6 -26 | 3.02 | 0.002 |
| Placebo effect (study end > baseline) | | | | |
| Left insula | 250 | -38 18 8 | 3.66 | <0.0005 |
| Right insula | 107 | 26 32 0 | 2.72 | 0.004 |
| Bilateral PFC, subgenual region and ACC | 3311 | 12 30 28 | 4.57 | <0.0005 |

MNI coordinates, p and T values refer to the maximum peak within the cluster revealed by the ANOVA on the PERPT activations. Abbreviations: ACC: anterior cingulate cortex; MNI: Montreal neurological institute; PFC: prefrontal cortex; ROI: region of interest.

9.5.2.3 Correlation analysis on PERPT

Correlation analysis between clinical scores and brain activation in the PERPT indicates a significant negative correlation between CGI-I scores and brain activation in the rostro-medial PFC produced by paroxetine (cluster size=877 in MNI 2 58 -0, t=4.35, p<0.0001). Since low CGI-I scores indicate better clinical conditions, these data indicate a direct association with clinical improvement (Figure 34a). No significant correlation between brain activation and clinical scores was observed in the placebo group.

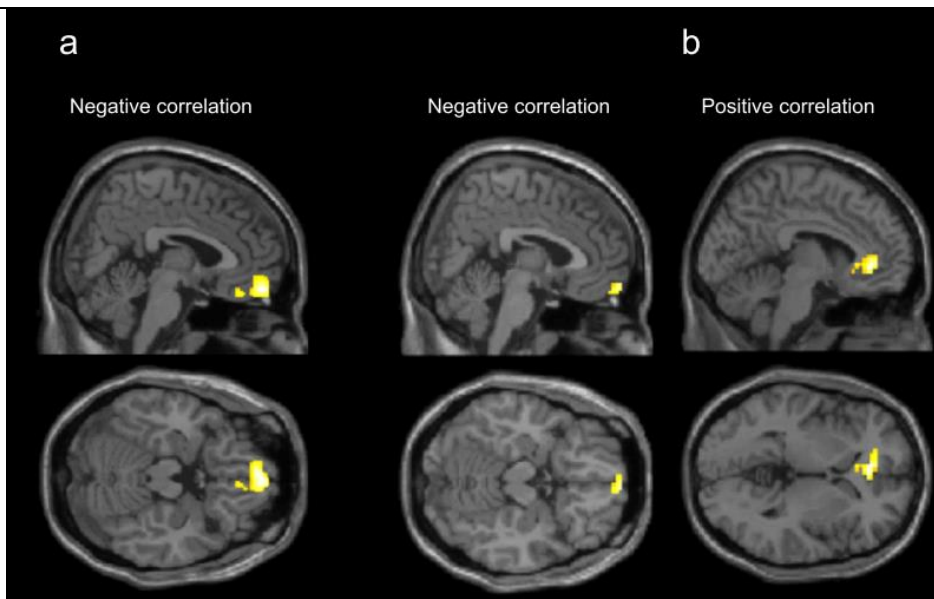


Figure 34 Correlation of paroxetine effect on PERPT or resting and CGI scores

Correlation ($p < 0.001$) between CGI-I scores and (a) activation produced by the PERPT, and (b) changes in resting state ICA “Anterior Paralimbic” component induced by paroxetine. Color maps represent t-values (black, $t = 0$; red, $t = 1$; yellow, $t = 3$; white, $t = 5$). Note that both paradigms showed a negative correlation with clinical score in the same areas of rostral-medial PFC. Placebo did not produce any effects (data not shown).

9.5.2.4 ANOVA on resting state task

Results from the two-way ANOVA treatment x time interactions showed that paroxetine treatment reduced the value of all ICA components when compared to placebo (Figure 35), suggesting an attenuation of functional connectivity. Specifically, a significant attenuation of connectivity of the ‘Default Mode’ component was produced in the right thalamus by paroxetine at study-end versus baseline when compared with placebo (cluster size=57, $t=2.53$ in MNI 9 -24 3, $p=0.007$). Paroxetine-induced attenuation of connectivity versus placebo was observed measuring the ‘Posterior Insular’ component in the right insula (cluster size=88, $t=3.19$ in MNI 33 -12 0, $p=0.001$) and in the perigenual regions BA12 and BA32 (cluster size=44, $t=2.64$ in -3 42 0, $p=0.005$). Paroxetine also reduced versus placebo connectivity of the anterior paralimbic component, in the the subgenual ACC (cluster size=89, $t=2.98$ in MNI 0 9 -12, $p=0.002$). Conversely, placebo treatment significantly increased functional connectivity in the subgenual region BA24 and BA35 at study-end vs. baseline (cluster size=58, $t=2.96$ in MNI 6 21 -, $p=0.002$). Finally,

the analysis of the 'Fronto-Parietal' component showed significant interaction at the level of the anterior left insula (cluster size=67, $t=2.68$ in MNI -36 15 6, $p=0.005$), a result driven by paroxetine that attenuated the signal at study-end while placebo did not. See Figure 35 for a summary of these results.

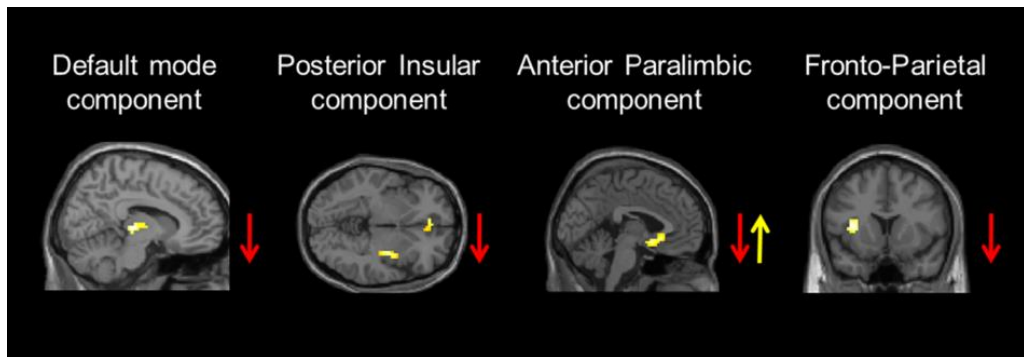


Figure 35 Resting state effect of treatment

Resting state maps of the ANOVA 2 x 2 interactions between treatment and time (paroxetine vs. placebo, study-end vs. baseline). Threshold was $p < 0.05$ at voxel level, color maps representing t-value at single voxel (black, $t = 0$; red, $t = 1$; yellow, $t = 2$; white, $t = 2.5$). The brain regions significantly affected are thalamus and midbrain for the 'Default Mode' component, the ACC and posterior insula for the 'Posterior Insular' component, the orbitofrontal and subgenual cortex for the 'Anterior Paralimbic' component, and the anterior insula for the 'Fronto-Parietal' component. Arrows represent the increase and the decrease of activation found at study-end vs. baseline for paroxetine (red arrow) and placebo (yellow arrow).

9.5.2.5 Correlation analysis on resting state data

Correlation analysis between CGI-I clinical scores and ICA 'anterior paralimbic' component showed a significant negative correlation between CGI-I scores (low score indicates improvement) and brain functional connectivity in the rostro-medial PFC produced by paroxetine (cluster size=32, $t=3.53$ in MNI 3 63 -15, $p=0.001$) (Figure 34b). Positive correlation was instead observed in the subgenual cortex, in the paroxetine group (cluster size=75, $t=4.79$ in MNI -6 39 -3, $p<0.0001$) and in the left orbitofrontal region in the placebo group (cluster size=114, $t=4.62$, in MNI -36 45 -6, $p<0.0001$).

9.6 Discussion and Conclusions

To our knowledge, this was the first placebo-controlled fMRI study evaluating paroxetine treatments in SAD that implements resting state analysis. In this present study two small groups of SAD subjects were exposed to paroxetine or placebo for 8 weeks, which is considered equivalent to a chronic treatment. Significant effects of paroxetine treatment were observed with the clinical score CGI-I and fMRI. Functional MRI showed consistent changes in structures of the fear, stress and anxiety circuit in two different procedures, the high-distressing PERPT and the non-intrusive resting state ICA analysis. Significant effects, but of more difficult interpretation, were also obtained with EFPT, a task shown to be sensitive to anxiolytics in healthy volunteers (Paulus et al. 2005). The lack of significant effects on the visuomotor task confirms that no unspecific effects were generated by the drug on fMRI results.

At baseline, the PERPT and EFPT fMRI tasks produced robust activation maps, as previously described in literature (Paulus et al. 2005) and in study 1 of this dissertation for EFPT and in study 4 for PERPT. PERPT generated generally stronger activations and activated additional brain regions – also seen in study 4- including primary and extra striate visual cortex, right inferior frontal gyrus, medial frontal gyrus, and ACC, known to be engaged in self-referential processing (Northoff et al. 2006).

The resting-state spatial Independent Component Analysis robustly isolated the spatial components reported in studies 2 and 3 of this dissertation and widely reported in literature (Barkhof et al. 2014). Only those networks overlapping with the fear, stress and anxiety circuit were considered when assessing paroxetine effects. These components were those corresponding to the Default Mode, posterior Insula, anterior paralimbic and fronto-parietal networks (see Figure 31).

Chronic treatment with paroxetine attenuated the activation produced by PERPT in medial PFC, subgenual PFC and ACC. These areas are known to be involved in emotion regulation and top-down modulation of anxiety in healthy subjects, with rostral ACC presumed to control the amygdala's response to stressful and aversive stimuli (Etkin et al. 2011). Notably, recent findings suggest ACC as a mediator from anxiety sensitivity to

subjective anxiety (Harrison et al. 2015). Attenuation of threat-related medial prefrontal cortex activation by acute administration of another SSRI (citalopram) has been previously reported (Harmer et al. 2006; Simmons et al. 2009).

The analysis on the connectivity in the four ICA-extracted components of interest showed that paroxetine treatment reduced connectivity in all components when compared to placebo. Specifically, paroxetine reduced thalamus connectivity to the default mode network. Reduced connectivity in posterior right insula, pregenual regions and subgenual ACC were seen when comparing paroxetine vs placebo. Remarkably, a recent seed-based study identified that higher social anxiety severity in SAD subjects correlated with lower amygdala-ACC/mPFC connectivity (Dodhia et al. 2014). In Dohia's study, this atypical connectivity was reversed by the administration of intranasal oxytocin. These could seem to be results opposite to ours. However, it is important to note the differences in the interpretation of seed-based functional connectivity and ICA-based functional network connectivity that were discussed in section 7.1. From our methods, it cannot be determined whether our decrease in intra-network connectivity was related to an experimentally induced internetwork coupling. Interestingly, another recent set of results revealed simultaneous decreased connectivity of the orbitofrontal gyrus and increased connectivity of the middle frontal gyrus in SAD patients versus controls (Geiger et al. 2015). This suggests that both hypo-connectivity in the executive control network and hyper-connectivity between the orbitofrontal cortex and the amygdala may reflect a disturbance in the balance between top-down and bottom-up control processes in SAD patients.

In the present study, the EFPT results drove activation of amygdala in both placebo and paroxetine groups at baseline and a similar significant attenuation over time. The interaction between paroxetine and placebo groups measured at basal and study-end, the effects were of activation, at variance with the attenuation reported in the early anxiolytic literature in healthy volunteers (Paulus et al. 2005; Arce et al. 2008; Simmons et al. 2009). However, other discrepant results like ours have been reported, showing SSRI to increase amygdala activation (Tendolkar et al. 2011), placebo to reduce it (Furmark et al. 2008) or SAD patients displaying lower amygdala activation than healthy volunteers

(Britton et al. 2010; Phan et al. 2006). The heterogeneity of these results suggest that the results of this paradigm may depend on setup-specific conditions (Freitas-Ferrari et al. 2010) or different phenotype-driven neural expressions of SAD (Furmark et al. 2008).

The analysis of correlation between clinical improvement (as reflected by CGI) and task activation revealed significant a significant correlation between PERPT BOLD activation and the improvement of CGI-I clinical scores in the rostro-medial PFC (Brodmann area 11) of SAD subjects in the paroxetine group. Remarkably, the same Brodmann area was identified to show a significant correlation between CGI-I clinical scores and ICA network functional connectivity. The fact that the symptom-provoking PERPT showed the same sensitivity to clinical improvement than the passive resting-state experiment enhances the interest for further exploring Independent Component Analysis as a basis for fMRI-based clinical improvement biomarkers. Notably, the only area identified to show this behavior is recently being highlighted as a potential candidate of study to disentangle the neural basis of social anxiety disorder (Sylvester et al. 2012; Geiger et al. 2015; Duval et al. 2015). A recent study applying connectivity and graph theory on a nonclinical population found that SAD symptoms were associated with weakened connectivity of the parahippocampal gyrus and ventromedial prefrontal cortex/medial orbitofrontal cortex, but not in insula nor amygdala (Kajimura et al. 2015). Altered ventrolateral prefrontal cortex (VLPFC) has also been observed in SAD patients using near infrared spectroscopy during a verbal fluency task (Yokoyama et al. 2015)

In conclusion, the selected fMRI paradigms and analysis methods showed significant sensitivity to the effects of paroxetine treatment of SAD. Treatment effects were identified in areas related to the processing of fear stress and anxiety, which are known to be altered in SAD. Remarkably, Independent Component Analysis revealed sensitivity to clinical improvement in the same areas and direction than the symptom-provocation task. While there is an evident need of further exploration and replication of these results, we conclude that our results strengthen the set of published evidence that fMRI can become a powerful tool for drug discovery.

10 Ethical considerations

All the experiments presented in this document have been planned and executed with strict observation of the Declaration of Helsinki (WMA 2013) and the applicable ethical committees, including CEIC-IMAS for studies 1,2,4 and 5; the Mental Health Research Institute of Victoria and Melbourne Health Research and Ethics Committees for study 3. Study 5 was posted on clinicaltrials.gov with reference NCT00470483.

Some additional ethical considerations are discussed below, covering the possible inferences done through this dissertation, and some common areas of concern in the field of neuroimaging.

10.1 Limitations of the inference through this thesis' results

Like in many other scientific disciplines, the inference of the results found in this work shall be contained until wide replication of these results is obtained and a full understanding of the underlying biophysical principles is developed.

As described in the section 2 of this dissertation, neuroimaging through functional magnetic resonance imaging relies in a long and complex chain of measurements and assumptions. Leaving aside possible execution errors, multiple unaccounted variables could influence the neuroimaging results. These variables could be affecting in the physics, physiology, psychology, technology or analysis methods and even be coincident in different experimental setups (Savoy 2005). Neuroimaging is not free of optimistic attempts to predict outcomes from too small datasets (Whelan & Garavan 2014) so experimental replication on robust sample sizes is convenient. When we seek for result replication we should include both similar and distinct experimental approaches to rule out the effect of random and deterministic effects, respectively. The experiments in studies 1 and 2 have been replicated in multiple setups, not without some diverging results. However, studies 3 to 5 involved much more novel tasks and analysis methods. Therefore, care should still be taken before inferring out from their results as the scientific community would need first to try to replicate these experiments.

10.2 Neuroethics

Unfortunately, when a neuroimaging study presents results in the shape of a set of colored regions on an anatomical image, the potential confounds or unaccounted variables are frequently not represented. Non-rational automatic thinking can lead to the belief that the relationship between the stimulus or condition and those colored areas is proven. However, like it happens with basic statistics when we see a difference between the mean values of two groups, we know that a number of context variables and metrics (i.e. variance or sample size) need to be accounted before these results are inferred into knowledge on the observed phenomenon. Most of the research disciplines are vulnerable to this (Ioannidis 2005), but the complexity of the brain and the related analysis methods make it a deeper concern in neuroimaging. These concerns have raised in the scientific community the feeling that neuroethics can play a significant role in the field of neuroimaging and our society in general (Levy 2008).

Having made a hypothesis before the experiment was executed is a generally adopted best practice. However, the hypothesis itself is not guaranteeing the validity of inference made out of the results. In fact, confirmation bias is a well-known phenomenon of human psychology, described as a tendency to search for evidence that supports the hypothesis we are assessing, rather than evidence that refutes it. It can also lead to the interpretation of ambiguous evidence so that it supports our hypothesis (Nickerson 1998).

Unfortunately, confirmation bias can also affect the progress of science. This phenomenon would make a scientist to pay more attention to evidence confirming the own hypothesis or beliefs and disregard disconfirming evidences. This can combine with the availability heuristic: The mental shortcut driving the belief that if something can be recalled, it is more frequent than alternative solutions which are not as readily recalled (Tversky & Kahneman 1973). Because, in presence of confirmation bias, confirming instances are more easily recalled, memory searches can lead us to conclude that our hypothesis is true. This is the same mechanism that leads people to believe that car accidents are more likely to happen after being shocked by witnessing one. Even when judging own experiences, perceived ease of recall can play a significant role in the

interpretation of the implications of the recalled experiences (Schwarz et al. 1991). The scientific community needs to pay special attention to impartiality and to contextualization of results to avoid this.

Most of the peer-reviewed articles are targeted to the scientific community. However, since the decade of the brain, the influence of neuroimaging has expanded to the broader community. Suddenly, the consumers of neuroscience studies have expanded to include marketing, legal, economics or divulgation interests, to name a few. A search in general news identified a large part of them had a mostly optimistic tone, while scientific issues such as validity were seldom discussed (Racine et al. 2005).

The “neuro-policy” trend identified by Racine et al, attempting to use fMRI to promote political or personal interests is becoming particularly concerning: The apparition of neuroimaging results in courts and legislatures is becoming frequent (Rosen & Savoy 2012). In these contexts the audience may not be trained enough to interpret these results with guarantees. In fact, research has shown that neuroimaging results are highly persuasive and are taken more seriously than other kinds of data in decision making (McCabe & Castel 2008). Racine et al also described “neurorealism”, where fMRI investigations can make a phenomenon uncritically real, objective or effective in the eyes of the public, despite the complexity of the data acquisition and processing. Under this phenomenon, general beliefs seem to be confirmed by the “visual proof” of brain activity.

A study that interviewed over 2000 members of the general community identified that reading about neuroscience in divulgation media could have both positive and negative effects in neuroscience literacy (Herculano-Houzel 2002). Historically, wide press coverage has shown to influence even health professionals, modulating the adoption of certain practices, such as what happened with the promotion of lobotomy to treat certain psychiatric diseases (Diefenbach et al. 1999), initiating one of the darkest episodes of neuroscience. Unfortunately, and the effect of popular press on medical practice remains as a concern today (Singh et al. 2007; Gilbert & Ovidia 2011; Schmitz et al. 2003). A high scientific criticism can be expected in the interpretation of fMRI data for pharmacology research, but the need to pay high attention to the methods and data interpretation to

support drug development is an overt concern in the neuroscientific community (Wise & Preston 2010). Developing a formal widespread education on neuroimaging to researchers and research consumers start seeming necessary to avoid the risks of misusing this science (Savoy 2012).

10.3 A new window to the brain: Privacy of the subjects

Despite the complexity of fMRI studies and the calls for caution in its interpretation, fMRI is clearly advancing at a high speed. Protocols based in fMRI are every day giving more information about the subject under study. Psychiatric pathology, emotional state or treatment response are characteristics of the individual that typically would be not revealed without one's participation. However, as we have seen in this work, novel techniques can give increasing detail about these conditions. This has raised concerns on the protection of privacy of the subject under study (Farah 2012). Like it happens with DNA sampling, the amount of information that can be extracted from the individual's data is not always predefined as new knowledge and analysis techniques can be developed after the data collection. Unlike DNA, fMRI results can be driven not only by the genetic heritage, but also by the subject's experience and cognition. This can be a concern in applications related to moral beliefs or crime (Littlefield 2009). Strict anonymity of research studies of medical files seems to be more necessary than ever to protect the subject's privacy to the current or future capacity of fMRI analyses.

On the other hand, the amount of information that today can be obtained from an individual's fMRI scan is still scarce. This is why fMRI studies often seek for large population samples before a conclusion can be drawn. As a result, individual's privacy may still be fairly well protected by the limitations in the science and technology behind fMRI (Farah et al. 2009). In fact, as introduced in section 10.1, it is likely that the general public's expectations on the degree of detail obtained by the individual is above the actual capacity of the technique. This could bring to an unjustified discomfort by the volunteers, as the perceived degree of privacy violation done by an exploration is modulated by the individual's expectations on the kind and quantity of data obtained by the technique (Baker et al. 2013). In this scenario, an overt communication of the actual degree of detail

obtained from the individual may reduce the subjects discomfort and may even ease recruitment for research studies.

If subsequent studies of this or parallel works continue objectivizing treatment response in psychiatric diseases, these research techniques may start being applied in the clinical context. This could significantly modify treatment adjustment practices, which today still rely mainly on self-reports from the individual. Despite self-reports from psychiatric patients can be misleading or complex to decode, a “the machine says you’re better” scenario where a neuroimaging test drives drug dosing or replacement would be likely to be considered too disruptive by patients and practitioners. The short term expectations for these techniques should not exceed the support to drug discovery research and being a bedside support technique in the clinical practice.

In future research, informed consents may need to be updated to detail the information that is expected to be inferred from the individual through the imaging exploration. Responsible and anonymous usage of these fMRI datasets is necessary to protect individual’s privacy and other rights. Public and private institutions may need to keep updating the criteria used in their ethical committees following the developments in fMRI techniques.

11 Conclusions

The review of the state of the art revealed that the usage of fMRI in clinical psychiatry research is in an incipient stage, while there is clear socioeconomic need to enhance the success rate of drug discovery.

The results of our emotional face processing experiment revealed that not only fMRI task activation, but also functional connectivity measurements shall be considered as potential biomarkers to characterize severity of social anxiety disorder.

Independent component analysis provides whole-brain functional connectivity measurements that are anatomically reproducible across studies and are sensitive to the subject's emotional state.

Our novel symptom-provoking task revealed a non-linear relationship between symptom severity and task-induced activations in brain structures mediating top-down emotion regulation.

In the pilot clinical trial using a standard pharmacological treatment on SAD patients, both the symptom-provocation task and the resting state analysis revealed that effect size on ventromedial prefrontal cortex (Brodmann area 11) was sensitive to clinical improvement as revealed by the CGI scale.

Despite it is clear that extensive works are still needed, these results provide evidence that fMRI-based measurements, including ICA of resting-state data, are sensitive to the expression of social anxiety disorder. Therefore, these techniques are valid candidates as SAD treatment response biomarkers for clinical research.

12 Publications derived from this thesis

The works presented in this thesis have contributed to the development of the following peer-reviewed publications. The results presented in studies 1 to 5 are reproduced from these publications with permission of the editors.

Study 1 (Journal's 2014 impact factor: 5.9)

Pujol, J, B J Harrison, Hector Ortiz, Joan Deus, Carles Soriano-Mas, M López-Solà, M Yücel, et al. 2009. **"Influence of the Fusiform Gyrus on Amygdala Response to Emotional Faces in the Non-Clinical Range of Social Anxiety."** *Psychological Medicine* 39 (7). pp 1177–87. Results reproduced with permission of the editor.

Study 2 (Journal's 2014 impact factor: 9.7)

Harrison, Ben J, Jesus Pujol, Marina López-Solà, Rosa Hernández-Ribas, Joan Deus, Hector Ortiz, Carles Soriano-Mas, et al. 2008. **"Consistency and Functional Specialization in the Default Mode Brain Network."** *Proceedings of the National Academy of Sciences of the United States of America* 105 (28). pp 9781–86. Results reproduced with permission of the editor, copyright © by the National Academy of Sciences.

Study 3 (Journal's 2014 impact factor: 3.23)

Harrison, Ben J., Jesus Pujol, Hector Ortiz, Alex Fornito, Christos Pantelis, and Murat Yücel. 2008. **"Modulation of Brain Resting-State Networks by Sad Mood Induction."** *PLoS ONE* 3 (3). Results reproduced under the CC license granted by the editor.

Study 4 (Journal's 2014 impact factor: 5.9)

Pujol, J., M. Giménez, Hector Ortiz, Carles Soriano-Mas, M. López-Solà, M. Farré, Joan Deus, et al. 2013. **"Neural Response to the Observable Self in Social Anxiety Disorder."** *Psychological Medicine* 43 (1). Pp 721-731. Results reproduced with permission of the editor.

Study 5 (Journal's 2014 impact factor: 4.4)

Giménez, Mónica, Hector Ortiz, Carles Soriano-Mas, Marina López-Solà, Magí Farré, Joan Deus, Rocio Martín-Santos, et al. 2014. **"Functional Effects of Chronic Paroxetine versus Placebo on the Fear, Stress and Anxiety Brain Circuit in Social Anxiety Disorder: Initial Validation of an Imaging Protocol for Drug Discovery."** *European Neuropsychopharmacology* 24 (1). pp 105–16. Results reproduced with permission of the editor.

13 Bibliography

- Adams, C.P. & Van Vu, B., 2010. Spending on new drug development. *Health Economics*, 19(2), pp.130–141.
- Aguirre, G.K., Zarahn, E. & D’Esposito, M., 1997. Empirical Analyses of BOLD fMRI Statistics. *NeuroImage*, 5(3), pp.199–212.
- Ahrens, L.M., Mühlberger, A., Pauli, P. & Wieser, M.J., 2015. Impaired visuocortical discrimination learning of socially conditioned stimuli in social anxiety. *Social cognitive and affective neuroscience*, 10(7), pp.929–37.
- Åhs, F., Furmark, T., Michelgård, Å., Långström, B., Appel, L., Wolf, O.T., Kirschbaum, C. & Fredrikson, M., 2006. Hypothalamic Blood Flow Correlates Positively With Stress-Induced Cortisol Levels in Subjects With Social Anxiety Disorder. *Psychosomatic Medicine*, 68(6), pp.859–862.
- Akaike, H., 1974. A new look at the statistical model identification. *IEEE Transactions on Automatic Control*, 19(6), pp.716–723.
- Allen, E.A., Damaraju, E., Plis, S.M., Erhardt, E.B., Eichele, T. & Calhoun, V.D., 2014. Tracking Whole-Brain Connectivity Dynamics in the Resting State. *Cerebral Cortex*, 24(3), pp.663–676.
- Alonso, J., Angermeyer, M.C., Bernert, S., Bruffaerts, R., Brugha, T.S., Bryson, H., de Girolamo, G., Graaf, R., et al., 2004. Disability and quality of life impact of mental disorders in Europe: results from the European Study of the Epidemiology of Mental Disorders (ESEMeD) project. *Acta psychiatrica Scandinavica. Supplementum*, (420), pp.38–46.
- Ampère, A.-M., 1826. *Théorie des phénomènes électro-dynamiques, uniquement déduite de l’expérience*, Paris: Méquignon-Marvis.
- Andrews, P.W., Bharwani, A., Lee, K.R., Fox, M. & Thomson, J.A., 2015. Is serotonin an upper or a downer? The evolution of the serotonergic system and its role in depression and the antidepressant response. *Neuroscience and biobehavioral reviews*, 51, pp.164–88.
- Andrews-Hanna, J.R., Reidler, J.S., Huang, C. & Buckner, R.L., 2010. Evidence for the default network’s role in spontaneous cognition. *Journal of neurophysiology*, 104(1), pp.322–35.

- APA, 2000. *Diagnostic Criteria from DSM-IV-TR*, American Psychiatric Association Washington, DC.
- APA, A.P.A., 2013. *Diagnostic and Statistical Manual of Mental Disorders (DSM-5®)*,
- Appelhans, B.M. & Luecken, L.J., 2006. Heart rate variability as an index of regulated emotional responding. *Review of General Psychology*, 10(3), pp.229–240.
- Arbabshirani, M.R., Havlicek, M., Kiehl, K.A., Pearlson, G.D. & Calhoun, V.D., 2013. Functional network connectivity during rest and task conditions: a comparative study. *Human brain mapping*, 34(11), pp.2959–71.
- Arce, E., Simmons, A.N., Lovero, K.L., Stein, M.B. & Paulus, M.P., 2008. Escitalopram effects on insula and amygdala BOLD activation during emotional processing. *Psychopharmacology*, 196(4), pp.661–72.
- Argyropoulos, S. V, Hood, S.D., Adrover, M., Bell, C.J., Rich, A.S., Nash, J.R., Rich, N.C., Witchel, H.J., et al., 2004. Tryptophan depletion reverses the therapeutic effect of selective serotonin reuptake inhibitors in social anxiety disorder. *Biological psychiatry*, 56(7), pp.503–9.
- Ashburner, J., 2012. SPM: a history. *NeuroImage*, 62(2), pp.791–800.
- Ashburner, J. & Friston, K.J., 2005. Unified segmentation. *NeuroImage*, 26(3), pp.839–851.
- Azevedo, F.A.C., Carvalho, L.R.B., Grinberg, L.T., Farfel, J.M., Ferretti, R.E.L., Leite, R.E.P., Jacob Filho, W., Lent, R., et al., 2009. Equal numbers of neuronal and nonneuronal cells make the human brain an isometrically scaled-up primate brain. *The Journal of comparative neurology*, 513(5), pp.532–41.
- Backs, R.W. & Seljos, K.A., 1994. Metabolic and cardiorespiratory measures of mental effort: the effects of level of difficulty in a working memory task. *International journal of psychophysiology : official journal of the International Organization of Psychophysiology*, 16(1), pp.57–68.
- Baker, D.A., Schweitzer, N.J. & Risko, E.F., 2013. Perceived Access to Self-relevant Information Mediates Judgments of Privacy Violations in Neuromonitoring and Other Monitoring Technologies. *Neuroethics*, 7(1), pp.43–50.
- Baker, S.C., Frith, C.D. & Dolan, R.J., 1997. The interaction between mood and cognitive function studied with PET. *Psychological Medicine*, 27(3), pp.565–578.
- Bandettini, P.A., Wong, E.C., Jesmanowicz, A., Hinks, R.S. & Hyde, J.S., 1994. Spin-echo and gradient-echo epi of human brain activation using bold contrast: A comparative study at 1.5 T. *NMR in Biomedicine*, 7(1-2), pp.12–20.

- Barch, D.M., Sabb, F.W., Carter, C.S., Braver, T.S., Noll, D.C. & Cohen, J.D., 1999. Overt verbal responding during fMRI scanning: empirical investigations of problems and potential solutions. *NeuroImage*, 10(6), pp.642–657.
- Barkhof, F., Haller, S. & Rombouts, S.A.R.B., 2014. Resting-state functional MR imaging: a new window to the brain. *Radiology*, 272(1), pp.29–49.
- Barks, S.K., Parr, L.A. & Rilling, J.K., 2015. The default mode network in chimpanzees (*Pan troglodytes*) is similar to that of humans. *Cerebral cortex (New York, N.Y. : 1991)*, 25(2), pp.538–44.
- Barrett, L.F., Mesquita, B., Ochsner, K.N. & Gross, J.J., 2007. The experience of emotion. *Annual review of psychology*, 58, pp.373–403.
- Becerra, L., Upadhyay, J., Chang, P.-C., Bishop, J., Anderson, J., Baumgartner, R., Schwarz, A.J., Coimbra, A., et al., 2013. Parallel buprenorphine pHMRI responses in conscious rodents and healthy human subjects. *The Journal of pharmacology and experimental therapeutics*, 345, pp.41–51.
- Beck, A.T., Epstein, N., Brown, G. & Steer, R.A., 1988. An inventory for measuring clinical anxiety: Psychometric properties. *Journal of Consulting and Clinical Psychology*, 56(6), pp.893–897.
- Beckmann, C.F., 2012. Modelling with independent components. *NeuroImage*, 62(2), pp.891–901.
- Beckmann, C.F., DeLuca, M., Devlin, J.T. & Smith, S.M., 2005. Investigations into resting-state connectivity using independent component analysis. *Philosophical transactions of the Royal Society of London. Series B, Biological sciences*, 360(1457), pp.1001–1013.
- Behrens, T.E.J. & Sporns, O., 2012. Human connectomics. *Current opinion in neurobiology*, 22(1), pp.144–53.
- Behzadi, Y. & Liu, T.T., 2005. An arteriolar compliance model of the cerebral blood flow response to neural stimulus. *NeuroImage*, 25(4), pp.1100–11.
- Bell, a J. & Sejnowski, T.J., 1995. An information-maximization approach to blind separation and blind deconvolution. *Neural computation*, 7(6), pp.1129–1159.
- Beneke, M. & Rasmus, W., 1992. “Clinical Global Impressions” (ECDEU): some critical comments. *Pharmacopsychiatry*, 25(4), pp.171–6.
- Benítez, C.I.P., Smith, K., Vasile, R.G., Rende, R., Edelen, M.O. & Keller, M.B., 2008. Use of Benzodiazepines and Selective Serotonin Reuptake Inhibitors in Middle-Aged and

Older Adults With Anxiety Disorders: A Longitudinal and Prospective Study. *The American Journal of Geriatric Psychiatry*, 16(1), pp.5–13.

Bergström, M., Grahnén, A. & Långström, B., 2003. Positron emission tomography microdosing: a new concept with application in tracer and early clinical drug development. *European journal of clinical pharmacology*, 59(5-6), pp.357–66.

Birbaumer, N., Grodd, W., Diedrich, O., Klose, U., Erb, M., Lotze, M., Schneider, F., Weiss, U., et al., 1998. fMRI reveals amygdala activation to human faces in social phobics. *Neuroreport*, 9(6), pp.1223–6.

Birn, R.M., Bandettini, P.A., Cox, R.W., Jesmanowicz, A. & Shaker, R., 1998. Magnetic field changes in the human brain due to swallowing or speaking. *Magnetic Resonance in Medicine*, 40(1), pp.55–60.

Birn, R.M., Cox, R.W. & Bandettini, P.A., 2004. Experimental designs and processing strategies for fMRI studies involving overt verbal responses. *NeuroImage*, 23(3), pp.1046–58.

Birn, R.M., Diamond, J.B., Smith, M. a. & Bandettini, P. a., 2006. Separating respiratory-variation-related fluctuations from neuronal-activity-related fluctuations in fMRI. *NeuroImage*, 31(4), pp.1536–1548.

Birn, R.M., Molloy, E.K., Patriat, R., Parker, T., Meier, T.B., Kirk, G.R., Nair, V.A., Meyerand, M.E., et al., 2013. The effect of scan length on the reliability of resting-state fMRI connectivity estimates. *NeuroImage*, 83, pp.550–8.

Birn, R.M., Murphy, K. & Bandettini, P.A., 2008. The effect of respiration variations on independent component analysis results of resting state functional connectivity. *Human Brain Mapping*, 29(7), pp.740–750.

Birn, R.M., Smith, M. a., Jones, T.B. & Bandettini, P. a., 2008. The respiration response function: The temporal dynamics of fMRI signal fluctuations related to changes in respiration. *NeuroImage*, 40(2), pp.644–654.

Bishop, S., Duncan, J., Brett, M. & Lawrence, A.D., 2004. Prefrontal cortical function and anxiety: controlling attention to threat-related stimuli. *Nature Neuroscience*, 7(2), pp.184–188.

Biswal, B., Yetkin, F.Z., Haughton, V.M., Hyde, J.S., Zerrin Yetkin, F., Haughton, V.M. & Hyde, J.S., 1995. Functional connectivity in the motor cortex of resting human brain using echo-planar MRI. *Magnetic resonance in medicine : official journal of the Society of Magnetic Resonance in Medicine / Society of Magnetic Resonance in*

Medicine, 34(4), pp.537–541.

Biswal, B.B., Mennes, M., Zuo, X.-N., Gohel, S., Kelly, C., Smith, S.M., Beckmann, C.F., Adelstein, J.S., et al., 2010. Toward discovery science of human brain function. *Proceedings of the National Academy of Sciences of the United States of America*, 107(10), pp.4734–4739.

Blair, K.S., Geraci, M., Otero, M., Majestic, C., Odenheimer, S., Jacobs, M., Blair, R.J.R. & Pine, D.S., 2011. Atypical modulation of medial prefrontal cortex to self-referential comments in generalized social phobia. *Psychiatry research*, 193(1), pp.38–45.

Blamire, a M., Ogawa, S., Ugurbil, K., Rothman, D., McCarthy, G., Ellermann, J.M., Hyder, F., Rattner, Z., et al., 1992. Dynamic mapping of the human visual cortex by high-speed magnetic resonance imaging. *Proceedings of the National Academy of Sciences of the United States of America*, 89(22), pp.11069–11073.

Blamire, A.M., 2012. The Yale experience in first advancing fMRI. *NeuroImage*, 62(2), pp.637–640.

Blanco, C., Bragdon, L.B., Schneier, F.R. & Liebowitz, M.R., 2013. The evidence-based pharmacotherapy of social anxiety disorder. *The international journal of neuropsychopharmacology / official scientific journal of the Collegium Internationale Neuropsychopharmacologicum (CINP)*, 16(1), pp.235–49.

Blanco, C., Schneier, F.R., Schmidt, A., Blanco-Jerez, C.-R., Marshall, R.D., Sánchez-Lacay, A. & Liebowitz, M.R., 2003. Pharmacological treatment of social anxiety disorder: a meta-analysis. *Depression and anxiety*, 18(1), pp.29–40.

Bloch, F., 1946. Nuclear induction. *Physical Review*, 70(7-8), pp.460–474.

Borsook, D., Becerra, L. & Hargreaves, R., 2006. A role for fMRI in optimizing CNS drug development. *Nature reviews. Drug discovery*, 5(5), pp.411–424.

Braboszcz, C. & Delorme, A., 2011. Lost in thoughts: neural markers of low alertness during mind wandering. *NeuroImage*, 54(4), pp.3040–7.

Brett, M., Anton, J.-L., Valabregue, R. & Poline, J.-B., 2002. Region of interest analysis using an SPM toolbox. In *8th International Conference on Functional Mapping of the Human Brain*. Sendai, Japan: Neuroimage, p. Vol 16, No 2.

Brett, M., Johnsrude, I.S. & Owen, A.M., 2002. The problem of functional localization in the human brain. *Nature reviews. Neuroscience*, 3(3), pp.243–249.

Bright, M.G. & Murphy, K., 2015. Is fMRI “noise” really noise? Resting state nuisance regressors remove variance with network structure. *NeuroImage*, 114, pp.158–169.

- Britton, J.C., Stewart, S.E., Killgore, W.D.S., Rosso, I.M., Price, L.M., Gold, A.L., Pine, D.S., Wilhelm, S., et al., 2010. Amygdala activation in response to facial expressions in pediatric obsessive-compulsive disorder. *Depression and anxiety*, 27(7), pp.643–51.
- Brookes, M.J., Woolrich, M., Luckhoo, H., Price, D., Hale, J.R., Stephenson, M.C., Barnes, G.R., Smith, S.M., et al., 2011. Investigating the electrophysiological basis of resting state networks using magnetoencephalography. *Proceedings of the National Academy of Sciences of the United States of America*, 108(40), pp.16783–8.
- Brown, G.G., Ostrowitzki, S., Stein, M.B., von Kienlin, M., Liu, T.T., Simmons, A., Wierenga, C., Stein, O.Y., et al., 2015. Temporal profile of brain response to alprazolam in patients with generalized anxiety disorder. *Psychiatry research*.
- Browning, M., Reid, C., Cowen, P.J., Goodwin, G.M. & Harmer, C.J., 2007. A single dose of citalopram increases fear recognition in healthy subjects. *Journal of psychopharmacology (Oxford, England)*, 21(7), pp.684–90.
- Brühl, A.B., Delsignore, A., Komossa, K. & Weidt, S., 2014. Neuroimaging in Social Anxiety Disorder—a meta-analytic review resulting in a new neurofunctional model. *Neuroscience & Biobehavioral Reviews*, 47, pp.260–280.
- Bullmore, E., Long, C., Suckling, J., Fadili, J., Calvert, G., Zelaya, F., Carpenter, T.A., Brammer, M., et al., 2001. Colored noise and computational inference in fMRI time series analysis: resampling methods in time and wavelet domains. Institute of Psychiatry KCL, London UK. *Human brain mapping*, 78(6), p.2001.
- Burghardt, N.S., Sullivan, G.M., McEwen, B.S., Gorman, J.M. & LeDoux, J.E., 2004. The selective serotonin reuptake inhibitor citalopram increases fear after acute treatment but reduces fear with chronic treatment: a comparison with tianeptine. *Biological psychiatry*, 55(12), pp.1171–8.
- Busner, J., Targum, S.D. & Miller, D.S., 2009. The Clinical Global Impressions scale: errors in understanding and use. *Comprehensive psychiatry*, 50(3), pp.257–62.
- Buxton, R.B. & Frank, L.R., 1997. A model for the coupling between cerebral blood flow and oxygen metabolism during neural stimulation. *Journal of cerebral blood flow and metabolism: official journal of the International Society of Cerebral Blood Flow and Metabolism*, 17(1), pp.64–72.
- Buxton, R.B., Wong, E.C. & Frank, L.R., 1998. Dynamics of blood flow and oxygenation changes during brain activation: the balloon model. *Magn Reson Med*, 39(17), pp.855–864.

- Calhoun, V., Adali, T., Pearlson, G. & Pekar, J., 2001a. A method for making group inferences from functional MRI data using independent component analysis. *Human brain mapping*, 14(3), pp.140–51.
- Calhoun, V., Adali, T., Pearlson, G. & Pekar, J., 2001b. Spatial and temporal independent component analysis of functional MRI data containing a pair of task-related waveforms. *Human Brain Mapping*, 13(1), pp.43–53.
- Calhoun, V.D. & Adali, T., 2006. Unmixing fMRI with Independent Component Analysis ©. *IEEE Engineering in Medicine and Biology Magazine*, 25(April), pp.79–90.
- Calhoun, V.D. & Adali, T., 2012. Multisubject independent component analysis of fMRI: a decade of intrinsic networks, default mode, and neurodiagnostic discovery. *IEEE reviews in biomedical engineering*, 5, pp.60–73.
- Calhoun, V.D., Adali, T. & Pekar, J.J., 2004. A method for comparing group fMRI data using independent component analysis: application to visual, motor and visuomotor tasks. *Magnetic Resonance Imaging*, 22(9), pp.1181–1191.
- Calhoun, V.D., Adali, T., Pekar, J.J. & Pearlson, G.D., 2003. Latency (in)sensitive ICA. *NeuroImage*, 20(3), pp.1661–1669.
- Calhoun, V.D., Kiehl, K. a & Pearlson, G.D., 2008. Modulation of temporally coherent brain networks estimated using ICA at rest and during cognitive tasks. *Human brain mapping*, 29(7), pp.828–38.
- Calhoun, V.D., Miller, R., Pearlson, G. & Adali, T., 2014. The Chronnectome: Time-Varying Connectivity Networks as the Next Frontier in fMRI Data Discovery. *Neuron*.
- Calhoun, V.D., Potluru, V.K., Phlypo, R., Silva, R.F., Pearlmuter, B. a., Caprihan, A., Plis, S.M. & Adali, T., 2013. Independent Component Analysis for Brain fMRI Does Indeed Select for Maximal Independence. *PLoS ONE*, 8(8), p.e73309.
- Camara, W.J., Nathan, J.S. & Puente, A.E., 2000. Psychological test usage: Implications in professional psychology. *Professional Psychology: Research and Practice*, 31(2), pp.141–154.
- Campbell, D.W., Sareen, J., Paulus, M.P., Goldin, P.R., Stein, M.B. & Reiss, J.P., 2007. Time-varying amygdala response to emotional faces in generalized social phobia. *Biological psychiatry*, 62(5), pp.455–63.
- Canton, J., Scott, K.M. & Glue, P., 2012. Optimal treatment of social phobia: systematic review and meta-analysis. *Neuropsychiatric disease and treatment*, 8, pp.203–15.
- Caseras, X., Mataix-Cols, D., Trasovares, M.V., López-Solà, M., Ortiz, H., Pujol, J., Soriano-

- Mas, C., Giampietro, V., et al., 2010. Dynamics of brain responses to phobic-related stimulation in specific phobia subtypes. *European Journal of Neuroscience*, 32(8), pp.1414–1422.
- Cavallo, A., Lungu, O., Becchio, C., Ansuini, C., Rustichini, A. & Fadiga, L., 2015. When gaze opens the channel for communication: Integrative role of IFG and MPFC. *NeuroImage*.
- Çetin, M.S., Christensen, F., Abbott, C.C., Stephen, J.M., Mayer, A.R., Cañive, J.M., Bustillo, J.R., Pearlson, G.D., et al., 2014. Thalamus and posterior temporal lobe show greater inter-network connectivity at rest and across sensory paradigms in schizophrenia. *NeuroImage*, 97, pp.117–26.
- Chang, C. & Glover, G.H., 2009. Effects of model-based physiological noise correction on default mode network anti-correlations and correlations. *NeuroImage*, 47(4), pp.1448–59.
- Chang, C., Metzger, C.D., Glover, G.H., Duyn, J.H., Heinze, H.-J. & Walter, M., 2013. Association between heart rate variability and fluctuations in resting-state functional connectivity. *NeuroImage*, 68, pp.93–104.
- Choi, S., Cichocki, A. & Amari, S.-I., 2000. Flexible Independent Component Analysis. *Journal of VLSI signal processing systems for signal, image and video technology*, 26(1-2), pp.25–38.
- Chumbley, J.R. & Friston, K.J., 2009. False discovery rate revisited: FDR and topological inference using Gaussian random fields. *NeuroImage*, 44(1), pp.62–70.
- Clark, D.M., Ehlers, A., McManus, F., Hackmann, A., Fennell, M., Campbell, H., Flower, T., Davenport, C., et al., 2003. Cognitive therapy versus fluoxetine in generalized social phobia: a randomized placebo-controlled trial. *Journal of consulting and clinical psychology*, 71(6), pp.1058–1067.
- Clark, D.M. & Mcmanus, F., 2002. Information Processing in Social Phobia. , 3223(1995).
- Clark, D.M. & Teasdale, J.D., 1985. Constraints on the effects of mood on memory. *Journal of Personality and Social Psychology*, 48(6), pp.1595–1608.
- Collins, J.M., 2005. Imaging and other biomarkers in early clinical studies: One step at a time or re-engineering drug development? *Journal of Clinical Oncology*, 23(24), pp.5417–5419.
- Comon, P., 1994. Independent component analysis, A new concept? *Signal Processing*, 36(3), pp.287–314.

- Cools, R., Roberts, A.C. & Robbins, T.W., 2008. Serotonergic regulation of emotional and behavioural control processes. *Trends in cognitive sciences*, 12(1), pp.31–40.
- Cooney, R.E., Atlas, L.Y., Joormann, J., Eugène, F. & Gotlib, I.H., 2006. Amygdala activation in the processing of neutral faces in social anxiety disorder: is neutral really neutral? *Psychiatry research*, 148(1), pp.55–9.
- Cordes, D., Haughton, V.M., Arfanakis, K., Carew, J.D., Turski, P.A., Moritz, C.H., Quigley, M.A. & Meyerand, M.E., 2001. Frequencies Contributing to Functional Connectivity in the Cerebral Cortex in “Resting-state” Data. *AJNR Am. J. Neuroradiol.*, 22(7), pp.1326–1333.
- Correa, N., Adali, T. & Calhoun, V.D., 2007. Performance of blind source separation algorithms for fMRI analysis using a group ICA method. *Magnetic resonance imaging*, 25(5), pp.684–94.
- Costa e Silva, J.A., 2013. Personalized medicine in psychiatry: new technologies and approaches. *Metabolism: clinical and experimental*, 62 Suppl 1, pp.S40–4.
- Cox, R.W., 1996. AFNI: software for analysis and visualization of functional magnetic resonance neuroimages. *Computers and biomedical research, an international journal*, 29(3), pp.162–173.
- Cox, W.J. & Kenardy, J., 1993. Performance anxiety, social phobia, and setting effects in instrumental music students. *Journal of Anxiety Disorders*, 7(1), pp.49–60.
- Croft, L.J., Rankin, P.M., Liégeois, F., Banks, T., Cross, J.H., Vargha-Khadem, F. & Baldeweg, T., 2013. To speak, or not to speak? The feasibility of imaging overt speech in children with epilepsy. *Epilepsy research*, 107(1-2), pp.195–9.
- Cryan, J.F. & Sweeney, F.F., 2011. The age of anxiety: Role of animal models of anxiolytic action in drug discovery. *British Journal of Pharmacology*, 164(4), pp.1129–1161.
- Cumming, P., 2014. PET Neuroimaging: The White Elephant Packs His Trunk? *NeuroImage*, 84, pp.1094–1100.
- Damadian, R., 1971. Tumor detection by nuclear magnetic resonance. *Science (New York, N.Y.)*, 171(3976), pp.1151–3.
- Damasio, a R., Grabowski, T.J., Bechara, A., Damasio, H., Ponto, L.L., Parvizi, J. & Hichwa, R.D., 2000. Subcortical and cortical brain activity during the feeling of self-generated emotions. *Nature neuroscience*, 3(10), pp.1049–1056.
- Davidson, J.R., Miner, C.M., De Vaughn-Geiss, J., Tupler, L. a, Colket, J.T. & Potts, N.L., 1997. The Brief Social Phobia Scale: a psychometric evaluation. *Psychological*

medicine, 27(1), pp.161–166.

- Davidson, J.R., Potts, N.L., Richichi, E.A., Ford, S.M., Krishnan, K.R., Smith, R.D. & Wilson, W., 1991. The Brief Social Phobia Scale.
- Davis, M.J. & Hill, M.A., 1999. Signaling Mechanisms Underlying the Vascular Myogenic Response. *Physiol Rev*, 79(2), pp.387–423.
- Dechent, P., Schütze, G., Helms, G., Merboldt, K.D. & Frahm, J., 2011. Basal cerebral blood volume during the poststimulation undershoot in BOLD MRI of the human brain. *Journal of cerebral blood flow and metabolism : official journal of the International Society of Cerebral Blood Flow and Metabolism*, 31(1), pp.82–89.
- Deco, G., Ponce-Alvarez, a., Mantini, D., Romani, G.L., Hagmann, P. & Corbetta, M., 2013. Resting-State Functional Connectivity Emerges from Structurally and Dynamically Shaped Slow Linear Fluctuations. *Journal of Neuroscience*, 33(27), pp.11239–11252.
- Demenescu, L.R., Kortekaas, R., Cremers, H.R., Renken, R.J., van Tol, M.J., van der Wee, N.J.A., Veltman, D.J., den Boer, J.A., et al., 2013. Amygdala activation and its functional connectivity during perception of emotional faces in social phobia and panic disorder. *Journal of psychiatric research*, 47(8), pp.1024–31.
- Devue, C. & Brédart, S., 2011. The neural correlates of visual self-recognition. *Consciousness and cognition*, 20(1), pp.40–51.
- Diedrichsen, J. & Shadmehr, R., 2005. Detecting and adjusting for artifacts in fMRI time series data. *NeuroImage*, 27(3), pp.624–34.
- Diefenbach, G.J., Diefenbach, D., Baumeister, A. & West, M., 1999. Portrayal of lobotomy in the popular press: 1935-1960. *Journal of the history of the neurosciences*, 8(1), pp.60–9.
- Dodhia, S., Hosanagar, a, Fitzgerald, D. a, Labuschagne, I., Wood, a G., Nathan, P.J. & Phan, K.L., 2014. Modulation of resting-state amygdala-frontal functional connectivity by oxytocin in generalized social anxiety disorder. *Neuropsychopharmacology*, 39(9), pp.2061–2069.
- Downing, N.S., Aminawung, J.A., Shah, N.D., Krumholz, H.M. & Ross, J.S., 2014. Clinical trial evidence supporting FDA approval of novel therapeutic agents, 2005-2012. *JAMA*, 311(4), pp.368–77.
- Du, Y., Liu, J., Sui, J., He, H., Pearlson, G.D. & Calhoun, V.D., 2014. Exploring difference and overlap between schizophrenia , schizoaffective and bipolar disorders using resting-state brain functional networks. *36th Annual International Conference of the IEEE*

Engineering in Medicine and Biology Society, pp.1517–1520.

- Duong, T.Q., Yacoub, E., Adriany, G., Hu, X., Uğurbil, K. & Kim, S.-G., 2003. Microvascular BOLD contribution at 4 and 7 T in the human brain: Gradient-echo and spin-echo fMRI with suppression of blood effects. *Magnetic Resonance in Medicine*, 49(6), pp.1019–1027.
- Duval, E.R., Javanbakht, A. & Liberzon, I., 2015. Neural circuits in anxiety and stress disorders: a focused review. *Therapeutics and clinical risk management*, 11, pp.115–26.
- Dziobek, I., Bahnemann, M., Convit, A. & Heekeren, H.R., 2010. The role of the fusiform-amygdala system in the pathophysiology of autism. *Archives of general psychiatry*, 67(4), pp.397–405.
- Ekman, P., Levenson, R.W. & Friesen, W. V., 1983. Autonomic nervous system activity distinguishes among emotions. *Science (New York, N.Y.)*, 221(4616), pp.1208–10.
- Engel, S. a., Glover, G.H. & Wandell, B. a., 1997. Retinotopic organization in human visual cortex and the spatial precision of functional MRI. *Cerebral Cortex*, 7(2), pp.181–192.
- Erecińska, M. & Dagani, F., 1990. Relationships between the neuronal sodium/potassium pump and energy metabolism. Effects of K⁺, Na⁺, and adenosine triphosphate in isolated brain synaptosomes. *The Journal of general physiology*, 95(4), pp.591–616.
- ESR, 2015. Medical imaging in personalised medicine: a white paper of the research committee of the European Society of Radiology (ESR). *Insights into imaging*, 6(2), pp.141–55.
- Etkin, A., Egner, T. & Kalisch, R., 2011. Emotional processing in anterior cingulate and medial prefrontal cortex. *Trends in cognitive sciences*, 15(2), pp.85–93.
- Etkin, A. & Wager, T.D., 2007. Functional neuroimaging of anxiety: a meta-analysis of emotional processing in PTSD, social anxiety disorder, and specific phobia. *The American journal of psychiatry*, 164(10), pp.1476–1488.
- Evans, K.C., Wright, C.I., Wedig, M.M., Gold, A.L., Pollack, M.H. & Rauch, S.L., 2008. A functional MRI study of amygdala responses to angry schematic faces in social anxiety disorder. *Depression and Anxiety*, 25(6), pp.496–505.
- Farah, M.J., 2012. Neuroethics: The Ethical, Legal, and Societal Impact of Neuroscience. *Annual Review of Psychology*, 63(1), pp.571–591.
- Farah, M.J., Smith, M.E., Gawuga, C., Lindsell, D. & Foster, D., 2009. Brain imaging and brain privacy: a realistic concern? *Journal of cognitive neuroscience*, 21(1), pp.119–

127.

- Faria, V., Appel, L., Åhs, F., Linnman, C., Pissioti, A., Frans, Ö., Bani, M., Bettica, P., et al., 2012. Amygdala subregions tied to SSRI and placebo response in patients with social anxiety disorder. *Neuropsychopharmacology : official publication of the American College of Neuropsychopharmacology*, 37(10), pp.2222–32.
- FDA, U.F. and drug administration, 2015. Applications for Food and Drug Administration Approval to Market a New Drug: Accelerated Approval of New Drugs for Serious or Life-Threatening Illnesses, 21 CFR §314h. Available at: <http://www.accessdata.fda.gov/scripts/cdrh/cfdocs/cfcfr/CFRSearch.cfm?CFRPart=314> [Accessed August 27, 2015].
- Fedota, J.R. & Stein, E.A., 2015. Resting-state functional connectivity and nicotine addiction: prospects for biomarker development. *Annals of the New York Academy of Sciences*, 1349(1), pp.64–82.
- Fehm, L., Pelissolo, A., Furmark, T. & Wittchen, H.-U., 2005. Size and burden of social phobia in Europe. *European neuropsychopharmacology : the journal of the European College of Neuropsychopharmacology*, 15(4), pp.453–62.
- Fehm, L. & Schmidt, K., 2006. Performance anxiety in gifted adolescent musicians. *Journal of anxiety disorders*, 20(1), pp.98–109.
- Feinberg, D.A. & Yacoub, E., 2012. The rapid development of high speed, resolution and precision in fMRI. *NeuroImage*, 62(2), pp.720–5.
- First, M.B., Spitzer, R.L., Gibbon, M. & Williams, J.B., 2002. *Structured Clinical Interview for DSM-IV-TR Axis I Disorders, Research Version, Non-patient Edition. (SCID-I/NP)*, New York: Biometrics Research, New York State Psychiatric Institute.
- Fischer, A.G., Jocham, G. & Ullsperger, M., 2014. Dual serotonergic signals: a key to understanding paradoxical effects? *Trends in cognitive sciences*, 19(1), pp.21–26.
- Fischl, B., Salat, D.H., van der Kouwe, A.J.W., Makris, N., Ségonne, F., Quinn, B.T. & Dale, A.M., 2004. Sequence-independent segmentation of magnetic resonance images. *NeuroImage*, 23 Suppl 1, pp.S69–84.
- Fleming, T.R., 1996. Surrogate End Points in Clinical Trials: Are We Being Misled? *Annals of Internal Medicine*, 125(7), p.605.
- Fornito, A. & Bullmore, E.T., 2010. What can spontaneous fluctuations of the blood oxygenation-level-dependent signal tell us about psychiatric disorders? *Current opinion in psychiatry*, 23(3), pp.239–249.

- Fox, P., Raichle, M., Mintun, M. & Dence, C., 1988. Nonoxidative glucose consumption during focal physiologic neural activity. *Science*, 241(4864), pp.462–464.
- Fox, P.T. & Raichle, M.E., 1986. Focal physiological uncoupling of cerebral blood flow and oxidative metabolism during somatosensory stimulation in human subjects. *Proceedings of the National Academy of Sciences of the United States of America*, 83(4), pp.1140–1144.
- Frahm, J., Merboldt, K.-D. & Hänicke, W., 1993. Functional MRI of human brain activation at high spatial resolution. *Magnetic Resonance in Medicine*, 29(1), pp.139–144.
- François, C., Despiéglé, N., Maman, K., Saragoussi, D. & Auquier, P., 2010. Anxiety disorders, major depressive disorder and the dynamic relationship between these conditions: treatment patterns and cost analysis. *Journal of medical economics*, 13(1), pp.99–109.
- Frank, R. & Hargreaves, R., 2003. Clinical biomarkers in drug discovery and development. *Nature reviews. Drug discovery*, 2(7), pp.566–580.
- Freitas-Ferrari, M.C., Hallak, J.E.C., Trzesniak, C., Filho, A.S., Machado-de-Sousa, J.P., Chagas, M.H.N., Nardi, A.E. & Crippa, J.A.S., 2010. Neuroimaging in social anxiety disorder: a systematic review of the literature. *Progress in neuro-psychopharmacology & biological psychiatry*, 34(4), pp.565–80.
- Frick, A., Howner, K., Fischer, H., Kristiansson, M. & Furmark, T., 2013. Altered fusiform connectivity during processing of fearful faces in social anxiety disorder. *Translational psychiatry*, 3(10), p.e312.
- Friston, K., 2002. Beyond P < 0.05: What Can Neuroimaging Tell Us About Distributed Circuitry? *Annual Review of Neuroscience*, 25(1), pp.221–250.
- Friston, K., Worsley, K., Frackowiak, R., Mazziotta, J. & Evans, A., 1994. Assessing the significance of focal activations using their spatial extent. *Hum Brain Mapp*.
- Friston, K.J., Buechel, C., Fink, G.R., Morris, J., Rolls, E. & Dolan, R.J., 1997. Psychophysiological and modulatory interactions in neuroimaging. *NeuroImage*, 6(3), pp.218–29.
- Friston, K.J., Frith, C.D., Liddle, P.F. & Frackowiak, R.S.J., 1991. Comparing Functional (PET) Images: The Assessment of Significant Change. *Journal of Cerebral Blood Flow & Metabolism*, 11(4), pp.690–699.
- Friston, K.J., Holmes, a. P., Worsley, K.J., Poline, J.-P., Frith, C.D. & Frackowiak, R.S.J., 1995.

- Statistical parametric maps in functional imaging: A general linear approach. *Human Brain Mapping*, 2(4), pp.189–210.
- Friston, K.J., Holmes, A., Poline, J.B., Price, C.J. & Frith, C.D., 1996. Detecting activations in PET and fMRI: levels of inference and power. *NeuroImage*, 4(3 Pt 1), pp.223–35.
- Friston, K.J., Jezzard, P. & Turner, R., 1994. Analysis of functional MRI time-series. *Human Brain Mapping*, 1(2), pp.153–171.
- Friston, K.J., Mechelli, A., Turner, R. & Price, C.J., 2000. Nonlinear responses in fMRI: the Balloon model, Volterra kernels, and other hemodynamics. *NeuroImage*, 12(4), pp.466–77.
- Friston, K.J., Penny, W.D., Ashburner, J., Kiebel, S.J. & Nichols, T.E., 2007. *Statistical parametric mapping : the analysis of functional brain images*,
- Friston, K.J., Penny, W.D. & Glaser, D.E., 2005. Conjunction revisited. *NeuroImage*, 25(3), pp.661–667.
- Friston, K.J., Zarahn, E., Josephs, O., Henson, R.N. & Dale, a M., 1999. Stochastic designs in event-related fMRI. *NeuroImage*, 10(5), pp.607–619.
- Fu, C.H.Y., Steiner, H. & Costafreda, S.G., 2013. Predictive neural biomarkers of clinical response in depression: a meta-analysis of functional and structural neuroimaging studies of pharmacological and psychological therapies. *Neurobiology of disease*, 52, pp.75–83.
- Fukunaga, M., Horovitz, S.G., van Gelderen, P., de Zwart, J.A., Jansma, J.M., Ikonomidou, V.N., Chu, R., Deckers, R.H.R., et al., 2006. Large-amplitude, spatially correlated fluctuations in BOLD fMRI signals during extended rest and early sleep stages. *Magnetic resonance imaging*, 24(8), pp.979–92.
- Furmark, T., Appel, L., Henningsson, S., Ahs, F., Faria, V., Linnman, C., Pissiota, A., Frans, O., et al., 2008. A Link between Serotonin-Related Gene Polymorphisms, Amygdala Activity, and Placebo-Induced Relief from Social Anxiety. *Journal of Neuroscience*, 28(49), pp.13066–13074.
- Furmark, T., Tillfors, M., Marteinsdottir, I., Fischer, H., Pissiota, A., Långström, B. & Fredrikson, M., 2002. Common changes in cerebral blood flow in patients with social phobia treated with citalopram or cognitive-behavioral therapy. *Archives of general psychiatry*, 59(5), pp.425–433.
- Gaebler, M., Daniels, J.K., Lamke, J.-P., Fydrich, T. & Walter, H., 2013. Heart rate variability and its neural correlates during emotional face processing in social anxiety disorder.

Biological psychology, 94(2), pp.319–30.

Gati, J.S., Menon, R.S., Uğurbil, K. & Rutt, B.K., 1997. Experimental determination of the BOLD field strength dependence in vessels and tissue. *Magnetic Resonance in Medicine*, 38(2), pp.296–302.

Gautama, T. & Van Hulle, M.M., 2005. Estimating the global order of the fMRI noise model. *NeuroImage*, 26(4), pp.1211–7.

Gazzaniga, M.S., 2011. Shifting Gears: Seeking New Approaches for Mind/Brain Mechanisms. *Annual Review of Psychology*, 64(1), p.120920151208003.

Geiger, M.J., Domschke, K., Ipser, J., Hattingh, C., Baldwin, D.S., Lochner, C. & Stein, D.J., 2015. Altered executive control network resting-state connectivity in social anxiety disorder. *The World Journal of Biological Psychiatry*, 2975(October), pp.1–11.

van Gelderen, P., Duyn, J.H., Ramsey, N.F., Liu, G. & Moonen, C.T.W., 2012. The PRESTO technique for fMRI. *NeuroImage*, 62(2), pp.676–81.

Genovese, C.R., Lazar, N.A. & Nichols, T., 2002. Thresholding of statistical maps in functional neuroimaging using the false discovery rate. *NeuroImage*, 15(4), pp.870–8.

Gentili, C., Cristea, I.A., Angstadt, M., Klumpp, H., Tozzi, L., Phan, K.L. & Pietrini, P., 2015. Beyond emotions: A meta-analysis of neural response within face processing system in social anxiety. *Experimental Biology and Medicine*, pp.1–13.

Gentili, C., Gobbini, M.I., Ricciardi, E., Vanello, N., Pietrini, P., Haxby, J. V & Guazzelli, M., 2008. Differential modulation of neural activity throughout the distributed neural system for face perception in patients with Social Phobia and healthy subjects. *Brain research bulletin*, 77(5), pp.286–92.

Gilbert, F. & Ovadia, D., 2011. Deep brain stimulation in the media: over-optimistic portrayals call for a new strategy involving journalists and scientists in ethical debates. *Frontiers in integrative neuroscience*, 5, p.16.

Gilbert, P., 2001. Evolution and social anxiety. The role of attraction, social competition, and social hierarchies. *The Psychiatric clinics of North America*, 24(4), pp.723–51.

Giménez, M., Pujol, J., Ortiz, H., Soriano-Mas, C., López-Solà, M., Farré, M., Deus, J., Merlo-Pich, E., et al., 2012. Altered brain functional connectivity in relation to perception of scrutiny in social anxiety disorder. *Psychiatry research*, 202(3), pp.214–23.

Gitelman, D.R., Penny, W.D., Ashburner, J. & Friston, K.J., 2003. Modeling regional and psychophysiological interactions in fMRI: the importance of hemodynamic

deconvolution. *NeuroImage*, 19(1), pp.200–207.

Glover, G.H., Li, T.Q. & Ress, D., 2000. Image-based method for retrospective correction of physiological motion effects in fMRI: RETROICOR. *Magnetic resonance in medicine*, 44(1), pp.162–7.

Gobbini, M.I. & Haxby, J. V., 2007. Neural systems for recognition of familiar faces. *Neuropsychologia*, 45(1), pp.32–41.

Goldin, P.R., Manber, T., Hakimi, S., Canli, T. & Gross, J.J., 2009. Neural bases of social anxiety disorder: emotional reactivity and cognitive regulation during social and physical threat. *Archives of general psychiatry*, 66(2), pp.170–80.

Goldin, P.R., Manber-Ball, T., Werner, K., Heimberg, R. & Gross, J.J., 2009. Neural mechanisms of cognitive reappraisal of negative self-beliefs in social anxiety disorder. *Biological psychiatry*, 66(12), pp.1091–9.

Goudriaan, A.E., Veltman, D.J., van den Brink, W., Dom, G. & Schmaal, L., 2013. Neurophysiological effects of modafinil on cue-exposure in cocaine dependence: a randomized placebo-controlled cross-over study using pharmacological fMRI. *Addictive behaviors*, 38(2), pp.1509–17.

Grant, B.F., Hasin, D.S., Blanco, C., Stinson, F.S., Chou, S.P., Goldstein, R.B., Dawson, D. a, Smith, S.M., et al., 2005. The epidemiology of social anxiety disorder in the United States: results from the National Epidemiologic Survey on Alcohol and Related Conditions. *The Journal of clinical psychiatry*, 66(11), pp.1351–61.

Gray, N.A., Milak, M.S., DeLorenzo, C., Ogden, R.T., Huang, Y.-Y., Mann, J.J. & Parsey, R. V., 2013. Antidepressant treatment reduces serotonin-1A autoreceptor binding in major depressive disorder. *Biological psychiatry*, 74(1), pp.26–31.

Greicius, M.D. & Menon, V., 2004. Default-mode activity during a passive sensory task: uncoupled from deactivation but impacting activation. *Journal of cognitive neuroscience*, 16(9), pp.1484–92.

Griffeth, V.E.M. & Buxton, R.B., 2011. A theoretical framework for estimating cerebral oxygen metabolism changes using the calibrated-BOLD method: modeling the effects of blood volume distribution, hematocrit, oxygen extraction fraction, and tissue signal properties on the BOLD signal. *NeuroImage*, 58(1), pp.198–212.

Griffeth, V.E.M., Perthen, J.E. & Buxton, R.B., 2011. Prospects for quantitative fMRI: investigating the effects of caffeine on baseline oxygen metabolism and the response to a visual stimulus in humans. *NeuroImage*, 57(3), pp.809–16.

- Grimm, O., Gass, N., Weber-Fahr, W., Sartorius, A., Schenker, E., Spedding, M., Risterucci, C., Schweiger, J.I., et al., 2015. Acute ketamine challenge increases resting state prefrontal-hippocampal connectivity in both humans and rats. *Psychopharmacology*, 232(21-22), pp.4231–4241.
- Gusnard, D.A., Akbudak, E., Shulman, G.L. & Raichle, M.E., 2001. Medial prefrontal cortex and self-referential mental activity: relation to a default mode of brain function. *Proceedings of the National Academy of Sciences of the United States of America*, 98(7), pp.4259–64.
- Gutiérrez-Zotes, J.A., Bayón, C., Montserrat, C., Valero, J., Labad, A., Cloninger, C.R. & Fernández-Aranda, F., 2004. Inventario del Temperamento y el Carácter-Revisado (TCI-R). Baremación y datos normativos en una muestra de población general. / Temperament and Character Inventory Revised (TCI-R). Standardization and normative data in a general population sample. *Actas Españolas de Psiquiatría*, 32(1), pp.8–15.
- Haase, A., Frahm, J., Matthaei, D., Hänicke, W. & Merboldt, K.-D., 1986. FLASH imaging: rapid NMR imaging using low flip-angle pulses. 1986. *Journal of magnetic resonance (San Diego, Calif. : 1997)*, 67, pp.258–266.
- Hagmann, P., Cammoun, L., Gigandet, X., Meuli, R., Honey, C.J., Wedeen, V.J. & Sporns, O., 2008. Mapping the structural core of human cerebral cortex. *PLoS biology*, 6(7), p.e159.
- Hariri, A.R., Mattay, V.S., Tessitore, A., Kolachana, B., Fera, F., Goldman, D., Egan, M.F. & Weinberger, D.R., 2002. Serotonin transporter genetic variation and the response of the human amygdala. *Science (New York, N.Y.)*, 297(5580), pp.400–3.
- Harmer, C.J., Bhagwagar, Z., Perrett, D.I., Völlm, B. a, Cowen, P.J. & Goodwin, G.M., 2003. Acute SSRI Administration Affects the Processing of Social Cues in Healthy Volunteers. *Neuropsychopharmacology*, 28(1), pp.148–152.
- Harmer, C.J., Mackay, C.E., Reid, C.B., Cowen, P.J. & Goodwin, G.M., 2006. Antidepressant drug treatment modifies the neural processing of nonconscious threat cues. *Biological psychiatry*, 59(9), pp.816–20.
- Harmer, C.J., Shelley, N.C., Cowen, P.J. & Goodwin, G.M., 2004. Increased positive versus negative affective perception and memory in healthy volunteers following selective serotonin and norepinephrine reuptake inhibition. *American Journal of Psychiatry*, 161(7), pp.1256–1263.
- Harrison, B.J., Fullana, M.A., Soriano-Mas, C., Via, E., Pujol, J., Martínez-Zalacaín, I.,

- Tinoco-Gonzalez, D., Davey, C.G., et al., 2015. A neural mediator of human anxiety sensitivity. *Human brain mapping*, 36(10), pp.3950–8.
- Harrison, B.J., Pujol, J., López-Solà, M., Hernández-Ribas, R., Deus, J., Ortiz, H., Soriano-Mas, C., Yücel, M., et al., 2008. Consistency and functional specialization in the default mode brain network. *Proceedings of the National Academy of Sciences of the United States of America*, 105(28), pp.9781–9786.
- Haxby, J. V., Haxby, J. V., Hoffman, E. a, Hoffman, E. a, Gobbini, M.I. & Gobbini, M.I., 2002. Human neural systems for face recognition and social communication. *Biological psychiatry*, 51(1), pp.59–67.
- Haxby, J. V., Hoffman, E.A. & Gobbini, M.I., 2000. The distributed human neural system for face perception. *Trends in Cognitive Sciences*, 4(6), pp.223–233.
- Haykin, S. & Chen, Z., 2005. The Cocktail Party Problem. *Neural Computation*, 17(9), pp.1875–1902.
- Hedges, D.W., Brown, B.L. & Shwalb, D.A., 2009. A direct comparison of effect sizes from the clinical global impression-improvement scale to effect sizes from other rating scales in controlled trials of adult social anxiety disorder. *Human psychopharmacology*, 24(1), pp.35–40.
- Heimberg, R.G., 2002. Cognitive-behavioral therapy for social anxiety disorder: current status and future directions. *Biological Psychiatry*, 51(1), pp.101–108.
- Heimberg, R.G.G., Horner, K.J.J., Juster, H.R.R., Safren, S. a a, Brown, E.J.J., Schneier, F.R.R. & Liebowitz, M.R.R., 1999. Psychometric properties of the Liebowitz Social Anxiety Scale. *Psychological medicine*, 29(1), pp.199–212.
- Heiser, N.A., Turner, S.M., Beidel, D.C. & Roberson-Nay, R., 2009. Differentiating social phobia from shyness. *Journal of anxiety disorders*, 23(4), pp.469–76.
- Hensler, J.G., 2006. Serotonergic modulation of the limbic system. *Neuroscience & Biobehavioral Reviews*, 30(2), pp.203–214.
- Herculano-Houzel, S., 2002. Do You Know Your Brain? A Survey on Public Neuroscience Literacy at the Closing of the Decade of the Brain. *The Neuroscientist*, 8(2), pp.98–110.
- Horley, K., Williams, L.M., Gonsalvez, C. & Gordon, E., 2004. Face to face: Visual scanpath evidence for abnormal processing of facial expressions in social phobia. *Psychiatry Research*, 127(1-2), pp.43–53.
- Hutchinson, E.B., Stefanovic, B., Koretsky, A.P. & Silva, A.C., 2006. Spatial flow-volume

dissociation of the cerebral microcirculatory response to mild hypercapnia. *NeuroImage*, 32(2), pp.520–30.

Hyvärinen, a. & Oja, E., 2000. Independent component analysis: Algorithms and applications. *Neural Networks*, 13(4-5), pp.411–430.

Iadecola, C. & Reis, D.J., 1990. Continuous monitoring of cerebrocortical blood flow during stimulation of the cerebellar fastigial nucleus: a study by laser-Doppler flowmetry. *Journal of cerebral blood flow and metabolism : official journal of the International Society of Cerebral Blood Flow and Metabolism*, 10(5), pp.608–617.

Iancu, I., Levin, J., Hermesh, H., Dannon, P., Poreh, A., Ben-Yehuda, Y., Kaplan, Z., Marom, S., et al., 2006. Social phobia symptoms: prevalence, sociodemographic correlates, and overlap with specific phobia symptoms. *Comprehensive psychiatry*, 47(5), pp.399–405.

Iannetti, G.D. & Wise, R.G., 2007. BOLD functional MRI in disease and pharmacological studies: room for improvement? *Magnetic resonance imaging*, 25(6), pp.978–88.

Illes, J., Kirschen, M.P. & Gabrieli, J.D.E., 2003. From neuroimaging to neuroethics. *Nature neuroscience*, 6(3), p.205.

Ioannidis, J.P.A., 2005. Why most published research findings are false. *PLoS medicine*, 2(8), p.e124.

Ivannikov, M.V. & Macleod, G.T., 2013. Mitochondrial Free Ca²⁺ Levels and Their Effects on Energy Metabolism in Drosophila Motor Nerve Terminals. *Biophysical Journal*, 104(11), pp.2353–2361.

Jafri, M.J., Pearlson, G.D., Stevens, M. & Calhoun, V.D., 2008. A method for functional network connectivity among spatially independent resting-state components in schizophrenia. *NeuroImage*, 39(4), pp.1666–81.

Johnstone, T., Somerville, L.H., Alexander, A.L., Oakes, T.R., Davidson, R.J., Kalin, N.H. & Whalen, P.J., 2005. Stability of amygdala BOLD response to fearful faces over multiple scan sessions. *NeuroImage*, 25(4), pp.1112–23.

Kaitin, K.I., 2010. Deconstructing the drug development process: the new face of innovation. *Clinical pharmacology and therapeutics*, 87(3), pp.356–61.

Kajimura, S., Kochiyama, T., Nakai, R., Abe, N. & Nomura, M., 2015. Fear of negative evaluation is associated with altered brain function in nonclinical subjects. *Psychiatry Research: Neuroimaging*.

Kanwisher, N., McDermott, J. & Chun, M.M., 1997. The fusiform face area: a module in

human extrastriate cortex specialized for face perception. *The Journal of neuroscience : the official journal of the Society for Neuroscience*, 17(11), pp.4302–4311.

Katz, R., 2004. Biomarkers and surrogate markers: an FDA perspective. *NeuroRx : the journal of the American Society for Experimental NeuroTherapeutics*, 1(2), pp.189–195.

Kemeny, S., Ye, F.Q., Birn, R. & Braun, A.R., 2005. Comparison of continuous overt speech fMRI using BOLD and arterial spin labeling. *Human Brain Mapping*, 24(3), pp.173–183.

Kemper, V.G., De Martino, F., Vu, A.T., Poser, B.A., Feinberg, D.A., Goebel, R. & Yacoub, E., 2015. Sub-millimeter T2 weighted fMRI at 7 T: comparison of 3D-GRASE and 2D SE-EPI. *Frontiers in Neuroscience*, 9, p.163.

Keyeux, a, Ochrymowicz-Bemelmans, D. & Charlier, a a, 1995. Induced response to hypercapnia in the two-compartment total cerebral blood volume: influence on brain vascular reserve and flow efficiency. *Journal of cerebral blood flow and metabolism : official journal of the International Society of Cerebral Blood Flow and Metabolism*, 15(6), pp.1121–1131.

Kilts, C.D., Kelsey, J.E., Knight, B., Ely, T.D., Bowman, F.D., Gross, R.E., Selvig, A., Gordon, A., et al., 2006. The neural correlates of social anxiety disorder and response to pharmacotherapy. *Neuropsychopharmacology : official publication of the American College of Neuropsychopharmacology*, 31(10), pp.2243–53.

Kim, J., Van Dijk, K.R. a. A., Libby, A. & Napadow, V., 2013. Frequency-Dependent Relationship Between Resting-State Functional Magnetic Resonance Imaging Signal Power and Head Motion Is Localized Within Distributed Association Networks. *Brain Connectivity*, 4(1), p.131218075844008.

Kiviniemi, V., Kantola, J.-H., Jauhiainen, J., Hyvärinen, A. & Tervonen, O., 2003. Independent component analysis of nondeterministic fMRI signal sources. *NeuroImage*, 19(2), pp.253–260.

Kiviniemi, V.J., Haanpää, H., Kantola, J.-H., Jauhiainen, J., Vainionpää, V., Alahuhta, S. & Tervonen, O., 2005. Midazolam sedation increases fluctuation and synchrony of the resting brain BOLD signal. *Magnetic resonance imaging*, 23(4), pp.531–7.

Klein, A., Andersson, J., Ardekani, B.A., Ashburner, J., Avants, B., Chiang, M.-C., Christensen, G.E., Collins, D.L., et al., 2009. Evaluation of 14 nonlinear deformation algorithms applied to human brain MRI registration. *NeuroImage*, 46(3), pp.786–

- Klumbies, E., Braeuer, D., Hoyer, J. & Kirschbaum, C., 2014. The Reaction to Social Stress in Social Phobia: Discordance between Physiological and Subjective Parameters S. Kotz, ed. *PLoS ONE*, 9(8), p.e105670.
- Knutson, B., Wolkowitz, O.M., Cole, S.W., Chan, T., Moore, E. a., Johnson, R.C., Terpstra, J., Turner, R. a., et al., 1998. Selective alteration of personality and social behavior by serotonergic intervention. *American Journal of Psychiatry*, 155(3), pp.373–379.
- Kola, I. & Landis, J., 2004. Can the pharmaceutical industry reduce attrition rates? *Nature reviews. Drug discovery*, 3(8), pp.711–715.
- Koutstaal, W., Wagner, A.. D., Rotte, M., Maril, a., Buckner, R.. L. & Schacter, D.. L., 2001. Perceptual specificity in visual object priming: Functional magnetic resonance imaging evidence for a laterality difference in fusiform cortex. *Neuropsychologia*, 39(2), pp.184–199.
- Krasnow, B., Tamm, L., Greicius, M., Yang, T., Glover, G., Reiss, A. & Menon, V., 2003. Comparison of fMRI activation at 3 and 1.5 T during perceptual, cognitive, and affective processing. *NeuroImage*, 18(4), pp.813–826.
- Krüger, G. & Glover, G.H., 2001. Physiological noise in oxygenation-sensitive magnetic resonance imaging. *Magnetic Resonance in Medicine*, 46(4), pp.631–637.
- Kummar, S., Kinders, R., Gutierrez, M.E., Rubinstein, L., Parchment, R.E., Phillips, L.R., Ji, J., Monks, A., et al., 2009. Phase 0 clinical trial of the poly (ADP-ribose) polymerase inhibitor ABT-888 in patients with advanced malignancies. *Journal of clinical oncology : official journal of the American Society of Clinical Oncology*, 27(16), pp.2705–11.
- Kwong, K., Kwong, K., Belliveau, J., Belliveau, J., Chesler, D., Chesler, D., Goldberg, I., Goldberg, I., et al., 1992. Dynamic magnetic resonance imaging of human brain activity during primary sensory stimulation. *Proc Natl Acad Sci U S A*, 89(12), pp.5675–5679.
- Laird, A.R., Robinson, J.L., McMillan, K.M., Tordesillas-Gutiérrez, D., Moran, S.T., Gonzales, S.M., Ray, K.L., Franklin, C., et al., 2010. Comparison of the disparity between Talairach and MNI coordinates in functional neuroimaging data: validation of the Lancaster transform. *NeuroImage*, 51(2), pp.677–83.
- Lancaster, J.L., Tordesillas-Gutiérrez, D., Martinez, M., Salinas, F., Evans, A., Zilles, K., Mazziotta, J.C. & Fox, P.T., 2007. Bias between MNI and talairach coordinates

- analyzed using the ICBM-152 brain template. *Human Brain Mapping*, 28(11), pp.1194–1205.
- Lappin, G. & Garner, R.C., 2003. Big physics, small doses: the use of AMS and PET in human microdosing of development drugs. *Nature reviews. Drug discovery*, 2(3), pp.233–240.
- Laufs, H., Krakow, K., Sterzer, P., Eger, E., Beyerle, a., Salek-Haddadi, a. & Kleinschmidt, a., 2003. Electroencephalographic signatures of attentional and cognitive default modes in spontaneous brain activity fluctuations at rest. *Proceedings of the National Academy of Sciences*, 100(19), pp.11053–11058.
- Lauterbur, P.C., 1973. Image Formation by Induced Local Interactions: Examples Employing Nuclear Magnetic Resonance. *Nature*, 242(5394), pp.190–191.
- Lee, M.H., Smyser, C.D. & Shimony, J.S., 2013. Resting-state fMRI: a review of methods and clinical applications. *AJNR. American journal of neuroradiology*, 34(10), pp.1866–72.
- Lee, T.-W., Girolami, M. & Sejnowski, T.J., 1999. Independent Component Analysis Using an Extended Infomax Algorithm for Mixed Subgaussian and Supergaussian Sources. *Neural Computation*, 11(2), pp.417–441.
- Levy, N., 2008. Introducing Neuroethics. *Neuroethics*, 1(1), pp.1–8.
- Lewis, P.A., Critchley, H.D., Smith, A.P. & Dolan, R.J., 2005. Brain mechanisms for mood congruent memory facilitation. *NeuroImage*, 25(4), pp.1214–23.
- Li, Y.-O., Adali, T. & Calhoun, V.D., 2007. Estimating the number of independent components for functional magnetic resonance imaging data. *Human brain mapping*, 28(11), pp.1251–1266.
- Liao, W., Qiu, C., Gentili, C., Walter, M., Pan, Z., Ding, J., Zhang, W., Gong, Q., et al., 2010. Altered effective connectivity network of the amygdala in social anxiety disorder: a resting-state FMRI study. *PLoS ONE*, 5(12), p.e15238.
- Lieberman, M.D. & Cunningham, W. a., 2009. Type I and Type II error concerns in fMRI research: Re-balancing the scale. *Social Cognitive and Affective Neuroscience*, 4(4), pp.423–428.
- Liebowitz, M.R., 1987. Social phobia. *Modern Problems of pharmacopsychiatry*, 22, pp.141–173.
- Liebowitz, M.R., Gotman, J.M., Fyer, A.J. & Klein, D.F., 1985. Social Phobia: Review of a Neglected Anxiety Disorder. *Archives of General Psychiatry*, 42(7), pp.729–736.

- Liebowitz, M.R., Mangano, R.M., Bradwejn, J. & Asnis, G., 2005. A randomized controlled trial of venlafaxine extended release in generalized social anxiety disorder. *The Journal of clinical psychiatry*, 66(2), pp.238–47.
- Linden, D.E.J., 2012. The challenges and promise of neuroimaging in psychiatry. *Neuron*, 73(1), pp.8–22.
- Lindquist, M.A., Meng Loh, J., Atlas, L.Y. & Wager, T.D., 2009. Modeling the hemodynamic response function in fMRI: efficiency, bias and mis-modeling. *NeuroImage*, 45(1 Suppl), pp.S187–98.
- Lipsitz, J.D. & Schneier, F.R., 2000. Social phobia. Epidemiology and cost of illness. *Pharmacoeconomics*, 18(1), pp.23–32.
- Littlefield, M., 2009. Constructing the Organ of Deceit. *Science, Technology & Human Values*, 34(3), pp.365–392.
- Liu, F., Guo, W., Fouche, J.-P., Wang, Y., Wang, W., Ding, J., Zeng, L., Qiu, C., et al., 2015. Multivariate classification of social anxiety disorder using whole brain functional connectivity. *Brain structure & function*, 220(1), pp.101–15.
- Liu, G., Sobering, G., Duyn, J. & Moonen, C.T.W., 1993. A functional MRI technique combining principles of echo-shifting with a train of observations (PRESTO). *Magnetic Resonance in Medicine*, 30(6), pp.764–768.
- Logothetis, N.K., 2008. What we can do and what we cannot do with fMRI. *Nature*, 453(7197), pp.869–878.
- Lorberbaum, J.P., Kose, S., Johnson, M.R., Arana, G.W., Sullivan, L.K., Hamner, M.B., Ballenger, J.C., Lydiard, R.B., et al., 2004. Neural correlates of speech anticipatory anxiety in generalized social phobia. *Neuroreport*, 15(18), pp.2701–5.
- Lu, H., Zou, Q., Gu, H., Raichle, M.E., Stein, E.A. & Yang, Y., 2012. Rat brains also have a default mode network. *Proceedings of the National Academy of Sciences*, 109(10), pp.3979–3984.
- De Luca, M., Beckmann, C.F., De Stefano, N., Matthews, P.M. & Smith, S.M., 2006. fMRI resting state networks define distinct modes of long-distance interactions in the human brain. *NeuroImage*, 29(4), pp.1359–67.
- Maas, L.C. & Renshaw, P.F., 1999. Post-registration spatial filtering to reduce noise in functional MRI data sets. *Magnetic Resonance Imaging*, 17(9), pp.1371–1382.
- Macaluso, M. & Preskorn, S.H., 2012. How Biomarkers Will Change Psychiatry. *Journal of Psychiatric Practice*, 18(2), pp.118–121.

- Mandeville, J.B., Marota, J.J., Ayata, C., Zaharchuk, G., Moskowitz, M. a, Rosen, B.R. & Weisskoff, R.M., 1999. Evidence of a cerebrovascular postarteriole windkessel with delayed compliance. *Journal of cerebral blood flow and metabolism : official journal of the International Society of Cerebral Blood Flow and Metabolism*, 19(6), pp.679–689.
- Mansfield, P., 1977. Multi-planar image formation using NMR spin echoes. *Journal of Physics C: Solid State Physics*, 10(3), pp.L55–L58.
- Martin, M., 1990. On the induction of mood. *Clinical Psychology Review*, 10(6), pp.669–697.
- Mathew, S.J., Price, R.B. & Charney, D.S., 2008. Recent advances in the neurobiology of anxiety disorders: implications for novel therapeutics. *American journal of medical genetics. Part C, Seminars in medical genetics*, 148C(2), pp.89–98.
- Mazziotta, J.C., Toga, A.W., Evans, A., Fox, P. & Lancaster, J., 1995. A probabalistic atlas of the human brain: theory and rationale for its development. *NeuroImage*, 2(2), pp.89–101.
- McCabe, D.P. & Castel, A.D., 2008. Seeing is believing: the effect of brain images on judgments of scientific reasoning. *Cognition*, 107(1), pp.343–52.
- McClure, E.B., Adler, A., Monk, C.S., Cameron, J., Smith, S., Nelson, E.E., Leibenluft, E., Ernst, M., et al., 2007. fMRI predictors of treatment outcome in pediatric anxiety disorders. *Psychopharmacology*, 191(1), pp.97–105.
- McKeown, M.J.M.S., 1998. Analysis of fMRI data by blind separation into independent spatial components. *Human Brain Mapping*, 6(June 1997), pp.160–188.
- Mendlowicz, M. V & Stein, M.B., 2000. Reviews and Overviews Quality of Life in Individuals With Anxiety Disorders. *Psychiatry Interpersonal and Biological Processes*, 157(5), pp.669–682.
- Meng, M., Cherian, T., Singal, G. & Sinha, P., 2012. Lateralization of face processing in the human brain. *Proceedings of the Royal Society B: Biological Sciences*, 279(1735), pp.2052–2061.
- Mennin, D.S., Fresco, D.M., Heimberg, R.G., Schneier, F.R., Davies, S.O. & Liebowitz, M.R., 2002. Screening for social anxiety disorder in the clinical setting: using the Liebowitz Social Anxiety Scale. *Journal of Anxiety Disorders*, 16(6), pp.661–673.
- Menon, R.S., Ogawa, S., Tank, D.W. & U?urbil, K., 1993. 4 Tesla gradient recalled echo characteristics of photic stimulation-induced signal changes in the human primary

visual cortex. *Magnetic Resonance in Medicine*, 30(3), pp.380–386.

Merlo Pich, E., 2011. Understanding pharmacology in humans: Phase I and Phase II (data generation). *Current opinion in pharmacology*, 11(5), pp.557–62.

Mikl, M., Marecek, R., Hlustík, P., Pavlicová, M., Drastich, A., Chlebus, P., Brázdil, M. & Krupa, P., 2008. Effects of spatial smoothing on fMRI group inferences. *Magnetic resonance imaging*, 26(4), pp.490–503.

Minzenberg, M.J. & Carter, C.S., 2007. The quest for developing new treatments from imaging techniques: promises, problems and future potential. *Expert Opinion on Drug Discovery*, 2(8), pp.1029–1033.

Molliver, M.E., 1987. Serotonergic neuronal systems: what their anatomic organization tells us about function. *Journal of clinical psychopharmacology*, 7(6 Suppl), p.3S–23S.

Morcom, A.M. & Fletcher, P.C., 2007. Does the brain have a baseline? Why we should be resisting a rest. *NeuroImage*, 37(4), pp.1073–1082.

Morris, J.S., Friston, K.J., Büchel, C., Frith, C.D., Young, a W., Calder, a J. & Dolan, R.J., 1998. A neuromodulatory role for the human amygdala in processing emotional facial expressions. *Brain : a journal of neurology*, 121 (Pt 1, pp.47–57.

Mueller, E.M., Panitz, C., Nestoriuc, Y., Stemmler, G. & Wacker, J., 2014. Panic Disorder and Serotonin Reuptake Inhibitors Predict Coupling of Cortical and Cardiac Activity. *Neuropsychopharmacology*, 39(2), pp.507–514.

Munos, B., 2009. Lessons from 60 years of pharmaceutical innovation. *Nature reviews. Drug discovery*, 8(12), pp.959–968.

Murphy, K., Bodurka, J. & Bandettini, P.A., 2007. How long to scan? The relationship between fMRI temporal signal to noise ratio and necessary scan duration. *NeuroImage*, 34(2), pp.565–74.

Myrick, H., Anton, R.F., Li, X., Henderson, S., Randall, P.K. & Voronin, K., 2008. Effect of naltrexone and ondansetron on alcohol cue-induced activation of the ventral striatum in alcohol-dependent people. *Archives of general psychiatry*, 65(4), pp.466–75.

Naganawa, S., Norris, D.G., Zysset, S. & Mildner, T., 2002. Regional differences of fMR signal changes induced by hyperventilation: Comparison between SE-EPI and GE-EPI at 3-T. *Journal of Magnetic Resonance Imaging*, 15(1), pp.23–30.

Nakao, T., Sanematsu, H., Yoshiura, T., Togao, O., Murayama, K., Tomita, M., Masuda, Y. & Kanba, S., 2011. fMRI of patients with social anxiety disorder during a social

situation task. *Neuroscience research*, 69(1), pp.67–72.

Nathan, P.J., Phan, K.L., Harmer, C.J., Mehta, M.A. & Bullmore, E.T., 2014. Increasing pharmacological knowledge about human neurological and psychiatric disorders through functional neuroimaging and its application in drug discovery. *Current opinion in pharmacology*, 14, pp.54–61.

NICE, 2013. Social Anxiety Disorder.

Nichols, T.E., 2012. Multiple testing corrections, nonparametric methods, and random field theory. *NeuroImage*, 62(2), pp.811–5.

Nickerson, R.S., 1998. Confirmation bias: A ubiquitous phenomenon in many guises. *Review of General Psychology*, 2(2), pp.175–220.

NIH, U.S.N.I. of H., 2015. Glossary of Clinical Trials. Available at: <https://clinicaltrials.gov/ct2/info/glossary> [Accessed July 12, 2015].

Nitschke, J.B., Sarinopoulos, I., Oathes, D.J., Johnstone, T., Whalen, P.J., Davidson, R.J. & Kalin, N.H., 2009. Anticipatory activation in the amygdala and anterior cingulate in generalized anxiety disorder and prediction of treatment response. *The American journal of psychiatry*, 166(3), pp.302–10.

Northoff, G., Heinzl, A., de Greck, M., Bermpohl, F., Dobrowolny, H. & Panksepp, J., 2006. Self-referential processing in our brain—A meta-analysis of imaging studies on the self. *NeuroImage*, 31(1), pp.440–457.

Odeblad, E. & Lindström, G., 1955. Some Preliminary Observations on the Proton Magnetic Resonance in Biologic Samples. *Acta Radiologica*, (43), pp.459–476.

Ogawa, S. & Lee, T., 1990. Brain magnetic resonance imaging with contrast dependent on blood oxygenation. *Proceedings of the ...*, 87(24), pp.9868–72.

Ogawa, S., Tank, D.W., Menon, R., Ellermann, J.M., Kim, S.G., Merkle, H. & Ugurbil, K., 1992. Intrinsic signal changes accompanying sensory stimulation: functional brain mapping with magnetic resonance imaging. *Proceedings of the National Academy of Sciences of the United States of America*, 89(13), pp.5951–5955.

Oldfield, R.C., 1971. The assessment and analysis of handedness: The Edinburgh inventory. *Neuropsychologia*, 9(1), pp.97–113.

Orloff, J., Douglas, F., Pinheiro, J., Levinson, S., Branson, M., Chaturvedi, P., Ette, E., Gallo, P., et al., 2009. The future of drug development: advancing clinical trial design. *Nature reviews. Drug discovery*, 8(12), pp.949–957.

- Oshio, K. & Feinberg, D.A., 1991. GRASE (Gradient-and Spin-Echo) imaging: A novel fast MRI technique. *Magnetic Resonance in Medicine*, 20(2), pp.344–349.
- Parkes, L.M., Schwarzbach, J. V., Bouts, A. a., Deckers, R.H.R., Pullens, P., Kerskens, C.M. & Norris, D.G., 2005. Quantifying the spatial resolution of the gradient echo and spin echo BOLD response at 3 Tesla. *Magnetic Resonance in Medicine*, 54(6), pp.1465–1472.
- Pauling, L. & Coryell, C.D., 1936. The Magnetic Properties and Structure of Hemoglobin, Oxyhemoglobin and Carbonmonoxyhemoglobin. *Proceedings of the National Academy of Sciences of the United States of America*, 22(4), pp.210–6.
- Paulus, M.P., Feinstein, J.S., Castillo, G., Simmons, A.N. & Stein, M.B., 2005. Dose-dependent decrease of activation in bilateral amygdala and insula by lorazepam during emotion processing. *Archives of general psychiatry*, 62(3), pp.282–288.
- Paulus, M.P. & Stein, M.B., 2007. Role of functional magnetic resonance imaging in drug discovery. *Neuropsychology review*, 17(2), pp.179–88.
- Peterson, A., Thome, J., Frewen, P. & Lanius, R.A., 2014. Resting-state neuroimaging studies: a new way of identifying differences and similarities among the anxiety disorders? *Canadian journal of psychiatry. Revue canadienne de psychiatrie*, 59(6), pp.294–300.
- Phan, K.L., Coccaro, E.F., Angstadt, M., Kreger, K.J., Mayberg, H.S., Liberzon, I. & Stein, M.B., 2013. Corticolimbic brain reactivity to social signals of threat before and after sertraline treatment in generalized social phobia. *Biological psychiatry*, 73(4), pp.329–36.
- Phan, K.L., Fitzgerald, D.A., Nathan, P.J. & Tancer, M.E., 2006. Association between amygdala hyperactivity to harsh faces and severity of social anxiety in generalized social phobia. *Biological psychiatry*, 59(5), pp.424–9.
- Phan, K.L., Wager, T., Taylor, S.F. & Liberzon, I., 2002. Functional neuroanatomy of emotion: a meta-analysis of emotion activation studies in PET and fMRI. *NeuroImage*, 16(2), pp.331–48.
- Phelps, E. a, 2006. Emotion and cognition: insights from studies of the human amygdala. *Annual review of psychology*, 57(Miller 2003), pp.27–53.
- Phelps, E.A. & LeDoux, J.E., 2005. Contributions of the amygdala to emotion processing: from animal models to human behavior. *Neuron*, 48(2), pp.175–87.
- Popa, D., Popescu, A.T. & Paré, D., 2009. Contrasting activity profile of two distributed

cortical networks as a function of attentional demands. *The Journal of neuroscience : the official journal of the Society for Neuroscience*, 29(4), pp.1191–1201.

di Prisco, G., Cocca, E., Parker, S.K. & Detrich, H.W., 2002. Tracking the evolutionary loss of hemoglobin expression by the white-blooded Antarctic icefishes. *Gene*, 295(2), pp.185–191.

Pujol, J., Giménez, M., Ortiz, H., Soriano-Mas, C., López-Solà, M., Farré, M., Deus, J., Merlo-Pich, E., et al., 2013. Neural response to the observable self in social anxiety disorder. *Psychological Medicine*, 43(1), pp.721–731.

Pujol, J., Martí-Vilalta, J., Arboix, A. & Capdevila, A., 1988. Resonancia magnética en neurología: análisis de 240 casos. *Medicina Clínica*, 91, pp.530–534.

Pujol, J., Reixach, J., Harrison, B.J., Timoneda-Gallart, C., Vilanova, J.C. & Pérez-Alvarez, F., 2008. Posterior cingulate activation during moral dilemma in adolescents. *Human Brain Mapping*, 29(8), pp.910–921.

Pujol, J., Vendrell, P., Deus, J., Mataró, M., Capdevila, A. & Martí-Vilalta, J.L., 1995. Study of cerebral activity with functional magnetic resonance. *Medicina clínica*, 104(1), pp.1–5.

Purcell, E.E., Torrey, H. & Pound, R.R., 1946. Resonance Absorption by Nuclear Magnetic Moments in a Solid. *Physical Review*, 69(1-2), pp.37–38.

Quadflieg, S., Mohr, A., Mentzel, H.-J.J., Miltner, W.H.R. & Straube, T., 2008. Modulation of the neural network involved in the processing of anger prosody: The role of task-relevance and social phobia. *Biological Psychology*, 78(2), pp.129–137.

Racine, E., Bar-Ilan, O. & Illes, J., 2005. fMRI in the public eye. *Nature reviews. Neuroscience*, 6(2), pp.159–64.

Raichle, M.E., 2013. The Brain's Default Mode Network. *Annual review of neuroscience*, 38(1), p.150504162358003.

Raichle, M.E., MacLeod, a M., Snyder, A.Z., Powers, W.J., Gusnard, D. a & Shulman, G.L., 2001. A default mode of brain function. *Proceedings of the National Academy of Sciences of the United States of America*, 98(2), pp.676–682.

Rapee, R.M. & Heimberg, R.G., 1997. A cognitive-behavioral model of anxiety in social phobia. *Behaviour Research and Therapy*, 35(8), pp.741–756.

Rayshubskiy, A., Wojtasiewicz, T.J., Mikell, C.B., Bouchard, M.B., Timerman, D., Youngerman, B.E., McGovern, R.A., Otten, M.L., et al., 2014. Direct, intraoperative observation of ~0.1 Hz hemodynamic oscillations in awake human cortex:

- implications for fMRI. *NeuroImage*, 87, pp.323–31.
- Reich, J., Goldenberg, I., Vasile, R., Goisman, R. & Keller, M., 1994. A prospective follow-along study of the course of social phobia. *Psychiatry Research*, 54(3), pp.249–258.
- Rissanen, J., 1983. A Universal Prior for Integers and Estimation by Minimum Description Length. *The Annals of Statistics*, 11(2), pp.416–431.
- Riwkes, S., Goldstein, A. & Gilboa-Schechtman, E., 2015. The temporal unfolding of face processing in social anxiety disorder — a MEG study. *NeuroImage: Clinical*, 7(August), pp.678–687.
- Rosazza, C. & Minati, L., 2011. Resting-state brain networks: literature review and clinical applications. *Neurological Sciences*, 32(5), pp.773–785.
- Rosazza, C., Minati, L., Ghielmetti, F., Mandelli, M.L. & Bruzzone, M.G., 2011. Functional Connectivity during Resting-State Functional MR Imaging: Study of the Correspondence between Independent Component Analysis and Region-of-Interest-Based Methods. *American Journal of Neuroradiology*, 33(1), pp.180–187.
- Rosen, B.R. & Savoy, R.L., 2012. fMRI at 20: Has it changed the world? *NeuroImage*, 62(2), pp.1316–1324.
- Ruscio, A.M., Brown, T.A., Chiu, W.T., Sareen, J., Stein, M.B. & Kessler, R.C., 2008. Social fears and social phobia in the USA: results from the National Comorbidity Survey Replication. *Psychological medicine*, 38(1), pp.15–28.
- Sacks, L. V, Shamsuddin, H.H., Yasinskaya, Y.I., Bouri, K., Lanthier, M.L. & Sherman, R.E., 2014. Scientific and regulatory reasons for delay and denial of FDA approval of initial applications for new drugs, 2000-2012. *JAMA*, 311(4), pp.378–84.
- Sareen, J., Campbell, D.W., Leslie, W.D., Malisza, K.L., Stein, M.B., Paulus, M.P., Kravetsky, L.B., Kjernisted, K.D., et al., 2007. Striatal Function in Generalized Social Phobia: A Functional Magnetic Resonance Imaging Study. *Biological Psychiatry*, 61(3), pp.396–404.
- Sareen, J., Chartier, M., Paulus, M.P. & Stein, M.B., 2006. Illicit drug use and anxiety disorders: findings from two community surveys. *Psychiatry research*, 142(1), pp.11–7.
- Sato, A., Sato, Y. & Uchida, S., 2001. Regulation of regional cerebral blood flow by cholinergic fibers originating in the basal forebrain. *International Journal of Developmental Neuroscience*, 19(3), pp.327–337.
- Savoy, R.L., 2012. Evolution and current challenges in the teaching of functional MRI and

functional brain imaging. *NeuroImage*, 62(2), pp.1201–7.

Savoy, R.L., 2005. Experimental design in brain activation MRI: cautionary tales. *Brain research bulletin*, 67(5), pp.361–7.

Schmitz, J., Krämer, M., Tuschen-Caffier, B., Heinrichs, N. & Blechert, J., 2011. Restricted autonomic flexibility in children with social phobia. *Journal of child psychology and psychiatry, and allied disciplines*, 52(11), pp.1203–11.

Schmitz, M.F., Filippone, P. & Edelman, E.M., 2003. Social Representations of Attention Deficit/Hyperactivity Disorder, 1988–1997. *Culture & Psychology*, 9(4), pp.383–406.

Schneier, F.R., 2011. Pharmacotherapy of social anxiety disorder. *Expert opinion on pharmacotherapy*, 12(4), pp.615–25.

Schneier, F.R., Johnson, J., Hornig, C.D., Liebowitz, M.R. & Weissman, M.M., 1992. Social phobia. Comorbidity and morbidity in an epidemiologic sample. *Archives of general psychiatry*, 49(4), pp.282–8.

Schultz, R.T., 2005. Developmental deficits in social perception in autism: The role of the amygdala and fusiform face area. *International Journal of Developmental Neuroscience*, 23(2-3 SPEC. ISS.), pp.125–141.

Schwarz, N., Bless, H., Strack, F., Klumpp, G., Rittenauerschatka, H. & Simons, A., 1991. Ease of Retrieval as Information - Another Look at the Availability Heuristic. *Journal of Personality and Social Psychology*, 61(2), pp.195–202.

Segal, Z. V, Kennedy, S., Gemar, M., Hood, K., Pedersen, R. & Buis, T., 2006. Cognitive reactivity to sad mood provocation and the prediction of depressive relapse. *Archives of general psychiatry*, 63(7), pp.749–55.

Shin, L.M. & Liberzon, I., 2010. The Neurocircuitry of Fear, Stress, and Anxiety Disorders. *Neuropsychopharmacology*, 35(1), pp.169–191.

Shmueli, K., van Gelderen, P., de Zwart, J.A., Horovitz, S.G., Fukunaga, M., Jansma, J.M. & Duyn, J.H., 2007. Low-frequency fluctuations in the cardiac rate as a source of variance in the resting-state fMRI BOLD signal. *NeuroImage*, 38(2), pp.306–20.

Shu, D.-G.G., Luo, H.-L.L., Conway Morris, S., Zhang, X.-L.L., Hu, S.-X.X., Chen, L.-Z.Z., Han, J., Zhu, M., et al., 1999. Lower Cambrian vertebrates from South China. *Nature*, 402(6757), pp.42–46.

Shulman, G.L., Fiez, J. a., Corbetta, M., Buckner, R.L., Miezin, F.M., Raichle, M.E. & Petersen, S.E., 1997. Common Blood Flow Changes across Visual Tasks: II. Decreases in Cerebral Cortex. *Journal of cognitive neuroscience*, 9(5), pp.648–63.

- Simmons, A.N., Arce, E., Lovero, K.L., Stein, M.B. & Paulus, M.P., 2009. Subchronic SSRI administration reduces insula response during affective anticipation in healthy volunteers. *The International Journal of Neuropsychopharmacology*, 12(08), p.1009.
- Singh, J., Hallmayer, J. & Illes, J., 2007. Interacting and paradoxical forces in neuroscience and society. *Nature reviews. Neuroscience*, 8(2), pp.153–60.
- Sladky, R., Höflich, A., Atanelov, J., Kraus, C., Baldinger, P., Moser, E., Lanzenberger, R. & Windischberger, C., 2012. Increased neural habituation in the amygdala and orbitofrontal cortex in social anxiety disorder revealed by fMRI. *PloS one*, 7(11), p.e50050.
- Smith, S.M., Miller, K.L., Moeller, S., Xu, J., Auerbach, E.J., Woolrich, M.W., Beckmann, C.F., Jenkinson, M., et al., 2012. Temporally-independent functional modes of spontaneous brain activity. *Proceedings of the National Academy of Sciences of the United States of America*, 109(8), pp.3131–6.
- Snitz, B.E., MacDonald, A., Cohen, J.D., Cho, R.Y., Becker, T. & Carter, C.S., 2005. Lateral and medial hypofrontality in first-episode schizophrenia: functional activity in a medication-naïve state and effects of short-term atypical antipsychotic treatment. *The American journal of psychiatry*, 162(12), pp.2322–9.
- Snyder, A.Z. & Raichle, M.E., 2012. A brief history of the resting state: the Washington University perspective. *NeuroImage*, 62(2), pp.902–10.
- Sorger, B., Goebel, R., Schiltz, C. & Rossion, B., 2007. Understanding the functional neuroanatomy of acquired prosopagnosia. *NeuroImage*, 35(2), pp.836–852.
- Spielberger, C.D., 1983. Manual for the State-Trait Anxiety Inventory STAI (Form Y) (“Self-Evaluation Questionnaire”).
- Spitzer, R.L., 1999. Validation and Utility of a Self-report Version of PRIME-MD<SUBTITLE>The PHQ Primary Care Study</SUBTITLE>. *JAMA*, 282(18), p.1737.
- Sorns, O., 2012. From simple graphs to the connectome: networks in neuroimaging. *NeuroImage*, 62(2), pp.881–6.
- Stafford, J.M., Jarrett, B.R., Miranda-Dominguez, O., Mills, B.D., Cain, N., Mihalas, S., Lahvis, G.P., Lattal, K.M., et al., 2014. Large-scale topology and the default mode network in the mouse connectome. *Proceedings of the National Academy of Sciences*, 111(52), pp.18745–18750.
- Stahl, S.M., 1998. Mechanism of action of serotonin selective reuptake inhibitors. *Journal of Affective Disorders*, 51(3), pp.215–235.

- Staugaard, S.R., 2010. Threatening faces and social anxiety: A literature review. *Clinical Psychology Review*, 30(6), pp.669–690.
- Stein, D.J., Cameron, A., Amrein, R., Montgomery, S. a & Africa, S., 2002. Moclobemide is effective and well tolerated in the long-term pharmacotherapy of social anxiety disorder with or without comorbid anxiety disorder. , 17(4), pp.161–170.
- Stein, M.B., Goldin, P.R., Sareen, J., Zorrilla, L.T.E. & Brown, G.G., 2002. Increased amygdala activation to angry and contemptuous faces in generalized social phobia. *Archives of general psychiatry*, 59(11), pp.1027–1034.
- Stein, M.B. & Kean, Y.M., 2000. Disability and quality of life in social phobia: Epidemiologic findings. *American Journal of Psychiatry*, 157(10), pp.1606–1613.
- Stein, M.B., Pollack, M.H., Bystritsky, A., Kelsey, J.E. & Mangano, R.M., 2004. Efficacy of low and higher dose extended-release venlafaxine in generalized social anxiety disorder: a 6-month randomized controlled trial. *Psychopharmacology*, 177(3), pp.280–288.
- Stein, M.B., Simmons, A.N., Feinstein, J.S. & Paulus, M.P., 2007. Increased amygdala and insula activation during emotion processing in anxiety-prone subjects. *American Journal of Psychiatry*, 164(2), pp.318–327.
- Stein, M.B. & Stein, D.J., 2008. Social anxiety disorder. *The Lancet*, 371(9618), pp.1115–1125.
- Straube, T., Kolassa, I.-T., Glauer, M., Mentzel, H.-J. & Miltner, W.H.R., 2004. Effect of task conditions on brain responses to threatening faces in social phobics: an event-related functional magnetic resonance imaging study. *Biological psychiatry*, 56(12), pp.921–30.
- Straube, T., Mentzel, H.J. & Miltner, W.H.R., 2005. Common and distinct brain activation to threat and safety signals in social phobia. *Neuropsychobiology*, 52(3), pp.163–168.
- Strother, S., La Conte, S., Kai Hansen, L., Anderson, J., Zhang, J., Pulapura, S. & Rottenberg, D., 2004. Optimizing the fMRI data-processing pipeline using prediction and reproducibility performance metrics: I. A preliminary group analysis. *NeuroImage*, 23, pp.S196–S207.
- Stuhldreher, N., Leibing, E., Leichsenring, F., Beutel, M.E., Herpertz, S., Hoyer, J., Konnopka, A., Salzer, S., et al., 2014. The costs of social anxiety disorder: the role of symptom severity and comorbidities. *Journal of affective disorders*, 165, pp.87–94.
- Sylvester, C.M., Corbetta, M., Raichle, M.E., Rodebaugh, T.L., Schlaggar, B.L., Sheline, Y.I.,

- Zorumski, C.F. & Lenze, E.J., 2012. Functional network dysfunction in anxiety and anxiety disorders. *Trends in neurosciences*, 35(9), pp.527–35.
- Tailby, C., Masterton, R.A.J., Huang, J.Y., Jackson, G.D. & Abbott, D.F., 2015. Resting state functional connectivity changes induced by prior brain state are not network specific. *NeuroImage*, 106, pp.428–40.
- Talairach, J. & Tournoux, P., 1988. *Co-planar stereotaxic atlas of the human brain* T. Medical, ed., Thieme Medical.
- Tang, Y., Nyengaard, J.R., De Groot, D.M. & Gundersen, H.J., 2001. Total regional and global number of synapses in the human brain neocortex. *Synapse (New York, N.Y.)*, 41(3), pp.258–73.
- Temple, R., 1999. Are surrogate markers adequate to assess cardiovascular disease drugs? *JAMA : the journal of the American Medical Association*, 282(8), pp.790–795.
- Tendolkar, I., van Wingen, G., Urner, M., Verkes, R.J. & Fernández, G., 2011. Short-term duloxetine administration affects neural correlates of mood-congruent memory. *Neuropsychopharmacology: official publication of the American College of Neuropsychopharmacology*, 36(11), pp.2266–75.
- The Lancet editors, 2009. Phase 0 trials: a platform for drug development? *The Lancet*, 374(9685), p.176.
- Thulborn, K.R., Waterton, J.C., Matthews, P.M. & Radda, G.K., 1982. Oxygenation dependence of the transverse relaxation time of water protons in whole blood at high field. *Biochimica et Biophysica Acta (BBA) - General Subjects*, 714(2), pp.265–270.
- Tillfors, M., Furmark, T., Marteinsdottir, I., Fischer, H., Pissiota, A., Långström, B. & Fredrikson, M., 2001. Cerebral blood flow in subjects with social phobia during stressful speaking tasks: A PET study. *American Journal of Psychiatry*, 158(8), pp.1220–1226.
- Tinoco-González, D., Fullana, M.A., Torrents-Rodas, D., Bonillo, A., Vervliet, B., Pailhez, G., Farré, M., Andión, O., et al., 2015. Conditioned Subjective Responses to Socially Relevant Stimuli in Social Anxiety Disorder and Subclinical Social Anxiety. *Clinical Psychology & Psychotherapy*, 22(3), pp.221–231.
- Torrubia, R., Ávila, C., Moltó, J. & Caseras, X., 2001. The Sensitivity to Punishment and Sensitivity to Reward Questionnaire (SPSRQ) as a measure of Gray's anxiety and impulsivity dimensions. *Personality and Individual Differences*, 31(6), pp.837–862.

- Trist, D.G. & Bye, A., 2014. Editorial overview: Neurosciences: Clinical pharmacology today in neuroscience drug discovery. *Current Opinion in Pharmacology*, 14, pp.v–vi.
- Trower, P. & Gilbert, P., 1989. New theoretical conceptions of social anxiety and social phobia. *Clinical Psychology Review*, 9(1), pp.19–35.
- Tsuji, Y. & Shimada, S., 2015. Socially Anxious Tendencies Affect Autonomic Responses during Eye Gaze Perception. , (October), pp.1646–1652.
- Turner, R., Jezzard, P., Wen, H., Kwong, K.K., Le Bihan, D., Zeffiro, T. & Balaban, R.S., 1993. Functional mapping of the human visual cortex at 4 and 1.5 Tesla using deoxygenation contrast EPI. *Magnetic Resonance in Medicine*, 29(2), pp.277–279.
- Tversky, A. & Kahneman, D., 1973. Availability: A heuristic for judging frequency and probability. *Cognitive Psychology*, 5(2), pp.207–232.
- Uğurbil, K., 2012. Development of functional imaging in the human brain (fMRI); the University of Minnesota experience. *NeuroImage*, 62(2), pp.613–9.
- Uludağ, K., Müller-Bierl, B. & Uğurbil, K., 2009. An integrative model for neuronal activity-induced signal changes for gradient and spin echo functional imaging. *NeuroImage*, 48(1), pp.150–65.
- Valenzuela, M., Bartrés-Faz, D., Beg, F., Fornito, a, Merlo-Pich, E., Müller, U., Öngür, D., Toga, a W., et al., 2011. Neuroimaging as endpoints in clinical trials: Are we there yet? Perspective from the first Provence workshop. *Molecular Psychiatry*, 16(11), pp.1064–1066.
- Veit, R., Flor, H., Erb, M., Hermann, C., Lotze, M., Grodd, W. & Birbaumer, N., 2002. Brain circuits involved in emotional learning in antisocial behavior and social phobia in humans. *Neuroscience Letters*, 328(3), pp.233–236.
- Vincent, J.L., Patel, G.H., Fox, M.D., Snyder, A.Z., Baker, J.T., Van Essen, D.C., Zempel, J.M., Snyder, L.H., et al., 2007. Intrinsic functional architecture in the anaesthetized monkey brain. *Nature*, 447(7140), pp.83–86.
- Vincent, J.L., Snyder, A.Z., Fox, M.D., Shannon, B.J., Andrews, J.R., Raichle, M.E. & Buckner, R.L., 2006. Coherent spontaneous activity identifies a hippocampal-parietal memory network. *Journal of neurophysiology*, 96(6), pp.3517–31.
- Waites, A.B., Stanislavsky, A., Abbott, D.F. & Jackson, G.D., 2005. Effect of prior cognitive state on resting state networks measured with functional connectivity. *Human Brain Mapping*, 24(1), pp.59–68.
- Wechsler, D., 1999. *Manual for the Wechsler abbreviated intelligence scale (WASI)*, San

Antonio, Texas: The Psychological Corporation.

Wechsler, D., 1981. *WAIS-R manual: Wechsler adult intelligence scale-revised*, Psychological Corporation.

Weiskopf, N., Hutton, C., Josephs, O. & Deichmann, R., 2006. Optimal EPI parameters for reduction of susceptibility-induced BOLD sensitivity losses: a whole-brain analysis at 3 T and 1.5 T. *NeuroImage*, 33(2), pp.493–504.

Whalen, P.J., Johnstone, T., Somerville, L.H., Nitschke, J.B., Polis, S., Alexander, A.L., Davidson, R.J. & Kalin, N.H., 2008. A functional magnetic resonance imaging predictor of treatment response to venlafaxine in generalized anxiety disorder. *Biological psychiatry*, 63(9), pp.858–63.

Whelan, R. & Garavan, H., 2014. When optimism hurts: inflated predictions in psychiatric neuroimaging. *Biological psychiatry*, 75(9), pp.746–8.

White, B.R., Snyder, A.Z., Cohen, A.L., Petersen, S.E., Raichle, M.E., Schlaggar, B.L. & Culver, J.P., 2009. Resting-state functional connectivity in the human brain revealed with diffuse optical tomography. *NeuroImage*, 47(1), pp.148–156.

White, T., O’Leary, D., Magnotta, V., Arndt, S., Flaum, M. & Andreasen, N.C., 2001. Anatomic and functional variability: the effects of filter size in group fMRI data analysis. *NeuroImage*, 13(4), pp.577–588.

WHO, 1992. *The ICD-10 classification of mental and behavioural disorders: clinical descriptions and diagnostic guidelines*, Geneva: World Health Organization.

Wise, R.G. & Preston, C., 2010. What is the value of human FMRI in CNS drug development? *Drug discovery today*, 15(21-22), pp.973–80.

Wittich, C.M., Burkle, C.M. & Lanier, W.L., 2012. Ten common questions (and their answers) about off-label drug use. *Mayo Clinic Proceedings*, 87(10), pp.982–990.

WMA, 2013. Declaration of Helsinki: ethical principles for medical research involving human subjects. *JAMA*, 310(20), pp.2191–4.

Woolrich, M.W., Ripley, B.D., Brady, M. & Smith, S.M., 2001. Temporal autocorrelation in univariate linear modeling of FMRI data. *NeuroImage*, 14(6), pp.1370–86.

Worsley, K.J., Evans, A.C., Marrett, S. & Neelin, P., 1992. A Three-Dimensional Statistical Analysis for CBF Activation Studies in Human Brain. *Journal of Cerebral Blood Flow & Metabolism*, 12(6), pp.900–918.

Worsley, K.J. & Friston, K.J., 1995. Analysis of fMRI time-series revisited--again.

NeuroImage, 2(3), pp.173–81.

- Worsley, K.J., Marrett, S., Neelin, P., Vandal, a. C., Friston, K.J. & Evans, a. C., 1996. A unified statistical approach for determining significant signals in images of cerebral activation. *Human Brain Mapping*, 4(1), pp.58–73.
- Yacoub, E., Ugurbil, K. & Harel, N., 2006. The spatial dependence of the poststimulus undershoot as revealed by high-resolution BOLD- and CBV-weighted fMRI. *Journal of cerebral blood flow and metabolism : official journal of the International Society of Cerebral Blood Flow and Metabolism*, 26(5), pp.634–644.
- Yokoyama, C., Kaiya, H., Kumano, H., Kinou, M., Umekage, T., Yasuda, S., Takei, K., Nishikawa, M., et al., 2015. Dysfunction of ventrolateral prefrontal cortex underlying social anxiety disorder: A multi-channel NIRS study. *NeuroImage: Clinical*, 8, pp.455–461.
- Zhang, X., Ross, T.J., Salmeron, B.J., Yang, S., Yang, Y. & Stein, E.A., 2011. Single subject task-related BOLD signal artifact in a real-time fMRI feedback paradigm. *Human brain mapping*, 32(4), pp.592–600.
- Zhao, F., Wang, P., Hendrich, K., Ugurbil, K. & Kim, S.-G., 2006. Cortical layer-dependent BOLD and CBV responses measured by spin-echo and gradient-echo fMRI: insights into hemodynamic regulation. *NeuroImage*, 30(4), pp.1149–60.
- van Zijl, P.C.M., Hua, J. & Lu, H., 2012. The BOLD post-stimulus undershoot, one of the most debated issues in fMRI. *NeuroImage*, 62(2), pp.1092–102.
- Ziv, M., Goldin, P.R., Jazaieri, H., Hahn, K.S. & Gross, J.J., 2013. Is there less to social anxiety than meets the eye? Behavioral and neural responses to three socio-emotional tasks. *Biology of mood & anxiety disorders*, 3(1), p.5.
- Zubeidat, I., Salinas, J.M. & Sierra, J.C., 2008. Exploration of the psychometric characteristics of the Liebowitz Social Anxiety Scale in a Spanish adolescent sample. *Depression and anxiety*, 25(11), pp.977–87.
- Zuo, Z., Wang, R., Zhuo, Y., Xue, R., St Lawrence, K.S. & Wang, D.J.J., 2013. Turbo-FLASH based arterial spin labeled perfusion MRI at 7 T. *PloS one*, 8(6), p.e66612.
- van der Zwaag, W., Francis, S., Head, K., Peters, A., Gowland, P., Morris, P. & Bowtell, R., 2009. fMRI at 1.5, 3 and 7 T: characterising BOLD signal changes. *NeuroImage*, 47(4), pp.1425–34.

